Free Vibrations and Static Deformations of Composite Laminates and Sandwich Plates using Ritz Method

Berkan Alanbay

Dissertation submitted to the Faculty of the
Virginia Polytechnic Institute and State University
in partial fulfillment of the requirements for the degree of

Doctor of Philosophy
in
Aerospace Engineering

Romesh C. Batra, Co-chair
Rakesh K. Kapania, Co-chair
Mayuresh J. Patil
Michael K. Philen
Joseph A. Schetz

November 18, 2020
Blacksburg, Virginia

Keywords: Free Vibrations, Composite Plates, Ritz Method, Jacobi Polynomials, Sandwich Structures, Stress Recovery Scheme

Free Vibrations and Static Deformations of Composite Laminates and Sandwich Plates using Ritz Method

Berkan Alanbay

(ABSTRACT)

In this study, Ritz method has been employed to analyze the following problems: free vibrations of plates with curvilinear stiffeners, the lowest 100 frequencies of thick isotropic plates, free vibrations of thick quadrilateral laminates and free vibrations and static deformations of rectangular laminates, and sandwich structures. Admissible functions in the Ritz method are chosen as a product of the classical Jacobi orthogonal polynomials and weight functions that exactly satisfy the prescribed essential boundary conditions while maintaining orthogonality of the admissible functions. For free vibrations of plates with curvilinear stiffeners, made possible by additive manufacturing, both plate and stiffeners are modeled using a first-order shear deformation theory. For the thick isotropic plates and laminates, a third-order shear and normal deformation theory is used. The accuracy and computational efficiency of formulations are shown through a range of numerical examples involving different boundary conditions and plate thicknesses. The above formulations assume the whole plate as an equivalent single layer. When the material properties of individual layers are close to each other or thickness of the plate is small compared to other dimensions, the equivalent single-layer plate (ESL) theories provide accurate solutions for vibrations and static deformations of multilayered structures. If, however, sufficiently large differences in material properties of individual layers such as those in sandwich structure that consist of stiff outer face sheets (e.g., carbon fiber-reinforced epoxy composite) and soft core (e.g., foam) exist, multilayered structures may exhibit complex kinematic behaviors. Hence, in such case, C_z^0 conditions, namely, piecewise continuity of displacements and the interlaminar continuity of transverse stresses must be taken into account. Here, Ritz formulations are extended for ESL and

layerwise (LW) N^{th}-order shear and normal deformation theories to model sandwich structures with various face-to-core stiffness ratios. In the LW theory, the C^0 continuity of displacements is satisfied. However, the continuity of transverse stresses is not satisfied in both ESL and LW theories leading to inaccurate transverse stresses. This shortcoming is remedied by using a one-step well-known stress recovery scheme (SRS). Furthermore, analytical solutions of three-dimensional linear elasticity theory for vibrations and static deformations of simply supported sandwich plates are developed and used to investigate the limitations and applicability of ESL and LW plate theories for various face-to-core stiffness ratios. In addition to natural frequency results obtained from ESL and LW theories, the solutions of the corresponding 3-dimensional linearly elastic problems obtained with the commercial finite element method (FEM) software, ABAQUS, are provided. It is found that LW and ESL (even though its higher order) theories can produce accurate natural frequency results compared to FEM with considerably lesser number of degrees of freedom.

Free Vibrations and Static Deformations of Composite Laminates and Sandwich Plates using Ritz Method

Berkan Alanbay

(GENERAL AUDIENCE ABSTRACT)

In everyday life, plate-like structures find applications such as boards displaying advertisements, signs on shops and panels on automobiles. These structures are typically nailed, welded, or glued to supports at one or more edges. When subjected to disturbances such as wind gusts, plate-like structures vibrate. The frequency (number of cycles per second) of a structure in the absence of an applied external load is called its natural frequency that depends upon plate's geometric dimensions, its material and how it is supported at the edges. If the frequency of an applied disturbance matches one of the natural frequencies of the plate, then it will vibrate violently. To avoid such situations in structural designs, it is important to know natural frequencies of a plate under different support conditions. One would also expect the plate to be able to support the designed structural load without breaking; hence a knowledge of plate's deformations and stresses developed in it is equally important. These require mathematical models that adequately characterize their static and dynamic behavior. Most mathematical models are based on plate theories. Although plates are three-dimensional (3D) objects, their thickness is small as compared to the in-plane dimensions. Thus, they are analyzed as 2D objects using assumptions on the displacement fields and using quantities averaged over the plate thickness. These provide many plate theories, each with its own computational efficiency and fidelity (degree to which it reproduces behavior of the 3-D object).Hence, a plate theory can be developed to provide accurately a quantity of interest. Some issues are more challenging for low-fidelity plate theories than others. For example, the greater the plate thickness, the higher the fidelity of plate theories required for obtaining accurate natural frequencies and deformations. Another challenging

issue arises when a sandwich structure consists of strong face-sheets (e.g., made of carbon fiber-reinforced epoxy composite) and a soft core (e.g., made of foam) embedded between them. Sandwich structures exhibit more complex behavior than monolithic plates. Thus, many widely used plate theories may not provide accurate results for them. Here, we have used different plate theories to solve problems including those for sandwich structures. The governing equations of the plate theories are solved numerically (i.e., they are approximately satisfied) using the Ritz method named after Walter Ritz and weighted Jacobi polynomials. It is shown that these provide accurate solutions and the corresponding numerical algorithms are computationally more economical than the commonly used finite element method. To evaluate accuracy of a plate theory, we have analytically solved (i.e., the governing equations are satisfied at every point in the problem domain) equations of 3D theory of linear elasticity. The results presented in this research should help structural designers.

To my parents and my beautiful wife

Acknowledgments

First and foremost, I would like to express my deepest gratitude to my advisors, Professors Rakesh K. Kapania and Romesh C. Batra. Professor Kapania has offered me not only high-quality training in research, but also numerous research opportunities to strategically shape my academic path. Since I began my Ph.D. studies in 2016, Professor Kapania's dedication and excellence in both teaching and advising have been essential ingredients for my research. In the last two years of my Ph.D. work, I have also had the privilege to closely work with Professor Batra. Without a doubt, his insights and unending quest for excellence have substantially contributed to my work. His passion for research has left a lasting impression on me. I have been blessed to have advisors with such and innate wisdom! This dissertation would not have been possible without their conscientious support, encouragement, and guidance.

I would also like to thank Dr. Mayuresh J. Patil, Dr. Michael Philen, and Dr. Joseph A. Schetz for serving on my committee. In addition, I extend my sincere appreciation to Dr. Daniel Hammerand, with whom I worked in a DARPA-funded project in 2018. Working with him was an invaluable experience. He consistently provided me with insight valuable for both the project and for my personal research.

During my time in the Aerospace Engineering doctoral program at Virginia Tech, I was extremely fortunate to encounter a number of amazing, brilliant, and steadfast friends and colleagues. I sincerely thank my friends and colleagues in Professor Kapania's research group, Dr. Wei Zhao, Dr. Rikin Gupta, Dr. Karanpreet Singh, Jitish Miglani, Junhyeon Seo, Manasi Palwankar, Siddhant Desai, and Varakini Sanmugadas, for their academic support and sincere friendship. Likewise, I thank my friends and colleagues in Professor Batra's research groups, Lisha Yuan, Dongho Kim, Devin Burns, Akshay Dahiya, and Balachandar Guduri, for investing their time and effort in providing invaluable feedback. Our weekly

meetings were instrumental in guiding my research. I truly enjoyed sharing the same office with Rikin. He has been a wonderful friend and an amazing colleague. It was a great pleasure to collaborate with Karanpreet. I also owe thanks to Lisha for sharing her knowledge with me on third-order shear and normal deformation plate theory when I first joined Professor Batra's research group. She has been both helpful and kind in answering my numerous questions.

I express my sincere appreciation to Steve Edwards and Tim Tomlin for their technical guidance and assistance in IT-related issues. I also gratefully acknowledge the help and computing resources received from Virginia Tech's Advanced Research Computing Center.

I am very grateful for the financial support that I received from Metalsa Structural Products Inc., NASA PAAW project (grant NRA NNX14AL36A), DARPA (grant SB172-005-0162). The work reported in Chapters three through six was supported by the U.S. Office of Naval Research grants N00014-18-1-2548 and N00014-20-1-2876 to Virginia Polytechnic Institute and State University with Dr. Batra as the principal investigator.

I would like to acknowledge the support and unconditional love of my parents, Hülya and Ali Naki, and my brother, Bayram Bora. Their emotional support and endless care have given me the strength and courage to persevere in my academic endeavors.

I will forever be thankful to my family in the USA, Wayne and Betty Coleman, for their sincere love and consistent support. I met them in the Blacksburg Tango Community in 2016. Since then, they have become my family here and have never made me feel alone even when the road got tough. Their presence in my life in Blacksburg has always been a true blessing.

My deepest appreciation goes to my beautiful and loving wife, Şengül. Her love and presence are a tremendous inspiration for meeting every challenge that comes our way!

Contents

List of Figures

List of Tables

Chapter 1

Introduction

Chapter 1. Introduction

Over the past several years, design engineers have been challenged to address ever higher performance requirements. The changes in structural design requirements have pushed researchers and engineers to look for more efficient structural members and configurations that are lightweight yet strong enough to withstand desired strength requirements. Plates and shells are utilized extensively in many engineering fields. To achieve lightweight design, usually, two typical approaches are adopted; (1) use of reinforcements like stiffeners in plates and shells and their structural optimization (size, shape, and topology), and (2) use of advanced materials, like composites. Furthermore, the efficient utilization of stiffeners and advanced materials require mathematical models that adequately predict the static and dynamic behaviors of structures under various loads. Most of these models are based on plate and shell theories, and the quality of their predictions depend upon simplifying kinematic assumptions in developing the theories. Hence, it is crucial to select a proper structural theory based on the complexity of the problem. Multilayered composite structures made of various materials have complex static and dynamic behaviors due to distinct material properties of individual layers. Thus, many of the classical equivalent single layer plate and shell theories fail to capture these complex behaviors. Understanding deficiencies in our knowledge of the behavior of laminated and sandwich structures is central to coming closer to effectively and rationally designing them, and possibly improving upon the theories.

The main objective of this dissertation is to develop more accurate and efficient methods, and investigate limitations and applicability of currently available plate theories to ensure the efficient utilization of composites. In this study, equations of various plate theories are numerically solved by using the Ritz method and the weighted Jacobi polynomials as admissible functions. Below we have briefly reviewed composite materials, plate and shell theories and the Ritz method.

1.1 Composite Materials

A composite material, or simply a composite, is a mixture of two or more different constituents which are insoluble in one another. The resulting composite offers tailor-made properties that cannot be achieved with any of the individual components. Generally, composite materials are obtained by embodying the structural constituents, such as fibers, particles, flakes, lamina and filler, in a continuous matrix material. While structural constituents are the principal load-carrying members, the matrix material holds them in place, seals the structure from mechanical damage and protects it from environmental deterioration.

A laminate (Figure 1.1) is a combination of lamina, a typical sheet of a composite material, to achieve the desired stiffness and other properties. For example, the effective properties of a laminate composed of unidirectional fiber-reinforced laminas can be tailored by varying the orientation of fibers and their volume fractions in each lamina.

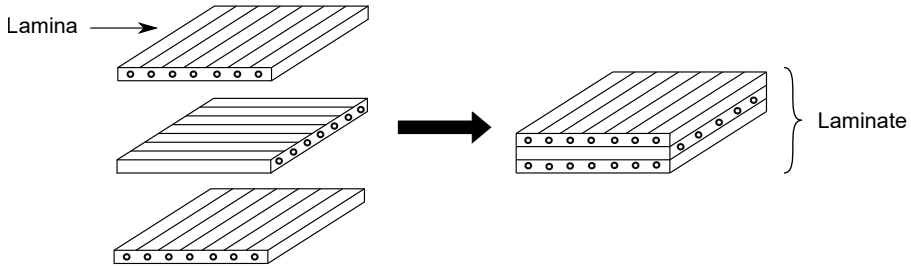

Figure 1.1: Lamina and laminate

A typical sandwich structure (Figure 1.2), a special kind of laminate, consists of outer thin face-sheets of a strong material (e.g., glass/carbon fiber-reinforced epoxy composite) and a thick core of soft, lightweight material (e.g., honeycomb, foam, and balsa wood) embedded between them [1]. Often, an analogy between sandwich construction and I-beam with a high section modulus is made. Since the facesheets are separated by the core, they can have very high bending stresses like those in flanges of the beam. The primary role of the core, like

the web of the beam, is to carry shear stresses while stabilizing the facesheets.

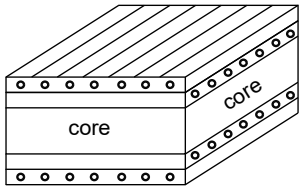

Figure 1.2: Configuration of a traditional sandwich structure

1.2 Brief Overview of Plate Theories

Even though a plate geometry is three-dimensional (3-D), the high computational expense of 3-D analyses has led to the development of plate theories based on simplifying kinematic assumptions. For example, the classical (or the Love-Kirchhoff) plate theory (CPT) does not consider both transverse shear and normal deformations and rotary inertia. Although the CPT provides acceptable solutions for thin (thickness/side length, $h/b < 0.01$) and moderately thick plates ($0.01 < h/b < 0.05$) [2], predictions become inaccurate for thicker plates. By accounting for both transverse shear and rotary inertia, Mindlin [3] proposed a first-order shear deformation theory (FSDT) and successfully applied it to study deformations of moderately thick plates. For $h/b \geq 0.1$, these simplifications may give erroneous results for some problems. These limitations of the FSDT led to the development of higher-order shear deformation theories (HSDT) and higher-order shear and normal deformable theories (HSNDT). Detailed examinations and reviews of HSDT and HSNDT are given in [4, 5, 6, 7]. Carrera and Brischetto [8] and Noor et al. [9] have, respectively, reviewed 82 and 556 papers.

The analysis of laminates can be arduous because of possible combinations of several different isotropic and/or anisotropic materials. In general, when analyzing deformations of homogeneous plates, it is assumed that at all material points displacements are described by the same functional relation between coordinates in the current and the reference con-

figurations. For multilayered structures, this assumption is invalid because differences in mechanical properties of individual layers introduce requirements of continuity of surface tractions and displacements across an interface between two layers. The former requirement can be satisfied only if the normal component (perpendicular to the interface) of displacement gradients is discontinuous across an interface. A displacement-based equivalent single layer (ESL) theory does not satisfy the continuity of surface tractions across an interface; accordingly, through-the-thickness stresses obtained from constitutive laws and plate theory displacements are generally inaccurate. These drawbacks of the ESL theories led to the development of zig-zag [10, 11, 12, 13] and layer-wise theories for multilayered plates and shells. Layer-wise theories that use mixed formulations (i.e., Reissner's mixed variational theorem [14, 15, 16]) a priori satisfy the C_0^z requirements. However, they introduce considerably more unknowns into the problem, hence the computational cost is high. For more detailed examination of layer-wise theories the reader should consult reviews by Reddy [17], Carrera and Brischetto [8], Khandan et al. [18], and Liew et al. [6].

1.3 Ritz method

A common technique for numerically solving initial boundary value problems is the finite element method (FEM). Compared to the FEM, the Ritz method uses global basis functions which a priori satisfy essential boundary conditions. The Ritz method can provide superior results with lesser degrees of freedoms (DoFs) than the FEM [19, 20]. Meirovitch and Kwak [19] attribute the enormous success of the FEM to two main reasons: (1) It can solve nonlinear problems for bodies of complex geometries, and (2) the low-order complete polynomial basis functions with compact support give matrices of small bandwidth. They also stated that the Ritz method could yield superior accuracy for the same number of degrees of freedom (DoFs) as those in the FEM. Furthermore, the convergence of high frequencies

computed with the FEM requires a large number of DoFs that increases the total CPU time.

1.3.1 Ritz Admissible Functions

In the Ritz method, the displacement is assumed as a linear combination of admissible functions. As long as the essential boundary conditions are satisfied, the Ritz method is applicable for any set of linearly independent admissible functions that form a complete set; completeness helps in the convergence of the solution as the number of basis functions is increased. However, the choice of admissible functions significantly affects accuracy of results and computational resources needed for the analysis. Selecting admissible functions that satisfy all essential boundary conditions has been the most serious drawback of the Ritz method. Over the years, many trial functions have been proposed. Among them, simple polynomials are the most commonly used trial functions due to their simplicity and fast convergence rate. However, it is well known that numerical instability and ill-conditioning issues arise when polynomials of very high degree are employed [21, 22]. Fletcher [23] explains this as follows: these polynomials become numerically linearly dependent, and the mass and the stiffness matrices become singular due to ill-conditioning with the consideration of higher-order terms in the polynomials.

The use of orthogonal polynomials has been proposed to overcome this ill-conditioning. Bhat [24] used orthogonal polynomials as trial functions, and developed boundary characteristic orthogonal polynomials by using the Gram-Schmidt process. In this method, the first term of the orthogonal polynomials is selected as the polynomial of the least order that satisfies the essential boundary conditions. Bhat later used these orthogonal polynomials to solve for a variety of problems [25, 26, 27]. Chakraverty, Bhat, and Stiharu [28] have reported that the method proposed by Bhat has received more than 100 citations, and that it produces more accurate results while using a simple implementation.

Singhvi and Kapania [29] proposed the use of classical Chebyshev polynomials in the Ritz method to study free torsional vibration and buckling of doubly symmetric thin-walled beams. They relaxed the requirements on the choice of admissible functions by implementing a penalty method in which the essential boundary conditions are simulated by artificial springs with large stiffness coefficients. Singhvi and Kapania also reported that when they used the Chebyshev polynomials, mass and stiffness matrices remained positive definite for higher modes, unlike that in simple polynomials. Smith, Bradford, and Oehlers [30] studied the numerical convergence of simple and orthogonal polynomials for a unilateral plate buckling problem by using the Ritz method. When they used the classical orthogonal polynomials, namely Chebyshev types 1 and 2, Legendre, Hermite, and Laguerre, the trial functions were defined as the product of the boundary function, which enforces the essential boundary conditions, and the classical orthogonal polynomials. Later, Zhou et al. [31] introduced a similar approach called the Chebyshev-Ritz method. In this method, admissible functions are constructed by multiplying the Chebyshev polynomials with a boundary function as suggested by Smith, Bradford, and Oehlers [30]. However, considerable doubts have arisen over advantages of using the classical orthogonal polynomials multiplied by a boundary function. Since the orthogonality of classical polynomials is valid with a particular weight function (for example, Chebyshev polynomials of the first kind are orthogonal on the interval $[-1, 1]$ with respect to the weight function $1/\sqrt{1-x^2}$, multiplying these polynomials with other than their specific weight function may lead to the loss of orthogonality

1.3.2 Jacobi Polynomials

Since the classical orthogonal Jacobi polynomials are eigenfunctions of singular Sturm–Liouville problems [32], they possess nice properties such as good rates of convergence and orthogonality [33]. Jacobi polynomials are general polynomials orthogonal on the interval $[-1, 1]$. By

adjusting the shape parameters of the Jacobi polynomials, other classical orthogonal polynomials, such as Gegenbauer, Legendre, Chebychev, and Zernike, can be obtained. This ease of modifying the Jacobi weight function helps in satisfying all essential boundary conditions without loss of orthogonality. Therefore, better numerical stability and condition number of the stiffness and the mass matrices can be achieved. Furthermore, submatrices of the mass matrices are diagonal. Another advantage of the Jacobi polynomials is the ease of generating them using the following three-term recursive formula:

$$\begin{aligned} 2n\, c_n\, c_{2n-2}\, P_n^{(\alpha,\beta)}(\xi) = c_{2n-1}\, (c_{2n-2}\, c_{2n}\, \xi + \alpha^2 - \beta^2)\, P_{n-1}^{(\alpha,\beta)}(\xi) \\ -2(n-1+\alpha)(n-1+\beta)\, c_{2n}\, P_{n-2}^{(\alpha,\beta)}(\xi) \end{aligned} \tag{1.1}$$

in which

$$c_n = n + \alpha + \beta$$

$$P_0^{(\alpha,\beta)}(t) = 1; \qquad P_1^{(\alpha,\beta)}(t) = \frac{\alpha-\beta}{2} + (1 + \frac{\alpha-\beta}{2})t$$

The derivative of Jacobi polynomials is given by [34]

$$\frac{\mathrm{d}}{\mathrm{d}t}\left[P_n^{(\alpha,\beta)}(t)\right] = \frac{1}{2}\,(n+\alpha+\beta+1)\, P_{n-1}^{(\alpha+1,\beta+1)}(t) \tag{1.2}$$

1.4 Objectives of the Dissertation Proposal

The overall aim of this work can be stated as follows:

- Develop new methodologies based on various plate theories that use weighted Jacobi polynomials as basis functions in the Ritz method and demonstrate efficiency of this methodology.

1.4. Objectives of the Dissertation Proposal

- Develop an approach for studying free vibrations of curvilinear stiffened quadrilateral plates by using Ritz method and weighted Jacobi polynomials. It is known that the use of curvilinear stiffeners provides a significantly larger design space than that by straight stiffeners; thus more efficient components can be developed by using curvilinear stiffeners. The approach using the Ritz method does not depend on a FE mesh that facilitates changing locations and shapes of stiffeners. In future, this can be extended to develop an equivalent plate model of built-up aircraft wings consisting of curvilinear spars and ribs for their rapid evaluation and optimization.

- Develop a third-order shear and normal deformable plate theory (TSNDT) based Ritz method for free vibrations of thick isotropic plates and compute up to lowest 100 frequencies and corresponding mode shapes which are important in vibro-acoustic applications, and represent the mid-frequency (high-frequency) range for thin (thick) plates. The traditional FEM is well established and mature for finding low frequencies. However, it is computationally more expensive for high frequencies. We note that there are probabilistic techniques such as the Statistical Energy Analysis for analyzing the high-frequency range. However, we have not seen how its computational cost compares with that of the FEM.

- Extend the TSNDT based Ritz method for analyzing quadrilateral laminates, and delineate effects of skew angles, the number of layers, and the thickness-to-side ratio on frequencies computed with the Ritz method, the FSDT based shell elements (S4 and S4R), and 20-node brick elements (C3D20) in Abaqus. These comparisons demonstrate the accuracy and efficiency of the present method and establish when to use the FSDT based shell elements in Abaqus for studying free vibrations of skew laminates.

- Present the three-dimensional linear theory of elasticity (LET) based lowest 12 distinct analytical natural frequencies of sandwich composite plates having different face-sheet

to core stiffness and density ratios, and find limits of applicability of using the TSNDT for sandwich structures.

- Develop N^{th}-order shear and normal deformable ESL and LW plate theories based on Ritz method for free vibrations and static deformations of sandwich plates having various face-to-core stiffness ratios. Assertain the critical ESL and LW plate theory orders for predicting natural frequency and stress results within 5% of their analytical values.

1.5 Layout of the Proposal

The main body of the proposal consists of four chapters mostly focusing on free vibrations of plates, starting from an isotropic single layer plate and progressing to laminated and sandwich composite plates. The common thing in all chapters is the use of the Ritz method and of the weighted Jacobi polynomials as basis functions to numerically solve governing equations of different plate theories. The analysis of static deformations is proposed for future work. Starting with the second chapter, the contents of the proposal are listed below.

The second chapter presents an approach for accurate and efficient analysis of free vibration of curvilinearly stiffened quadrilateral plates. The formulations for both the plate and stiffeners are based on the first-order shear deformation theory (FSDT). The Jacobi polynomials up to degree 30 in each of the two directions for both the plate and stiffeners are used.

The third chapter focuses on obtaining up to the lowest 100 free vibration frequencies and corresponding mode shapes of isotropic elastic plates with thickness to side ratio varying from 0.001 to 0.5 by using a TSNDT. It is shown that this approach requires fewer degrees of freedom than those in the FEM. The presently computed results agree well with those from either analytical or numerical solutions of the corresponding 3-dimensional LET equations

obtained with the commercial FE software, Abaqus.

In chapter four, the work is extended to solve frequencies of thick quadrilateral laminates. The method is applied first to find the lowest few (6 in most examples) frequencies of isotropic cantilever plates of different skew angles and thickness to side length ratios. Subsequently, presently computed natural frequencies of laminated composite plates for varying skew angles, thickness to side ratios, number of layers, and stacking sequences are compared with those obtained from converged solutions using either shell or brick elements in Abaqus. It is demonstrated that the TSNDT/Ritz method provides accurate frequencies. Three-dimensional mode shapes are presented for a better understanding of the dynamic behavior of skew quadrilateral laminates

The fifth chapter provides the lowest 12 distinct analytical frequencies and the corresponding mode shapes of simply supported cross-ply laminates and sandwich plates by using the state-space approach to solve 3D LET equations. Limits of applicability and the error in frequencies computed using a TSNDT are provided. The dependence of the relative error between the TSNDT and 3D analytical solutions upon the face-sheet to the core stiffness (FCSR) and mass density ratio (FCDR) is delineated for sandwich structures.

In Chapter 6, we analyzed the free vibration and static deformations of laminated and sandwich composite plates using a variable order equivalent single layer (ESL) theory and layer-wise plate theories. In chapter five, we evaluated the accuracy of the TSNDT in predicting the lowest 12 natural frequencies of sandwich structures with the soft core by comparing results with those found from the 3D-LET. Here, the purpose is to see whether or not the use of a variable order ESL plate theory can remove limitations of the TSNDT in accurately predicting the natural frequencies. Furthermore, we assess the accuracy and computational efficiency of the layer-wise theory in analyzing static and

The face-sheet to core stiffness ratio in Chapter 5 was varied by modifying the elastic constant C_{11} of Aragonite crystals with other elastic constants expressed in terms of C_{11}. It does not precisely inform us which material direction elastic modulus (i.e., E_{11}, E_{33}) has the most dominant role on the response of plates. Hence, in this chapter, we considered the sandwich plates with typical industrial face and core materials.

Bibliography

[1] Birman, V. and Kardomateas, G. A., 2018, "Review of current trends in research and applications of sandwich structures," Composites Part B: Engineering, **142**(1), pp. 221–240.

[2] Leissa, A. W., 1973, "The free vibration of rectangular plates," Journal of Sound and Vibration, **31**(3), pp. 257–293.

[3] Mindlin, R. D., 1951, "Influence of rotatory inertia and shear on flexural motions of isotropic, elastic plates," Journal of Applied Mechanics, **18**, pp. 31–38.

[4] Kapania, R. K. and Raciti, S., 1989, "Recent Advances in analysis of laminated beams and plates, Part I: Shear effects and buckling," AIAA Journal, **27**(7), pp. 923–935.

[5] Batra, R. C., Vidoli, S., and Vestroni, F., 2002, "Plane wave solutions and modal analysis in higher order shear and normal deformable plate theories," Journal of Sound and Vibration, **257**(1), pp. 63–88.

[6] Liew, K. M., Pan, Z. Z., and Zhang, L. W., 2019, "An overview of layerwise theories for composite laminates and structures: Development, numerical implementation and application," Composite Structures, **216**, pp. 240–259.

[7] Kapania, R. K. and Raciti, S., 1989, "Recent advances in analysis of laminated beams

and plates, part II: Vibrations and wave propagation," AIAA Journal, **27**(7), pp. 935–946.

[8] Carrera, E. and Brischetto, S., 2009, "A survey with numerical assessment of classical and refined theories for the analysis of sandwich plates," Applied Mechanics Reviews, **62**(1), p. p. 010803.

[9] Noor, A. K., Burton, W. S., and Bert, C. W., 1996, "Computational models for sandwich panels and shells," Applied Mechanics Reviews, **49**(3), pp. 155–199.

[10] Carrera, E., 2003, "Historical review of zig-zag theories for multilayered plates and shells," Applied Mechanics Reviews, **56**(3), pp. 287–308.

[11] Lekhnitskii, S. G., 1935, "Strength calculation of composite beams," Vestnik inzhen i tekhnikov, **9**, pp. 137–148.

[12] Ren, J. G., 1986, "Bending theory of laminated plate," Composites Science and Technology, **27**(3), pp. 225–248.

[13] Gherlone, M., 2013, "On the use of zigzag functions in equivalent single layer theories for laminated composite and sandwich beams: a comparative study and some observations on external weak layers," Journal of Applied Mechanics, **80**(6), p. 061004.

[14] Reissner, E., 1984, "On a certain mixed variational theorem and a proposed application," International Journal for Numerical Methods in Engineering, **20**(7), pp. 1366–1368.

[15] Reissner, E., 1986, "On a mixed variational theorem and on shear deformable plate theory," International Journal for Numerical Methods in Engineering, **23**(2), pp. 193–198.

[16] Carrera, E., 1999, "A reissner's mixed variational theorem applied to vibration analysis of multilayered shell," Journal of Applied Mechanics, **66**(1), pp. 68–78.

BIBLIOGRAPHY

[17] Reddy, J. N., 1993, "An evaluation of equivalent-single-layer and layerwise theories of composite laminates," Composite Structures, **25**(1-4), pp. 21–35.

[18] Khandan, R., Noroozi, S., Sewell, P., and Vinney, J., 2012, "The development of laminated composite plate theories: a review," Journal of Materials Science, **47**(16), pp. 5901–10.

[19] Meirovitch, L. and Kwak, M. K., 1990, "Convergence of the classical Rayleigh-Ritz method and the finite element method," AIAA Journal, **28**(8), pp. 1509–1516.

[20] Wang, C. M., Wang, Y. C., and Reddy, J. N., 2002, "Problems and remedy for the Ritz method in determiningstress resultants of corner supported rectangular plates," Computers and Structures, **80**(2), pp. 145–154.

[21] Ilanko, S., Monterrubio, L., and Mochida, Y., 2015, *The Rayleigh-Ritz Method for Structural Analysis*, John Wiley & Sons.

[22] Kapania, R. K. and Liu, Y., 2000, "Static and vibration analyses of general wing structures using equivalent-plate Models," AIAA Journal, **38**(7), pp. 1269–1277.

[23] Fletcher, C. A. J., 1987, *Computational Galerkin Methods*, Springer-Verlag New.

[24] Bhat, R., 1985, "Natural frequencies of rectangular plates using characteristic orthogonal polynomials in Rayleigh-Ritz method," Journal of Sound and Vibration, **102**(4), pp. 493–499.

[25] Bhat, R., 1987, "Flexural vibration of polygonal plates using characteristic orthogonal polynomials in two variables," Journal of Sound and Vibration, **114**(1), pp. 65–71.

[26] Bhat, R., 1987, "Rayleigh-Ritz method with separate deflection expressions for structural segments," Journal of Sound and Vibration, **115**(1), pp. 174–177.

BIBLIOGRAPHY

[27] Bhat, R., 2015, "Vibration of beams using novel boundary characteristic orthogonal polynomials satisfying all boundary conditions," Advances in Mechanical Engineering, **7**(4), p. 1687814015578355.

[28] Chakraverty, S., Bhat, R., and Stiharu, I., 1999, "Recent research on vibration of structures using boundary characteristic orthogonal polynomials in the Rayleigh-Ritz method," Shock and Vibration Digest, **31**(3), pp. 187–194.

[29] Singhvi, S. and Kapania, R. K., 1994, "Comparison of simple and Chebychev polynomials in Rayleigh-Ritz analysis," Journal of Engineering Mechanics, **120**(10), pp. 2126–2135.

[30] Smith, S. T., Bradford, M. A., and Oehlers, D. J., 1999, "Numerical Convergence of simple and orthogonal polynomials for the unilateral plate buckling problem using the Rayleigh–Ritz method," International Journal for Numerical Methods in Engineering, **44**(11), pp. 1685–1707.

[31] Zhou, D., Cheung, Y. K., Au, F. T., and Lo, S. H., 2002, "Three-dimensional vibration analysis of thick rectangular plates using Chebyshev polynomial and Ritz method," International Journal of Solids and Structures, **39**(26), pp. 6339–6353.

[32] Caruntu, D. I., 2007, "Classical Jacobi polynomials, closed-form solutions for transverse vibrations," Journal of Sound and Vibration, **306**(3-5), pp. 467–494.

[33] Ditkowski, A. and Kats, R., 2019, "On spectral approximations with nonstandard weight functions and their Implementations to generalized chaos expansions," Journal of Scientific Computing, **79**(3), pp. 1981–2005.

[34] Szegö, G., 1939, *Orthogonal polynomials*, Vol. 23, American Mathematical Society, Providence, Rhode Island.

Chapter 2

Free Vibration of Curvilinearly Stiffened Quadrilateral Plates

The contents of this chapter have appeared in Journal of Vibration and Acoustics. [1]

[1] **Alanbay, B.**, Singh, K., and Kapania, R. K., 2020, "Vibration of Curvilinearly Stiffened Plates Using Ritz Method with Orthogonal Jacobi Polynomials," Journal of Vibration and Acoustics, 142(1), p. 011009.

2.1 Abstract

This paper presents a general approach for the free vibration analysis of curvilinearly stiffened rectangular and quadrilateral plates using Ritz method by employing classical orthogonal Jacobi polynomials. Both the plate and stiffeners are modeled using first-order shear deformation theory (FSDT). The displacement and rotations of the plate and stiffeners are approximated by separate sets of Jacobi polynomials. The ease of modification of the Jacobi polynomials enables the Jacobi weight function to satisfy geometric boundary conditions without loss of orthogonality. The distinctive advantage of Jacobi polynomials, over other polynomial-based trial functions, lies in that their use eliminates the well-known ill-conditioning issues when a high number of terms are used in the Ritz method; e.g., to obtain higher modes required for vibro-acoustic analysis. In this paper, numerous case studies are undertaken by considering various sets of boundary conditions. The results are verified both with the detailed Finite Element Analysis (FEA) using commercial software MSC.NASTRAN, and with those available in the open literature. New formulation and results include: (i) exact boundary condition enforcement through Jacobi weight function for FSDT, (ii) formulation of quadrilateral plates with curvilinear stiffeners, (iii) use of higher-order Gauss quadrature scheme for required integral evaluations to obtain higher modes. It is demonstrated that the presented method provides good numerical stability and highly accurate results. The given new numerical results and convergence studies may serve as benchmark solutions for validating the new computational techniques.

2.2 Introduction

Stiffened plates are widely used in different engineering applications such as submarines [1], aircraft [2], and pressure vessels and pipes [3]. With the advancement in manufacturing

technologies, e.g., additive manufacturing, it is possible to make use of curvilinearly stiffened structures[4]. Kapania, Li and Kapoor [5] indicated that under certain design conditions, curvilinear stiffeners can help in reducing the weight of the structure while still satisfying the required constraints. Furthermore, it has been shown that curvilinear stiffeners provide a significantly larger design space while designing the aircraft wings [2, 5, 6, 7] . Designing local stiffened panels is also one of the important tasks while designing the aircraft wings [8]. Following the work of Kapania, Li and Kapoor, a number of studies have been conducted to study the use of curvilinear stiffeners in plates and shells both at Virginia Tech and at other places. Shi, Kapania and Dong [9, 10] studied the vibration and buckling analysis of isotropic curvilinearly stiffened plates using finite element (FE) model by using First-order Shear Deformation Theory (FSDT) in the presence of in-plane loads. They modeled the plate and stiffener separately. Their formulation has a benefit of not requiring to place nodes at the plate interface of the panel and stiffener. Similarly, Zhao and Kapania [11, 12] developed a FE model for buckling and vibration analyses of curvilinearly stiffened composite panels. Research showed that it is possible to improve the free vibration response, buckling and pre-stressed vibration responses simultaneously by tailoring stiffener shape and placement [13, 14, 15]. Tamijani and Kapania conducted buckling and vibration analysis of curvilinearly stiffened plates by using Chebyshev-Ritz method [16, 17] and mesh-free method [18, 19].

Finite element analysis (FEA) is one of the most robust and reliable engineering tools for analyzing various engineering problems. However, FE may require significant amount of model preparation time for generating a reliable mesh. The Ritz Method can be an alternative method for getting accurate solutions especially in the preliminary design stage and/or when higher modes are needed, for example, for studying vibro-acoustic response of stiffened plates. The Ritz method has advantages over FEM for being simple and less time consuming (except when a large number of complex integrals need to be performed). However, the

Ritz method has also some drawbacks and challenges. For example, the choice of Ritz trial functions plays an important role and can significantly affect the analysis results. The trial functions should satisfy the essential boundary conditions and form a complete set. Due to their simplicity and fast convergence rate, simple polynomials are widely used as Ritz trial functions. Liew et al. [20, 21, 22] studied bending, buckling, deflection and vibration of various shaped plates with and without stiffeners using pb-2 Ritz method based on simple polynomials. Despite the mentioned advantages of the simple polynomials, well-known ill-conditioning issues can arise while using more number of terms for the trials functions in the Ritz method; e.g., to obtain higher modes [23]. To overcome this issue, Bhat [24] used the orthogonal polynomials as the Ritz trial functions. The author developed boundary characteristic orthogonal polynomials by the use of Gram-Schmidt procedure and used them for variety of problems [25, 26]. Later, Kapania et al. [27, 28, 29] used Chebyshev polynomials as the trial functions to solve generally laminated plates using FSDT. Since the Chebychev polynomials do not satisfy the essential boundary conditions, the authors used the penalty method to relax the restriction on selection of admissible functions. In the penalty method, essential boundary conditions are simulated by artificial springs with large stiffness coefficients. It should be noted that in the selection of the stiffness coefficients, great care should be taken to ensure boundary conditions are correctly satisfied and the mass and stiffness matrices do not become ill conditioned.

In a previous study [30], the classical orthogonal Jacobi polynomials as the Ritz trial functions were introduced for solution of rectangular plates using classical plate theory (CPT). Since the classical orthogonal Jacobi polynomials are eigenfunctions of singular Sturm-Liouville problems [31], they possesses such important properties as good rate of convergence and orthogonality measure [32]. Jacobi polynomials are the general form of many orthogonal polynomials which are orthogonal in the interval [-1,1]. By adjusting the shape parameters

of the Jacobi polynomials, the other classical orthogonal polynomials such as Gegenbauer, Legendre, Chebychev and Zernike can be obtained. This ease of manipulating Jacobi weight function can help in satisfying all essential boundary geometric boundary conditions without loss of orthogonality [32]. Furthermore, by using three terms recursive formula the trial function can easily be generated and implemented in the computer code.

The current study extends our previous work [30] on Jacobi polynomials based Ritz method to study the vibration of curvilinearly stiffened rectangular and quadrilateral plates, using FSDT for modeling both plate and stiffener. The Jacobi polynomials are used as trial functions in the Ritz method. First, the methodology is described in detail in Section 2. Later, in Section 3, different configurations of stiffeners under different sets of boundary conditions are studied and the results compared with those in available literature and obtained using a detailed FEM analysis employing MSC.NASTRAN, commercially available software. Convergence studies are also presented in order to study the effect of the number of terms used on the accuracy of the higher modes frequencies.

2.3 Formulation for stiffened plates

2.3.1 Formulation for the plate

Consider a curvilinearly stiffened quadrilateral plate of uniform thickness h_p as shown in Figure 2.1. The plane strain energy, U_p, and the kinetic energy, T_p, can be expressed by

$$U_p = \frac{1}{2}\int_V \{\epsilon_p\}^T [E_p] \{\epsilon_p\} \, dV \tag{2.1}$$

$$T_p = \frac{1}{2}\int_V \rho \{\dot{u}_p\}^T \{\dot{u}_p\} \, dV \tag{2.2}$$

where $\{\epsilon\}$ and V are strain tensor and volume of the quadrilateral plate, respectively.

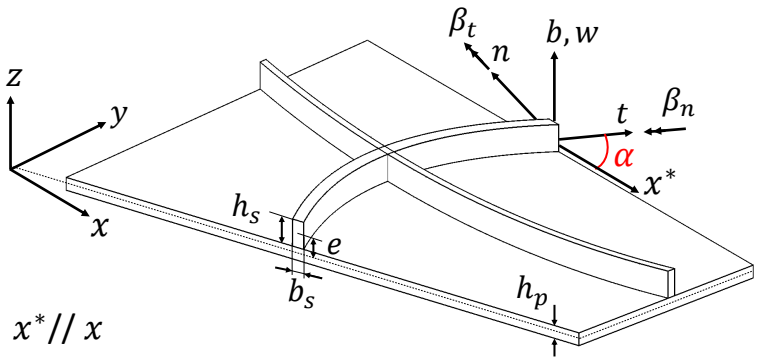

Figure 2.1: Curvilinearly stiffened quadrilateral plate and related coordinate systems

The plate material property matrix, $[E_p]$, is given by

$$[E_p] = \begin{bmatrix} \frac{E}{1-\nu^2} & \frac{E\nu}{1-\nu^2} & 0 & 0 & 0 \\ \frac{E\nu}{1-\nu^2} & \frac{E}{1-\nu^2} & 0 & 0 & 0 \\ 0 & 0 & G & 0 & 0 \\ 0 & 0 & 0 & \kappa G & 0 \\ 0 & 0 & 0 & 0 & \kappa G \end{bmatrix} \tag{2.3}$$

where E, G, ν, κ are Young's modulus, shear modulus, Poisson's ratio, and shear correction factor, respectively. The shear correction factor is taken as $\kappa = 5/6$ and shear modulus is $G = E/[2(1+\nu)]$.

Considering FSDT, the displacement fields of the plate, $\{u_p\}$, can be expressed as [33]:

$$\begin{aligned} u(x,y,z,t) &= z\,\beta_x(x,y,t) \\ v(x,y,z,t) &= z\,\beta_y(x,y,t) \\ w(x,y,z,t) &= w_0(x,y,t) \end{aligned} \tag{2.4}$$

in which, as shown in Figure 2.1, u, v, w are displacements in the x, y, z directions, respec-

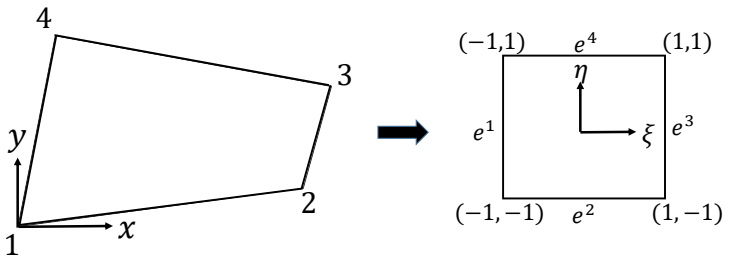

Figure 2.2: Transformation from global to natural coordinate system

tively and β_x and β_y are the rotations about y and $-x$ axis, respectively. Subscript 0 refers to the motion for the point in the middle plane. Note that only bending and shear effects are considered thus the in-plane displacements of the middle plane, u_0 and v_0, are ignored.

From Eqn. (2.4), the generalized strains can be obtained by using Green's definitions,

$$\{\epsilon_p\} = \begin{Bmatrix} \epsilon_x \\ \epsilon_y \\ \gamma_{xy} \\ \gamma_{xz} \\ \gamma_{zx} \end{Bmatrix} = \begin{Bmatrix} \dfrac{\partial u}{\partial x} \\ \dfrac{\partial v}{\partial y} \\ \dfrac{\partial u}{\partial y} + \dfrac{\partial v}{\partial x} \\ \dfrac{\partial u}{\partial z} + \dfrac{\partial w}{\partial x} \\ \dfrac{\partial v}{\partial z} + \dfrac{\partial w}{\partial y} \end{Bmatrix} = \begin{Bmatrix} z\dfrac{\partial \beta_x}{\partial x} \\ z\dfrac{\partial \beta_y}{\partial y} \\ z\left(\dfrac{\partial \beta_x}{\partial y} + \dfrac{\partial \beta_y}{\partial x}\right) \\ \beta_x + \dfrac{\partial w}{\partial x} \\ \beta_y + \dfrac{\partial w}{\partial y} \end{Bmatrix} \tag{2.5}$$

For the convenience of the integral computations and to efficiently use the orthogonal properties of the classical Jacobi polynomials, a transformation from global (x, y) to natural (ξ, η) coordinates is performed, a quadrilateral plate in (x, y) mapped to a square in (ξ, η), as illustrated in Figure 2.2.

The transformation is defined by the following formulation [28]:

$$x = \sum_{i=1}^{4} N_i(\xi,\eta)\, x_i, \qquad y = \sum_{i=1}^{4} N_i(\xi,\eta)\, y_i \tag{2.6}$$

where (x_i, y_i) are the coordinates of the corner points of the quadrilateral plate and N_i are isoparametric shape functions given as,

$$\begin{aligned} N_1(\xi,\eta) &= \frac{1}{4}(1-\xi)(1-\eta), \qquad & N_2(\xi,\eta) &= \frac{1}{4}(1+\xi)(1-\eta) \\ N_3(\xi,\eta) &= \frac{1}{4}(1+\xi)(1+\eta), \qquad & N_4(\xi,\eta) &= \frac{1}{4}(1-\xi)(1+\eta) \end{aligned} \tag{2.7}$$

Using Ritz method, the transverse deflection and rotations can be expressed as a function of transformed coordinates ξ and η,

$$\begin{aligned} w_0 &= \{\phi_{IJ}\}^T \{q_w\} = \sum_{i=0}^{I}\sum_{j=0}^{J} W_{ij}(t)\phi_i(\xi)\phi_j(\eta) \\ \beta_x &= \{\psi_{KL}\}^T \{q_x\} = \sum_{k=0}^{K}\sum_{l=0}^{L} X_{kl}(t)\psi_k(\xi)\psi_l(\eta) \\ \beta_y &= \{\psi_{MN}\}^T \{q_y\} = \sum_{m=0}^{M}\sum_{n=0}^{N} Y_{mn}(t)\psi_m(\xi)\psi_n(\eta) \end{aligned} \tag{2.8}$$

or in matrix form,

$$\{d_p\} = \begin{Bmatrix} w_0 \\ \beta_x \\ \beta_y \end{Bmatrix} = \begin{bmatrix} \{\phi_{IJ}\} & 0 & 0 \\ 0 & \{\psi_{KL}\} & 0 \\ 0 & 0 & \{\psi_{MN}\} \end{bmatrix} \begin{Bmatrix} q_w \\ q_x \\ q_y \end{Bmatrix} = [H_p]\{q_p\} \tag{2.9}$$

where *I, J, K, L, M, N* are integers; $\{d_p\}$ represents the displacement and rotation components of the plate; $\{q_p\}$ is time dependent Ritz coefficients vector; $\{\phi_{IJ}\}$, $\{\psi_{KL}\}$ and $\{\psi_{MN}\}$

are Ritz basis function vectors, which are expressed as,

$$\begin{aligned}
\{q_w\} &= \begin{bmatrix} W_{00} & W_{01} & \dots & W_{0J} & W_{10} \dots & W_{1J} & \dots & W_{IJ} \end{bmatrix}^T \\
\{q_x\} &= \begin{bmatrix} X_{00} & X_{01} & \dots & X_{0L} & X_{10} \dots & X_{1L} & \dots & X_{KL} \end{bmatrix}^T \\
\{q_y\} &= \begin{bmatrix} Y_{00} & Y_{01} & \dots & Y_{0N} & Y_{10} \dots & Y_{1N} & \dots & Y_{MN} \end{bmatrix}^T
\end{aligned} \tag{2.10}$$

and,

$$\begin{aligned}
\{\phi_{IJ}\} &= \begin{bmatrix} \phi_0(\xi)\phi_0(\eta) & \phi_0(\xi)\phi_1(\eta & \dots & \phi_I(\xi)\phi_J(\eta) \end{bmatrix}^T \\
\{\psi_{KL}\} &= \begin{bmatrix} \psi_0(\xi)\psi_0(\eta) & \psi_0(\xi)\psi_1(\eta & \dots & \psi_K(\xi)\psi_L(\eta) \end{bmatrix}^T \\
\{\psi_{MN}\} &= \begin{bmatrix} \psi_0(\xi)\psi_0(\eta) & \psi_0(\xi)\psi_1(\eta & \dots & \psi_M(\xi)\psi_N(\eta) \end{bmatrix}^T
\end{aligned} \tag{2.11}$$

in which $\phi_n(s)$, $\psi_n(s)$ can be chosen as,

$$\begin{aligned}
&\mu_n(s) = W(s) P_n^{(2e_q^{i+2}, 2e_q^i)}(s) \\
&W(s) = (1-s)^{e_q^{i+2}} (1+s)^{e_q^i} \\
&s = \xi, \eta; \quad \mu = \phi, \psi
\end{aligned} \tag{2.12}$$

where $P_n^{(\alpha,\beta)}(s)$ are Jacobi polynomials, which are orthogonal on the interval $[-1, 1]$ with respect to the weight function $W(s) = (1-s)^\alpha (1+s)^\beta$.

The Jacobi weight function, $(1-s)^{e_q^{i+2}}(1+s)^{e_q^i}$ in Eqn. (2.12), is used to enforce the boundary conditions. The exponents e_q^i take values corresponding to the boundary conditions along each edge. The subscript q refers to the displacement components, $d_p = \{w_0, \beta_x, \beta_y\}^T$ and the superscript i refers to the corresponding edge number, as illustrated in Figure 2.2. If the displacements or rotations are restrained for i^{th} edge, e_q^i takes value of one, otherwise zero.

The detailed expressions for different boundary conditions are presented in Supplement II (Table 2.10). The three term recursive formula for the Jacobi polynomials is given by:

$$\begin{aligned} 2n\, c_n\, c_{2n-2}\, P_n^{(\alpha,\beta)}(\xi) = c_{2n-1}\,(c_{2n-2}\, c_{2n}\, \xi + \alpha^2 - \beta^2)\, P_{n-1}^{(\alpha,\beta)}(\xi) \\ -2(n-1+\alpha)(n-1+\beta)\, c_{2n}\, P_{n-2}^{(\alpha,\beta)}(\xi) \end{aligned} \tag{2.13}$$

in which

$$c_n = n + \alpha + \beta$$

$$P_0^{(\alpha,\beta)}(t) = 1; \qquad P_1^{(\alpha,\beta)}(t) = \frac{\alpha-\beta}{2} + (1 + \frac{\alpha-\beta}{2})t$$

The derivative of Jacobi polynomials is given by [34]

$$\frac{\mathrm{d}}{\mathrm{d}t}\left[P_n^{(\alpha,\beta)}(t)\right] = \frac{1}{2}\,(n+\alpha+\beta+1)\, P_{n-1}^{(\alpha+1,\beta+1)}(t) \tag{2.14}$$

To associate the derivatives with respect to the global coordinates x and y, the chain rule can be implemented as [35]

$$\begin{Bmatrix} \dfrac{\partial}{\partial x} \\ \dfrac{\partial}{\partial y} \end{Bmatrix} = \left([J]^{-1}\right)^T \begin{Bmatrix} \dfrac{\partial}{\partial \xi} \\ \dfrac{\partial}{\partial \eta} \end{Bmatrix} = \begin{bmatrix} \bar{J}_{11} & \bar{J}_{21} \\ \bar{J}_{12} & \bar{J}_{22} \end{bmatrix} \begin{Bmatrix} \dfrac{\partial}{\partial \xi} \\ \dfrac{\partial}{\partial \eta} \end{Bmatrix} \tag{2.15}$$

where the inverse Jacobian matrix is

$$\left([J]^{-1}\right) = \begin{bmatrix} \dfrac{\partial x}{\partial \xi} & \dfrac{\partial x}{\partial \eta} \\ \dfrac{\partial y}{\partial \xi} & \dfrac{\partial y}{\partial \eta} \end{bmatrix}^{-1} = \begin{bmatrix} \bar{J}_{11} & \bar{J}_{12} \\ \bar{J}_{21} & \bar{J}_{22} \end{bmatrix} \tag{2.16}$$

From Eqns. (2.5) and (2.15), the plate strains can be writen in the following form,

$$\{\epsilon_p\} = \begin{Bmatrix} \epsilon_x \\ \epsilon_y \\ \gamma_{xy} \\ \gamma_{xz} \\ \gamma_{zx} \end{Bmatrix} = \begin{bmatrix} 0 & 0 & z\bar{J}_{11} & z\bar{J}_{21} & 0 & 0 & 0 & 0 \\ 0 & 0 & 0 & 0 & z\bar{J}_{12} & z\bar{J}_{22} & 0 & 0 \\ 0 & 0 & z\bar{J}_{12} & z\bar{J}_{22} & z\bar{J}_{11} & z\bar{J}_{21} & 0 & 0 \\ \bar{J}_{12} & \bar{J}_{22} & 0 & 0 & 0 & 0 & 0 & 1 \\ \bar{J}_{11} & \bar{J}_{21} & 0 & 0 & 0 & 0 & 1 & 0 \end{bmatrix} \{\bar{\epsilon}_p\} \tag{2.17}$$
$$= [L_p]\,\{\bar{\epsilon}_p\}$$

where $\{\bar{\epsilon}_p\}$ is

$$\{\bar{\epsilon}_p\} = \left\{ \frac{\partial w_0}{\partial \xi}, \frac{\partial w_0,}{\partial \eta}, \frac{\partial \beta_x}{\partial \xi}, \frac{\partial \beta_x,}{\partial \eta}, \frac{\partial \beta_y}{\partial \xi}, \frac{\partial \beta_y,}{\partial \eta}, \beta_x, \beta_y \right\}^T \tag{2.18}$$

or,

$$\{\bar{\epsilon}_p\} = [B_p]\,\{d_p\} \tag{2.19}$$

in which

$$[B_p] = \begin{bmatrix} [\phi_{IJ,\xi\eta}] & 0 & 0 \\ 0 & [\psi_{KL,\xi\eta}] & 0 \\ 0 & 0 & [\psi_{MN,\xi\eta}] \\ 0 & \{\psi_{KL}\} & 0 \\ 0 & 0 & \{\psi_{MN}\} \end{bmatrix} \tag{2.20}$$

where

$$
\begin{aligned}
[\phi_{IJ,\xi\eta}] &= \begin{bmatrix} \phi_0'(\xi)\phi_0(\eta) & \phi_0'(\xi)\phi_1(\eta) & \dots & \phi_I'(\xi)\phi_J(\eta) \\ \phi_0(\xi)\phi_1'(\eta) & \phi_0(\xi)\phi_1'(\eta) & \dots & \phi_I(\xi)\phi_J'(\eta) \end{bmatrix} \\
[\psi_{KL,\xi\eta}] &= \begin{bmatrix} \psi_0'(\xi)\psi_0(\eta) & \psi_0'(\xi)\psi_1(\eta) & \dots & \psi_K'(\xi)\psi_L(\eta) \\ \psi_0(\xi)\psi_0'(\eta) & \psi_0(\xi)\psi_1'(\eta) & \dots & \psi_K(\xi)\psi_L'(\eta) \end{bmatrix} \\
[\psi_{MN,\xi\eta}] &= \begin{bmatrix} \psi_0'(\xi)\psi_0(\eta) & \psi_0'(\xi)\psi_1(\eta) & \dots & \psi_M'(\xi)\psi_N(\eta) \\ \psi_0(\xi)\psi_0'(\eta) & \psi_0(\xi)\psi_1'(\eta) & \dots & \psi_M(\xi)\psi_N'(\eta) \end{bmatrix}
\end{aligned}
\tag{2.21}
$$

Substituting Eqns. (2.18) and (2.20) into Eqn. (2.1) gives,

$$
U_p = \frac{1}{2}\int_V \{q_p\}^T [B_p]^T [L_p]^T [E_p] [L_p] [B_p] \{q_p\} \, dV \tag{2.22}
$$

The strain energy of the plate also can be written in the following form

$$
U_p = \frac{1}{2}\{q_p\}^T [K_p] \{q_p\} \tag{2.23}
$$

The comparison of Eqns. (2.22) and (2.23) gives

$$
[K_p] = \int_{-1}^{1}\int_{-1}^{1}\int_{-h_p/2}^{h_p/2} [B_p]^T [L_p]^T [E_p] [L_p] [B_p] \, |J| \, \mathrm{d}z \, \mathrm{d}\xi \, \mathrm{d}\eta \tag{2.24}
$$

where $|J|$ is the determinant of the Jacobian matrix.

For plate mass matrix calculations, the velocity vector, $\{\dot{u}_p\}$, can be expressed as [35]

$$\{\dot{u}_p\} = \left\{\frac{\partial u_p}{\partial t}\right\} = \begin{Bmatrix} z\dfrac{\partial \beta_x}{\partial t} \\ z\dfrac{\partial \beta_y}{\partial t} \\ \dfrac{\partial w_0}{\partial t} \end{Bmatrix} = \begin{bmatrix} 0 & z & 0 \\ 0 & 0 & z \\ 1 & 0 & 0 \end{bmatrix} \begin{Bmatrix} \dfrac{\partial w_0}{\partial t} \\ \dfrac{\partial \beta_x}{\partial t} \\ \dfrac{\partial \beta_y}{\partial t} \end{Bmatrix} = [Z]\,[H_p]\,\{\dot{q}_p\} \tag{2.25}$$

Substituting Eqn. (2.25) into Eqn. (2.2) gives

$$T_p = \frac{1}{2}\int_V \rho\,\{\dot{q}_p\}^T\,[H_p]^T\,[ZZ]\,[H_p]\,\{\dot{q}_p\}\,dV \tag{2.26}$$

in which

$$[ZZ] = [Z]^T\,[Z] \begin{bmatrix} 1 & 0 & 0 \\ 0 & z^2 & 0 \\ 0 & 0 & z^2 \end{bmatrix} \tag{2.27}$$

The kinetic energy of the plate also can be written in the following form,

$$T_p = \frac{1}{2}\,\{\dot{q}\}^T\,[M]\,\{\dot{q}\} \tag{2.28}$$

The comparison of Eqns. (2.26) and (2.28) gives

$$[M_p] = \int_{-1}^{1}\int_{-1}^{1}\int_{-h_p/2}^{h_p/2} \rho\,[H_p]^T\,[ZZ]\,[H_p]\,|J|\,\mathrm{d}z\,\mathrm{d}\xi\,\mathrm{d}\eta \tag{2.29}$$

2.3.2 Formulation for the curvilinear stiffener

A curvilinear blade stiffener lying on quadrilateral plate of uniform height h_s, width b_s is also shown in Figure 2.1. The local coordinates are defined by t, n and b in tangential, normal, and binormal directions respectively, as shown in Figure 2.1. The stiffener coordinates can be represented by using B-spline parametric equation with knot vector of $[-1,-1,-1,1,1,1]$

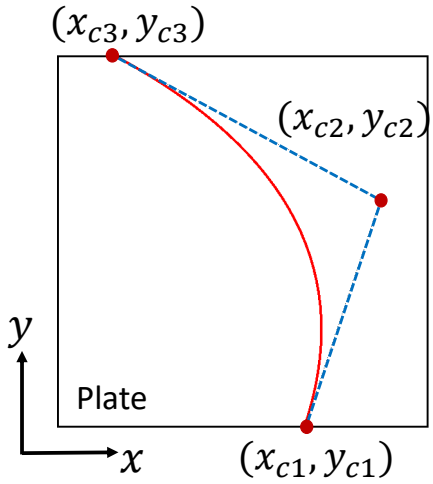

Figure 2.3: B-spline control points for stiffener definition

as

$$x_s = \sum_{i=1}^{3} N_i^s(\zeta)\, x_{ci}, \qquad y_s = \sum_{i=1}^{3} N_i^s(\zeta)\, y_{ci} \tag{2.30}$$

where x and y are global coordinates; the B-spline parameter, ζ, is ranging from -1 to 1; (xc_i, yc_i) are the control points of the stiffener, as shown Figure 2.3 and $N_i^s(\zeta)$ are b-spline shape functions given as,

$$\begin{aligned} N_1^s(\zeta) &= \frac{1}{4} - \frac{\zeta}{2} + \frac{\zeta^2}{4} \\ N_2^s(\zeta) &= \frac{1}{2} - \frac{\zeta^2}{2} \\ N_3^s(\zeta) &= \frac{1}{4} + \frac{\zeta}{2} + \frac{\zeta^2}{4} \end{aligned} \tag{2.31}$$

The curve length Γ can be defined as [36]

$$\Gamma = \int_{-1}^{1} |J_s|\, d\zeta \tag{2.32}$$

2.3. Formulation for stiffened plates

The stiffener strain energy, U_s, and the kinetic energy, T_s, can be written as

$$U_s = \frac{1}{2}\int_\Gamma \{\epsilon_s\}^T [D_s] \{\epsilon_s\} \, d\Gamma \tag{2.33}$$

$$T_p = \frac{1}{2}\int_\Gamma \{\dot{u}_s\}^T [m_s] \{\dot{u}_s\} \, d\Gamma \tag{2.34}$$

The strain-displacement relation of the stiffener is assumed as [11]

$$\{\epsilon_s\} = \begin{Bmatrix} \gamma_b \\ \kappa_t \\ \kappa_n \end{Bmatrix} = \begin{bmatrix} \frac{1}{|J_s|}\frac{\mathrm{d}}{\mathrm{d}\zeta} & 1 & 0 \\ 0 & \frac{1}{|J_s|}\frac{\mathrm{d}}{\mathrm{d}\zeta} & \frac{1}{R} \\ 0 & -\frac{1}{R} & \frac{1}{|J_s|}\frac{\mathrm{d}}{\mathrm{d}\zeta} \end{bmatrix} \begin{Bmatrix} w_b \\ \beta_t \\ \beta_n \end{Bmatrix} = [L_s] \{d_s\} \tag{2.35}$$

where the curvature $1/R$, the determinant of Jacobian matrix for the curved beam, $|J_s|$, are defined in [36] as

$$\frac{1}{R} = \left(\frac{\mathrm{d}x_s}{\mathrm{d}\zeta}\frac{\mathrm{d}^2 y_s}{\mathrm{d}\zeta^2} - \frac{\mathrm{d}y_s}{\mathrm{d}\zeta}\frac{\mathrm{d}^2 x_s}{\mathrm{d}\zeta^2}\right) \Big/ \left(|J_s|\right)^3 \tag{2.36}$$

$$|J_s| = \sqrt{\left(\frac{\mathrm{d}x_s}{\mathrm{d}\zeta}\right)^2 + \left(\frac{\mathrm{d}y_s}{\mathrm{d}\zeta}\right)^2} \tag{2.37}$$

The stiffener material and mass property matrices are given by

$$\{D_s\} = \begin{bmatrix} G_s A_s \kappa & 0 & 0 \\ 0 & E_s I_n & 0 \\ 0 & 0 & G_s J_t \end{bmatrix}, \quad [m_s] = \rho_s \begin{bmatrix} A_s & 0 & 0 \\ 0 & I_n & 0 \\ 0 & 0 & I_n + I_b \end{bmatrix} \tag{2.38}$$

where E_s, G_s, ρ_s and $A_s = b_s h_s$ are the Young's modulus, shear modulus, density and cross-sectional area of the stiffener, respectively; $J_t \approx (1/3) h_s b_s^3$ is the torsional constant of the stiffer; $I_n = (1/12) b_s h_s^3 + e^2 A_s$ and $I_b = (1/12) b_s^3 h_s$ are the second moment of inertia about n

and b axes, respectively and $e = 1/2(h_p + h_s)$ is the stiffener eccentricity measured between the stiffener neutral line and the plate middle plane. For concentrically stiffened plate, the stiffener neutral line coincides with the plate middle plane and e takes the value of zero.

By assuming stiffener rotations β_t and β_n are infinitesimal, displacement components of the stiffener, $\{d_s\}$ can be related to those of the plate with the help of the relevant direction cosine matrix, $[\Lambda_s]$, as follows

$$\{d_s\} = \begin{Bmatrix} w_b \\ \beta_t \\ \beta_n \end{Bmatrix} = \begin{bmatrix} 1 & 0 & 0 \\ 0 & n_x & n_y \\ 0 & -n_y & n_x \end{bmatrix} \begin{Bmatrix} w_0 \\ \beta_x \\ \beta_y \end{Bmatrix} = [\Lambda_s]\{d_p\} \tag{2.39}$$

where

$$n_x = cos(\alpha) = \frac{x_s'}{|J_s|}, \qquad n_y = sin(\alpha) = \frac{y_s'}{|J_s|} \tag{2.40}$$

where α is the angle between the stiffener tangential direction t and x axis of the global coordinate system and the prime $'$ represents the differential operator of $d()/d\zeta$. The α values are calculated at each Gauss point while evaluating the integrals in the Ritz solution.

Substituting Eqn. (2.39) into Eqn. (2.35) gives $\{\epsilon_s\}$ in terms of global coordinates

$$\{\epsilon_s\} = [L_s][\Lambda_s]\{d_p\} \tag{2.41}$$

By using Eqn. (2.40) and chain rule, the diagonal terms of $[L_s]$ matrix defined in Eqn. (2.35) can be expressed as;

$$\frac{1}{|J_s|}\frac{\mathrm{d}}{\mathrm{d}\zeta} = \left(\frac{1}{|J_s|}\frac{\mathrm{dx}}{\mathrm{d}\zeta}\right)\frac{\partial}{\partial x} + \left(\frac{1}{|J_s|}\frac{\mathrm{dy}}{\mathrm{d}\zeta}\right)\frac{\partial}{\partial y} = n_x\frac{\partial}{\partial x} + n_y\frac{\partial}{\partial y} \tag{2.42}$$

Since the Ritz trial functions are in defined in natural coordinates ξ and η, the derivatives

with respect to the global coordinates x and y in Eqn. (2.42) are needed to be related to those with respect to natural coordinates ξ and η by using Eqn. (2.15). From Eqns. (2.41), (2.40), and (2.15), the stiffener strains can be expressed as

$$\{\epsilon_s\} = [T_J]\,\{\bar{\epsilon}_p\} \tag{2.43}$$

where $\{\bar{\epsilon}_p\}$ is given in Eqn. (2.19), and

$$[T_J] = \begin{bmatrix} t_{11} & t_{12} & 0 & 0 & 0 & 0 & t_{17} & t_{18} \\ 0 & 0 & t_{23} & t_{24} & t_{25} & t_{26} & t_{27} & t_{28} \\ 0 & 0 & -t_{25} & -t_{26} & t_{23} & t_{24} & -t_{28} & t_{27} \end{bmatrix} \tag{2.44}$$

in which

$$\begin{aligned} t_{11} &= \bar{J}_{11}n_x + \bar{J}_{12}n_y, & t_{12} &= \bar{J}_{21}n_x + \bar{J}_{22}n_y, \\ t_{23} &= \bar{J}_{11}n_x^2 + \bar{J}_{12}n_xn_y, & t_{24} &= \bar{J}_{21}n_x^2 + \bar{J}_{22}n_xn_y, \\ t_{25} &= \bar{J}_{12}n_y^2 + \bar{J}_{11}n_xn_y, & t_{26} &= \bar{J}_{22}n_y^2 + \bar{J}_{21}n_xn_y, \\ t_{17} &= n_x, & t_{18} &= n_y, \\ t_{27} &= -n_y/R, & t_{28} &= n_x/R \end{aligned} \tag{2.45}$$

Substituting Eqns. (2.43) and (2.19) into Eqn. (2.33), then considering Eqn. (2.32) for integration by substitution, the stiffness matrix for the stiffener can be derived as

$$[K_s] = \int_{-1}^{1} [B_p]^T\,[T_J]^T\,[D_s]\,[T_J]\,[B_p]\,|J_s|\,\mathrm{d}\zeta \tag{2.46}$$

Similarly, using Eqns. (2.34), (2.9) and the direction cosine matrix, the mass matrix of

stiffener can be written as

$$[M_s] = \int_{-1}^{1} [H_p]^T [\Lambda_s]^T [m_s] [\Lambda_s] [H_p] |J_s| \, \mathrm{d}\zeta \tag{2.47}$$

After employing Hamilton's principle, the natural frequencies of the stiffened plate can be obtained the eigenvalue problem in following form

$$\left[(K_p + K_s) - \omega^2 (M_p + M_s) \right] \{q\} = 0 \tag{2.48}$$

The required integral evaluations are performed by using Gauss quadrature. Since the Ritz functions can contain higher-order Jacobi polynomials, a high-order Gauss quadrature scheme, provided by Hale and Townsend [37], is implemented. This numerical quadrature is seen to be very efficient despite the fact that tensor product of Jacobi polynomials up to 30×30 were used here.

2.4 Results and Discussion

In this section, the methodology explained in the previous section is applied on numerous case studies considering various plates and stiffener shapes and size parameters with different sets of boundary conditions. First, the accuracy of the present method and the generated FEA models are validated by comparing with Liew et al. results [21]. Then, for some new cases, accuracy assessments are carried out by comparing the results obtained from the present approach with those from the FEM. Parametric studies are also presented in order to study the effect of the number of terms used on the accuracy of the higher modes frequencies. For the FEM modeling, MSC.NASTRAN is used for conducting the free vibration analysis. The mesh size in the FEM model is taken to be very refined, around $10,000$ CTRIA3 shell

elements for plate modeling and 150 CBAR beam elements for a single stiffener, is used in the MSC.NASTRAN. In addition to the frequencies, the mode shapes obtained using the present method and those found by the FEM are compared in Supplement I. In the mode shape figures, the red color represents the absolute maximum deflection, and the blue color the undeformed state. Note: In this study and the paper by Liew et al. [21], eccentric stiffeners are considered with ignoring in-plane displacements at the plate mid-plane. Due to this reason, the height of the stiffener to the plate height ratio (h_s/h_p) is limited to be below 4.

The case studies can be categorized as follows:

a) Straight Stiffeners on Rectangular Plate

b) Curvilinear Stiffeners on Rectangular Plate

c) Curvilinear Stiffeners on Quadrilateral Plate

2.4.1 Straight Stiffeners on Rectangular Plate

Validation studies are performed on the SSSS and CCCC rectangular plates with one central longitudinal and two orthogonal stiffeners as shown in Figures 2.4 and 2.5. In the figures, a and b denotes the width and height of the rectangular plates. The coordinates of the control points for the stiffeners are also shown in the figure. Letters "S" and "C" represent simply supported and clamped boundary conditions, respectively. In Table 2.1, the frequency parameters are obtained by setting $I, J, K, L, M, N = 14$ (Degree Set). It can be seen from the Table 2.1 that a good agreement is observed in the frequency parameters for both cases. In Table 2.2, convergence studies are presented for the case of two orthogonal stiffeners. It is known that, in order to observe the accuracy of the higher mode approximation, higher number polynomial terms or degree set are required. However, with the use of the simple

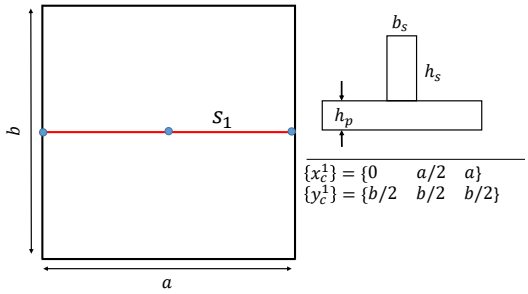

Figure 2.4: Rectangular plate with one central longitudinal stiffener

polynomials as Ritz trial functions, the ill-conditioning issues do not allow the use of higher number of terms in the trial functions. As mentioned earlier, the key advantage of the Jacobi polynomials is that they allow the use of higher number of terms in Ritz trial functions to approximate the frequency parameters closely to the detailed FEM results. It can be seen from the Table 2.2 that for higher modes like, 30^{th}, 40^{th} and 50^{th} mode, using a small degree set can result in significant error. But, after using enough degree set of about 20 or 30, close approximation can be achieved without facing any ill-conditioning issues.

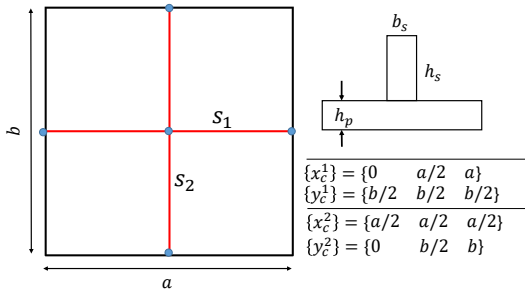

Figure 2.5: Rectangular plate with two orthogonal stiffeners

Finally, a third configuration is studied in this case study with arbitrary straight stiffeners on a rectangular plate as shown in Figure 2.6. Table 2.3 presents the convergence of the frequency parameters regarding various degree sets and comparison with the FEM. It has been seen that upto 20 modes, even the degree set of 12 is sufficient to provide upper bound values of the frequency parameters. However, for higher modes, the accuracy of the solution

Table 2.1: Comparison studies of frequency parameters ($\lambda = (\omega b^2\pi^2)\sqrt{\rho t/D}$) of rectangular plate with straight stiffeners

	(a)			(b)		
Mode	Present	Liew	FEM	Present	Liew	FEM
(i) Two Orthogonal Stiffeners						
1	2.1977	2.2017	2.1924	4.3659	4.3664	4.3046
2	5.7090	5.7167	5.6577	8.7209	8.7274	8.5669
3	5.7090	5.7167	5.6577	8.7209	8.7274	8.5680
4	8.0313	8.0552	8.0141	11.0108	11.0143	10.9957
5	11.1759	11.1909	11.0717	14.8659	14.8754	14.7034
6	11.6680	11.6785	11.4491	16.2267	16.2504	15.6911
(ii) One longitudinal Stiffener						
1	2.1014	2.1057	2.0978	4.0282	4.0285	3.9928
2	5.0002	5.009	4.9949	7.4362	7.4374	7.4320
3	5.6980	5.7049	5.6499	8.7084	8.7109	8.5581
4	7.9996	8.0219	7.9880	10.9713	10.9732	10.9614
5	9.8573	9.8659	9.8566	13.2368	13.2374	13.2299
6	11.5041	11.5174	11.3592	15.4924	15.5071	15.2127

Note: $a/b = 1, h_p/b = 0.01, h_s/h_p = 1.5, b_s/b = 0.01$
Boundary Conditions: (a) SSSS (b) CCCC

is dramatically influenced with the used degree set.

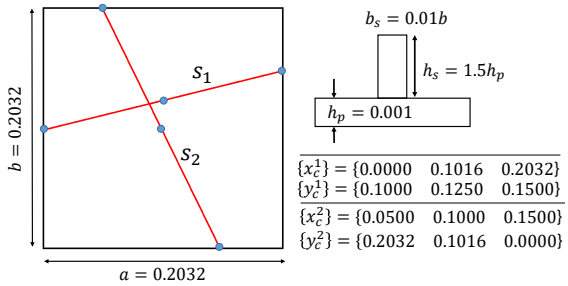

Figure 2.6: Rectangular plate with two arbitrary straight stiffeners

2.4.2 Curvilinear Stiffeners on Rectangular Plate

In this case study, different configurations of curvilinear stiffeners are considered on rectangular plates. First, two configurations are studied with one curvilinear stiffener and then,

Table 2.2: Convergence studies of frequency parameters of two orthogonal stiffeners ($\lambda = (\omega b^2\pi^2)\sqrt{\rho t/D}$)

Mode	Degree Set					FEM
	10	12	14	20	30	
(i) $a/b = 1$; CCCC Plate						
5	14.8871	14.8732	14.8659	14.8546	14.8470	14.7034
10	24.0469	23.9997	23.9752	23.9394	23.9177	23.6314
20	37.5558	37.5527	37.5524	37.5513	37.5500	37.5313
25	47.8065	46.1890	46.0850	46.0818	46.0813	46.0624
30	60.1564	58.0761	57.7339	57.4510	57.2996	56.2376
40	81.7347	73.7331	72.4430	72.3762	72.3572	71.9586
50	122.8050	94.5363	88.3756	87.4831	87.2772	86.3727
(ii) $a/b = 3$; SSSS Plate						
5	5.5719	5.5437	5.5427	5.5409	5.5395	5.4627
10	7.8704	7.8700	7.8699	7.8699	7.8698	7.8572
20	16.2130	13.8269	13.7502	13.7001	13.6815	13.5355
25	20.5850	18.7351	18.4553	16.1101	16.1087	16.0330
30	25.2907	21.8783	20.5680	19.6607	19.6565	19.5217
40	39.2524	31.3282	27.5035	24.4850	24.0967	23.9050
50	51.8998	42.3902	37.6786	30.8533	30.0939	30.0136
Note: $h_p/b = 0.01, h_s/b = 1.5, b_s/b = 0.01$						

with a two-stiffener configuration. For these configurations, different values of aspect ratio (a/b) and stiffener-to-plate height ratio (h_s/h_p) are considered. A rectangular plate with one curvilinear stiffener, in Figures 2.7 and 2.8, and with two curvilinear stiffeners, in Figures 2.9 and 2.10, are shown along with the details of the geometric dimensions. Tables 2.4 to 2.7 present the comparison and convergence studies for the various case studies. A similar trend has been observed as in previous section. The present results are in close agreement with the FEM results for both lower and higher modes when enough polynomial terms are used in the Ritz trial function.

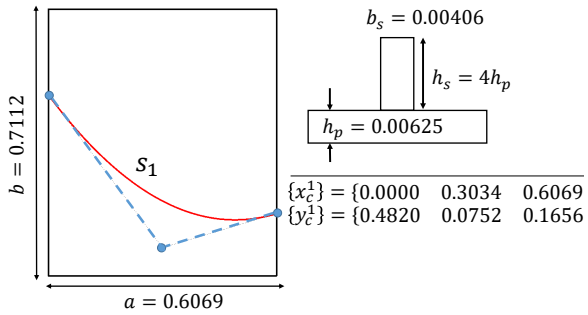

Figure 2.7: Rectangular plate with one curvilinear stiffener

Table 2.3: Comparison and convergence studies of frequency parameters of SSSS rectangular plate with two arbitrary straight stiffeners ($\lambda = (\omega b^2\pi^2)\sqrt{\rho t/D}$)

Mode	Degree Set					FEM
	10	12	14	20	30	
1	2.1849	2.1823	2.1804	2.1763	2.1742	2.1439
2	5.4015	5.3976	5.3946	5.3887	5.3856	5.3957
3	5.7666	5.7592	5.7546	5.7461	5.7413	5.6415
4	8.5567	8.5448	8.5366	8.5209	8.5132	8.4405
5	10.6970	10.6860	10.6791	10.6675	10.6606	10.7243
6	11.5341	11.5169	11.5088	11.4932	11.4836	11.2615
10	18.9547	18.9054	18.8719	18.8369	18.8179	18.5027
20	34.0538	33.6025	33.5134	33.4190	33.3813	32.9741
30	53.5544	49.7157	48.8328	48.4307	48.3309	47.5471
50	196.0236	89.8407	77.6551	75.4999	75.3167	74.9273

2.4.3 Curvilinear Stiffeners on Quadrilateral Plate

Lastly, in a first study of its kind, the curvilinear stiffeners are considered for a quadrilateral plate. The geometric dimensions including the corners' coordinates and control points of the stiffener are presented in the Figures 2.11 and 2.12. For both the cases, the Young's modulus $= 73\ GPa$, Poisson's ratio $= 0.33$ and density, $\rho = 2837\ kg/m^3$ are used for both the stiffener and the plate. As can be seen from Tables 2.8 and 2.9, that for the quadrilateral plates with curvilinear stiffeners, the present method can accurately evaluate the natural frequencies of higher modes.

Table 2.4: Comparison and convergence studies of frequency parameters ($\lambda = (\omega b^2\pi^2)\sqrt{\rho t/D}$) of SSSS rectangular plate ($a = 0.6069$, $b = 0.7112$) with one curvilinear stiffener

Mode	Degree Set				FEM
	10	14	20	30	
1	2.9742	2.9663	2.9598	2.9555	3.0234
2	5.8591	5.8414	5.8299	5.8223	5.7373
3	8.1144	8.0821	8.0622	8.0481	8.0388
4	10.4278	10.4131	10.4021	10.3955	10.3801
5	12.9719	12.8240	12.7611	12.7182	12.3811
6	14.4428	14.3865	14.3568	14.3384	14.2097
10	22.1465	22.0342	21.9857	21.9575	21.8093
20	42.0893	39.2775	39.1606	39.1020	38.8375
30	65.7954	58.6047	58.2636	58.1702	56.9711
50	204.3775	95.4173	90.2137	89.7746	88.7575

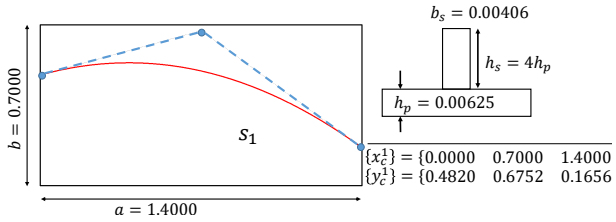

Figure 2.8: Rectangular plate with one curvilinear stiffener

2.5 Conclusion

In this paper, a method capable of solving vibration problem of curvilinearly stiffened rectangular and quadrilateral plates with various boundary conditions and geometric dimensions is developed. The displacement and rotations of the plate and stiffener are approximated by sets of Jacobi polynomials. The results are verified with the results available in open literature and by a detailed FEM using commercial software MSC.NASTRAN. Convergence studies are presented for studying the effect of the number of terms used on the accuracy of the solutions. The Jacobi Polynomials, with upto 30 degree set in each of the two directions for both plate and stiffeners, are used for the vibration analysis. It is observed in

Table 2.5: Comparison and convergence studies of frequency parameters ($\lambda = (\omega b^2\pi^2)\sqrt{\rho t/D}$) of CCCC rectangular plate ($a = 1.4,\ b = 0.7$) with one curvilinear stiffener

Mode	Degree Set				FEM
	10	14	20	30	
1	2.6698	2.6705	2.6699	2.6702	2.6233
2	3.8781	3.8791	3.8800	3.8840	3.8121
3	5.6136	5.6124	5.6231	5.6327	5.5719
4	6.5869	6.5841	6.5863	6.5876	6.5137
5	7.2931	7.2883	7.2904	7.2918	7.2380
6	8.4359	8.4141	8.4605	8.4845	8.3200
10	12.4861	12.4802	12.4806	12.4825	12.4223
20	22.1551	21.2173	21.1669	21.1803	20.9607
30	33.5219	30.1122	29.4891	29.5401	29.4406
50	69.2861	48.1187	43.5896	43.4355	43.1581

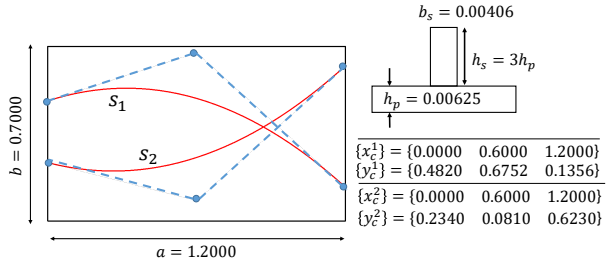

Figure 2.9: Rectangular plate with two curvilinear stiffeners

this study that unlike the simple polynomials [30], Jacobi polynomials do not possess any ill-conditioning issues in the authors' knowledge. A trend observed in the conducted studies suggests that to obtain natural frequencies for higher modes, a higher number of degree set is required in the Ritz trial function to achieve acceptable accuracy. Accurate and efficient integration of stiffness and mass coefficients is of great importance.

Table 2.6: Comparison and convergence studies of frequency parameters ($\lambda = (\omega b^2\pi^2)\sqrt{\rho t/D}$) of CCCC rectangular plate ($a = 1.2,\ b = 0.7$) with two curvilinear stiffeners

Mode	Degree Set				FEM
	10	14	20	30	
1	2.8593	2.8617	2.8591	2.8610	2.8150
2	4.6845	4.6960	4.6980	4.6954	4.6275
3	6.7506	6.7521	6.7550	6.7551	6.7213
4	7.6601	7.6110	7.6268	7.6620	7.5180
5	8.5826	8.5723	8.5967	8.5717	8.5840
6	11.0457	11.0177	11.0233	11.1118	10.9436
10	14.9698	14.9135	14.9384	14.9585	14.8710
20	25.7811	24.4272	24.3366	24.3917	24.2199
30	38.9245	33.9505	33.6428	33.6663	33.7785
50	74.7159	55.6277	51.8033	51.8313	51.8340

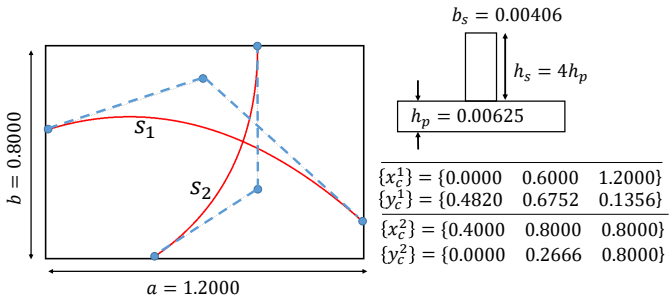

Figure 2.10: Rectangular plate with two curvilinear stiffeners

Table 2.7: Comparison and convergence studies of frequency parameters ($\lambda = (\omega b^2\pi^2)\sqrt{\rho t/D}$) of CCCC rectangular plate ($a = 1.2,\ b = 0.8$) with two curvilinear stiffeners

Mode	Degree Set				FEM
	10	14	20	30	
1	3.9674	3.9595	3.9572	3.9530	3.8041
2	6.1403	6.1064	6.1116	6.1138	5.9464
3	7.9872	7.9727	7.9722	7.9726	7.8741
4	9.5536	9.4564	9.4426	9.4358	9.0796
5	10.8060	10.7855	10.7656	10.7691	10.3538
6	12.4484	12.3775	12.3543	12.3491	12.0385
10	17.6465	17.5692	17.5607	17.5919	17.0975
20	30.1854	28.9819	28.7996	28.7458	28.1215
30	45.2707	40.2101	39.6440	39.8104	39.1728
50	87.6983	63.6027	60.2569	60.4463	59.7240

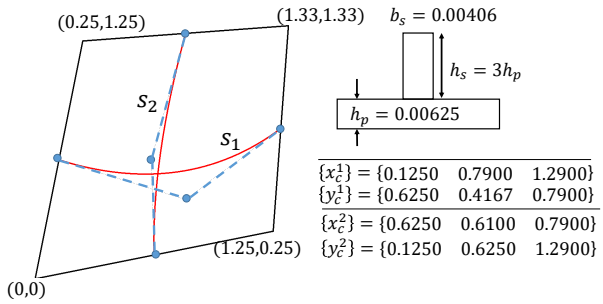

Figure 2.11: Quadrilateral plate with two curvilinear stiffeners (Case 1)

Table 2.8: Comparison and convergence studies of frequencies $[Hz]$ of CCCC quadrilateral plate with two curvilinear stiffeners (Case 1)

Mode	Degree Set				FEM
	10	14	20	30	
1	56.2199	56.1880	56.1656	56.1455	55.2868
2	106.1105	105.9447	105.8564	105.7950	104.0111
3	113.2358	113.0436	112.9463	112.8821	111.2852
4	139.5444	139.2810	139.1568	139.0870	137.1643
5	182.5730	182.3579	182.2457	182.1855	180.4298
6	187.2533	186.9154	186.7541	186.6701	184.8294
10	278.3449	277.3300	276.9289	276.7287	273.8292
20	492.5750	478.6192	476.7769	475.9567	469.2426
30	712.2670	663.5038	659.6955	658.4916	649.7203
50	1514.1801	1040.3537	1008.8254	1005.7611	994.5147

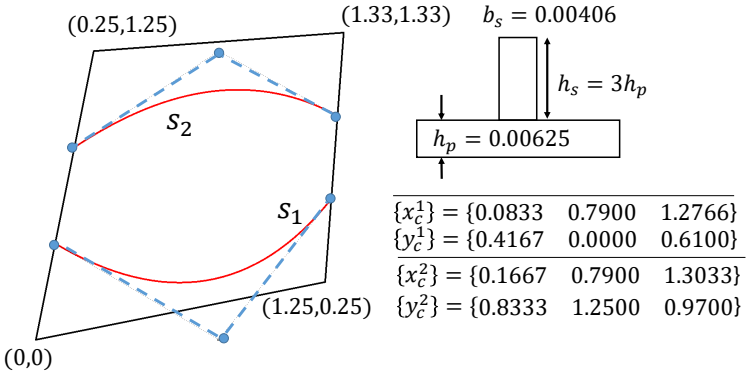

Figure 2.12: Quadrilateral plate with two curvilinear stiffeners (Case 2)

Table 2.9: Comparison and convergence studies of frequencies $[Hz]$ of CCCC quadrilateral plate with two curvilinear stiffeners (case 2)

Mode	Degree Set				FEM
	10	14	20	30	
1	46.49711	46.48868	46.478	46.47036	46.21285
2	88.15556	88.12435	88.09127	88.07212	87.58268
3	101.1748	101.1351	101.1051	101.0834	100.2853
4	141.6271	141.527	141.4275	141.363	139.8992
5	162.3894	162.3014	162.2462	162.2139	161.4215
6	176.6936	176.5759	176.4984	176.4456	174.9143
10	272.9932	272.7353	272.591	272.5001	270.1629
20	487.6229	470.9395	470.2213	469.8319	464.1293
30	699.5724	665.4078	663.7512	663.5902	660.9457
50	1510.363	1052.313	1028.866	1027.306	1015.549

Bibliography

[1] Xie, K., Chen, M., and Li, Z., 2017, "Free and Forced Vibration Analysis of Ring-Stiffened Conical–Cylindrical–Spherical Shells Through a Semi-Analytic Method," Journal of Vibration and Acoustics, **139**(3).

[2] Locatelli, D., Mulani, S. B., and Kapania, R. K., 2011, "Wing-box Weight Optimization Using Curvilinear Spars and Ribs (SpaRibs)," Journal of Aircraft, **48**(5), pp. 1671–1684.

[3] Doherty, C. G., Southward, S. C., and Hull, A. J., 2018, "Elastic Response of Acoustic Coating on Fluid-Loaded Rib-Stiffened Cylindrical Shells," Journal of Vibration and Acoustics, **141**(1).

[4] Locatelli, D., 2012, "Optimization of supersonic aircraft wing-box using curvilinear SpaRibs," PhD Thesis, Virginia Tech, Blacksburg, VA.

[5] Kapania, R. K., Li, J., and Kapoor, H., 2005, "Optimal design of unitized panels with curvilinear stiffeners," *AIAA 5th ATIO and16th Lighter-Than-Air Sys Tech. and Balloon Systems Conferences*, p. 7482.

[6] Zhao, W. and Kapania, R. K., 2018, "BLP Optimization of Composite Flying-wings with SpaRibs and Multiple Control Surfaces," *2018 AIAA/ASCE/AHS/ASC Structures, Structural Dynamics, and Materials Conference*, p. 2150.

BIBLIOGRAPHY

[7] Zhao, W., 2017, "Optimal Design and Analysis of Bio-inspired, Curvilinearly Stiffened Composite Flexible Wings," PhD Thesis, Virginia Tech, Blacksburg, VA.

[8] Liu, Q., Jrad, M., Mulani, S. B., and Kapania, R. K., 2016, "Global/local optimization of aircraft wing using parallel processing," AIAA Journal, pp. 3338–3348.

[9] Shi, P., Kapania, R. K., and Dong, C., 2015, "Vibration and buckling analysis of curvilinearly stiffened plates using finite element method," AIAA Journal, **53**(5), pp. 1319–1335.

[10] Shi, P., Kapania, R. K., and Dong, C., 2015, "Free vibration of curvilinearly stiffened shallow shells," Journal of Vibration and Acoustics, **137**(3), pp. 031006–031006–1515.

[11] Zhao, W. and Kapania, R. K., 2016, "Vibration Analysis of Curvilinearly Stiffened Composite Panel Subjected to In-Plane Loads," AIAA Journal, **55**(3), pp. 981–997.

[12] Zhao, W. and Kapania, R. K., 2016, "Buckling analysis of unitized curvilinearly stiffened composite panels," Composite Structures, **135**, pp. 365–382.

[13] Singh, K., Zhao, W., and Kapania, R. K., 2017, "Optimal Design of Curvilinearly Stiffened Shells," *58th AIAA/ASCE/AHS/ASC Structures, Structural Dynamics, and Materials Conference, AIAA SciTech Forum, (AIAA 2017-1830).*

[14] Singh, K., Zhao, W., and Kapania, R. K., 2017, "An Optimization Framework for Curvilinearly Stiffened Composite Pressure Vessels and Pipes," *ASME 2017 Pressure Vessels and Piping Conference*, Vol. 3A: Design and Analysis, p. V03AT03A066.

[15] Singh, K. and Kapania, R. K., 2018, "Optimal Design of Tow-Steered Composite Laminates with Curvilinear Stiffeners," *2018 AIAA/ASCE/AHS/ASC Structures, Structural Dynamics, and Materials Conference, AIAA SciTech Forum, (AIAA 2018-2243).*

BIBLIOGRAPHY

[16] Tamijani, A. Y. and Kapania, R. K., 2012, "Chebyshev-ritz approach to buckling and vibration of curvilinearly stiffened plate," AIAA Journal, **50**(5), pp. 1007–1018.

[17] Tamijani, A. Y., McQuigg, T., and Kapania, R. K., 2010, "Free vibration analysis of curvilinear-stiffened plates and experimental validation," Journal of Aircraft, **47**(1), pp. 192–200.

[18] Tamijani, A. Y. and Kapania, R. K., 2010, "Vibration of plate with curvilinear stiffeners using mesh-free method," AIAA Journal, **48**(8), pp. 1569–1581.

[19] Tamijani, A. Y. and Kapania, R. K., 2010, "Buckling and static analysis of curvilinearly stiffened plates using mesh-free method," AIAA Journal, **48**(12), pp. 2739–2751.

[20] Liew, K. and Wang, C., 1993, "pb-2 Rayleigh-Ritz method for general plate analysis," Engineering structures, **15**(1), pp. 55–60.

[21] Liew, K., Xiang, Y., Kitipornchai, S., and Lim, M., 1994, "Vibration of rectangular Mindlin plates with intermediate stiffeners," Journal of Vibration and Acoustics, **116**(4), pp. 529–535.

[22] Liew, K. and Wang, C., 1992, "Vibration analysis of plates by the pb-2 Rayleigh-Ritz method: mixed boundary conditions, reentrant corners, and internal curved supports," Journal of Structural Mechanics, **20**(3), pp. 281–292.

[23] Fletcher, C. A. J., 1984, "Traditional Galerkin Methods," *Computational Galerkin Methods*, Springer, pp. 1–71.

[24] Bhat, R., 1985, "Natural frequencies of rectangular plates using characteristic orthogonal polynomials in Rayleigh-Ritz method," Journal of Sound and Vibration, **102**(4), pp. 493–499.

BIBLIOGRAPHY

[25] Bhat, R., 1987, "Flexural vibration of polygonal plates using characteristic orthogonal polynomials in two variables," Journal of Sound and Vibration, **114**(1), pp. 65–71.

[26] Bhat, R. B., 2015, "Vibration of beams using novel boundary characteristic orthogonal polynomials satisfying all boundary conditions," Advances in Mechanical Engineering, **7**(4), p. 1687814015578355.

[27] Kapania, R. K. and Singhvi, S., 1992, "Free vibration analyses of generally laminated tapered skew plates," Composites Engineering, **2**(3), pp. 197–212.

[28] Kapania, R. K. and Lovejoy, A. E., 1996, "Free vibration of thick generally laminated cantilever quadrilateral plates." AIAA Journal, **34**(7), pp. 1474–1486.

[29] Kapania, R. K. and Lovejoy, A. E., 1998, "Free vibration of thick generally laminated quadrilateral plates having arbitrarily located point supports," Journal of Aircraft, **35**(6), pp. 958–965.

[30] Alanbay, B. and Kapania, R. K., 2018, "On the Use of Classical Jacobi Orthogonal Polynomials in the Ritz Method," *2018 AIAA/ASCE/AHS/ASC Structures, Structural Dynamics, and Materials Conference*, p. 1225.

[31] Caruntu, D. I., 2007, "Classical Jacobi polynomials, closed-form solutions for transverse vibrations," Journal of Sound and Vibration, **306**(3-5), pp. 467–494.

[32] Ditkowski, A. and Kats, R., 2016, "On Spectral Approximations With Nonstandard Weight Functions and Their Implementations to Generalized Chaos Expansions," arXiv preprint arXiv:1611.00242.

[33] Kitipornchai, S., Liew, K., Xiang, Y., and Wang, C., 1993, "Free vibration of isosceles triangular Mindlin plates," International journal of mechanical sciences, **35**(2), pp. 89–102.

BIBLIOGRAPHY

[34] Szego, G., 1967, *Orthogonal Polynomials: 3d Ed*, American Mathematical Society.

[35] Kapania, R. K. and Liu, Y., 2000, "Static and vibration analyses of general wing structures using equivalent-plate models," AIAA Journal, **38**(7), pp. 1269–1277.

[36] Martini, L. and Vitaliani, R., 1988, "On the polynomial convergent formulation of a C0 isoparametric skew beam element," Computers & Structures, **29**(3), pp. 437–449.

[37] Hale, N. and Townsend, A., 2013, "Fast and accurate computation of Gauss–Legendre and Gauss–Jacobi quadrature nodes and weights," SIAM Journal on Scientific Computing, **35**(2), pp. A652–A674.

Supplement I: Mode Shape Plots

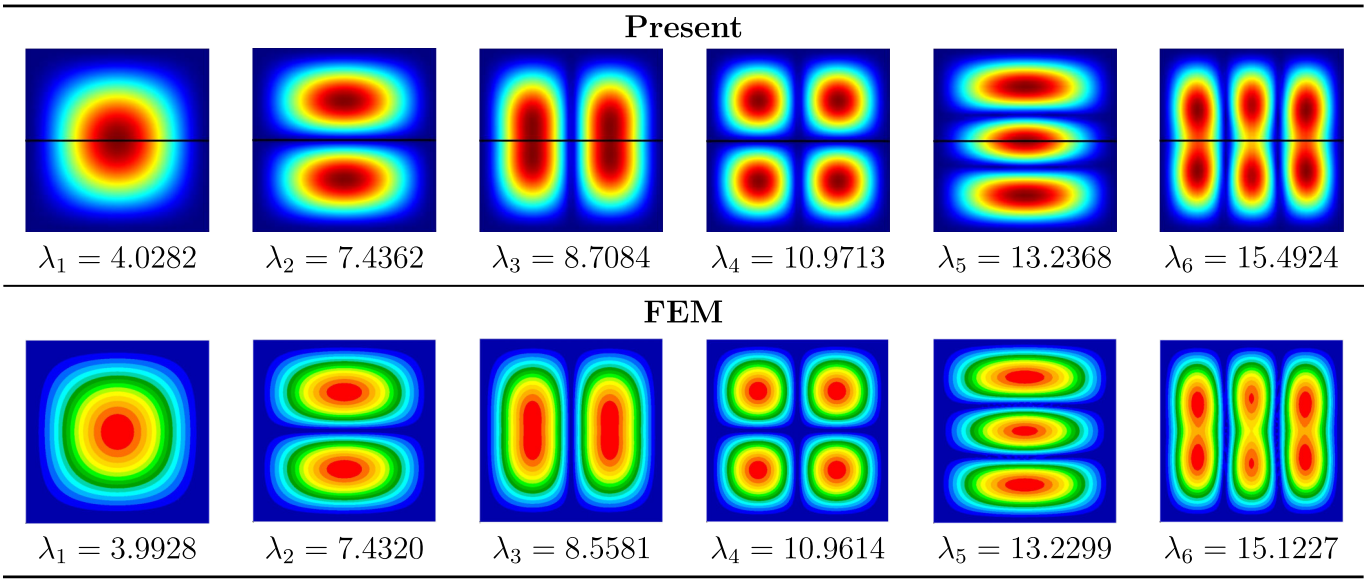

Figure 2.13: Comparison of mode shapes of CCCC rectangular plate with one central longitudinal stiffener (See Table 2.1)

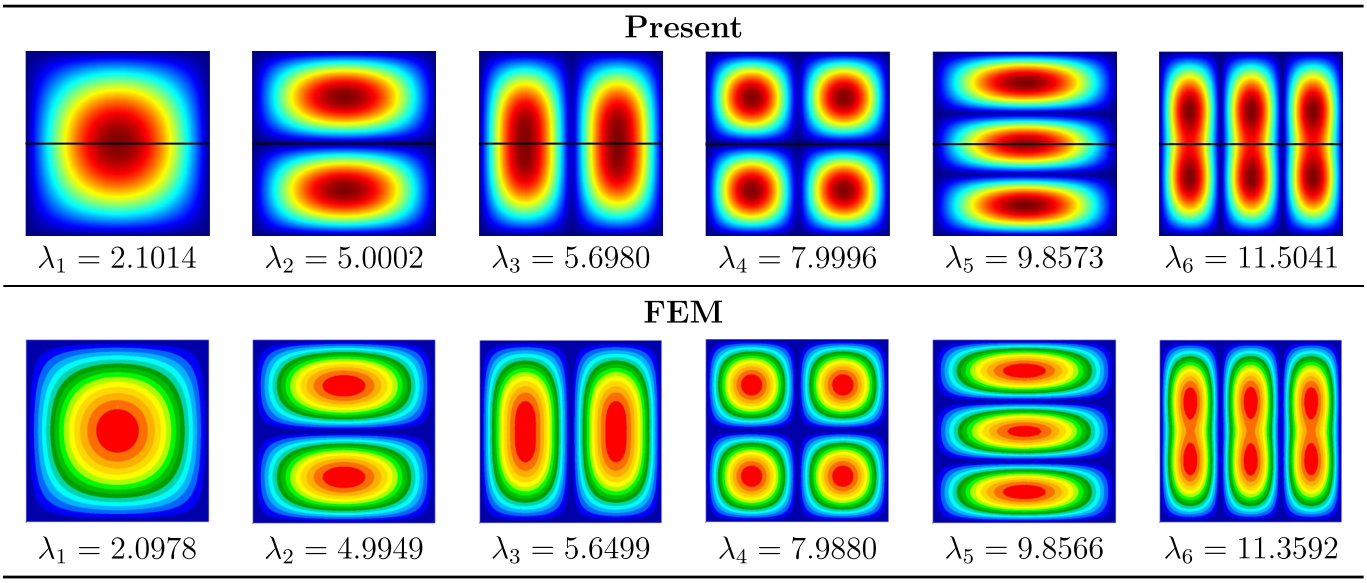

Figure 2.14: Comparison of mode shapes of SSSS rectangular plate with one central longitudinal stiffener (See Table 2.1)

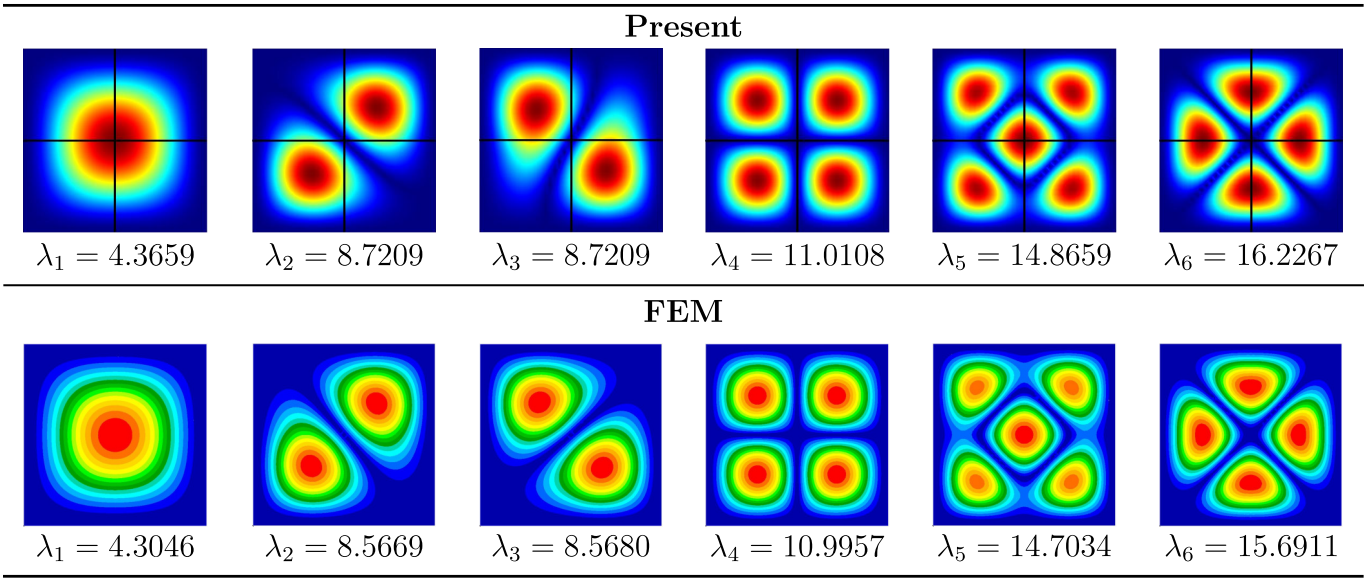

Figure 2.15: Comparison of mode shapes of CCCC rectangular plate with two orthogonal stiffeners (See Table 2.1)

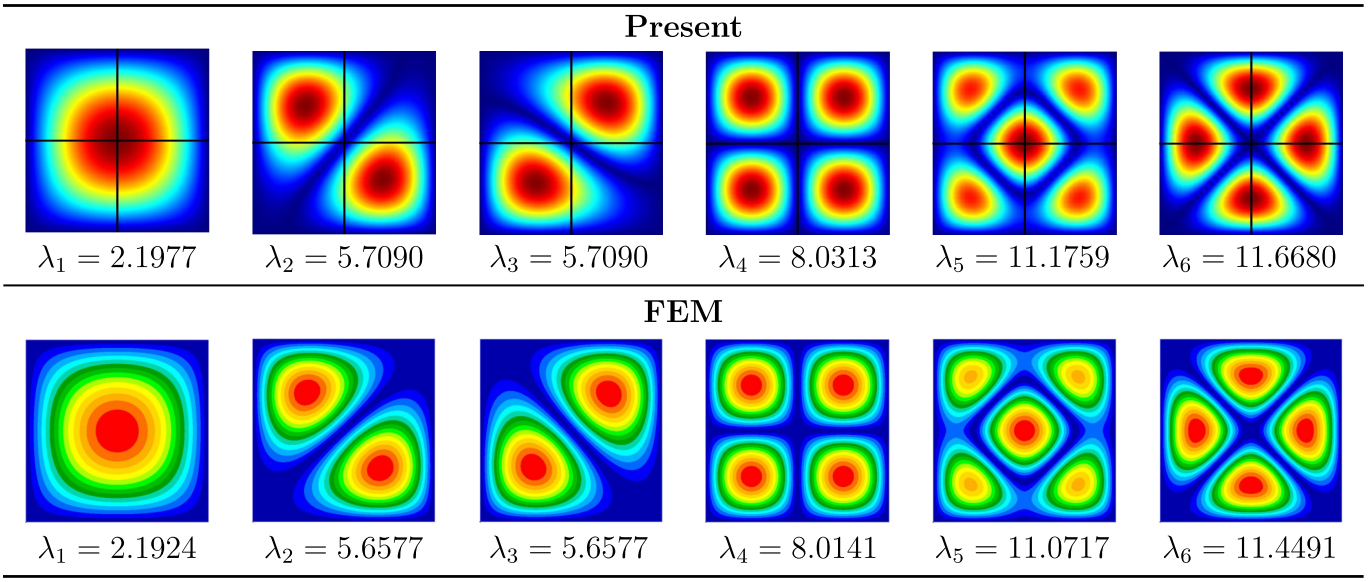

Figure 2.16: Comparison of mode shapes of SSSS rectangular plate with two orthogonal stiffeners (See Table 2.1)

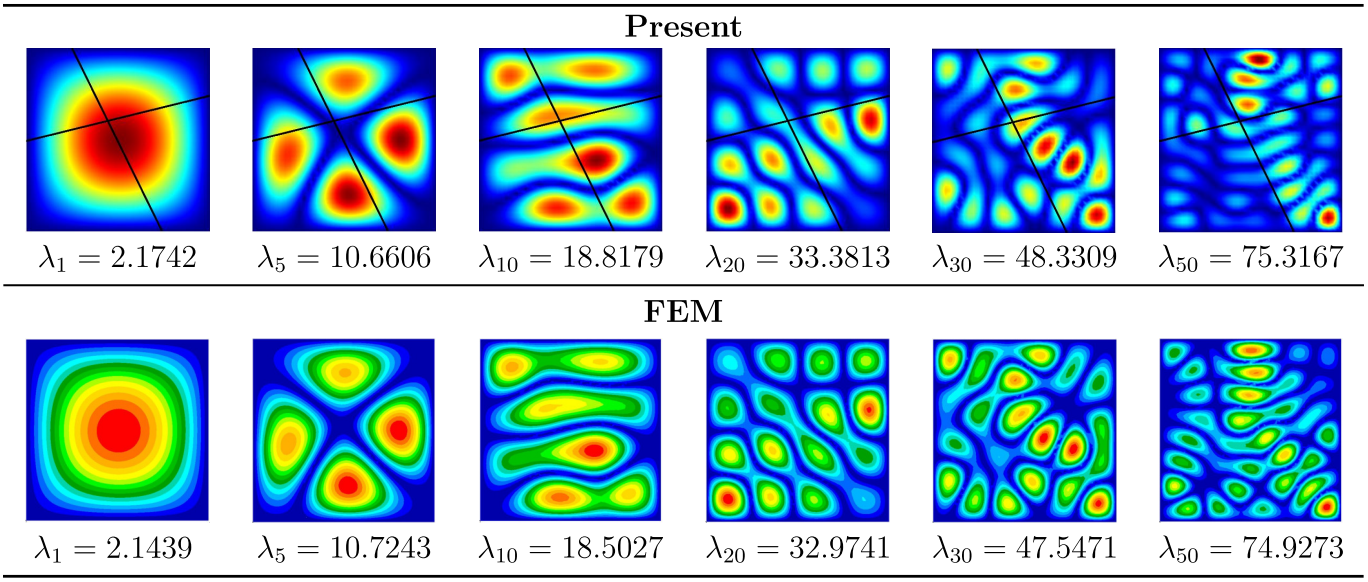

Figure 2.17: Comparison of mode shapes of SSSS rectangular plate with two arbitrary stiffeners (See Table 2.3)

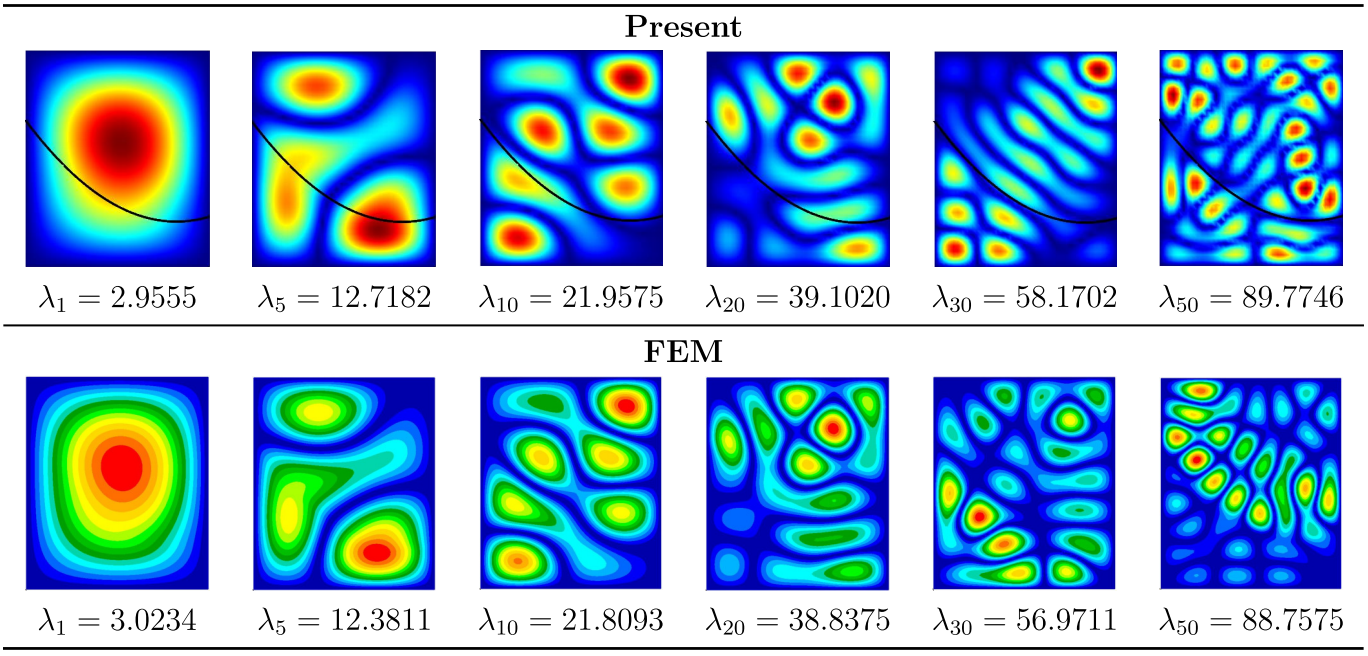

Figure 2.18: Comparison of mode shapes of SSSS rectangular plate with one curvilinear stiffener (See Table 2.4)

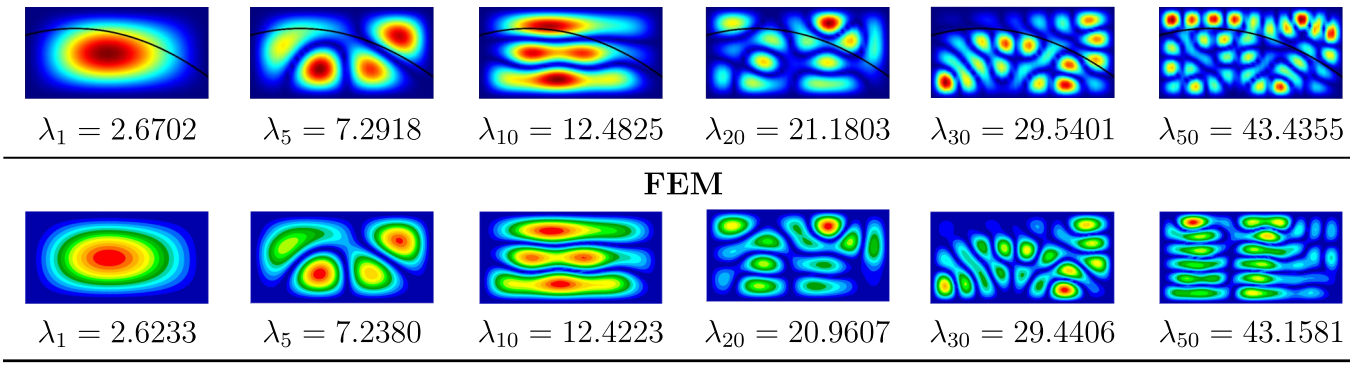

Figure 2.19: Comparison of mode shapes of CCCC rectangular plate with one curvilinear stiffener (See Table 2.5)

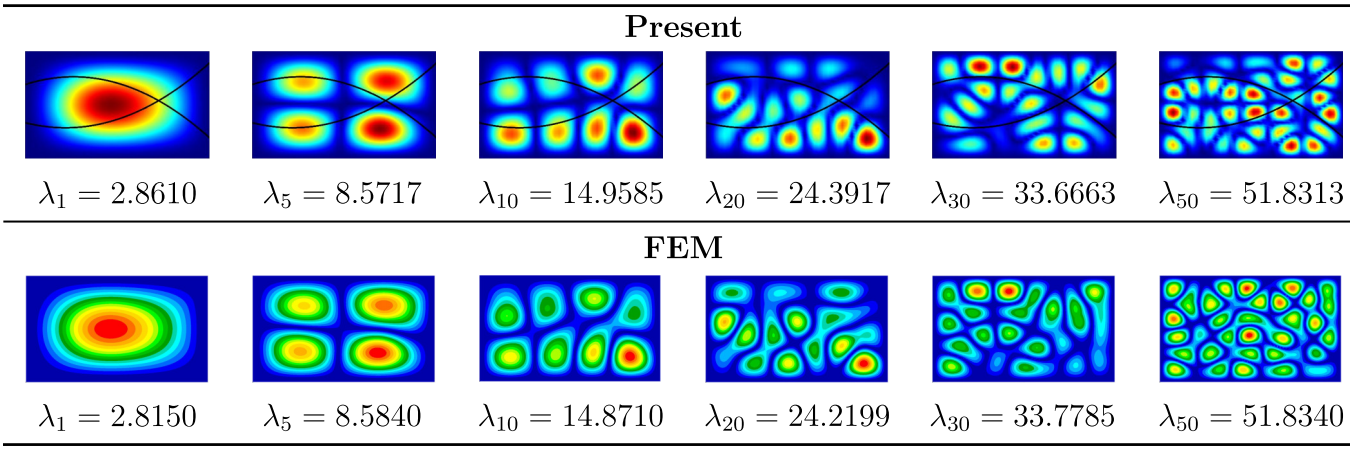

Figure 2.20: Comparison of mode shapes of CCCC rectangular plate with two curvilinear stiffeners (See Table 2.6)

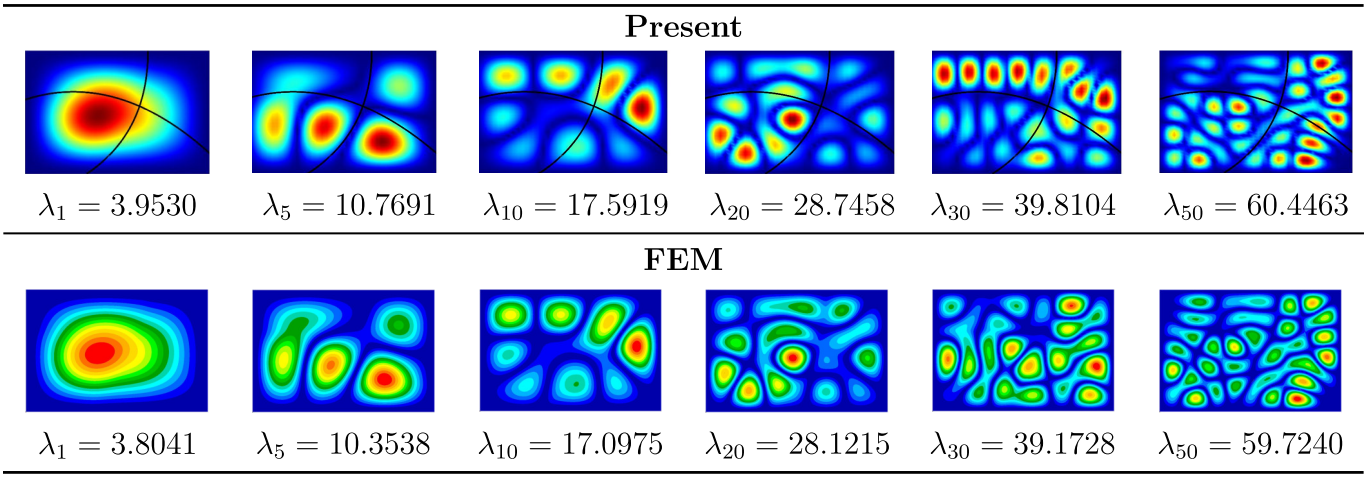

Figure 2.21: Comparison of mode shapes of CCCC rectangular plate with two curvilinear stiffeners (See Table 2.7)

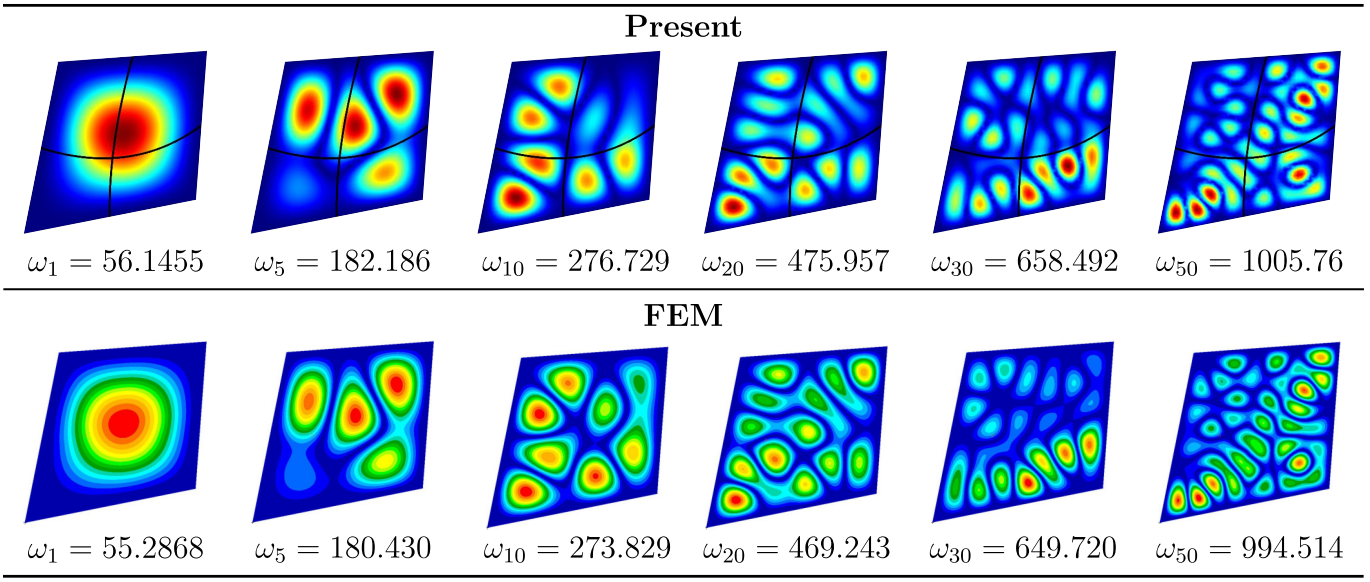

Figure 2.22: Comparison of mode shapes of CCCC quadrilateral plate with two curvilinear stiffeners (See Table 2.8)

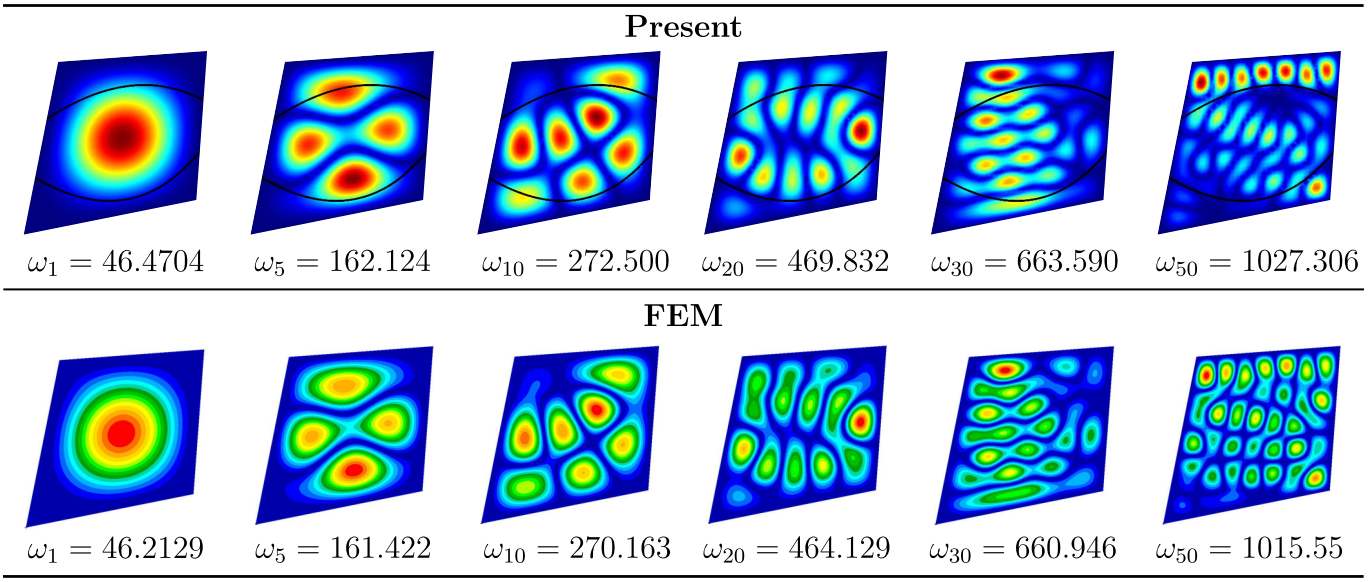

Figure 2.23: Comparison of mode shapes of CCCC quadrilateral plate with two curvilinear stiffeners (See Table 2.9)

Supplement II:

Table 2.10: Boundary condition realization using Jacobi weight function

Boundary Conditions	$W_w(\xi)$	$W_X(\xi)$	$W_Y(\xi)$	$W_w(\eta)$	$W_X(\eta)$	$W_Y(\eta)$
F-F	1	1	1	1	1	1
F-S	$(1-\xi)$	1	1	$(1-\eta)$	1	1
S-F	$(1+\xi)$	1	1	$(1+\eta)$	1	1
S-S	$(1-\xi)(1+\xi)$	1	1	$(1-\eta)(1+\eta)$	1	1
F-C	$(1-\xi)$	$(1-\xi)$	$(1-\xi)$	$(1-\eta)$	$(1-\eta)$	$(1-\eta)$
C-F	$(1+\xi)$	$(1+\xi)$	$(1+\xi)$	$(1+\eta)$	$(1+\eta)$	$(1+\eta)$
S-C	$(1-\xi)(1+\xi)$	$(1-\xi)$	$(1-\xi)$	$(1-\eta)(1+\eta)$	$(1-\eta)$	$(1-\eta)$
C-S	$(1-\xi)(1+\xi)$	$(1+\xi)$	$(1+\xi)$	$(1-\eta)(1+\eta)$	$(1+\eta)$	$(1+\eta)$
C-C	$(1-\xi)(1+\xi)$	$(1-\xi)(1+\xi)$	$(1-\xi)(1+\xi)$	$(1-\eta)(1+\eta)$	$(1-\eta)(1+\eta)$	$(1-\eta)(1+\eta)$

*F=Free, S=Simple supported, C=Clamped

Sample explanation for CSCS plate:
Edges 1,3 are clamped, hence, the displacement and rotations are restrained
Edges 2,4 are simply supported, consequently, only the displacements are restrained
Thus; the corresponding trial functions defined in Eqn. (2.12) for each direction can be written as below:
For the displacements:
$\phi_n(\xi) = (1-\xi)(1+\xi)P_n^{(2,2)}(\xi)$
$\phi_n(\eta) = (1-\eta)(1+\eta)P_n^{(2,2)}(\eta)$
For the rotations:
$\psi_n(\xi) = (1-\xi)(1+\xi)P_n^{(2,2)}(\xi)$
$\psi_n(\eta) = (1)P_n^{(0,0)}(\eta)$

Chapter 3

Up to lowest 100 frequencies of rectangular plates using Jacobi polynomials and TSNDT

The contents of this chapter have appeared in Journal of Sound and Vibration. [1]

[1] **Alanbay, B.**, Kapania, R. K., and Batra, R. C., 2020, "Up to Lowest 100 Frequencies of Rectangular Plates Using Jacobi Polynomials and TSNDT," Journal of Sound and Vibration, 480(1), p. 115352.

3.1 Abstract

This paper finds up to lowest 100 free vibration frequencies of isotropic elastic plates with thickness to side length ratio varying from 0.001 to 0.5 by using the Ritz method, a third-order shear and normal deformable plate theory (TSNDT), and weighted Jacobi polynomials as admissible functions that are mutually orthogonal and exactly satisfy essential boundary conditions. The numerical method is stable even for 18^{th} degree polynomials as basis functions. It is shown that this approach requires fewer degrees of freedom than those in the traditional finite element method (FEM) to find converged lowest 100 frequencies and the corresponding mode shapes. No shear correction factor is employed in the TSNDT. The presently computed results agree well with those from either analytical or numerical solutions of the corresponding 3-dimensional linearly elastic problems obtained with the commercial FE software, ABAQUS. Furthermore, results for plates made of incompressible material can be computed by setting Poisson's ratio = 0.49.

3.2 Introduction

Plates are widely used as structural components in many engineering applications such as automotive, aerospace, civilian, marine and other military structures. These components are not always thin plates; in fact, industrial and marine applications frequently involve thick plates. Understanding dynamics of thin/thick plates over a wide frequency range (e.g., the audio-frequency range for automotive and aerospace structures [1]), is of crucial importance to produce products with good vibration and noise performance. However, covering the entire range of frequency spectrum with deterministic methods is time-consuming for most approaches [2]. For instance, the traditional finite element method (FEM) can easily compute a few low frequencies with a reasonable computational cost. However, the cost significantly

increases for finding high frequencies. A deterministic method with a fast convergence rate and good computational efficiency for finding a large number of lowest frequencies will be useful for further understanding the dynamic characteristics of plate-like structures.

Even though a plate geometry is three-dimensional (3-D), the high computational expense of 3-D analyses has led to the development of plate theories based on simplifying kinematic assumptions. For example, the classical (or the Love-Kirchhoff) plate theory (CPT) does not consider both transverse shear and normal deformations and rotary inertia. Although the CPT provides acceptable solutions for thin (thickness/side length, h/b $<$ 0.01) and moderately thick plates (0.01$<$ h/b $<$ 0.05) [3], predictions become inaccurate for thicker plates. By accounting for both transverse shear and rotary inertia, Mindlin [4] proposed a first-order shear deformation theory (FSDT) and successfully applied it to study deformations of moderately thick plates. For $h/b \geq$ 0.1, these simplifications may give erroneous results for some problems. These limitations of the FSDT led to the development of higher-order shear deformation theories (HSDT) and high order shear and normal deformable theories (HSNDT). A detailed examination and review of HSDT and HSNDT are given in [5, 6, 7]. Carrera and Brischetto [8] and Noor et al. [9] have, respectively, reviewed 82 and 556 papers.

Many investigators, e.g., Mindlin and Medick [10], Hanna and Leissa [11], Carrera [12], Messina [13], Batra and Aimmanee [14, 15], have used different plate theories to characterize free vibrations of plates. The reader should consult books by Soedel [16], Mindlin [17], Leissa and Qatu [18] and Elishakoff [19] for additional works on equivalent single-layer plate theories.

Carrera [20] proposed a framework for efficiently deriving plate theories using a compact formulation, namely the Carrera Unified Formulation (CUF), in which the three displacement and/or transverse stress fields are expanded in the thickness coordinate using polynomials expansion of N-order. These are reviewed in [21] wherein details of CUF's implementation

are also described. Demasi [22, 23, 24, 25, 26, 27] presented a Generalized Unified Formulation (GUF) based on the CUF, and exhaustively reviewed the equivalent single layer, the layerwise, the mixed higher-order shear deformation, and the zigzag theories. In [27], he compared for different plate theories, the three displacements and the transverse stresses for simply supported laminates under bi-sinusoidal load on the top surface with the analytical solutions obtained by using the 3D-LET. As pointed out by both Carrera's group, and by Vel and Batra [28], there are no boundary layers observed for simply supported plates. Boscolo et al. [29, 30] obtained the lowest twelve natural frequencies of cross-ply laminates, having at least one pair of opposite edges simply supported, by using a layer-wise theory based on the CUF. They employed the Levy type analysis technique [29] and the dynamic stiffness method [30] that is only applicable when two opposite edges are simply supported. Dozio [31] also found the first 5 natural frequencies of cross-ply laminates using the CUF and the state-space method. Fazzolari and Carrera [32] used both the Ritz and the Galerkin formulations in conjunction with the CUF to compute the first six natural frequencies of simply supported angle-ply laminates. They used trigonometric functions as Ritz admissible functions. Fazzolari [33] obtained up to 10 lowest frequencies of metallic and functionally graded beams with arbitrary boundary conditions using refined variable-kinematics in quasi-3D beam theories. He used the principle of virtual displacements to derive governing equations, and numerically solved them by using the Ritz trial functions orthonormalized by the Gram-Schmidt process.

Even though the CUF is probably one of the most efficient ways to solve a problem, it requires several iterations to determine the least degree of complete polynomial basis functions in each direction [34]. Batra et al. [14, 15, 35, 36, 37, 38] have established the effectiveness and accuracy of the third-order shear and normal deformable plate theory (TSNDT) for analyzing thick plates by comparing predictions from the plate theory solutions with those from the 3D Linear Elasticity Theory (LET) equations derived either analytically or numerically by

the FEM.

The FEM is a widely used, well-established and general numerical method for solving initial boundary value problems. A key difference between the Ritz and the FE methods is that in the former the basis functions are defined over the entire domain and satisfy all essential boundary conditions. In the latter, the basis functions are usually polynomials that are defined piecewise over the domain, and their compact support is a small part of the domain. Meirovitch and Kwak [39] attribute the enormous success of the FEM to two main reasons: (1) It can solve nonlinear problems for bodies of complex geometries, and (2) the low-order complete polynomial basis functions with compact support give matrices of small bandwidth. They also stated that the Ritz method can yield superior accuracy for the same number of degrees of freedom (DoFs) as those in the FEM. Furthermore, the convergence of high frequencies computed with the FEM requires a large number of DoFs that increases the total CPU time. In order to accurately find higher frequencies, several techniques such as the discrete singular convolution method [40], the wave-based [41], and the hybrid FE−statistical energy analysis [42] are used. Each method has its own strengths and weaknesses.

This work differs from those of Demasi, Boscolo et al., and Dozio and Fazzolari in that we use the TSNDT to find the lowest 100 frequencies for rectangular plates under different boundary conditions at the edges. This is in contrast to the aforementioned works wherein only a few natural frequencies are computed. We determine the 100 frequencies by using the weighted Jacobi polynomials as basis functions in the Ritz method to numerically solve the TSNDT equations, and show that our results agree well with those found either analytically or numerically solving the 3-D LET equations with the commercial FE software, ABAQUS. The number of degrees of freedom (DoF) and the CPU time for the TSNDT to compute the lowest 100 frequencies was 1200 and 5 seconds, respectively; it was 2×10^6 and 3 hours for the ABAQUS solution.We note that for a rectangular plate with internal constraints,

3.2. Introduction

Filoche and Mayboroda [43], Sharma et al. [44], and Chattopadhyay and Batra [37] have used the FEM and, respectively, the Love-Kirchhoff, the FSDT, and the TSNDT to find the 100 lowest frequencies, the corresponding mode shapes and strain energies associated with them to analyze mode localization in the plate. Whereas it is easy to satisfy constraints of null displacements at points on a line normal to the plate mid-surface in the FEM, modifying basis functions in the Ritz method to meet this requirement is considerably arduous. Paik et al. [45] found first 100 buckling modes of an internally constrained clamped rectangular plate with the Mindlin plate theory and the FEM. These studies were aimed to show that some modes localize in one of the two plate regions separated by the line parallel to the smaller edge and passing through the fixed interior points.

It is well known that the quality (accuracy and rate of convergence) of the numerical solution and the efficiency of the computational algorithm strongly depend upon the choice of basis functions that must satisfy essential boundary conditions in the Ritz method. Although many different basis functions, such as simple polynomials [46], orthogonal polynomials generated using the Gram-Schmidt process [47, 48], and Chebyshev polynomials [49], have been employed in the literature, the orthogonality of the weighted Jacobi polynomials used here simplifies evaluation of many integrals and gives mass matrix which consists of diagonal submatrices. Alanbay and Kapania [50, 51] showed the efficiency of the Jacobi polynomials for studying free vibrations of thin plates, with and without stiffeners, using the CPT and the FSDT. We note that the orthogonal basis functions for the Ritz method can also be generated by taking the tensor product of eigenfunctions of free vibrations of a beam that are available in closed form for the Euler-Bernoulli and the Timoshenko beam theories; the former has been used, amongst others, by Datta and Verma [52] for a monolithic plate, and by Qin and Batra [53] for a sandwich plate to compute, respectively, 30 and 10 lowest frequencies.

The novelty of the present work is in demonstrating that the use of weighted orthogonal Jacobi polynomials as basis functions in the Ritz method to solve the TSNDT equations for the lowest 100 frequencies of a rectangular plate, under various boundary conditions, is computationally very efficient. The computed frequencies of both in-plane and out-of-plane (bending) vibration modes are very close to those found using the 3-D LET and the FE commercial software, ABAQUS.

3.3 Formulation of the Problem

Figure 3.1 shows a schematic sketch of a plate of length a, width b, thickness h, and the rectangular Cartesian co-ordinate axes used to describe its infinitesimal deformations from the stress-free initial configuration. We assume that the plane z=0 coincides with the plate mid-surface, the origin of the coordinate axes is at the plate centroid, and the plate material is linearly elastic, isotropic and homogeneous.

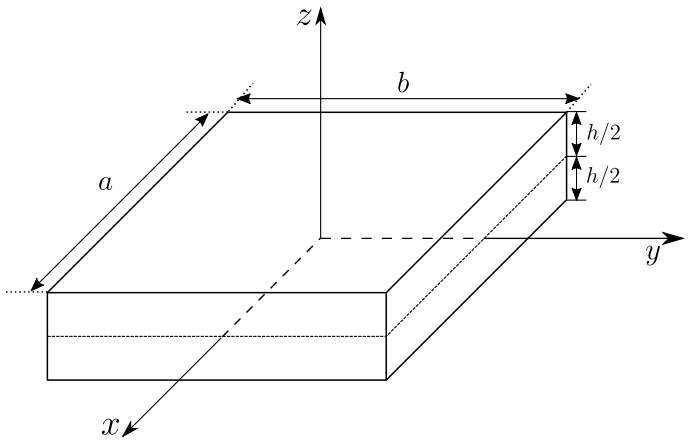

Figure 3.1: Schematic sketch of a rectangular plate, and of rectangular Cartesian coordinate axes

3.3.1 Brief review of the TSNDT

We use the TSNDT to analyze free vibrations of the plate; e.g., see Batra and Vidoli [6]. In the TSNDT, each displacement component, u_1,u_2,u_3, along the $x-$, the $y-$ and the $z-$axis, respectively, is expressed as a complete polynomial of degree 3 in the thickness (or the $z-$) coordinate. That is,

$$\mathbf{u}(\mathbf{x},\mathbf{y},\mathbf{z}) = \left\{ \begin{array}{c} u_1(x,y,z) \\ u_2(x,y,z) \\ u_3(x,y,z) \end{array} \right\} = \sum_{i=0}^{3} \left\{ \begin{array}{c} u_{1i}\,(x,y) \\ u_{2i}\,(x,y) \\ u_{3i}\,(x,y) \end{array} \right\} z^i \tag{3.1}$$

Thus, both transverse normal and shear deformations are considered. Recalling expressions for the infinitesimal strain tensor

$$\boldsymbol{\epsilon} = \{\epsilon_{xx} \;\; \epsilon_{yy} \;\; \epsilon_{zz} \;\; \gamma_{xy} \;\; \gamma_{xz} \;\; \gamma_{yz}\}^T = \{u_{1,x} \;\; u_{2,y} \;\; u_{3,z} \;\; u_{1,y}+u_{2,x} \;\; u_{1,z}+u_{3,x} \;\; u_{2,z}+u_{3,y}\}^T \tag{3.2}$$

and substituting for displacements from Eq. 3.1 into Eq. 3.2, we get

$$\boldsymbol{\epsilon} = \boldsymbol{Z}_i\,(z)\;\boldsymbol{L}\,\boldsymbol{d}_i\,(x,y)\,, \qquad i = 0,1,2,3 \tag{3.3}$$

Here

$$\mathbf{d}_i = [u_{1i} \;\; u_{2i} \;\; u_{3i}]^T\,, \qquad i = 0,1,2,3 \tag{3.4}$$

is the vector of generalized displacements defined on the plate mid-surface, $\boldsymbol{L}$ is the matrix of differential operators, elements of the matrix $\boldsymbol{Z_i}$ are powers of z, and a repeated index, unless otherwise noted, implies summation over the range of the index. Expressions for matrices $\boldsymbol{L}$

and $\boldsymbol{Z_i}$ are

$$\mathbf{L} = \begin{bmatrix} \frac{d}{dx} & 0 & 0 & \frac{d}{dy} & 0 & 0 & 1 & 0 \\ 0 & \frac{d}{dy} & 0 & \frac{d}{dx} & 0 & 0 & 0 & 1 \\ 0 & 0 & 1 & 0 & \frac{d}{dx} & \frac{d}{dy} & 0 & 0 \end{bmatrix}^T \tag{3.5}$$

$$\mathbf{Z}_i = \begin{bmatrix} z^i & 0 & 0 & 0 & 0 & 0 & 0 & 0 \\ 0 & z^i & 0 & 0 & 0 & 0 & 0 & 0 \\ 0 & 0 & i\,z^{i-1} & 0 & 0 & 0 & 0 & 0 \\ 0 & 0 & 0 & z^i & 0 & 0 & 0 & 0 \\ 0 & 0 & 0 & 0 & z^i & 0 & i\,z^{i-1} & 0 \\ 0 & 0 & 0 & 0 & 0 & z^i & 0 & i\,z^{i-1} \end{bmatrix} \tag{3.6}$$

We introduce non-dimensional coordinates (ξ,η) relating the natural and the global coordinates (see Figure 3.2) as

$$x = \frac{\xi\, a}{2}, \qquad y = \frac{\eta\, b}{2} \tag{3.7}$$

Thus, the plate sides extend from -1 to $+1$ in both the ξ and the η directions. The derivatives of a function with respect to ξ and η are related to those with respect to x and y as

$$\begin{Bmatrix} \phi_{,\xi} \\ \\ \phi_{,\eta} \end{Bmatrix} = \mathbf{J} \begin{Bmatrix} \phi_{,x} \\ \\ \phi_{,y} \end{Bmatrix} \tag{3.8}$$

where

$$\mathbf{J} = \begin{bmatrix} x_{,\xi} & y_{,\xi} \\ \\ x_{,\eta} & y_{,\eta} \end{bmatrix} \tag{3.9}$$

is the Jacobian matrix. Alternatively,

$$\begin{Bmatrix} \phi_{,x} \\ \phi_{,y} \end{Bmatrix} = \underbrace{\begin{bmatrix} \Gamma_{11} & \Gamma_{12} \\ \Gamma_{21} & \Gamma_{22} \end{bmatrix}}_{\mathbf{\Gamma}} \begin{Bmatrix} \phi_{,\xi} \\ \phi_{,\eta} \end{Bmatrix} \quad where \quad \mathbf{\Gamma} = \mathbf{J}^{-1} = \frac{1}{|\mathbf{J}|} \begin{bmatrix} J_{22} & -J_{12} \\ -J_{21} & J_{11} \end{bmatrix} \tag{3.10}$$

Using Eq. 3.10, we write Eq. 3.3 as

$$\boldsymbol{\epsilon} = \mathbf{Z_i} \begin{bmatrix} \Gamma_{11} & \Gamma_{12} & 0 & 0 & 0 & 0 & 0 & 0 & 0 \\ 0 & 0 & \Gamma_{21} & \Gamma_{22} & 0 & 0 & 0 & 0 & 0 \\ 0 & 0 & 0 & 0 & 0 & 0 & 0 & 0 & 1 \\ \Gamma_{21} & \Gamma_{22} & \Gamma_{11} & \Gamma_{12} & 0 & 0 & 0 & 0 & 0 \\ 0 & 0 & 0 & 0 & \Gamma_{11} & \Gamma_{12} & 0 & 0 & 0 \\ 0 & 0 & 0 & 0 & \Gamma_{21} & \Gamma_{22} & 0 & 0 & 0 \\ 0 & 0 & 0 & 0 & 0 & 0 & 1 & 0 & 0 \\ 0 & 0 & 0 & 0 & 0 & 0 & 0 & 1 & 0 \end{bmatrix} \begin{Bmatrix} u_{1i,\xi} \\ u_{1i,\eta} \\ u_{2i,\xi} \\ u_{2i,\eta} \\ u_{3i,\xi} \\ u_{3i,\eta} \\ u_{1i} \\ u_{2i} \\ u_{3i} \end{Bmatrix} = \mathbf{Z_i}\ \mathbf{T}\ \bar{\mathbf{d}}_\mathbf{i} \tag{3.11}$$

We assume the plate material obeys Hooke's law

$$\boldsymbol{\sigma} = \boldsymbol{C}\boldsymbol{\epsilon} \tag{3.12}$$

where

$$\boldsymbol{\sigma} = \{\sigma_{xx}\ \ \sigma_{yy}\ \ \sigma_{zz}\ \ \sigma_{xy}\ \ \sigma_{xz}\ \ \sigma_{yz}\}^T \tag{3.13}$$

and $\boldsymbol{C}$ is the 6×6 matrix of elastic constants that has 2 independent parameters for an isotropic material.

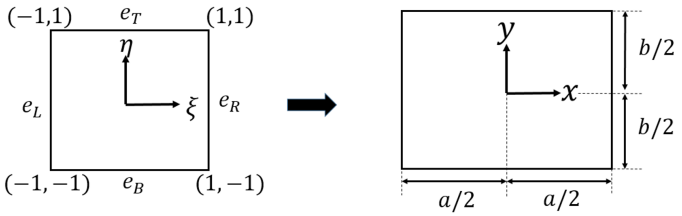

Figure 3.2: Transformation from natural to global coordinates in a rectangular plate

3.3.2 Ritz Method

Admissible Displacement Functions

We approximate displacement components in Eq. 3.4 as

$$\mathbf{d}_i = \begin{Bmatrix} u_{1i} \\ u_{2i} \\ u_{3i} \end{Bmatrix} = \sum_{j=0}^{m}\sum_{k=0}^{m} \begin{Bmatrix} N_{1i}^{jk}(\xi,\eta)\ q_{1i}^{jk} \\ N_{2i}^{jk}(\xi,\eta)\ q_{2i}^{jk} \\ N_{3i}^{jk}(\xi,\eta)\ q_{3i}^{jk} \end{Bmatrix} = \mathbf{H_i}\,\mathbf{q_i}, \qquad i = 0,1,2,3 \tag{3.14}$$

where the index i is not summed, $\mathbf{q}_i = [q_{1i}\ q_{2i}\ q_{3i}]^T$ is the vector of the generalized DoFs, and

$$\mathbf{H_i} = \begin{bmatrix} \mathbf{N_{1i}^T} & 0 & 0 \\ 0 & \mathbf{N_{2i}^T} & 0 \\ 0 & 0 & \mathbf{N_{3i}^T} \end{bmatrix} \tag{3.15}$$

Each term of the $\mathbf{N_{1i}}$, $\mathbf{N_{2i}}$, and $\mathbf{N_{3i}}$ vectors is written as the product of the Jacobi polynomials and a weight function that enforces the essential boundary condition prescribed at an edge

in the following form

$$\begin{aligned} N_{1i}^{jk}(\xi,\eta) &= W_{1i}\, P_j^{\left(2e_L^{1i},2e_R^{1i}\right)}(\xi)\; P_k^{\left(2e_B^{1i},2e_T^{1i}\right)}(\eta) \\ N_{2i}^{jk}(\xi,\eta) &= W_{2i}\, P_j^{\left(2e_L^{2i},2e_R^{2i}\right)}(\xi)\; P_k^{\left(2e_B^{2i},2e_T^{2i}\right)}(\eta) \\ N_{3i}^{jk}(\xi,\eta) &= W_{3i}\, P_j^{\left(2e_L^{3i},2e_R^{3i}\right)}(\xi)\; P_k^{\left(2e_B^{3i},2e_T^{3i}\right)}(\eta) \end{aligned} \tag{3.16}$$

Here

$$\begin{aligned} W_{1i} &= (1-\xi)^{e_R^{1i}}(1+\xi)^{e_L^{1i}}(1-\eta)^{e_T^{1i}}(1+\eta)^{e_B^{1i}} \\ W_{2i} &= (1-\xi)^{e_R^{2i}}(1+\xi)^{e_L^{2i}}(1-\eta)^{e_T^{2i}}(1+\eta)^{e_B^{2i}} \\ W_{3i} &= (1-\xi)^{e_R^{3i}}(1+\xi)^{e_L^{3i}}(1-\eta)^{e_T^{3i}}(1+\eta)^{e_B^{3i}} \end{aligned} \tag{3.17}$$

are weight functions, $P_n^{(\alpha,\beta)}(\xi)$ is the nth order Jacobi polynomial. These polynomials are orthogonal with respect to the weight $(1-\xi)^\alpha(1+\xi)^\beta$ on the interval $[-1,1]$, i.e.,

$$\int_{-1}^{1}(1-\xi)^\alpha(1+\xi)^\beta P_i^{(\alpha,\beta)}(\xi)\, P_j^{(\alpha,\beta)}(\xi)\; d\xi = f(\alpha,\beta,n)\,\delta_{ij}, \quad \alpha,\beta>-1 \tag{3.18}$$

where δ_{ij} is the Kronecker delta, and values of superscripts in Eqs. 3.16 and 3.17 depend upon the boundary conditions as mentioned below.

Boundary Conditions

Boundary conditions at a simply supported (S), a clamped (C), and a free (F) edge are specified as follows.

$$\begin{aligned}
S: &\quad v = w = 0,\ \sigma_{xx} = 0 \quad \text{on } \xi = -1,\ 1 \\
&\quad u = w = 0,\ \sigma_{yy} = 0 \quad \text{on } \eta = -1,\ 1 \\
C: &\quad u = v = w = 0 \quad \text{on } \xi = -1,\ 1;\ \eta = -1,\ 1 \\
F: &\quad \sigma_{xx} = \sigma_{xy} = \sigma_{xz} = 0 \quad \text{on } \xi = -1,\ 1 \\
&\quad \sigma_{yx} = \sigma_{yy} = \sigma_{yz} = 0 \quad \text{on } \eta = -1,\ 1
\end{aligned} \tag{3.19}$$

In the Ritz method, the admissible functions must satisfy the essential (i.e., displacement) boundary conditions. We enforce these by setting α and β equal to $2e_L^{ij}$, $2e_R^{ij}$, $2e_B^{ij}$ and $2e_T^{ij}$ in Eq. 3.16 and e_L^{ij}, e_R^{ij}, e_B^{ij} and e_T^{ij} in Eq. 3.17 for $i = 1, 2, 3$ and $j = 0, 1, 2, 3$. The subscripts L, R, B, and T, respectively, represent left, right, bottom and top edges of the plate. e_L^{ij}, e_R^{ij}, e_B^{ij}, and e_T^{ij} equal either 1.0 or 0 according as u_{ij} at the corresponding edge is prescribed or not. Values of e_L^{ij}, e_R^{ij}, e_B^{ij}, and e_T^{ij} are listed in Table 3.1 for different edge conditions.

Table 3.1: Weight function values for SSSS and CSFF plate

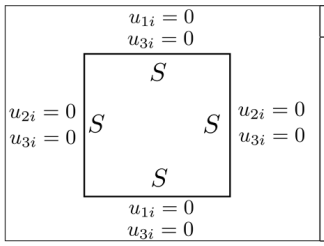

SSSS			CSFF		
u_{1i}	u_{2i}	u_{3i}	u_{1i}	u_{2i}	u_{3i}
$e_L^{1i} = 0$	$e_L^{2i} = 1$	$e_L^{3i} = 1$	$e_L^{1i} = 1$	$e_L^{2i} = 1$	$e_L^{3i} = 1$
$e_R^{1i} = 0$	$e_R^{2i} = 1$	$e_R^{3i} = 1$	$e_R^{1i} = 0$	$e_R^{2i} = 0$	$e_R^{3i} = 0$
$e_B^{1i} = 1$	$e_B^{2i} = 0$	$e_B^{3i} = 1$	$e_B^{1i} = 1$	$e_B^{2i} = 0$	$e_B^{3i} = 1$
$e_T^{1i} = 1$	$e_T^{2i} = 0$	$e_T^{3i} = 1$	$e_T^{1i} = 0$	$e_T^{2i} = 0$	$e_T^{3i} = 0$

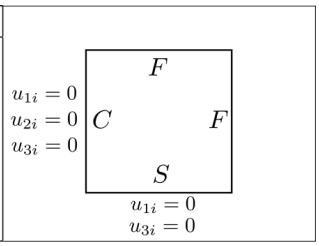

There are two advantages of using Jacobi polynomials, namely, the function used to satisfy an essential boundary condition is not arbitrary but is the actual weight of the Jacobi polynomials, and the orthogonality condition is defined with respect to this weight function.

Therefore, a better numerical stability and conditioning number of the stiffness and the mass matrices is achieved. Furthermore, submatrices of the mass matrices are diagonal. The second advantage is the ease of generating Jacobi polynomials and calculating their derivatives. The three-term recursive formula for Jacobi polynomials is,

$$\begin{aligned} 2n\, c_n\, c_{2n-2}\, P_n^{(\alpha,\beta)}(\xi) = c_{2n-1}\, (c_{2n-2}\, c_{2n}\, \xi + \alpha^2 - \beta^2)\, P_{n-1}^{(\alpha,\beta)}(\xi) \\ -2(n-1+\alpha)(n-1+\beta)\, c_{2n}\, P_{n-2}^{(\alpha,\beta)}(\xi) \end{aligned} \tag{3.20}$$

where

$$c_n = n + \alpha + \beta \tag{3.21}$$

$$P_0^{(\alpha,\beta)}(\xi) = 1; \qquad P_1^{(\alpha,\beta)}(\xi) = \frac{\alpha - \beta}{2} + \left(1 + \frac{\alpha + \beta}{2}\right) \xi \tag{3.22}$$

The formula for the derivative of a Jacobi polynomial is [54],

$$\frac{\mathrm{d}}{\mathrm{d}\xi}\left[P_n^{(\alpha,\beta)}(\xi)\right] = \frac{1}{2}\,(n + \alpha + \beta + 1)\, P_{n-1}^{(\alpha+1,\beta+1)}(\xi) \tag{3.23}$$

Strain Energy and Stiffness Matrix

The strain energy (U) of the plate is given by

$$U = \frac{1}{2}\int_V \boldsymbol{\sigma}^T \boldsymbol{\epsilon}\, dV \tag{3.24}$$

where V is the volume of the plate. By using Eq. 3.14, we rewrite Eq. 3.11 as

$$\epsilon = \mathbf{Z_i}\, \mathbf{T}\, \bar{\mathbf{B}}_\mathbf{i} \mathbf{q_i} \tag{3.25}$$

where

$$\bar{\mathbf{B}}_\mathbf{i} = \begin{bmatrix} \mathbf{N_{1i,\xi}} & \mathbf{N_{1i,\eta}} & 0 & 0 & 0 & 0 & \mathbf{N_{1i}} & 0 & 0 \\ 0 & 0 & \mathbf{N_{2i,\xi}} & \mathbf{N_{2i,\eta}} & 0 & 0 & 0 & \mathbf{N_{2i}} & 0 \\ 0 & 0 & 0 & 0 & \mathbf{N_{3i,\xi}} & \mathbf{N_{3i,\eta}} & 0 & 0 & \mathbf{N_{3i}} \end{bmatrix}^T \tag{3.26}$$

Substituting Eqs. 3.25 and 3.12 into Eq. 3.24 yields

$$U = \frac{1}{2}\int_A \boldsymbol{q_i}^T\, \bar{\boldsymbol{B}}_{\boldsymbol{i}}^T\, \boldsymbol{T}^T\, \boldsymbol{D_{ij}}\, \boldsymbol{T}^T\, \bar{\boldsymbol{B}}_{\boldsymbol{i}}\, \boldsymbol{q_j}\, dA = \frac{1}{2}\, \mathbf{q_i}^T\, \mathbf{K_{ij}}\, \mathbf{q_j} \tag{3.27}$$

where

$$\mathbf{K_{ij}} = \int_{-1}^{1}\int_{-1}^{1} \bar{\mathbf{B}}_\mathbf{i}^T\, \mathbf{T}^T\, \mathbf{D_{ij}}\, \mathbf{T}\, \bar{\mathbf{B}}_\mathbf{j}\ |\mathbf{J}|\, d\xi d\eta, \qquad i,j = 0,1,2,3 \tag{3.28}$$

$$\boldsymbol{D_{ij}} = \int_{-h/2}^{h/2} \boldsymbol{Z}_{\boldsymbol{i}}^T\, \boldsymbol{C}\, \boldsymbol{Z_j}\, dz \tag{3.29}$$

and indices on the right-hand side of Eq. 3.28 are not summed.

Kinetic Energy and Mass Matrix

The plate kinetic energy, T, is given by

$$T = \frac{1}{2}\int_V \rho\, \bar{v}^T \bar{v}\, dV \tag{3.30}$$

where ρ is the mass density, and

$$\bar{v} = \begin{Bmatrix} \dfrac{\partial u}{\partial t} \\ \dfrac{\partial v}{\partial t} \\ \dfrac{\partial w}{\partial t} \end{Bmatrix} = \begin{bmatrix} z^i & 0 & 0 \\ 0 & z^i & 0 \\ 0 & 0 & z^i \end{bmatrix} \begin{Bmatrix} \dot{u}_{1i} \\ \dot{u}_{2i} \\ \dot{u}_{3i} \end{Bmatrix} = \mathbf{Z_i^m}\dot{\mathbf{d}}_\mathbf{i}, \qquad i = 0,1,2,3 \tag{3.31}$$

the velocity vector. From Eq. 3.14, $\dot{\boldsymbol{d}}$ can be expressed in terms of admissible functions and the generalized DoFs as

$$\dot{\mathbf{d}}_\mathbf{i} = \mathbf{H}_\mathbf{i}\, \dot{\mathbf{q}}_\mathbf{i} \tag{3.32}$$

Substituting Eqs. 3.31 and 3.32 into Eq. 3.30 yields

$$T = \frac{1}{2} \int_V \rho\, \dot{\mathbf{q}}_\mathbf{i}^T\, \mathbf{H}_\mathbf{i}{}^T\, \mathbf{ZZ}_\mathbf{ij}\, \mathbf{H}_\mathbf{j}\, \dot{\mathbf{q}}_\mathbf{j}\, dV \tag{3.33}$$

where

$$\mathbf{ZZ}_\mathbf{ij} = \mathbf{Z}_\mathbf{i}^\mathbf{mT}\, \mathbf{Z}_\mathbf{j}^\mathbf{m} = \begin{bmatrix} z^{i+j} & 0 & 0 \\ 0 & z^{i+j} & 0 \\ 0 & 0 & z^{i+j} \end{bmatrix}, \qquad i,j = 0,1,2,3 \tag{3.34}$$

Setting

$$\mathbf{M}_\mathbf{ij} = \int_{-1}^{1}\int_{-1}^{1} \mathbf{H}_\mathbf{i}{}^T\, \mathbf{m}_\mathbf{ij}\, \mathbf{H}_\mathbf{j}\, |\mathbf{J}|\, d\xi d\eta \tag{3.35}$$

where

$$\mathbf{m}_\mathbf{ij} = \int_{-h/2}^{h/2} \rho\, \mathbf{ZZ}_\mathbf{ij}\, dz \tag{3.36}$$

we get

$$T = \frac{1}{2}\, \dot{\mathbf{q}}_\mathbf{i}^T\, \mathbf{M}_\mathbf{ij}\, \dot{\mathbf{q}}_\mathbf{j} \tag{3.37}$$

Free Vibration Analysis

The natural frequency, ω, and the corresponding mode shape $\{\boldsymbol{q}\}$ of the plate are obtained by solving the following eigenvalue problem:

$$\left[\mathbf{K} - \omega^2\, \mathbf{M}\right] \{\mathbf{q}\} = \{\mathbf{0}\} \tag{3.38}$$

In Eq. 3.38 $\boldsymbol{K}$ is the global stiffness matrix, $\boldsymbol{M}$ the global mass matrix, ω the natural frequency, and $\{\boldsymbol{q}\}$ the eigenvector. The global stiffness and mass matrices, $\boldsymbol{k}$ and $\boldsymbol{M}$, have the following expressions.

$$\mathbf{K} = \begin{bmatrix} \mathbf{K_{00}} & \frac{1}{2}\left(\mathbf{K_{01}} + \mathbf{K_{10}}^T\right) & \frac{1}{2}\left(\mathbf{K_{02}} + \mathbf{K_{20}}^T\right) & \frac{1}{2}\left(\mathbf{K_{03}} + \mathbf{K_{30}}^T\right) \\ \frac{1}{2}\left(\mathbf{K_{10}} + \mathbf{K_{01}}^T\right) & \mathbf{K_{11}} & \frac{1}{2}\left(\mathbf{K_{12}} + \mathbf{K_{21}}^T\right) & \frac{1}{2}\left(\mathbf{K_{13}} + \mathbf{K_{31}}^T\right) \\ \frac{1}{2}\left(\mathbf{K_{20}} + \mathbf{K_{02}}^T\right) & \frac{1}{2}\left(\mathbf{K_{21}} + \mathbf{K_{12}}^T\right) & \mathbf{K_{22}} & \frac{1}{2}\left(\mathbf{K_{23}} + \mathbf{K_{32}}^T\right) \\ \frac{1}{2}\left(\mathbf{K_{30}} + \mathbf{K_{03}}^T\right) & \frac{1}{2}\left(\mathbf{K_{31}} + \mathbf{K_{13}}^T\right) & \frac{1}{2}\left(\mathbf{K_{32}} + \mathbf{K_{23}}^T\right) & \mathbf{K_{33}} \end{bmatrix} \tag{3.39}$$

$$\mathbf{M} = \begin{bmatrix} \mathbf{M_{00}} & \frac{1}{2}\left(\mathbf{M_{01}} + \mathbf{M_{10}}^T\right) & \frac{1}{2}\left(\mathbf{M_{02}} + \mathbf{M_{20}}^T\right) & \frac{1}{2}\left(\mathbf{M_{03}} + \mathbf{M_{30}}^T\right) \\ \frac{1}{2}\left(\mathbf{M_{10}} + \mathbf{M_{01}}^T\right) & \mathbf{M_{11}} & \frac{1}{2}\left(\mathbf{M_{12}} + \mathbf{M_{21}}^T\right) & \frac{1}{2}\left(\mathbf{M_{13}} + \mathbf{M_{31}}^T\right) \\ \frac{1}{2}\left(\mathbf{M_{20}} + \mathbf{M_{02}}^T\right) & \frac{1}{2}\left(\mathbf{M_{21}} + \mathbf{M_{12}}^T\right) & \mathbf{M_{22}} & \frac{1}{2}\left(\mathbf{M_{23}} + \mathbf{M_{32}}^T\right) \\ \frac{1}{2}\left(\mathbf{M_{30}} + \mathbf{M_{03}}^T\right) & \frac{1}{2}\left(\mathbf{M_{31}} + \mathbf{M_{13}}^T\right) & \frac{1}{2}\left(\mathbf{M_{32}} + \mathbf{M_{23}}^T\right) & \mathbf{M_{33}} \end{bmatrix} \tag{3.40}$$

The required integrals are evaluated by using a high-order Gauss quadrature rules commensurate with the degree of polynomials in the Ritz basis functions; e.g., see Hale and Townsend [55]. The polynomials of degree 2m+2 appear in the expressions of the stiffness matrix of a CCCC plate. Since the $n-$point Gauss quadrature exactly integrates a polynomial of degree $2n-1$, we set the number of Gauss quadrature points $= (2m+3)/2$ (or the next higher integer).

No shear correction factor is used in the TSNDT.

3.4 Results

We take Poisson's ratio $\nu = 0.3$, and present below frequencies and mode shapes in terms of the non-dimensional frequency, λ, related to the dimensional frequency, ω, by

$$\lambda = \left(\frac{\omega b^2}{\pi^2}\right)\sqrt{\left(\frac{\rho h}{D}\right)} \tag{3.41}$$

Where $D = Eh^3/(12(1-\nu^2))$ is the flexural rigidity, and E Young's modulus. The approach is validated by comparing computed results for simply supported (SSSS) plates with the analytical solutions, and for other boundary conditions either with literature values or with those computed using the LET and the commercial FE software, ABAQUS.

3.4.1 Verification studies

To validate the accuracy of the present approach, first ten frequencies converged within 1% of their values, of a SSSS rectangular plate with $a/b = 2$ and $h/b = 0.1, 0.5$ are compared in Table 3.2 with the analytical solutions of Srinivas et al. [56] as augmented by Batra and Aimmanee [35] who also considered in-plane modes of vibration. For an SSSS rectangular plate, the displacement field

$$u_j = \mathrm{e}^{\mathrm{i}\omega t} U_j(z) \cos\left(\frac{m\pi x}{a}\right) \sin\left(\frac{n\pi y}{b}\right) \tag{3.42}$$

satisfies boundary conditions. Modes with either $m = 0$ or $n = 0$ correspond to in-plane deformations that have null transverse displacements. Mode shapes are classified as symmetric (s) and antisymmetric (a) about the plate mid-surface. It is clear that the first ten computed frequencies differ from their analytical values by atmost 0.6%. In Tables 3.3- 3.6, we have listed the first ten computed frequency parameters for different edge boundary conditions

Table 3.2: Comparison of the presently computed first ten frequencies of a SSSS rectangular plate with their exact values given by Srinivas et al. [56]. In column 1, (a) and (s) signify, respectively, asymettric and symettric modes; (2,1) implies the mode corresponds to $m = 2$ and $n = 1$ in Eq. 3.42

Mode	Present	Exact	% Error	Mode	Present	Exact	% Error
	(a) $h/b = 0.1$, $a/b = 2$				(a) $h/b = 0.5$, $a/b = 2$		
$1(s)(1,1)$	1.2237	1.2230	0.06	$1(s)(1,0)$	0.6523	0.6523	-0.00
$2(a)(2,1)$	1.9342	1.9332	0.06	$2(a)(1,1)$	0.8890	0.8881	0.10
$3(a)(3,1)$	3.0826	3.0836	-0.03	$3(a)(2,1)$	1.2613	1.2590	0.18
$4(s)(1,0)$	3.2617	3.2621	-0.01	$4(s)(0,1)$	1.3047	1.3047	-0.00
$5(a)(1,2)$	3.9716	3.9723	-0.02	$4(s)(2,0)$	1.3047	1.3047	-0.00
$6(a)(2,2)$	4.6224	4.6222	0.00	$5(s)(1,1)$	1.4587	1.4587	0.00
$6(a)(4,1)$	4.6224	4.6222	0.00	$6(a)(3,1)$	1.7684	1.7624	0.34
$7(a)(3,2)$	5.6789	5.6791	-0.00	$7(s)(2,1)$	1.8451	1.8451	0.00
$8(a)(5,1)$	6.5005	6.4993	0.02	$8(s)(3,0)$	1.9570	1.9570	-0.00
$9(s)(0,1)$	6.5234	6.5243	-0.01	$9(a)(1,2)$	2.1115	2.1018	0.46
$9(s)(2,0)$	6.5234	6.5243	-0.01	$10(a)(2,2)$	2.3440	2.3311	0.55
$10(a)(4,2)$	7.1038	7.1036	0.00	$10(a)(4,1)$	2.3440	2.3311	0.55

Table 3.3: Frequency parameters, $\lambda = (\omega b^2/\pi^2)\sqrt{\rho h/D})$, for a CCCC isotropic square plate

$\frac{h}{b}$	Solution	λ_1	λ_2	λ_3	λ_4	λ_5	λ_6	λ_7	λ_8	λ_9	λ_{10}
	Present	3.3212	6.3485	6.3485	8.9087	10.5055	10.6050	12.5223	12.5223	12.7168	12.7168
0.1	FEM [38]	3.3214	6.3482	6.3482	8.9062	10.5033	10.6038	12.5223	12.5223	12.7131	12.7131
	MLPG [38]	3.3449	6.3917	6.3917	8.9497	10.5267	10.6171	12.5524	12.5524	12.7466	12.7466
	Present	2.7330	4.7877	4.7877	6.2759	6.2759	6.4410	7.3526	7.4372	7.4552	8.7349
0.2	FEM [38]	2.7288	4.7779	4.7779	6.2745	6.2745	6.4252	7.3326	7.4338	7.4338	8.7078
	MLPG [38]	2.7388	4.8013	4.8013	6.2829	6.2837	6.4503	7.3694	7.4472	7.4472	8.6953
	Present	2.2262	3.6909	3.6909	4.1911	4.1911	4.8788	4.9594	5.4952	5.5783	6.0910
0.3	FEM [38]	2.2191	3.6763	3.6763	4.1893	4.1893	4.8564	4.9591	5.4684	5.5487	6.0881
	MLPG [38]	2.2228	3.6860	3.6864	4.1927	4.1931	4.8690	4.9654	5.4933	5.5889	6.0904
	Present	1.8452	2.9625	2.9625	3.1467	3.1467	3.7203	3.8899	4.3629	4.4284	4.5608
0.4	FEM [[38]	1.8363	2.9464	2.9464	3.1446	3.1446	3.7201	3.8651	4.3345	4.3960	4.5567
	MLPG [38]	1.8373	2.9504	2.9504	3.1465	3.1465	3.7247	3.8711	4.3514	4.4240	4.5571
	Present	1.5627	2.4602	2.4602	2.5192	2.5192	2.9767	3.2246	3.6134	3.6372	3.6661
0.5	FEM [38]	1.5529	2.4445	2.4445	2.5165	2.5165	2.9766	3.1997	3.5855	3.6313	3.6331
	MLPG [38]	1.5525	2.4458	2.4458	2.5176	2.5176	2.9800	3.2025	3.5974	3.6309	3.6536

and aspect ratios together with those found by Qian et al. [38] and Liew et al. [57] who used different numerical techniques. It should be noted that as opposed to other plate theories that generally ignore transverse normal strains, the present TSNDT based analysis captures the full spectrum of vibration frequencies in excellent agreement with 3D LET solutions.

3.4. Results

As pointed out by Srinivas et al., the CPT and the FSDT do not yield symmetric thickness modes (in-plane vibration modes). For $0.1 \leq h/b \leq 0.5$, the maximum difference in

Table 3.4: Frequency parameters, $\lambda = (\omega b^2/\pi^2)\sqrt{\rho h/D})$, for a CFCF isotropic square plate

$\frac{h}{b}$	Solution	λ_1	λ_2	λ_3	λ_4	λ_5	λ_6	λ_7	λ_8	λ_9	λ_{10}
	Present	2.1043	2.4483	3.9235	5.3880	5.8296	5.9489	6.9690	7.3612	9.7328	10.0752
0.1	FEM [38]	2.1060	2.4475	3.9241	5.3873	5.8292	5.9498	6.9676	7.3593	9.7332	10.0714
	MLPG [38]	2.1194	2.4777	3.9710	5.4241	5.8660	5.9698	6.8504	7.3393	9.7500	10.1149
	Present	1.8036	2.0403	2.9767	3.1949	4.1189	4.4208	5.3331	5.4384	5.4754	5.4829
0.2	FEM [38]	1.8013	2.0382	2.9774	3.1925	4.1108	4.4129	5.3320	5.4341	5.4668	5.4827
	MLPG [38]	1.8064	2.0491	2.9866	3.2101	4.1342	4.4464	5.3454	5.4149	5.4869	5.4927
	Present	1.5064	1.6698	1.9857	2.6142	3.1816	3.4192	3.5633	3.6558	3.9117	4.2229
0.3	FEM [38]	1.5022	1.6659	1.9859	2.6105	3.1696	3.4077	3.5621	3.6555	3.9114	4.2105
	MLPG [38]	1.5056	1.6704	1.9922	2.6183	3.1797	3.4252	3.5696	3.6618	3.9185	4.2351
	Present	1.2659	1.3829	1.4900	2.1902	2.5495	2.6770	2.7421	2.7542	2.9234	3.3039
0.4	FEM [38]	1.2606	1.3784	1.4902	2.1878	2.5367	2.6756	2.7413	2.7415	2.9230	3.3032
	MLPG [38]	1.2616	1.3803	1.4948	2.1901	2.5409	2.6804	2.7462	2.7516	2.9280	3.3074
	Present	1.0806	1.1665	1.1926	1.8769	2.1119	2.1443	2.1941	2.2966	2.3255	2.6152
0.5	FEM [38]	1.0746	1.1618	1.1926	1.8723	2.0999	2.1428	2.1931	2.2843	2.3249	2.6091
	MLPG [38]	1.0748	1.1626	1.1964	1.8751	2.1016	2.1462	2.1968	2.2900	2.3289	2.6136

Table 3.5: Frequency parameters, $\lambda = (\omega b^2/\pi^2)\sqrt{\rho h/D})$, for a SCSC isotropic square plate

h/b	Solution	λ_1	λ_2	λ_3	λ_4	λ_5	λ_6	λ_7	λ_8	λ_9	λ_{10}
0.1	Present	2.7186	5.0016	6.0549	6.5234	8.0548	8.8548	10.3923	11.4568	11.5171	12.1895
	FEM [38]	2.7187	5.0022	6.0535	6.5223	8.0524	8.8526	10.3895	11.4542	11.5178	12.1875
	MLPG [38]	2.7321	5.0457	6.0937	6.5223	8.0926	8.9531	10.4129	11.3839	11.5346	12.1707
0.2	Present	2.2962	3.2617	4.0872	4.6081	5.7660	6.0414	6.1320	6.5234	6.7674	7.3205
	FEM [38]	2.2935	3.2620	4.0840	4.5996	5.7656	6.0309	6.1314	6.5231	6.7583	7.3008
	MLPG [38]	2.2994	3.2620	4.1007	4.6197	5.7715	6.0519	6.1381	6.5282	6.7943	7.3510
0.3	Present	1.9123	2.1745	3.3376	3.5806	3.8479	4.0807	4.3489	4.6882	5.1667	5.2903
	FEM [38]	1.9081	2.1745	3.3311	3.5677	3.8471	4.0803	4.3489	4.6711	5.1666	5.2716
	MLPG [38]	1.9100	2.1745	3.3400	3.5766	3.8501	4.0841	4.3523	4.6823	5.1622	5.2954
0.4	Present	1.6156	1.6309	2.7838	2.8881	2.8969	3.0504	3.2617	3.7961	3.8758	4.2915
	FEM [38]	1.6105	1.6308	2.7740	2.8826	2.8874	3.0498	3.2618	3.7747	3.8755	4.2637
	MLPG [38]	1.6107	1.6308	2.7792	2.8864	2.8889	3.0523	3.2643	3.7803	3.8720	4.2809
0.5	Present	1.3047	1.3911	2.3119	2.3733	2.4234	2.4272	2.6094	2.9180	3.1011	3.1776
	FEM [38]	1.3047	1.3854	2.3111	2.3607	2.4090	2.4264	2.6093	2.9179	3.1008	3.1528
	MLPG [38]	1.3046	1.3850	2.3121	2.3637	2.4103	2.4284	2.6113	2.9174	3.0978	3.1559

the presently computed and the literature values of the first ten frequencies for plates with different edge conditions is 0.9%.

Table 3.6: Frequency parameters, $\lambda = (\omega b^2/\pi^2)\sqrt{\rho h/D}$), for a FFFF isotropic square plate

h/b	Solution	λ_1	λ_2	λ_3	λ_4	λ_5	λ_6	λ_7	λ_8	λ_9	λ_{10}
0.1	Present	1.2892	1.9205	2.3654	3.2378	3.2378	5.6226	5.6226	5.6563	6.1569	6.8779
	Ref [57]	1.2894	1.9205	2.3655	3.2387	–	5.6226	–	5.6591	6.1570	6.8779
0.2	Present	1.1866	1.7665	2.1535	2.8019	2.8019	4.0723	4.3340	4.3340	4.5934	4.6127
	Ref [57]	1.1864	1.7663	2.1532	2.8013	–	4.0722	4.3341	–	4.5909	4.6138
0.3	Present	1.0791	1.5868	1.9172	2.3942	2.3942	2.7147	2.8864	2.8864	3.0752	3.4830
	Ref [57]	–	–	–	–	–	–	–	–	–	–
0.4	Present	0.9790	1.4172	1.7017	2.0359	2.0590	2.0590	2.1616	2.1616	2.3064	2.6037
	Ref [57]	–	–	–	–	–	–	–	–	–	–
0.5	Present	0.8903	1.2691	1.5180	1.6285	1.7256	1.7256	1.7897	1.7897	1.8451	2.0722
	Ref [54]	0.8896	1.2680	1.5159	1.6285	1.7255	–	1.7864	–	1.8451	–

3.4.2 Effect of aspect ratio on mode shapes

In addition to the frequency parameters, 3-D mode shapes obtained using the present method and those found by analyzing 3-D deformations of the plate by the FEM are compared in Figures 3.3 and 3.4 for SSSS and CCCC square plates, respectively. The red color represents the absolute maximum deflection, and the blue color the undeformed state. The fringe plots are for magnitudes of deflections.

Figure 3.5 shows the effect of the aspect ratio on the mode shapes. It is observed that for thin plates ($h/b = 0.001, 0.01$), the first six modes are out-of-plane modes, i.e., correspond to bending deformations. With an increase in the aspect ratio, the number of out-of-plane modes decrease and are replaced by in-plane vibration modes

3.4.3 Effect of boundary conditions on the fundamental frequency parameter

The fundamental frequency parameter versus the aspect ratio (h/b) for different boundary conditions for square plates are plotted in Figures 3.6 and 3.7. For a fixed value of $h/b < 0.22$, the fundamental frequency parameter in the descending order are for the

	Mode 1	*Mode* 2	*Mode* 3	*Mode* 4	*Mode* 5	*Mode* 6
Boundary Condition : *SSSS*, $a/b = 1$, $h/b = 0.1$						
Present	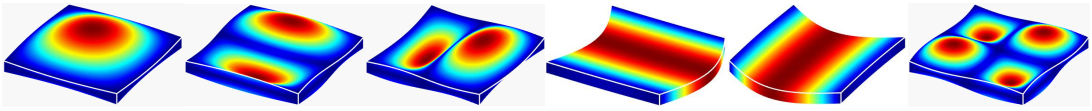					
	$\lambda_1 = 1.9342$	$\lambda_2 = 4.6224$	$\lambda_3 = 4.6224$	$\lambda_4 = 6.5234$	$\lambda_5 = 6.5234$	$\lambda_6 = 7.1038$
3DLET	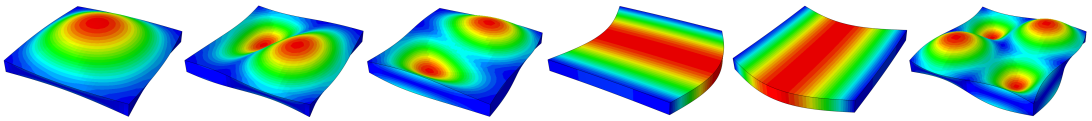					
	$\lambda_1 = 1.9335$	$\lambda_2 = 4.6201$	$\lambda_3 = 4.6201$	$\lambda_4 = 6.5230$	$\lambda_5 = 6.5230$	$\lambda_6 = 7.0975$

Figure 3.3: First six mode shapes and frequencies for the SSSS thick square plate with $h/b = 0.1$

CCCC, SCSC, CFCF, FFFF, SFSF, SCFF, CFFF edges. However, for $h/b >$ 0.22, the fundamental frequency parameter of the plate with SSSS edges becomes greater than that of the plate with the CFCF edges. The six zero frequencies of a FFFF plate are excluded from these plots. For $0 < h/b < 0.5$, the CCCC (FFFF) square plate has the maximum (minimum) fundamental frequency.

3.4.4 Comparison of results with different basis functions

Fundamental frequency parameters of incompressible square plates under different boundary conditions calculated using the present approach and taking the Poisson's ratio to be 0.49 are plotted in Figure 3.8 together with those found by Yuan and Batra [58] who used the TSNDT and the mixed FEM with 16x16 uniform FE mesh. They [58] considered displacements as unknowns at the nodes of a 9-node quadrilateral element and 4 interior nodes for the hydrostatic pressure. The results obtained from both approaches are in excellent agreement with each other. The frequency parameter, $\Omega = \omega h\sqrt{\rho/\mu}$, is used [58] here.

	Mode 1	*Mode* 2	*Mode* 3	*Mode* 4	*Mode* 5	*Mode* 6
Boundary Condition : *CCCC*, $a/b = 1$, $h/b = 0.1$						
Present	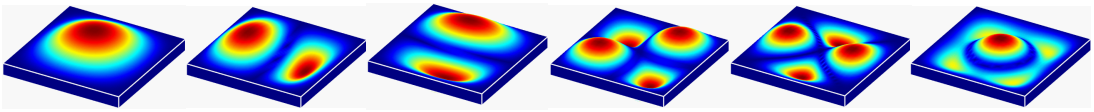					
	$\lambda_1 = 3.3212$	$\lambda_2 = 6.3475$	$\lambda_3 = 6.3475$	$\lambda_4 = 8.9072$	$\lambda_5 = 10.5055$	$\lambda_6 = 10.6049$
3DLET	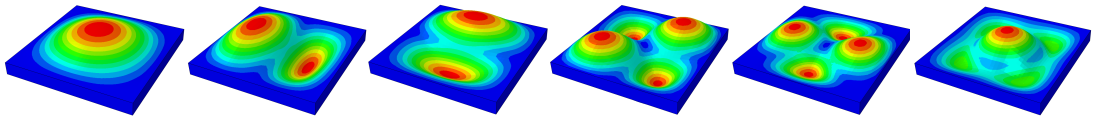					
	$\lambda_1 = 3.3031$	$\lambda_2 = 6.3140$	$\lambda_3 = 6.3140$	$\lambda_4 = 8.8566$	$\lambda_5 = 10.4518$	$\lambda_6 = 10.5509$

Figure 3.4: First six mode shapes and frequencies for the CCCC thick square plate with $h/b = 0.1$

3.4.5 Convergence studies

Present approach

In Figure 3.9, we have exhibited the convergence (within 1% of their values) of the $5^t h$, $10^t h$, 50^{th}, and 100^{th} frequency of a CCCC square plate with an increase in the degree of polynomials used in the Ritz method. Four values of $h = b = \tau = 0.001, 0.1, 0.3$ and 0.5 are considered. The same degree of polynomial is used for all generalized DoFs. It is seen that with an increase in τ, the degree of the polynomial needed for computing the 100^{th} lowest frequency decreases. It is because mode shapes of a thin plate are predominantly out-of-plane modes and have complicated wave patterns that can be well captured by higher order polynomials. We also need higher degree polynomials for computing mode shapes corresponding to high frequencies of a thick plate. Although the 4^{th} degree polynomials suffice to compute converged frequencies up to the 10^{th} mode, for the 50^{th} and the 100^{th} modes, polynomials of degree 10 and higher are needed. For the 100^{th} mode of the thin

plate, the convergence is achieved by using polynomials of degree 16. The size of matrices and the run time for different polynomial degrees are summarized in Table 3.7.

Table 3.7: For a CCCC square thick plate ($h/b = 0.2$) the number of DoFs and the run time for the present TSNDT/Ritz method

Polynomial Degree	# DoFs	Run Time (s)	Polynomial Degree	# DoFs	Run Time (s)
3	192	0.337	11	1728	19.8
4	300	0.592	12	2028	30.1
5	432	0.944	13	2352	43.4
6	588	1.36	14	2700	63.2
7	768	2.00	15	3072	89.9
8	972	3.01	16	3468	122
9	1200	4.75	17	3888	170
10	1452	12.7	18	4332	233

The FEM

We have also found the lowest 100 frequencies by analyzing plate's 3-D deformations with the commercial FE software, Abaqus, and employing different mesh seedings listed in Table 3.8 and 8-node brick elements (C3D in Abaqus terminology). We realize that the run time of these analyses depends on many factors, and there is no fair way to compare the computational requirements for a commercial software with those for the in-house code developed in MATLAB 2018b. However, the number of DoFs and the run time in the same machine provides a rough insight about the performance of the two methods. Both software were executed on Intel® Xeon(R) CPU E5-2665 0 at 2.40 GHz processor with 64 GB RAM running a Win 10 system. Fig. 10 illustrates the maximum mode prediction capabilities of different FE meshes. It is clear that the first 3 FE meshes with up to 137,781 DoFs did not give accurate frequencies of modes greater than 9, and accurate frequencies of the first 100 modes are achieved using the FEM with 2,120,493 DoFs and run time of approximately 3 h. However, the same first 100 frequencies were accurately computed using the present method with as few as 1200 DoFs and a run time of 4.75 s. For a few arbitrarily selected modes,

the polynomial degree for the present approach and the number of DoFs for the FEM are displayed in Fig. 11. The convergence of the FEM progressively worsens with an increase in the order of the frequency. Higher order mode shapes and the corresponding frequencies of a

Table 3.8: FE meshes and the run time for studying convergence using the commercial software, Abaqus, of the first 100 frequencies of a CCCC square plate ($h/b = 0.2$)

Case	Seeding (x, y, , z)	# Elements	# Nodes	# DoFs	Run Time (s)
1	40x40x6	9,600	11,767	35,301	102
2	40x40x20	32,000	35,301	105,903	211
3	80x80x6	38,400	45,927	137,781	285
4	80x80x10	64,000	72,171	216,513	578
5	80x80x15	96,000	104,976	314,928	1,695
6	80x80x20	128,000	137,781	413,343	2,059
7	100x100x15	150,000	163,216	489,648	3,250
8	120x120x20	288,000	307,461	922,383	7,849
9	150x150x30	675,000	706,831	2,120,493	11,085

CCCC square plate obtained with the two methods are presented in Figure 3.12. Since the higher modes are predominantly bending, contour plots are based on the deflection amplitude in the z-direction. The maximum discrepancy between results from the two approaches is less than 1%.

3.5 Conclusions

We have shown that the computational method using a third-order shear and normal deformation theory (TSNDT) and the weighted orthogonal Jacobi polynomials as the basis functions in the Ritz method to find the first 100 frequencies and the corresponding mode shapes is considerably more economical than the traditional finite element method (FEM). In the TSNDT, each displacement component is expressed as a complete polynomial of degree 3 in the thickness coordinate. The mutually orthogonal weighted Jacobi polynomials basis functions in the Ritz method satisfy the essential boundary conditions and may be of

degree 18 for finding the 100th lowest frequency. Computational resources needed for the present approach are considerably less that those needed for the traditional FEM.

h/b	$Mode\ 1$	$Mode\ 2$	$Mode\ 3$	$Mode\ 4$	$Mode\ 5$	$Mode\ 6$
			$Boundary\ Condition:\ SSSS,\ a/b = 1$			
0.001	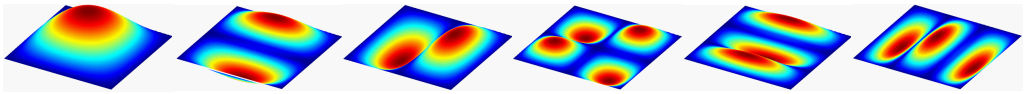					
	$\lambda_1 = 2.0000$	$\lambda_2 = 5.0000$	$\lambda_3 = 5.0000$	$\lambda_4 = 7.9999$	$\lambda_5 = 10.0019$	$\lambda_6 = 10.0019$
0.01	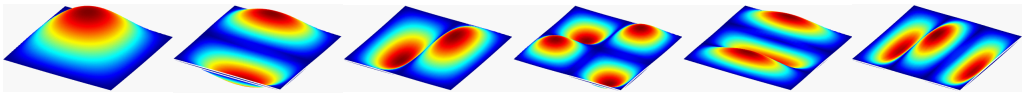					
	$\lambda_1 = 1.9993$	$\lambda_2 = 4.9956$	$\lambda_3 = 4.9956$	$\lambda_4 = 7.9888$	$\lambda_5 = 9.9846$	$\lambda_6 = 9.9846$
0.1	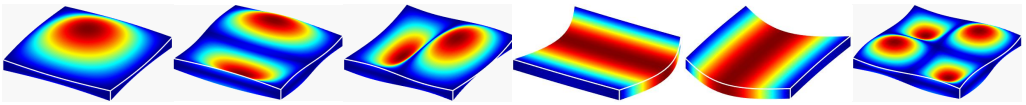					
	$\lambda_1 = 1.9342$	$\lambda_2 = 4.6224$	$\lambda_3 = 4.6224$	$\lambda_4 = 6.5234$	$\lambda_5 = 6.5234$	$\lambda_6 = 7.1038$
0.2	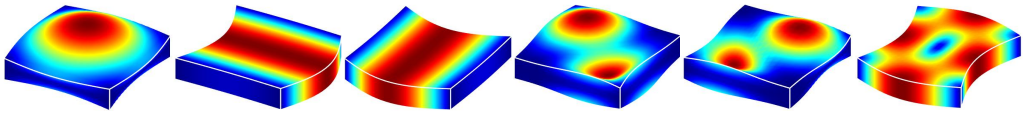					
	$\lambda_1 = 1.7760$	$\lambda_2 = 3.2617$	$\lambda_3 = 3.2617$	$\lambda_4 = 3.9011$	$\lambda_5 = 3.9011$	$\lambda_6 = 4.6127$
0.3	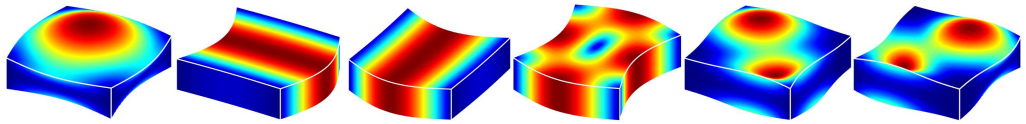					
	$\lambda_1 = 1.5902$	$\lambda_2 = 2.1745$	$\lambda_3 = 2.1745$	$\lambda_4 = 3.0752$	$\lambda_5 = 3.2458$	$\lambda_6 = 3.2458$
0.4	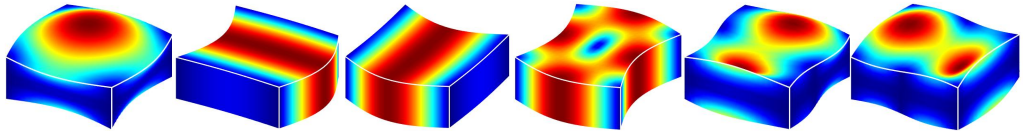					
	$\lambda_1 = 1.4145$	$\lambda_2 = 1.6309$	$\lambda_3 = 1.6309$	$\lambda_4 = 2.3064$	$\lambda_5 = 2.7344$	$\lambda_6 = 2.7344$
0.5	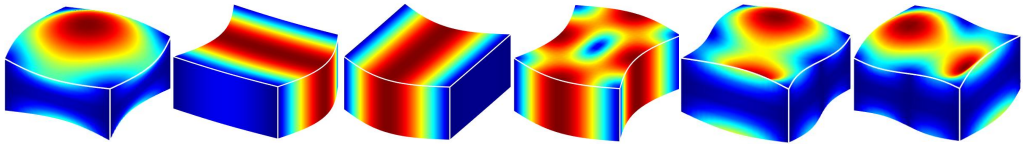					
	$\lambda_1 = 1.2613$	$\lambda_2 = 1.3047$	$\lambda_3 = 1.3047$	$\lambda_4 = 1.8451$	$\lambda_5 = 2.3440$	$\lambda_6 = 2.3440$

Figure 3.5: For different aspect ratios, presently computed mode shapes and frequencies for the SSSS plate

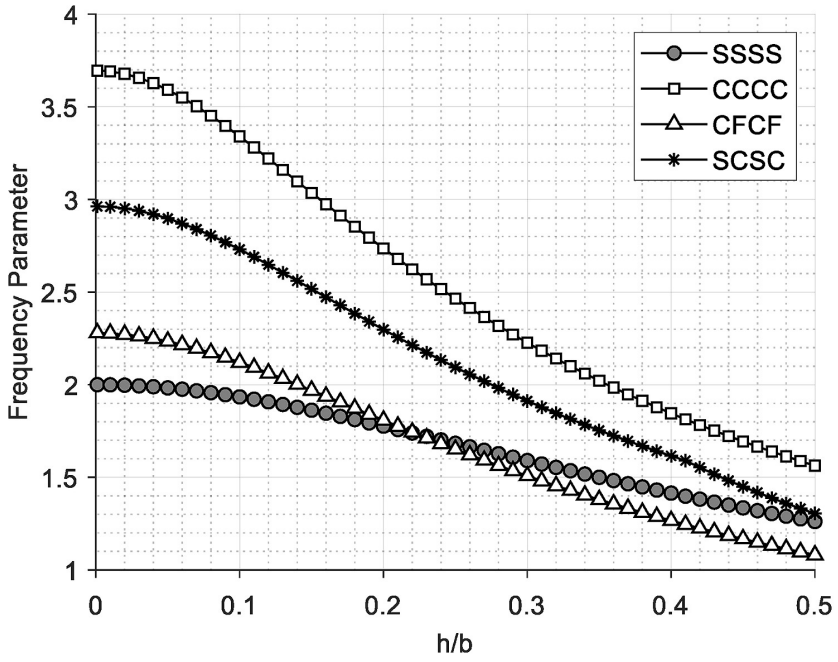

Figure 3.6: Fundamental frequency parameter versus aspect ratio of SSSS, CCCC, CFCF, and SCSC square plates

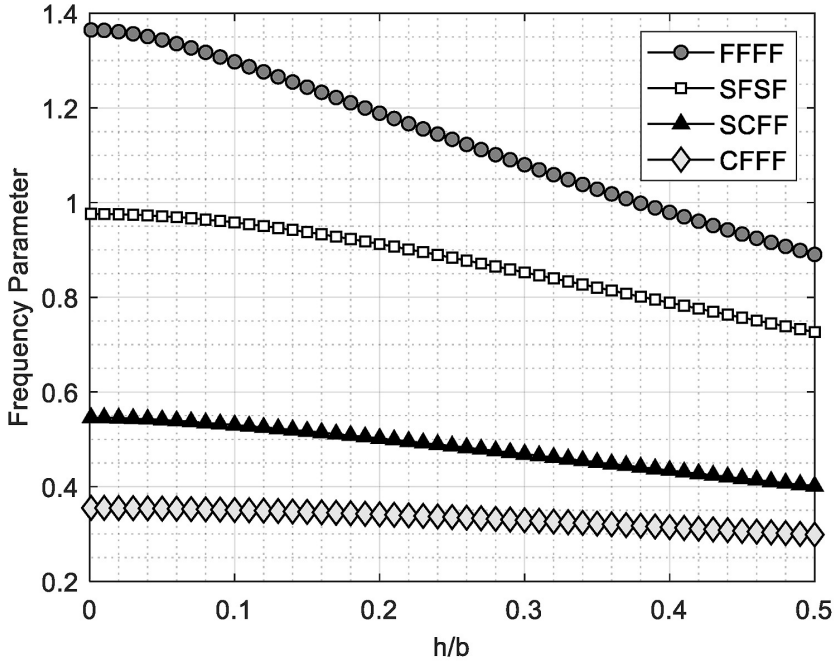

Figure 3.7: Fundamental frequency parameter versus aspect ratio of FFFF, SFSF, SCFF, and CFFF square plates

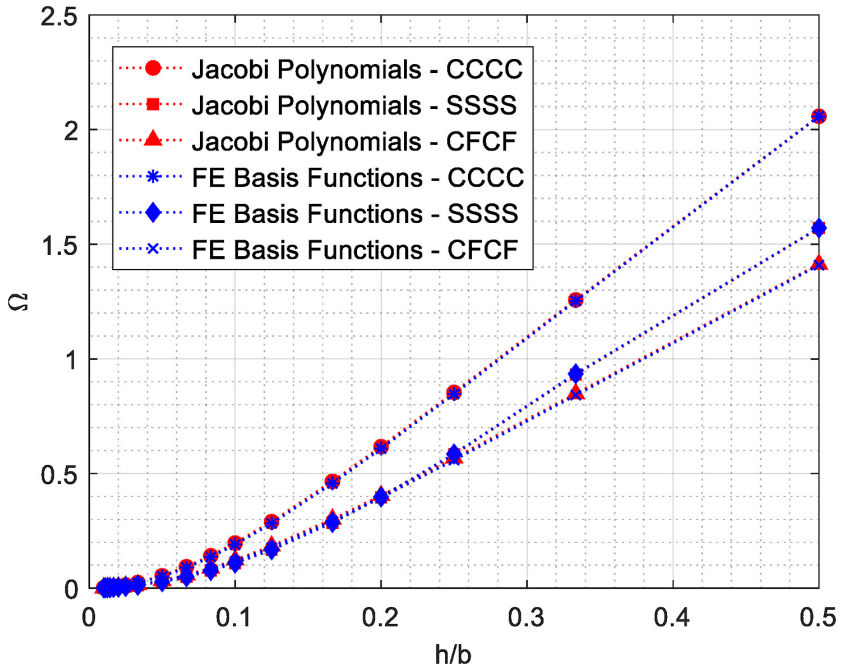

Figure 3.8: Comparison of the fundamental frequency parameters obtained by using the Jacobi polynomials and the FE hybrid basis functions for an incompressible plate

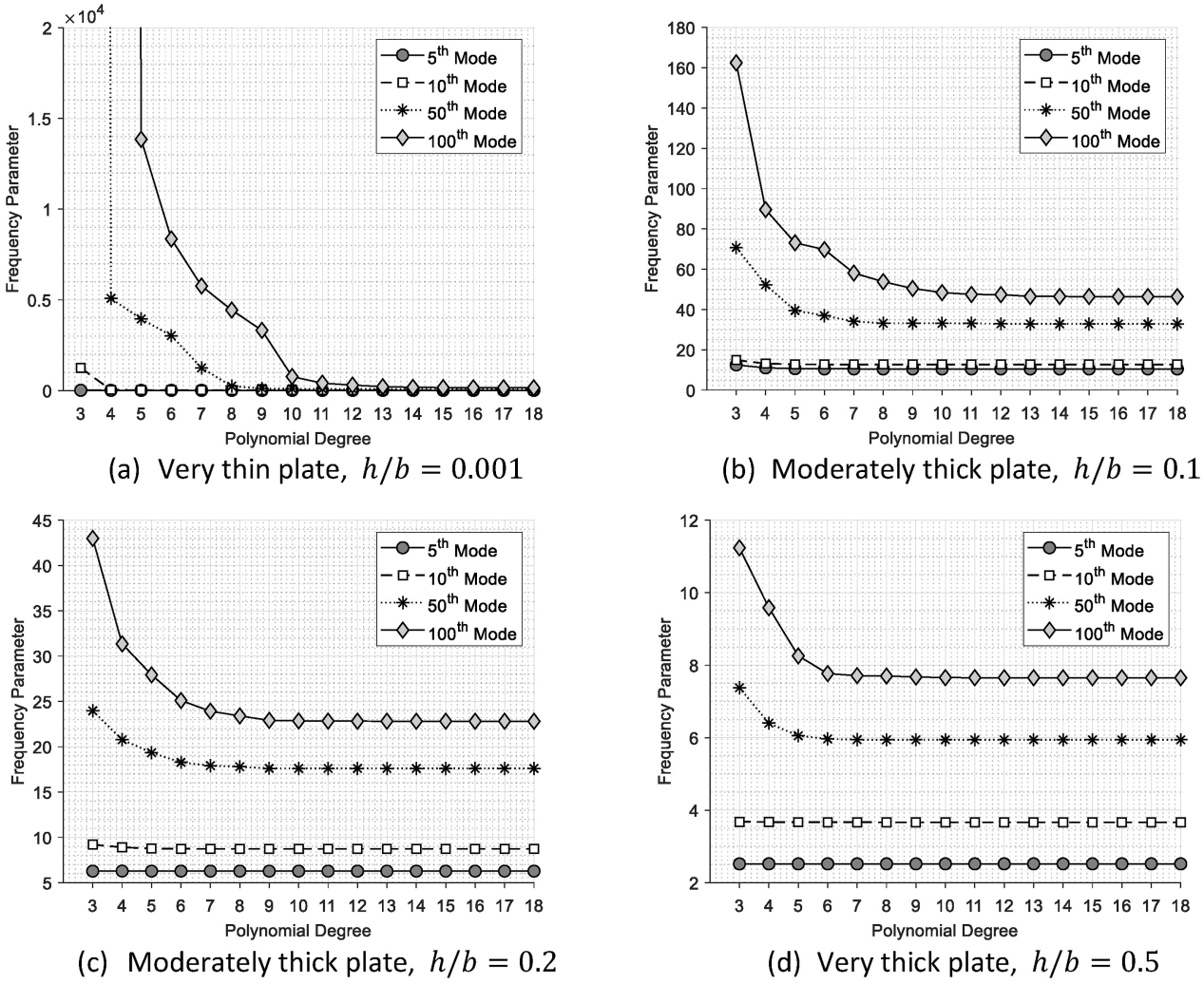

Figure 3.9: Convergence of frequencies with an increase in the degree of polynomial basis functions

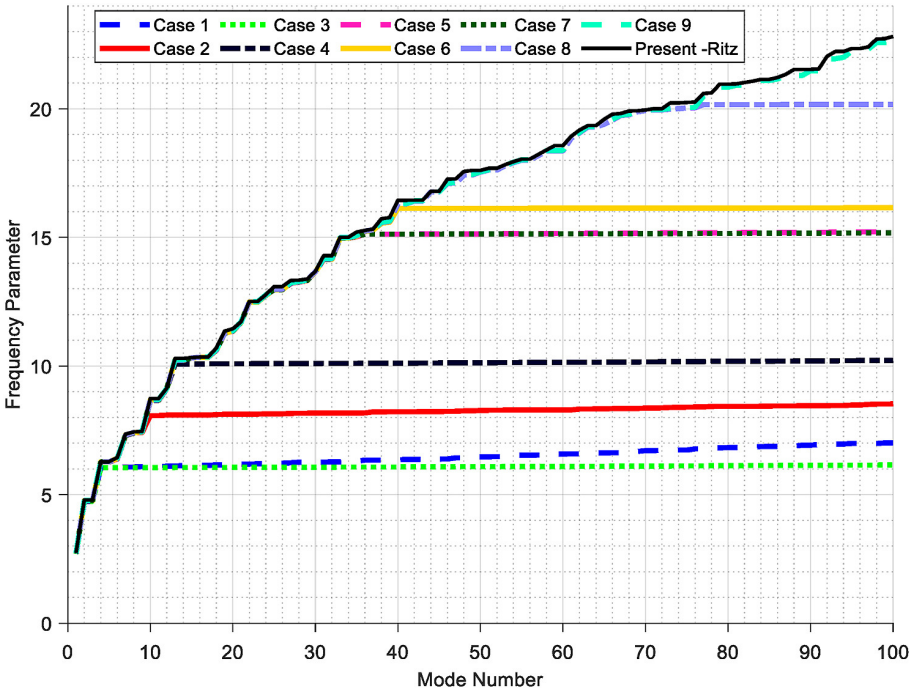

Figure 3.10: First 100 frequencies of a CCCC square thick plate ($h/b = 0.2$) obtained using ABAQUS (see Table 3.8 for the corresponding FE meshes) and the present formulation

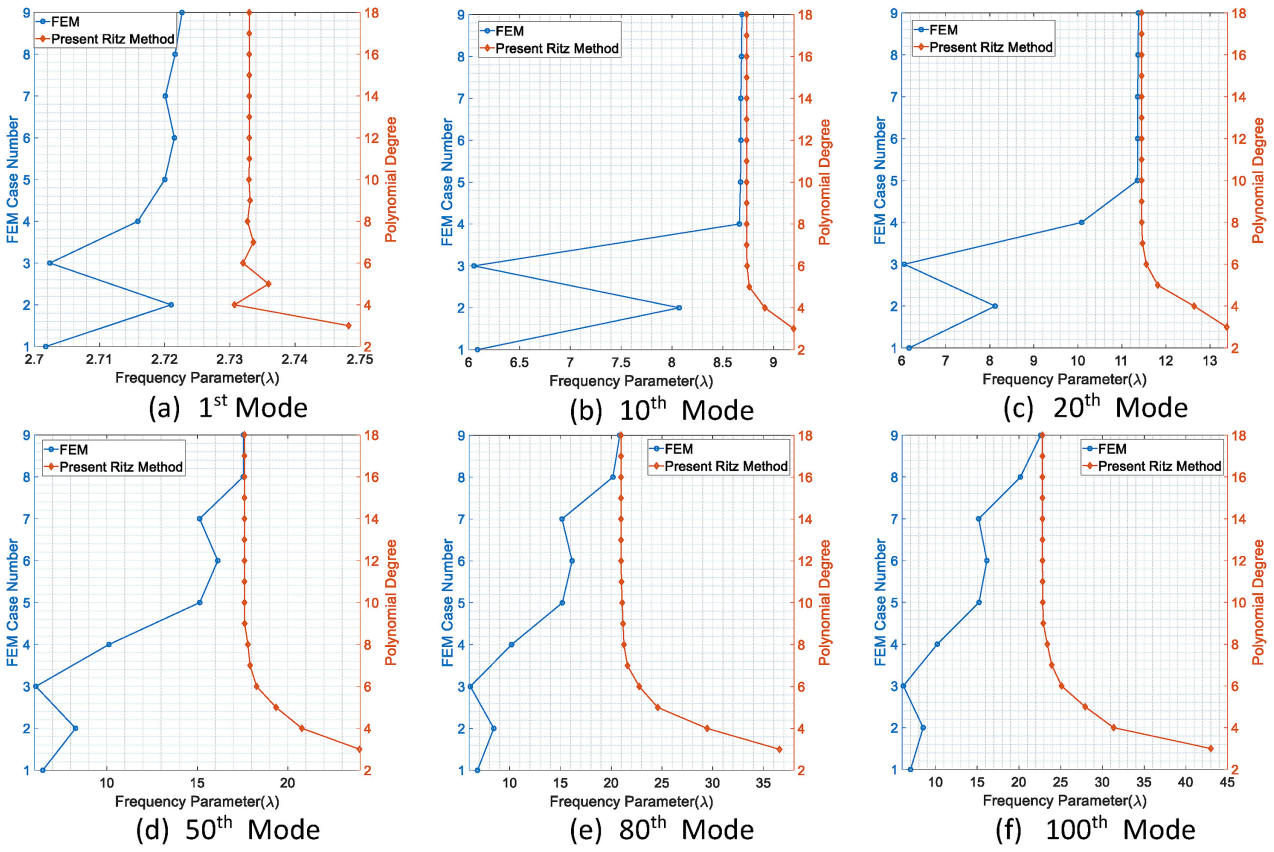

Figure 3.11: Convergence of frequencies from the FEM and the TSNDT Ritz method

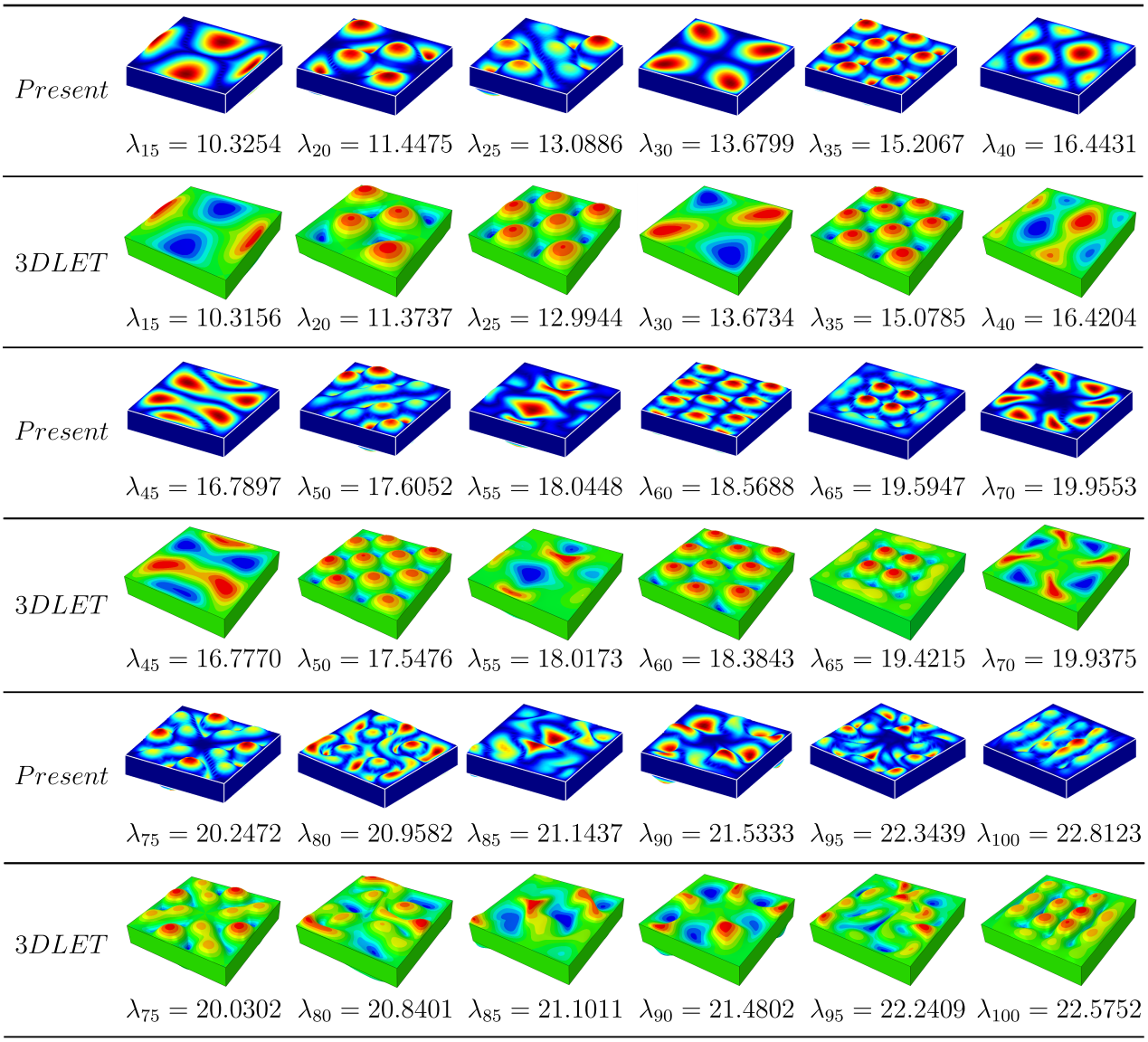

Figure 3.12: Comparison of higher-order mode shapes and frequencies computed using the TSNDT/Ritz and the FEM/ABAQUS

Bibliography

[1] Mace, B., Desmet, W., and Pluymers, B., 2013, "Mid-frequency methods in sound and vibration-part A," Journal of Sound and Vibration, **332**(8), pp. 1895 – 1896.

[2] Desmet, W., 2002, "Mid-frequency vibro-acoustic modelling: challenges and potential solutions," Proceedings of ISMA, **2**(2002).

[3] Leissa, A. W., 1973, "The free vibration of rectangular plates, J," Journal of Sound and Vibration, **31**(3), pp. 257–293.

[4] Mindlin, R. D., 1951, "Influence of rotatory inertia and shear on flexural motions of isotropic, elastic plates, J," Journal of Applied Mechanics, **18**, pp. 31–38.

[5] Kapania, R. K. and Raciti, S., 1989, "Recent Advances in analysis of laminated beams and plates Part I: shear effects and buckling," AIAA Journal, **27**(7), pp. 923–935.

[6] Batra, R. C., Vidoli, S., and Vestroni, F., 2002, "Plane wave solutions and modal analysis in higher order shear and normal deformable plate theories, J," Journal of Sound and Vibration, **257**(1), pp. 63–88.

[7] Liew, K. M., Pan, Z. Z., and Zhang, L. W., 2019, "An overview of layerwise theories for composite laminates and structures: development, numerical implementation and application," Composite Structures, **216**(1), pp. 240–259.

BIBLIOGRAPHY

[8] Carrera, E. and Brischetto, S., 2009, "A survey with numerical assessment of classical and refined theories for the analysis of sandwich plates, Appl," Applied Mechanics Reviews, **62**(1), p. 010803.

[9] Noor, A. K., Burton, W. S., and Bert, C. W., 1996, "Computational models for sandwich panels and shells, Appl," Applied Mechanics Reviews, **49**(3), pp. 155–199.

[10] Mindlin, R. C. and Medick, M. A., 1959, "Extensional vibrations of elastic plates, J," Journal of Applied Mechanics, **26**, pp. 145–151.

[11] Hanna, N. F. and Leissa, A. W., 1994, "A high order shear deformation theory for the vibration of thick plates, J," Journal of Sound and Vibration, **170**(4), pp. 545–555.

[12] Carrera, E., 1999, "A study of transverse normal stress effect on vibration of multilayered plates and shells, J," Journal of Sound and Vibration, **225**(5), pp. 803–829.

[13] Messina, A., 2001, "Two generalized higher order theories in free vibration studies of multilayered plates, J," Journal of Sound and Vibration, **242**(1), pp. 125–150.

[14] Batra, R. C. and Aimmanee, S., 2007, "Vibration of an incompressible isotropic linear elastic rectangular plate with a higher-order shear and normal deformable theory," Journal of Sound and Vibration, **307**(3), pp. 961–971.

[15] Batra, R. C. and Aimmanee, S., 2005, "Vibrations of thick isotropic plates with higher order shear and normal deformable plate theories," Computers & Structures, **83**(12), pp. 934–955.

[16] Soedel, W., 2004, *Vibrations of Shells and Plates, 3 ed.,*, CRC Press.

[17] Mindlin, R. D. and Yang, J., 2006, *An Introduction to the Mathematical Theory of Vibrations of Elastic Plates*, World Scientific.

BIBLIOGRAPHY

[18] Leissa, A. W. and Qatu, M. S., 2011, *Vibrations of Continuous Systems*, McGraw-Hill.

[19] Elishakoff, I., 2019, *Handbook on Timoshenko-Ehrenfest Beam and Uflyand-Mindlin Plate Theories, World Scientific*, World Scientific.

[20] Carrera, E., 2002, "Theories and finite elements for multilayered, anisotropic, composite plates and shells, Arch," Archives of Computational Methods in Engineering, **9**(2), pp. 87–140.

[21] Carrera, E., Cinefra, M., Petrolo, M., and Zappino, E., 2014, *Finite Element Analysis of Structures through Unified Formulation*, John Wiley & Sons.

[22] Demasi, L., 2008, "∞ 3 Hierarchy plate theories for thick and thin composite plates: the generalized unified formulation," Struct., **84**(3), pp. 256–270.

[23] Demasi, L., 2009, "∞ 6 mixed plate theories based on the generalized unified formulation," Part IV: Zig-zag theories, Compos. Struct., **87**(3), pp. 195–205.

[24] Demasi, L., 2009, "∞ 6 mixed plate theories based on the generalized unified formulation.: Part II: layerwise theories," Composite Structures, **87**(1), pp. 12–22.

[25] Demasi, L., 2009, "∞ 6 mixed plate theories based on the generalized unified formulation Part I: governing equations," Composite Structures, **87**(1), pp. 1–11.

[26] Demasi, L., 2009, "∞ 6 mixed plate theories based on the generalized unified formulation Part III: advanced mixed high order shear deformation theories," Composite Structures, **87**(3), pp. 183–194.

[27] Demasi, L., 2009, "∞6 mixed plate theories based on the generalized unified formulation Part V: results," Composite Structures, **88**(1), pp. 1–16.

[28] Vel, S. S. and Batra, R. C., 2000, "The generalized plane strain deformations of thick anisotropic composite laminated plates, Int," International Journal of Solids and Structures, **37**(5), pp. 715–733.

[29] Boscolo, M., "Analytical solution for free vibration analysis of composite plates with layer-wise displacement assumptions," Composite Structures, **100**(1), pp. 493–510.

[30] Boscolo, M. and Banerjee, J., "Layer-wise dynamic stiffness solution for free vibration analysis of laminated composite plates," Journal of Sound and Vibration, **333**(1), pp. 200–227.

[31] Dozio, L., 2014, "Exact vibration solutions for cross-ply laminated plates with two opposite edges simply supported using refined theories of variable order," Journal of Sound and Vibration, **333**(8), pp. 2347–2359.

[32] Fazzolari, F. A. and Carrera, E., 2011, "Advanced variable kinematics Ritz and Galerkin formulations for accurate buckling and vibration analysis of anisotropic laminated composite plates," Composite Structures, **94**(1), pp. 50–67.

[33] Fazzolari, F. A., 2016, "Quasi-3D beam models for the computation of eigenfrequencies of functionally graded beams with arbitrary boundary conditions, Compos," CO, **154**(1), pp. 239–255.

[34] Marco, P. and Carrera, E., 2020, "Methods and guidelines for the choice of shell theories," Acta Mech., **231**(1), p. 395–43.

[35] Batra, R. C. and Aimmanee, S., 2003, "Missing frequencies in previous exact solutions of free vibrations of simply supported rectangular plates," Journal of Sound and Vibration, **265**(1), pp. 887–896.

BIBLIOGRAPHY

[36] Batra, R. C., Qian, L. F., and Chen, L. M., 2004, "Natural frequencies of thick square plates made of orthotropic, trigonal, monoclinic, hexagonal and triclinic materials, J," Sound Vib., **270**(4), pp. 1074–1086.

[37] Chattopadhyay, A. P. and Batra, R. C., 2019, "Free and forced vibrations of monolithic and composite rectangular plates with interior constrained points," Journal of Vibration and Acoustics, **141**(1), p. 011018.

[38] Qian, L. F., Batra, R. C., and Chen, L. M., 2003, "Free and forced vibrations of thick rectangular plates using higher-order shear and normal deformable plate theory and meshless Petrov-Galerkin (MLPG) method, Comput," Computer Modeling in Engineering and Sciences, **4**(5), pp. 519–534.

[39] Meirovitch, L. and Kwak, M. K., 1990, "Convergence of the classical Rayleigh-Ritz method and the finite element method," AIAA Journal, **28**(8), pp. 1509–1516.

[40] Wei, G. W., Zhao, Y. B., and Xiang, Y., 2002, "A novel approach for the analysis of high-frequency vibrations," Journal of Sound and Vibration, **257**(2), pp. 207–246.

[41] Deckers, E., Atak, O., Coox, L., D'Amico, R., Devriendt, H., Jonckheere, S., Koo, K., Pluymers, B., Vandepitte, D., and Desmet, W., 2014, "The wave based method: an overview of 15 years of research," Wave Motion, **51**(4), pp. 550–565.

[42] Langley, R. S. and Cordioli, J. A., 2009, "Hybrid deterministic-statistical analysis of vibro-acoustic systems with domain couplings on statistical components, J," Journal of Sound and Vibration, **321**(3), pp. 893–912.

[43] Filoche, M. and Mayboroda, S., 2009, "Strong localization induced by one clamped point in thin plate vibrations, Phys," Physical Review Letters, **103**(1), p. 25430.

[44] Sharma, D., Gupta, S., and Batra, R., 2002, "Mode localization in composite laminates," Composite Structures, **94**(8), pp. 2620–2631.

[45] Paik, S., Gupta, S., and Batra, R., 2015, "Localization of buckling modes in plates and laminates," Composite Structures, **120**(1), pp. 79–89.

[46] Leissa, A. and Zhang, Z. D., 1983, "On the three-dimensional vibrations of the cantilevered rectangular parallelepiped," The Journal of the Acoustical Society of America, **73**.

[47] Liew, K. M., Hung, K. C., and Lim, M. K., 1993, "A continuum three-dimensional vibration analysis of thick rectangular plates," International Journal of Solids and Structures, **30**(24), pp. 3357–3379.

[48] Liew, K. M., Hung, K. C., and Lim, M. K., 1995, "Three-dimensional vibration of rectangular plates: effects of thickness and edge constraints," Journal of Sound and Vibration, **182**(5), pp. 709–727.

[49] Zhou, D., Cheung, Y. K., Au, F., and Lo, S. H., 2002, "Three-dimensional vibration analysis of thick rectangular plates using Chebyshev polynomial and Ritz method," International Journal of Solids and Structures, **39**(26), pp. 6339–6353.

[50] Alanbay, B. and Kapania, R. K., 2018, "On the use of classical Jacobi orthogonal polynomials in the Ritz method," AIAA/ASCE/AHS/ASC Structures, Structural Dynamics, and Materials Conference.

[51] Alanbay, B., Singh, K., and Kapania, R. K., 2020, "Vibration of curvilinearly stiffened plates using Ritz method with orthogonal Jacobi polynomials, J," Journal of Vibration and Acoustics, **142**(1), p. 011009.

BIBLIOGRAPHY

[52] Nabanita, D. and Verma, Y., 2017, "Accurate Eigenvector-based generation and computational insights of Mindlin's plate modeshapes for twin frequencies," International Journal of Mechanical Sciences, **123**(1), pp. 64–73.

[53] Qin, Z. and Batra, R. C., 2009, "Local slamming impact of sandwich composite hulls," International Journal of Solids and Structures, **46**(10), pp. 2011–2035.

[54] Szego, G., 1967, *Orthogonal Polynomials*, American Mathematical Society and Providence, Providence, Rhode Island.

[55] Hale, N. and Townsend, A., 2013, "Fast and accurate computation of Gauss-Legendre and Gauss-Jacobi quadrature nodes and weights, SIAM J," SIAM Journal on Scientific Computing, **35**(2), pp. A652–A674.

[56] Srinivas, S., Rao, C. J., and Rao, A. K., 1970, "An exact analysis for vibration of simply-supported homogeneous and laminated thick rectangular plates, J," Journal of Sound and Vibration, **12**(2), pp. 187–199.

[57] Liew, K. M., Hung, K. C., and Lim, M. K., 1995, "Free vibration studies on stress-free three-dimensional elastic solids, J," Applied Mechanics Reviews, **62**(1), pp. 159–165.

[58] Yuan, L. S. and Batra, R. C., 2019, "Vibrations of an incompressible linearly elastic plate using discontinuous finite element basis functions for pressure, J," Journal of Vibration and Acoustics, **141**(1), p. 051016.

Chapter 4

Free Vibration of Thick Quadrilateral Laminates Using TSNDT

The contents of this chapter have appeared in AIAA Journal. [1]

[1] **Alanbay, B.**, Kapania, R. K., and Batra, R. C., 2020, "Free Vibration of Thick Quadrilateral Laminates Using Third-Order Shear-Normal Deformation Theory," AIAA Journal, 58(10), p. 4580-4594.

4.1 Abstract

Free vibrations of thick and skew quadrilateral laminates have been analyzed by using the Ritz method and a third-order shear and normal deformable plate theory (TSNDT) that does not require a shear-correction factor. The weighted orthogonal Jacobi polynomials are employed as basis functions that exactly satisfy essential boundary conditions at the plate edges. An in-house-developed software is first verified by comparing computed frequencies with those either available in the literature or found by using the three-dimensional linear elasticity-theory-based finite-element-based commercial software ABAQUS. The method is applied first to find the lowest few (six in most examples) frequencies of isotropic cantilever plates of different skew angles and thickness-to-side length ratios. Subsequently, natural frequencies of laminated composite plates for various skew angles, thickness-to-side ratios, numbers of layers, and stacking sequences are compared with those obtained from converged solutions using either shell or brick elements in ABAQUS. It is demonstrated that the TSNDT/Ritz method provides highly accurate frequencies. Three-dimensional mode shapes are presented for a better understanding of the dynamic behavior of skew quadrilateral laminates.

4.2 Introduction

There is a significant interest in studying the dynamic behavior of isotropic and laminated quadrilateral plates. Robust techniques for accurately predicting their dynamic behavior are needed in many engineering fields, including the design of control surfaces in aircraft and missiles. An understanding of the vibration characteristics of these structures is crucial for efficiently developing their lightweight and durable designs. An often-used tool to accomplish this is a commercial finite element software that employs a first-order shear de-

formation theory (FSDT) and provides reasonably accurate frequencies for thin plates. For finding frequencies and mode shapes of thick and skew quadrilateral plates/laminates, we have developed a software using a third-order shear and normal deformable plate theory (TSNDT), the Ritz method, and the weighted orthogonal Jacobi polynomials as basis functions that is robust and provides accurate values of at least the lowest six frequencies and the corresponding mode shapes.

For skew polygonal plates, it is an arduous task to solve the threedimensional linear elasticity theory (3D-LET) equations for free vibrations. Thus, most analyses employ a plate theory. The quality of the solution depends upon simplifying kinematic assumptions in developing the plate theory such as the classical (or the Love–Kirchhoff) plate theory (CPT) [1], an FSDT [2, 3], a higher-order shear deformation theory (HSDT), and a higher-order shear and normal deformable theory (HSNDT). While the CPT neglects both transverse shear and normal deformations and requires a shear correction factor, an FSDT and an HSDT consider transverse shear deformations and rotary inertia, and they generally do not need a shear-correction factor. An HSNDT also considers transverse normal deformations and does not need a shear-correction factor. These and other plate theories are reviewed in Refs [4, 5, 6, 7], as well as in books by Soedel [8], Mindlin [9], Leissa and Qatu [10], and Elishakoff [11].

Free vibrations of skew quadrilateral plates have been reviewed by Liew and Wang [12] and McGee [13]. McGee and Leissa [14] and and Zhou et al. [15] have used the Ritz method and the 3D-LET equations to study free vibrations of thick cantilever plates of varying skew angles. Whereas McGee and Leissa [14] expressed the three displacement components in terms of polynomial functions of the three spatial coordinates, Zhou et al. [15] expressed them in terms of either algebraic or Chebyshev polynomials.

Lakshminarayana et al. [16] and Lee and Lee [17] examined free vibrations of a swept

thin symmetric laminate by using an FSDT and the finite element method (FEM). However, Kapania and Singhvi [18] employed the CPT in conjunction with the Ritz method to analyze the plate's vibrations explored in Refs. [16, 17]. Kapania and Lovejoy [19] extended the work reported in Ref. [18] by including transverse shear effects and using an FSDT. Gurses et al. [20] analyzed similar problems by employing a discrete singular convolution technique and an FSDT.

Carrerra [21] and Batra and Vidoli [22] have proposed K^th-order plate theories that account for transverse shear and normal deformations. By expanding the displacement and transverse stress fields in the thickness coordinate using polynomial expansions, Carrerra [21] provided a compact formulation [namely, the Carrera unified formulation (CUF)] for plate theories. By extending the CUF, Demasi [23, 24, 25, 26, 27, 28] presented a generalized unified formulation in which the three displacements and transverse stresses are approximated using different order polynomial expansions in the thickness coordinate; and the equivalent single layer, the layerwise, the mixed higher-order shear deformation, and the zigzag theories are captured. Batra and Vidoli [22] deduced both mixed and compatible plate theories; the former takes stresses and displacements as unknowns, and the latter only takes displacements and derives stresses from the plate theory displacements and constitutive relations. In Batra and Vidoli's mixed plate theory, the transverse shear and normal stresses are expanded in terms of polynomials of degree $(K + 2)$, whereas the three displacements and the in-plane stresses are expressed in terms of polynomials of degree K in the thickness coordinate. Batra et al. [5] have used a variable-order shear and normal deformable theory to study wave propagation and free vibrations of orthotropic plates.

Boscolo [29] and Boscolo and Banerjee [30] have used a CUF-based layerwise theory, the Levy analysis [29], and the dynamic stiffness method [30] to compute the lowest 12 natural frequencies of crossply laminates with a pair of simply supported edges. Dozio [31] employed

the CUF and the state-space method to find the first five natural frequencies of cross-ply laminates, and Fazzolari and Carrera [32] employed the Ritz and the Galerkin formulations to compute the first six natural frequencies of simply supported angle-ply laminates. They used trigonometric functions in the Ritz method. Fazzolari [33] used refined variable kinematics in quasi-three dimensional beam theories, the principle of virtual displacements to derive governing equations, and the Ritz trial functions orthonormalized by the Gram–Schmidt process to compute up to 10 lowest frequencies of beams under arbitrary boundary conditions. Even though the CUF is an efficient way to analyze plate deformations, it requires several iterations to determine the least degree of complete polynomial basis functions in each direction [34].

The effectiveness and accuracy of the FEM in solving the TSNDT equations to analyze dynamic characteristics of plates have been demonstrated by Batra and Aimmanee [35, 36] for thick isotropic and incompressible isotropic linear elastic rectangular plates, Qian and Batra [37] for designing bidirectionally graded plates for optimum natural frequencies, Chattopadhyay and Batra [38] for monolithic and composite rectangular plates with interior constrained points, and Yuan and Batra [39] for incompressible linearly elastic plates considering hydrostatic pressure as a variable by using discontinuous finite element basis functions. Also, Qian et al. [40] used the meshless local Petrov–Galerkin method to solve TSNDT equations for analyzing free and forced vibrations of thick rectangular plates.

The FEM is a widely used, well-established, and general numerical technique for solving initial boundary value problems. A key difference between the Ritz method and the FEM is that in the former, the basis functions are defined over the entire domain and satisfy all essential boundary conditions. In the latter, the basis functions are usually polynomials that are defined piecewise over the domain,their compact support is a small part of the domain, and essential boundary conditions can be imposed after the global stiffness matrix and the

global force vector have been assembled. Meirovitch and Kwak [41] attribute the enormous success of the FEM to two main reasons:

1. It can solve nonlinear problems for bodies of complex geometries.
2. The low-order complete polynomial basis functions with compact support give matrices of small bandwidth.

They also stated that the Ritz method can yield superior accuracy for the same number of degrees of freedom (DOFs) as those in the FEM. Furthermore, the convergence of high frequencies computed with the FEM requires a large number of DOFs that increases the total CPU time.

The novelty of the present work is in demonstrating that the use of weighted orthogonal Jacobi polynomials as basis functions in the Ritz method to solve the TSNDT equations for the lowest six frequencies of a skew quadrilateral laminate with either one or all four edges clamped is computationally very efficient. The computed frequencies and the corresponding mode shapes are very close to those found using the 3-D LET and the finite element (FE) commercial software, ABAQUS. Furthermore, by varying the skew angle, the number of layers, and the thickness-to side ratio, we examine how the present results and those from the FSDT-based shell elements S4 and S4R (in ABAQUS terminology) compare with those computed using the 3D-LET equations solved using 20-node brick elements (C3D20) in ABAQUS. It is found that for a thickness-to-side ratio of 0.2, natural frequencies for a clamped two-layered skew plate computed using the ABAQUS shell elements have errors of 11%. Moreover, the accuracy of the FSDT-based frequencies worsens with an increase in the plate skew angle and thickness-to-side ratio, as well as a decrease in the number of layers. However, the present approach provides accurate frequencies. It is well known that the accuracy and rate of convergence as well as the efficiency of the computational algorithm

strongly depend upon the choice of basis functions. We note that the orthogonality of the weighted Jacobi polynomials used here simplifies evaluation of many integrals, and it gives a mass matrix comprising diagonal submatrices that make the computational algorithm quite efficient; for example, see the works of Alanbay and Kapania [42] and Alanbay et al. [43] who studied free vibrations of stiffened thin plates using the CPT and the FSDT, and see the works of Alanbay et al. [44, 45] who studied the free vibrations of thick isotropic plates and sandwich structures. We note that basis functions generated by taking the tensor product of eigenfunctions of free vibrations of a beam are also orthogonal; and they have been used for finding frequencies, among others, by Datta and Verma [46] for a monolithic plate, and by Qin and Batra [47] for a sandwich plate.

The rest of the paper is organized as follows. Section II describes the problem formulation. In Sec. III, the accuracy of the present method is established by comparing the obtained results with those available in the literature for isotropic thick skew plates, for thin cantilever skew laminates, and for clamped thin skew laminates. Subsequently, parametric studies considering various skew angles, numbers of layers, and thickness-to-side ratios are presented to delineate their effects on the frequencies computed with the present method, the FSDT-based shell elements (S4 and S4R), and with 20-node brick elements (C3D20) in ABAQUS. These comparisons establish when to use the FSDT-based shell elements in ABAQUS for studying free vibrations of skew laminates

4.3 Formulation of the Problem

Figure 4.1 shows a schematic sketch of a quadrilateral laminate of uniform thickness with corner points 1–4 on its midsurface and the rectangular Cartesian coordinate axes used to describe its infinitesimal deformations from the stress-free initial configuration. We assume that the plane $x_3 = 0$ coincides with the plate midsurface shown with dashed lines; the origin

of the coordinate axes coincides with the corner point 1; and the material of each layer is linearly elastic, orthotropic, and homogeneous.

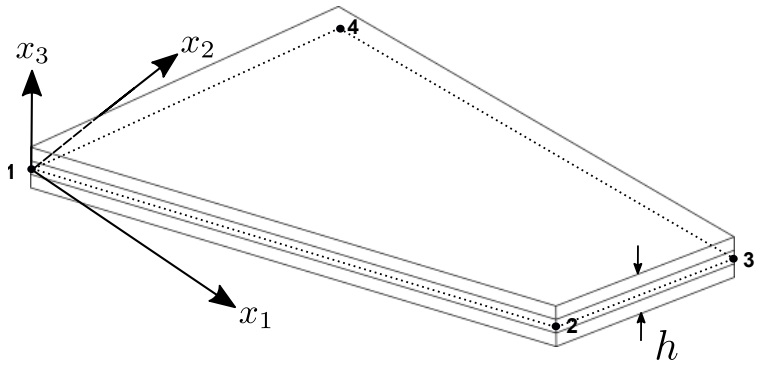

Figure 4.1: Schematic sketch of a quadrilateral laminated plate

4.3.1 Brief Review of the TSNDT

We use a TSNDT to analyze free vibrations of a plate (e.g., see the work of Batra and Vidoli [22]) and express each component u_i, of the displacement field as a complete polynomial of degree 3 in the thickness (or the x_3) coordinate. That is,

$$u_i\left(x_1, x_2, x_3, t\right) = \left(x_3\right)^j u_{ij}\left(x_1, x_2, t\right), \qquad i = 1, 2, 3 \ \textit{and} \ j = 0, 1, 2, 3 \tag{4.1}$$

where t denotes time. Eq. 4.1 implies that both transverse shear and normal deformations are considered. In this paper, a repeated index (unless noted otherwise) implies summation over the range of the index. Components of the infinitesimal strain tensor are related to displacement gradients as

$$\varepsilon_{ij} = \frac{1}{2}\left(u_{i,j} + u_{j,i}\right) \tag{4.2}$$

where u_{ij} equals the partial derivative of u_i with respect to x_j. Substituting for displacements from Eq. 4.1 into Eq. 4.2, we get

$$\boldsymbol{\epsilon} = \boldsymbol{Z}_i\left(x_3\right)\ \boldsymbol{L}\,\boldsymbol{d}_i\left(x_1, x_2\right), \qquad i = 0, 1, 2, 3 \tag{4.3}$$

where

$$\boldsymbol{\epsilon} = \left[\epsilon_{11}\ \ \epsilon_{22}\ \ \epsilon_{33}\ \ 2\epsilon_{23}\ \ 2\epsilon_{13}\ \ 2\epsilon_{12}\right]^T \tag{4.4}$$

$$\mathbf{d}_i = \left[u_{1i}\ \ u_{2i}\ \ u_{3i}\right]^T, \qquad i = 0, 1, 2, 3 \tag{4.5}$$

$$\mathbf{L} = \begin{bmatrix} \dfrac{\partial}{\partial x_1} & 0 & 0 & 0 & 0 & \dfrac{\partial}{\partial x_2} & 1 & 0 \\ 0 & \dfrac{\partial}{\partial x_2} & 0 & 0 & 0 & \dfrac{\partial}{\partial x_1} & 0 & 1 \\ 0 & 0 & 1 & \dfrac{\partial}{\partial x_2} & \dfrac{\partial}{\partial x_1} & 0 & 0 & 0 \end{bmatrix}^T,$$

$$\mathbf{Z}_i = \begin{bmatrix} (x_3)^i & 0 & 0 & 0 & 0 & 0 & 0 & 0 \\ 0 & (x_3)^i & 0 & 0 & 0 & 0 & 0 & 0 \\ 0 & 0 & i\,(x_3)^{i-1} & 0 & 0 & 0 & 0 & 0 \\ 0 & 0 & 0 & (x_3)^i & 0 & 0 & 0 & i\,(x_3)^{i-1} \\ 0 & 0 & 0 & 0 & (x_3)^i & 0 & i\,(x_3)^{i-1} & 0 \\ 0 & 0 & 0 & 0 & 0 & (x_3)^i & 0 & 0 \end{bmatrix} \tag{4.6}$$

We note that the vector $\boldsymbol{d_i}$ of generalized displacements is defined on the plate midsurface, $\boldsymbol{L}$ is the matrix of differential operators, and elements of the matrix $\boldsymbol{Z_i}$ contain powers of x_3.

For a linearly elastic material, the Cauchy stress tensor $\boldsymbol{\sigma}$, is related to the infinitesimal strain tensor by the constitutive relation

$$\sigma_{ij} = C_{ijmn}\epsilon_{mn} \quad i, j, m, n = 1, 2, 3; \quad C_{ijmn} = C_{mnij} = C_{jimn} \tag{4.7}$$

where $\boldsymbol{C}$ is a fourth-order elasticity tensor that has 2, 5, 9, and 21 independent components for an isotropic, transversely isotropic, orthotropic, and anisotropic material, respectively. For a homogeneous plate, elasticities have the same values at all material points.

We assume that all interior angles of a quadrilateral plate are between 15 and 165 deg. We use the one-to-one and onto transformations

$$x_1 = \sum_{i=1}^{4} N_i\left(\xi_1, \xi_2\right) x_1^i, \qquad x_2 = \sum_{i=1}^{4} N_i\left(\xi_1, \xi_2\right) x_2^i \tag{4.8}$$

between the quadrilateral plate midsurface in the (x_1, x_2) coordinate system and the 2×2 square in the (ξ_1, ξ_2) coordinate system as illustrated in Figure 4.2. In Eq. 4.8, (x_1^i, x_2^i) are coordinates of the corner i of the quadrilateral plate, and the function Ni is given by

$$\begin{aligned} N_1(\xi_1, \xi_2) &= \frac{1}{4}(1-\xi_1)(1-\xi_2), & N_2(\xi_1, \xi_2) &= \frac{1}{4}(1+\xi_1)(1-\xi_2) \\ N_3(\xi_1, \xi_2) &= \frac{1}{4}(1+\xi_1)(1+\xi_2), & N_4(\xi_1, \xi_2) &= \frac{1}{4}(1-\xi_1)(1+\xi_2) \end{aligned} \tag{4.9}$$

The mapping [Eq. 4.8] is one-to-one and has a differentiable inverse, provided that the determinant of the Jacobian matrix $\boldsymbol{J}$, defined by Eq. 4.11, is nonzero everywhere in the domain.

The derivatives of a function with respect to ξ_1 and ξ_1 are related to those with respect to x_1 and x_2 as

$$\begin{Bmatrix} \phi_{,\xi_1} \\ \phi_{,\xi_2} \end{Bmatrix} = \mathbf{J} \begin{Bmatrix} \phi_{,x_1} \\ \phi_{,x_2} \end{Bmatrix} \tag{4.10}$$

where

$$\mathbf{J} = \begin{bmatrix} x_{1,\xi_1} & x_{2,\xi_1} \\ x_{1,\xi_2} & x_{2,\xi_2} \end{bmatrix} \tag{4.11}$$

Alternatively,

$$\begin{Bmatrix} \phi_{,x_1} \\ \phi_{,x_2} \end{Bmatrix} = \underbrace{\begin{bmatrix} \Gamma_{11} & \Gamma_{12} \\ \Gamma_{21} & \Gamma_{22} \end{bmatrix}}_{\mathbf{\Gamma}} \begin{Bmatrix} \phi_{,\xi_1} \\ \phi_{,\xi_2} \end{Bmatrix} \quad \text{where} \quad \mathbf{\Gamma} = \mathbf{J}^{-1} = \frac{1}{|\mathbf{J}|} \begin{bmatrix} J_{22} & -J_{12} \\ -J_{21} & J_{11} \end{bmatrix} \tag{4.12}$$

Using Eq. 4.11, we write Eq. 4.3 as

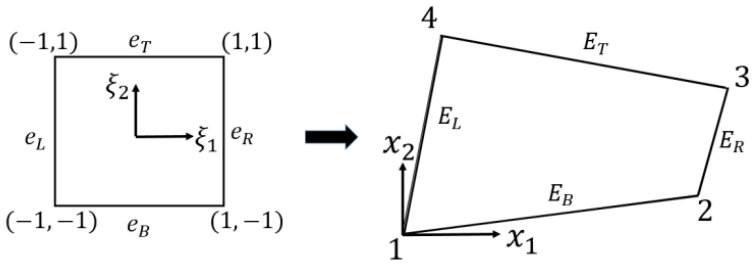

Figure 4.2: Schematic sketch of a quadrilateral laminated plate

$$\boldsymbol{\epsilon} = \mathbf{Z_i} \begin{bmatrix} \Gamma_{11} & \Gamma_{12} & 0 & 0 & 0 & 0 & 0 & 0 & 0 \\ 0 & 0 & \Gamma_{21} & \Gamma_{22} & 0 & 0 & 0 & 0 & 0 \\ 0 & 0 & 0 & 0 & 0 & 0 & 0 & 0 & 1 \\ \Gamma_{21} & \Gamma_{22} & \Gamma_{11} & \Gamma_{12} & 0 & 0 & 0 & 0 & 0 \\ 0 & 0 & 0 & 0 & \Gamma_{11} & \Gamma_{12} & 0 & 0 & 0 \\ 0 & 0 & 0 & 0 & \Gamma_{21} & \Gamma_{22} & 0 & 0 & 0 \\ 0 & 0 & 0 & 0 & 0 & 0 & 1 & 0 & 0 \\ 0 & 0 & 0 & 0 & 0 & 0 & 0 & 1 & 0 \end{bmatrix} \begin{Bmatrix} u_{1i,\xi_1} \\ u_{1i,\xi_2} \\ u_{2i,\xi_1} \\ u_{2i,\xi_2} \\ u_{3i,\xi_1} \\ u_{3i,\xi_2} \\ u_{1i} \\ u_{2i} \\ u_{3i} \end{Bmatrix} = \mathbf{Z_i}\ \mathbf{T}\ \bar{\mathbf{d}}_\mathbf{i} \tag{4.13}$$

Here, the matrix $\boldsymbol{T}$ consists of elements of the inverse Jacobian matrix that relate derivatives of a displacement component with respect to the natural coordinates to those with respect

to the global coordinates, and $\boldsymbol{d_i}$ is the vector of the generalized displacements and their derivatives with respect to ξ_1 and ξ_2.

4.3.2 Ritz Method

At any time t, the Hamiltonian is given by

$$\Pi = U - T = \sum_{k=1}^{p} \frac{1}{2} \int_{\bar{V}_k} \left(\boldsymbol{\varepsilon}^T \boldsymbol{\sigma}^k - \rho^k \, \dot{\boldsymbol{u}}^T \dot{\boldsymbol{u}} \right) d\bar{V}_k \tag{4.14}$$

where

$$\dot{\boldsymbol{u}} = \begin{Bmatrix} u_{1,t} \\ u_{2,t} \\ u_{3,t} \end{Bmatrix} = \begin{bmatrix} (x_3)^i & 0 & 0 \\ 0 & (x_3)^i & 0 \\ 0 & 0 & (x_3)^i \end{bmatrix} \begin{Bmatrix} u_{1i,t} \\ u_{2i,t} \\ u_{3i,t} \end{Bmatrix} = \mathbf{Z_i^m} \dot{\mathbf{d}}_\mathbf{i}, \qquad i = 0, 1, 2, 3 \tag{4.15}$$

A dot superimposed upon a variable indicates its partial derivative with respect to time t, $\bar{V}_k$ is the region occupied by the k^{th} lamina, and ρ_k is the mass density. Variables in Eq. 4.14 are expressed as functions of ξ_1, ξ_2 by using the transformation [Eq. 4.8]. Thus, the integration is on the 2×2 square domain. After having solved for displacements as functions of (ξ_1, ξ_2) displacements at a point (x_1, x_2) are found by determining the point in the ξ_1, ξ_2-plane into which the point (x_1, x_2) is mapped by the inverse of the transformation given in Eq. 4.8 or equivalently solving Eq. 4.8 for ξ_1, ξ_2.

For studying free vibrations of a plate, we assume that its displacements are harmonic in time with frequency ω. Substituting Eqs. 4.7, 4.12, and 4.14 into Eq. 4.13 and taking the variation in the energy functional with respect to the unknown generalized DOFs lead to the

following eigenvalue problem:

$$\left[\mathbf{K} - \omega^2\,\mathbf{M}\right]\{\mathbf{d}\} = \{\mathbf{0}\} \tag{4.16}$$

In Eq. 4.15, $\boldsymbol{K}$ is the global stiffness matrix, $\boldsymbol{M}$ is the global mass matrix, and $\{\boldsymbol{d}\}$ is the eigenvector. The global stiffness and mass matrices,$\boldsymbol{K}$ and $\boldsymbol{M}$, have the following expressions:

$$\mathbf{K} = \begin{bmatrix} \mathbf{K_{00}} & \frac{1}{2}\left(\mathbf{K_{01}} + \mathbf{K_{10}}^T\right) & \frac{1}{2}\left(\mathbf{K_{02}} + \mathbf{K_{20}}^T\right) & \frac{1}{2}\left(\mathbf{K_{03}} + \mathbf{K_{30}}^T\right) \\ \frac{1}{2}\left(\mathbf{K_{10}} + \mathbf{K_{01}}^T\right) & \mathbf{K_{11}} & \frac{1}{2}\left(\mathbf{K_{12}} + \mathbf{K_{21}}^T\right) & \frac{1}{2}\left(\mathbf{K_{13}} + \mathbf{K_{31}}^T\right) \\ \frac{1}{2}\left(\mathbf{K_{20}} + \mathbf{K_{02}}^T\right) & \frac{1}{2}\left(\mathbf{K_{21}} + \mathbf{K_{12}}^T\right) & \mathbf{K_{22}} & \frac{1}{2}\left(\mathbf{K_{23}} + \mathbf{K_{32}}^T\right) \\ \frac{1}{2}\left(\mathbf{K_{30}} + \mathbf{K_{03}}^T\right) & \frac{1}{2}\left(\mathbf{K_{31}} + \mathbf{K_{13}}^T\right) & \frac{1}{2}\left(\mathbf{K_{32}} + \mathbf{K_{23}}^T\right) & \mathbf{K_{33}} \end{bmatrix} \tag{4.17}$$

$$\mathbf{M} = \begin{bmatrix} \mathbf{M_{00}} & \frac{1}{2}\left(\mathbf{M_{01}} + \mathbf{M_{10}}^T\right) & \frac{1}{2}\left(\mathbf{M_{02}} + \mathbf{M_{20}}^T\right) & \frac{1}{2}\left(\mathbf{M_{03}} + \mathbf{M_{30}}^T\right) \\ \frac{1}{2}\left(\mathbf{M_{10}} + \mathbf{M_{01}}^T\right) & \mathbf{M_{11}} & \frac{1}{2}\left(\mathbf{M_{12}} + \mathbf{M_{21}}^T\right) & \frac{1}{2}\left(\mathbf{M_{13}} + \mathbf{M_{31}}^T\right) \\ \frac{1}{2}\left(\mathbf{M_{20}} + \mathbf{M_{02}}^T\right) & \frac{1}{2}\left(\mathbf{M_{21}} + \mathbf{M_{12}}^T\right) & \mathbf{M_{22}} & \frac{1}{2}\left(\mathbf{M_{23}} + \mathbf{M_{32}}^T\right) \\ \frac{1}{2}\left(\mathbf{M_{30}} + \mathbf{M_{03}}^T\right) & \frac{1}{2}\left(\mathbf{M_{31}} + \mathbf{M_{13}}^T\right) & \frac{1}{2}\left(\mathbf{M_{32}} + \mathbf{M_{23}}^T\right) & \mathbf{M_{33}} \end{bmatrix} \tag{4.18}$$

where

$$\mathbf{K_{ij}} = \int_{-1}^{1}\int_{-1}^{1} \bar{\mathbf{B}}_\mathbf{i}^T\,\mathbf{T}^T\,\mathbf{D_{ij}}\,\mathbf{T}\,\bar{\mathbf{B}}_\mathbf{j}\;|\mathbf{J}|\,d\xi_1 d\xi_2, \qquad i,j = 0,1,2,3 \tag{4.19}$$

$$\boldsymbol{M_{ij}} = \int_{-1}^{1}\int_{-1}^{1} \boldsymbol{H_i}^T \boldsymbol{m_{ij}} \boldsymbol{H_j} d\xi_1 d\xi_2, \qquad i,j = 0,1,2,3 \tag{4.20}$$

$$\bar{\mathbf{B}}_{\mathbf{i}} = \begin{bmatrix} \boldsymbol{\Phi}_{\mathbf{1}i,\boldsymbol{\xi}_1} & \boldsymbol{\Phi}_{\mathbf{1}i,\boldsymbol{\xi}_2} & 0 & 0 & 0 & 0 & \boldsymbol{\Phi}_{\mathbf{1}i} & 0 & 0 \\ 0 & 0 & \boldsymbol{\Phi}_{\mathbf{2}i,\boldsymbol{\xi}_1} & \boldsymbol{\Phi}_{\mathbf{2}i,\boldsymbol{\xi}_2} & 0 & 0 & 0 & \boldsymbol{\Phi}_{\mathbf{2}i} & 0 \\ 0 & 0 & 0 & 0 & \boldsymbol{\Phi}_{\mathbf{3}i,\boldsymbol{\xi}_1} & \boldsymbol{\Phi}_{\mathbf{3}i,\boldsymbol{\xi}_2} & 0 & 0 & \boldsymbol{\Phi}_{\mathbf{3}i} \end{bmatrix}^T \tag{4.21}$$

$$\boldsymbol{D_{ij}} = \sum_{k=1}^{p} \int_0^{h_k} \boldsymbol{Z_i}^T \boldsymbol{C}^k \boldsymbol{Z_j} dx_3, \quad \boldsymbol{m_{ij}} = \sum_{k=1}^{p} \int_{x_3^{(k)}}^{x_3^{(k+1)}} \rho^k \left(\boldsymbol{Z_i^m}\right)^T \boldsymbol{Z_j^m} dx_3, \quad i,j = 0,1,2,3 \tag{4.22}$$

$$\boldsymbol{H_i} = \begin{bmatrix} \boldsymbol{\Phi}_{\mathbf{1}i} & 0 & 0 \\ 0 & \boldsymbol{\Phi}_{\mathbf{2}i} & 0 \\ 0 & 0 & \boldsymbol{\Phi}_{\mathbf{3}i} \end{bmatrix} \tag{4.23}$$

The integrals are evaluated by using a high-order Gauss quadrature rule that depends upon the degree of polynomials of the integrands, e.g., see the work of Hale and Townsend [48]. Since the Jacobian of the mapping given by Eq. 4.8 has different values at the Gauss points, the mass and the stiffness matrices are non-diagonal.

We approximate u_{ij} as

$$u_{ij}(\xi_1,\xi_2) = \sum_{k=0}^{n_1}\sum_{l=0}^{n_2} T_k^{ij}(\xi_1)\, T_l^{ij}(\xi_2)\; q_{kl}^{ij} = \boldsymbol{\Phi}_{\mathbf{ij}}^{\mathbf{T}}\, \mathbf{q_{ij}}, \quad i = 1,2,3 \quad and \quad j = 0,1,2,3 \tag{4.24}$$

where indices i and j are not summed. Thus, there are 12 displacement components u_{ij}. Vectors ϕ_{ij} and q_{ij}, respectively, contain basis functions and unknown generalized DOFs. Furthermore,

$$\begin{aligned} T_k^{ij}(\xi_1) &= (1-\xi_1)^{e_R^{ij}} (1+\xi_1)^{e_L^{ij}}\; P_k^{\left(2e_L^{ij}, 2e_R^{ij}\right)}(\xi_1) \\ T_l^{ij}(\xi_2) &= (1-\xi_2)^{e_T^{ij}} (1+\xi_2)^{e_B^{ij}}\; P_l^{\left(2e_B^{ij}, 2e_T^{ij}\right)}(\xi_2) \end{aligned} \tag{4.25}$$

Here, $P_n^{\alpha,\beta}(\xi)$ is the n^{th}-degree Jacobi polynomial; and subscripts on e_L^{ij}, e_R^{ij}, e_B^{ij}, and e_T^{ij} denote, respectively, the left, the right, the bottom, and the top edges of the square shown

in Figure 4.2. These polynomials are orthogonal with respect to the weight $(1-\xi)^{\alpha}(1+\xi)^{\beta}$ on the interval $[-1,1]$, i.e.,

$$\int_{-1}^{1}(1-\xi)^{\alpha}\,(1+\xi)^{\beta}\,P_i^{(\alpha,\beta)}\,(\xi)\,P_j^{(\alpha,\beta)}\,(\xi)\;d\xi = f(\alpha,\beta,n)\,\delta_{ij}, \qquad \alpha,\beta>-1 \tag{4.26}$$

where δ_{ij} is the Kronecker delta. Quantities e_L^{ij}, e_R^{ij}, e_B^{ij}, and e_T^{ij} equal either 1.0 or 0, depending upon whether or not the displacement component u_{ij} at the corresponding edge is prescribed. For example, if the left edge of $\xi_1=-1$, is clamped and the other three edges are free, then to satisfy $u_i=0$ at the clamped edge, we set $e_L^{ij}=1$ and $e_B^{ij}=e_R^{ij}=e_T^{ij}=0$. In this paper, we study plates either with only the left edge clamped (i.e., cantilever plate) or all four edges clamped; and we do not discuss boundary conditions at a simply supported edge.

The three-term recursive formula for Jacobi polynomials is

$$\begin{aligned} 2n\,c_n\,c_{2n-2}\,P_n^{(\alpha,\beta)}(\xi) = {} & c_{2n-1}\,(c_{2n-2}\,c_{2n}\,\xi+\alpha^2-\beta^2)\,P_{n-1}^{(\alpha,\beta)}(\xi) \\ & -2(n-1+\alpha)(n-1+\beta)\,c_{2n}\,P_{n-2}^{(\alpha,\beta)}(\xi) \end{aligned} \tag{4.27}$$

where

$$c_n = n+\alpha+\beta \tag{4.28}$$

$$P_0^{(\alpha,\beta)}(\xi)=1; \qquad P_1^{(\alpha,\beta)}(\xi)=\frac{\alpha-\beta}{2}+\left(1+\frac{\alpha+\beta}{2}\right)\xi \tag{4.29}$$

The derivative of a Jacobi polynomial can be written as [49]

$$\frac{\mathrm{d}}{\mathrm{d}\xi}\left[P_n^{(\alpha,\beta)}(\xi)\right]=\frac{1}{2}\,(n+\alpha+\beta+1)\,P_{n-1}^{(\alpha+1,\beta+1)}(\xi) \tag{4.30}$$

4.4 Results

4.4.1 Isotropic Skew Plates

A schematic of an isotropic skew plate of side lengths a and b, thickness h, and skew angle α with respect to the x_1- axis is shown in Figure 4.3. Results are presented in terms of the nondimensional frequency parameter $\Omega = a^2\omega\sqrt{\rho/D}$ where $D = Eh^3/12(1-\nu^2)$. In Table 4.1, we list the first eight frequencies of a skew cantilever plate ($h/a = 0.2, 0.5, \alpha = 30deg$) for different degrees of Jacobi polynomials in ξ_1 and ξ_2 directions used as basis functions. The same degree polynomial is used for all generalized DOFs. It is seen that the relative difference between any two consecutive results for the same frequency is less than 1%, and the frequency parameters monotonically converge as the degree of the polynomial is increased. Unless stated otherwise, we have used polynomials of degree 14 in the both directions for the results presented below. To evaluate the accuracy of the present approach,

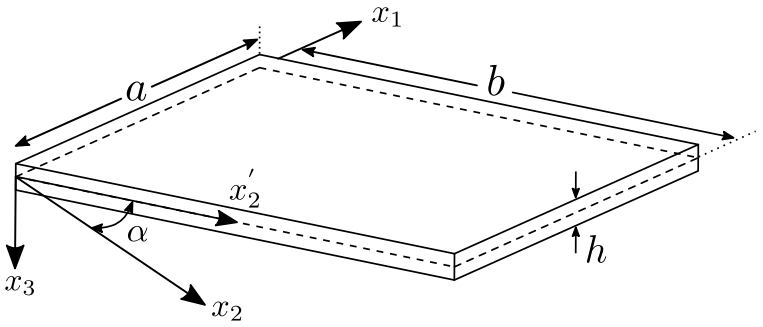

Figure 4.3: The schematic of the skew plate

we have listed in Table 4.2 the first eight frequencies of an isotropic skew cantilever plate for different values of h/a, and α along with those reported by McGee and Leissa [14] and Zhou et al. [15]. Also, for a better understanding of the dynamic behavior of laminated quadrilateral plates, the corresponding first eight three-dimensional mode shapes of the plate are presented in Figures 4.4 and 4.5 for $h/a = 0.2$ and 0.5, respectively. In the fringe plots

for the mode shapes, the blue color denotes the undeformed state and the red color the absolute maximum deflection. It is clear that the present results are in excellent agreement with those of Zhou et al. [15], who used Chebyshev polynomials as trial functions in the Ritz method. However, our results noticeably differ from those of McGee and Leissa [14], who used algebraic polynomials as trial functions; the difference is the maximum for $\alpha = 45$ deg. This large difference could be due to the well-known ill-conditioning issues encountered with using algebraic polynomials [50] that limit the degree of polynomials included in the trial functions.

Table 4.1: For different degrees of polynomials in the basis functions, the first eight frequency parameters for skewed cantilever thick isotropic plates with $a/b = 1$ and $\alpha = 30$ deg

Polynomial order	Ω_1	Ω_2	Ω_3	Ω_4	Ω_5	Ω_6	Ω_7	Ω_8
				$h/a = 0.2$				
6×6	3.7576	8.1131	11.137	19.767	21.503	24.551	30.876	31.694
7×7	3.7523	8.1065	11.112	19.751	21.494	24.550	30.859	31.658
9×9	3.7470	8.1031	11.086	19.738	21.489	24.548	30.851	31.620
11×11	3.7449	8.1023	11.074	19.734	21.487	24.547	30.849	31.601
14×14	3.7436	8.1019	11.065	19.731	21.487	24.547	30.848	31.588
				$h/a = 0.5$				
6×6	3.1809	4.4769	5.7306	9.8361	11.264	12.703	14.118	17.291
7×7	3.1792	4.4670	5.7281	9.8356	11.261	12.689	14.116	17.289
9×9	3.1775	4.4568	5.7257	9.8352	11.258	12.674	14.115	17.288
11×11	3.1766	4.4519	5.7246	9.8351	11.257	12.667	14.115	17.288
14×14	3.1759	4.4483	5.7239	9.8350	11.256	12.662	14.115	17.288

4.4.2 Thin Cantilever Skew Laminated Plates

In this section, the plate geometry exhibited in Figure 4.6 is similar to that of a sweptback wing. The current method is applied to find the first three frequencies of the symmetrically laminated skew cantilever plate with different stacking sequences. Each lamina is glass/epoxy [51] having, with respect to the material principal axes, $E_1 = 5.6$ megapounds per square inch (Msi), $E_2 = E_3 = 1.2$ Msi, $G_{12} = G_{13} = G_{23} = 0.6$ Msi, $\nu_{12} = \nu_{13} = 0.26$, $\nu_{23} = 0.34$,

Table 4.2: Comparison with those from the literature of the presently computed first eight frequency parameters for skewed cantilever thick isotropic plates with $a/b = 1$

α	Ω_1	Ω_2	Ω_3	Ω_4	Ω_5	Ω_6	Ω_7	Ω_8
				$h/b = 0.2$				
Present: 0°	3.3584	7.3810	10.9230	17.7236	22.5667	24.0642	26.2046	29.2848
Ref. [15]	3.3549	7.3744	10.9188	17.6976	22.5565	24.0336	26.1963	29.2837
Ref. [14]	3.3687	7.3397	10.9847	17.6949	23.6885	24.9997	26.2343	29.3881
FE [14]	3.3624	7.3941	10.9436	17.6728	22.1487	23.9502	26.2278	29.1873
Present: 15°	3.4551	7.5308	10.9802	18.2465	21.7421	25.6291	26.1816	30.0764
Ref. [15]	3.4511	7.5240	10.9746	18.2183	21.7257	25.6236	26.1544	30.0703
Ref. [14]	3.3989	7.5411	11.5005	18.0708	21.9487	25.5651	26.3655	30.6082
FE [14]	3.4650	7.5411	11.5005	18.0708	21.9487	25.5651	26.3655	30.6082
Present: 30°	3.7444	8.1021	11.0702	19.7324	21.4872	24.5469	30.8482	31.5957
Ref. [15]	3.7387	8.0942	11.0600	19.6967	21.4693	24.5441	30.8119	31.5784
Ref. [14]	3.7583	8.2944	11.8183	20.3724	22.5723	28.3452	31.3633	33.8068
FE [14]	3.7740	8.1276	11.1511	19.7461	21.2757	24.4965	30.6623	31.6052
Present: 45°	4.2013	9.5862	10.8383	20.9936	23.4723	23.7534	32.3021	36.6788
Ref. [15]	4.1923	9.5732	10.8193	20.9548	23.4641	23.7231	32.2737	36.6256
Ref. [14]	4.2809	10.4206	11.2917	23.5901	27.4819	33.4636	43.8769	47.2720
FE [14]	4.2679	9.6755	11.0507	21.1558	23.5722	23.6375	32.6347	36.7692
				$h/b = 0.5$				
Present: 0°	2.9432	4.3899	5.2049	10.5238	10.9833	11.7095	14.6482	15.0490
Ref. [15]	2.9336	4.3876	5.1925	10.5169	10.9367	11.7081	14.5988	15.0237
Ref. [14]	2.9463	4.4178	5.1815	10.5391	10.9792	11.7535	14.4674	16.1660
FE [14]	2.9397	4.3957	5.1470	10.5200	10.7864	11.6626	14.3273	14.4794
Present: 15°	3.0035	4.4132	5.3183	10.2813	11.0780	12.0399	14.1868	16.0106
Ref. [15]	2.9933	4.4110	5.3056	10.2760	11.0322	12.0367	14.1465	15.9724
Ref. [14]	3.0096	4.6232	5.3635	9.9399	10.6450	11.3436	12.5292	14.4180
FE [14]	3.0017	4.4244	5.2527	10.2640	10.8493	12.0043	13.7176	15.3277
Present: 30°	3.1763	4.4504	5.7243	9.8350	11.2565	12.6647	14.1147	17.2882
Ref. [15]	3.1649	4.4486	5.7105	9.8316	11.2146	12.6597	14.0731	17.2391
Ref. [14]	3.3164	4.6768	6.1756	11.3566	13.5265	13.5265	14.3425	15.9530
FE [14]	3.1809	4.4802	5.6351	9.8067	10.9455	12.5606	13.6732	16.5283
Present: 45°	3.4373	4.3586	6.6264	9.3973	11.1914	12.9639	14.5089	17.5424
Ref. [15]	3.4246	4.3582	6.6094	9.3954	11.1578	12.9582	14.4607	17.4797
Ref. [14]	3.8412	6.5555	7.6914	13.3667	18.6951	18.6951	18.9918	25.394
FE [14]	3.4554	4.4421	6.4876	9.4300	10.8145	13.0694	14.0382	16.7953

and $\rho = 4.94$ slug/ft3; (1 Msi= 10^6 Psi). The computed results and those from the literature are listed in Table 4.3 for the sweep angle $\beta = 30$ deg, aspect ratio (AR)= 3.111, taper ratio (TR) = 0.5, area S= 63 in^2, and total thickness = 0.14 in. The present results are in excellent agreement with those from the literature. The corresponding mode shapes are presented in Figure 4.7.

4.4.3 Clamped Thin Skew Laminated Plates

We now compare in Tables 4.4 and 4.5 the presently computed frequency parameters $\lambda = (a^2\omega/\pi^2 h)\sqrt{\rho/E_2})$, for clamped skew laminated plates (see Fig. 3) with those of Malekzadeh et al. [52], Fig. 3 The schematic of the skew plate. Wang [53], and Anlas and Goker [54]. Malekzadeh et al. [52] used a layerwise theory and the differential quadrature (DQ) method. Wang [53] and Anlas and Goker [54] used the Ritz method to solve the FSDT and the CPT equations, respectively. The following material properties are used for each lamina of the composite: $E_1 = 40$ GPa, $E_2 = E_3 = 1$ GPa, $\nu_{12} = \nu_{13} = \nu_{23} = 0.25$, $G_{12} = G_{13} = 0.6$ GPa, and $G_{23} = 0.5$ GPa. The present computed frequencies are in excellent agreement with those of Malekzadeh et al. [52] for all cases except for the sixth and the seventh frequencies of the [90°/0°/90°/0°/90°] plate having a skew angle of 45 deg. These differences could be due to Malekzadeh et al.'s [52] frequencies being not fully converged since they reported a difference of 29% in their sixth and seventh frequencies obtained with 11 and nine DQ grid points.

4.4.4 Comparison of Present Results with Those from FEM for Clamped Skew Laminates

For a crossply skew plate, we investigate effects of the number of layers, the plate thickness-to-side ratio, and the skew angle on the accuracy of the presently computed frequencies

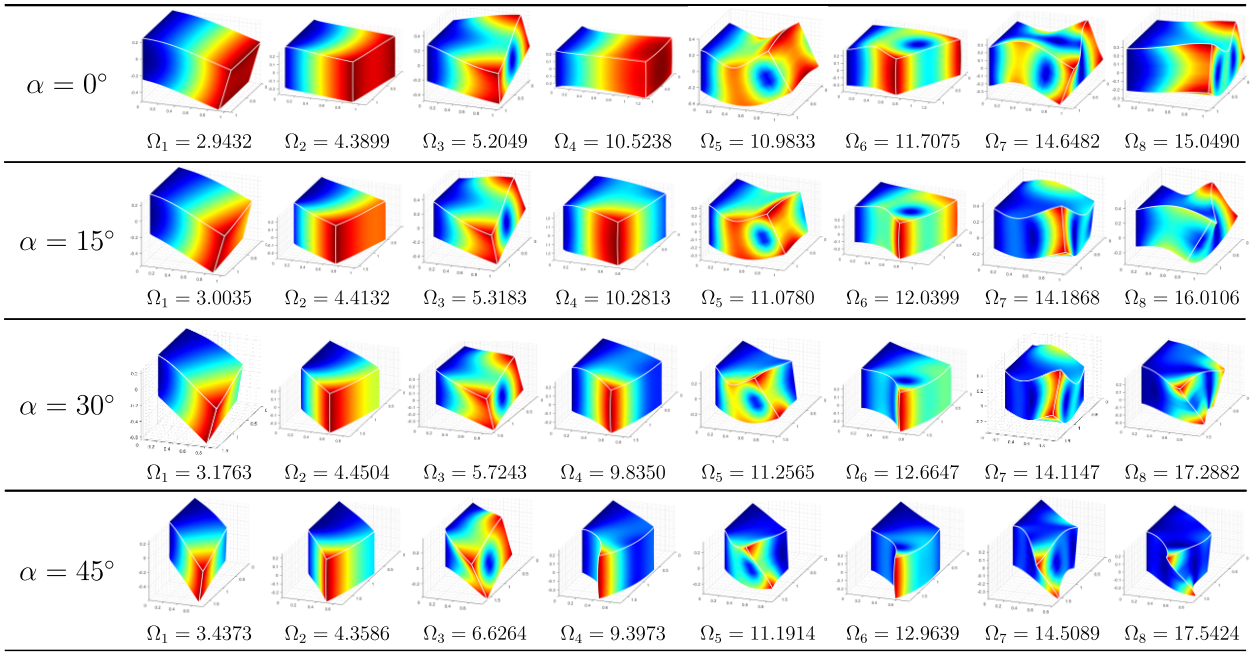

Figure 4.4: Mode shapes corresponding to the first eight frequencies for the cantilever skew isotropic plates with $h/a = 0.2$ and $a/b = 1$

relative to those obtained using 20-node brick (C3D20 and C3D20R) and four-node shell (S4 and S4R) FEs in ABAQUS. The shell elements are for the FSDT, and the letter "R" implies using a reduced Gauss quadrature rule to numerically compute the element integrals. We set $a = b = 10$ m for the plate depicted in Figure 4.3, and we assign the following values to the material properties for each lamina: $E_1 = 40$ GPa, $E_2 = E_3 = 1$ GPa, $\nu_{12} = \nu_{13} = \nu_{23} = 0.25$, $G_{12} = G_{13} = 0.6$ GPa, $G_{23} = 0.5$ GPa, and $\rho = 1800$ kg/m^3. First, we find the FE meshes to be used in ABAQUS for achieving 0.12% relative difference (rel. diff.) defined by

$$\left(\left|\omega^{\text{current mesh}} - \omega^{\text{previous mesh}}\right| / \omega^{\text{current mesh}}\right) \times 100$$

For the [90°/0°] laminate with $\alpha = 45$ deg, natural frequencies (in Hertz) of the first, third, and sixth modes of clamped [90°/0°] laminates are listed in Table 4.6 for different uniform FE meshes for C3D20, C3D20R, S4, and S4R elements. The FE meshes are identified as follows: for brick elements, $m \times n \times l$, and for shell elements, $m \times n$, where m, n, and l represent

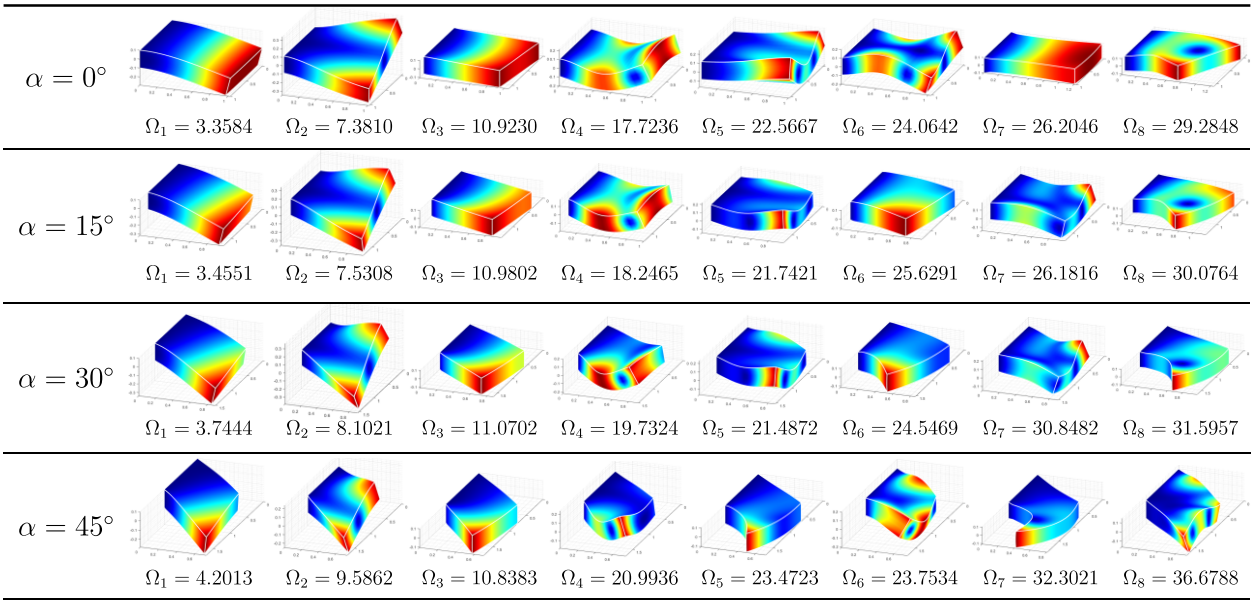

Figure 4.5: Mode shapes corresponding to the first eight frequencies for the cantilever skew isotropic plates with $h/a = 0.5$ and $a/b = 1$

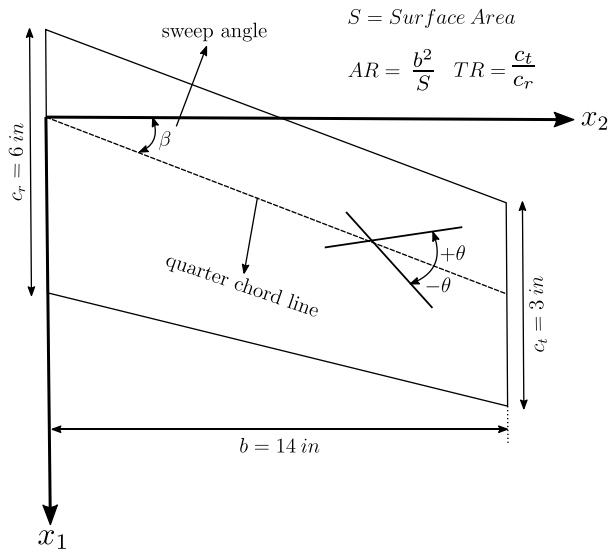

Figure 4.6: Geometry of a sweptback wing

the number of uniform elements along the x_1, the x_2', and the x_3 axes. It is clear that for C3D20 and C3D20R elements, the $60 \times 60 \times 8$ FE mesh (and for S4 and S4R elements, the 100×100 FE mesh) give converged frequencies. For the present method, in Table 4.7, we

Table 4.3: Comparison with those from the literature of the first three frequencies, in Hertz, of a thin laminated

Stacking Sequence	Mode No	Present Study	Kapania and Lovejoy [19]	Kapania and Singhvi [18]	Lakshminarayana et al. [16]:comp.	Lakshminarayana et al. [16]:exp.	Lee and Lee [17]
$[0_2/0]_s$	1	17.32	17.25	17.30	16.67	17.55	16.80
	2	83.82	83.77	84.44	80.40	83.80	81.03
	3	97.95	97.70	98.29	99.52	98.65	100.08
$[15_2/0]_s$	1	16.97	16.91	16.96	15.90	15.70	16.00
	2	76.82	76.73	77.28	73.20	73.60	75.08
	3	110.72	110.62	111.40	114.56	108.15	111.98
$[30_2/0]_s$	1	13.92	13.91	13.94	13.15	13.90	13.18
	2	69.39	69.30	69.65	66.67	65.70	67.61
	3	115.08	115.55	116.59	120.86	110.80	116.65
$[45_2/0]_s$	1	11.45	11.47	11.48	11.05	11.05	10.45
	2	59.91	59.97	60.13	59.13	57.01	59.01
	3	112.49	113.38	114.46	117.37	116.10	112.55
$[60_2/0]_s$	1	10.01	10.04	10.04	9.82	10.10	9.33
	2	53.28	53.38	53.48	53.5	52.75	52.98
	3	101.37	102.52	103.36	105.6	105.25	100.65
$[75_2/0]_s$	1	9.29	9.30	9.31	9.16	9.60	9.24
	2	49.62	49.63	49.78	49.84	50.30	52.98
	3	89.12	90.24	90.79	93.38	91.35	88.99
$[90_2/0]_s$	1	8.98	8.98	9.00	8.82	8.45	8.60
	2	47.87	47.82	48.01	47.41	45.45	47.43
	3	81.93	82.79	83.25	86.58	89.15	82.64

have listed the first, third, and sixth frequencies for different degrees of Jacobi polynomials. It can be seen that the eighth-degree Jacobi polynomials suffice. However, all results in this section are with the 11^{th}-degree polynomials.

In Tables 4.8 – 4.10, we have listed the first six frequencies for two-,four-, and eight-layered clamped skew laminates with the thicknessto-side ratio of 0.2 by taking results found using the C3D20 elements (387,411 DOFs) as the reference, calculating the percent errors

$$\left(\left|\omega^{\text{reference}} - \omega^{\text{current}}\right| / \omega^{\text{reference}} \times 100\right)$$

in other results. The maximum discrepancy in the present results (5,184 DoF) is 3%. Using C3D20R elements introduces a negligible error. It is found that with 11% error, the 2 layered laminate with the skew angle of 45° is the most critical case for the S4 elements.

The accuracy of S4 and S4R elements worsens with an increase in the skew angle and a decrease in the number of layers. For this problem, the maximum difference between the results obtained using the present method and those using C3D20 elements in Abaqus is 2.2%.

To study the effect of the thickness-to-side ratio, h/a, we consider h/a=0.1 and 0.01, (both a cantilever and a clamped plate), and list results in Tables 4.11 - 4.14. For the clamped plate, with a decrease in the thickness ratio, the % error between the C3D20 results and the present method and using S4 elements has been reduced. For $h/a = 0.1$, the error, respectively, equals 3.13 and 7% for the TSNDT and the S4 elements. However, for the cantilever plate, the error decreases to 2% both for the TSNDT and the S4 elements. For $h/a = 0.01$, frequencies from both the TSNDT and the S4 elements have negligible error.

The three-dimensional(3-D) mode shapes obtained using the present method were found to be essentially independent of the number of layers. Thus, for brevity, in Figures 4.8 - 4.12 the mode shapes are displayed only for the 2-layer plate.

4.4.5 Comparison of Computational Resources for Present Method and FEM Using ABAQUS

We have listed in Table 4.15 the DOFs and the CPU time for the present method and ABAQUS using C3D20 elements needed to find converged values of the lowest six frequencies for two-, four-, and six-layered cantilever laminates with $\alpha = 45^\circ$ and $h/b = 0.2$.The seedings of the FE meshes are based on the convergence study for which the results are reported in Table 4.6. For the present method, $11^{th}-$ degree polynomials are used in both ξ_1 and ξ_2 directions for all three laminates. For the two-, four-, and six-layered laminates, the total numbers of DOFs for the FEM, respectively, equal $387,411$, $741,699$, and $1,450,275$;

but, those for the present method equal 1758. The corresponding CPU times are 639, 2403, and 10,262 s for the FEM; and they are merely 13 s for the Ritz/TSNDT approach. We recognize that run times depend on many factors, and it is not fair to compare computational requirements for a commercial software with those for the in-house code developed in MATLAB 2018b. However, the number of DOFs and the CPU time for the same machine (Intel® Xeon® CPU E5-2665 0 at 2.40 GHz processor with 64 GB of RAM running a Windows 10 system) provide some insights about the performance of the two methods.

4.5 Conclusions

We have presented a computational method using a third-order shear and normal deformation plate theory (TSNDT) and weighted Jacobi polynomials as basis functions in the Ritz method to analyze free vibrations of thick skew quadrilateral laminates. For an improved understanding of the dynamic characteristics, we have also provided 3-dimensional mode shapes. It is shown that the current method provides accurate frequencies with fewer number of unknowns than those in the traditional finite element method (FEM). Even though the mass and the stiffness matrices in the present method have larger bandwidth than those in the FEM, the present approach requires less computational resources. It is found that the presently computed first six natural frequencies of clamped skew laminates with thickness/side length = 0.2 differ at most by 3% from those found by numerically solving the 3-D linear elasticity theory equations using brick elements, C3D20, in Abaqus. We note that the FSDT based shell elements provide frequencies that differ by 11% from those computed using either the 3-D FEM or the present TSNDT based method. Thus, one should be careful in using these shell elements in Abaqus when designing skew plates for critical applications.

Table 4.4: For three values of the skew angle, frequency parameters of clamped skew $[45°/-45°/45°/-45°/45°]$ laminate $(a/b = 1, h/a = 0.01)$; $m_1 \times m_2 = 8 \times 8$ means eight-degree Jacobi polynomials in each direction

α	Source	λ_1	λ_2	λ_3	λ_4	λ_5	λ_6	λ_7
	Present: $m_1 \times m_2 = 8 \times 8$	3.85	7.01	8.27	10.93	12.95	14.26	15.59
	Present: $m_1 \times m_2 = 11 \times 11$	3.85	7.02	8.27	10.93	12.95	14.26	15.59
0°	Present: $m_1 \times m_2 = 14 \times 14$	3.85	7.02	8.27	10.92	12.95	14.26	15.59
	Layerwise Theory [52]	3.85	7.01	8.27	10.91	12.93	14.25	15.57
	Ritz Method - FSDT [53]	3.90	7.15	8.46	11.21	13.32	14.74	16.13
	Ritz Method - CPT [54]	3.90	7.15	8.46	11.21	13.32	14.75	16.13
	Present: $m_1 \times m_2 = 8 \times 8$	4.48	8.21	9.66	12.49	15.20	16.91	17.66
	Present: $m_1 \times m_2 = 11 \times 11$	4.48	8.21	9.66	12.48	15.20	16.91	17.65
30°	Present: $m_1 \times m_2 = 14 \times 14$	4.48	8.21	9.66	12.48	15.20	16.91	17.65
	Layerwise Theory [52]	4.48	8.20	9.65	12.47	15.17	16.89	17.63
	Ritz Method - FSDT [53]	4.54	8.38	9.88	12.85	15.69	17.49	18.34
	Ritz Method - CPT [54]	4.54	8.38	9.88	12.85	15.69	17.49	18.35
	Present: $m_1 \times m_2 = 8 \times 8$	6.20	10.54	14.08	14.94	20.13	21.15	24.68
	Present: $m_1 \times m_2 = 11 \times 11$	6.20	10.54	14.07	14.93	20.13	21.14	24.68
45°	Present: $m_1 \times m_2 = 14 \times 14$	6.20	10.54	14.07	14.93	20.13	21.14	24.67
	Layerwise Theory [52]	6.20	10.52	14.05	14.91	20.13	21.16	24.62
	Ritz Method - FSDT [53]	6.31	10.82	14.50	15.47	21.06	22.08	25.89
	Ritz Method - CPT [54]	6.31	10.82	14.50	15.47	21.09	22.13	25.89

Table 4.5: For three values of the skew angle, frequency parameters of clamped skew [90°/0°/90°/0°/90°] laminate ($a/b = 1, h/a = 0.01$); $m_1 \times m_2 = 8 \times 8$ means eight-degree Jacobi polynomials in each direction

α	Source	λ_1	λ_2	λ_3	λ_4	λ_5	λ_6	λ_7
0°	Present: $m_1 \times m_2 = 8 \times 8$	4.19	6.60	10.16	11.20	11.48	14.75	17.65
	Present: $m_1 \times m_2 = 11 \times 11$	4.19	6.60	10.16	11.20	11.48	14.75	17.62
	Present: $m_1 \times m_2 = 14 \times 14$	4.19	6.60	10.16	11.20	11.48	14.75	17.62
	Layerwise Theory [52]	4.19	6.60	10.16	11.18	11.47	14.73	17.74
	Ritz Method - FSDT [53]	4.24	6.69	10.45	11.44	11.78	15.14	18.19
	Ritz Method - CPT [54]	4.24	6.69	10.45	11.44	11.78	15.14	18.29
30°	Present: $m_1 \times m_2 = 8 \times 8$	5.54	8.16	12.06	13.61	16.16	16.37	20.80
	Present: $m_1 \times m_2 = 11 \times 11$	5.54	8.16	12.06	13.61	16.15	16.37	20.75
	Present: $m_1 \times m_2 = 14 \times 14$	5.54	8.16	12.06	13.61	16.15	16.37	20.75
	Layerwise Theory [52]	5.53	8.16	12.05	13.60	16.16	16.36	20.94
	Ritz Method - FSDT [53]	5.63	8.33	12.40	14.13	16.74	16.96	21.70
	Ritz Method - CPT [54]	5.63	8.33	12.40	14.13	16.76	16.97	21.85
45°	Present: $m_1 \times m_2 = 8 \times 8$	8.22	11.44	15.55	19.93	20.31	24.14	25.27
	Present: $m_1 \times m_2 = 11 \times 11$	8.22	11.44	15.54	19.90	20.30	24.07	25.08
	Present: $m_1 \times m_2 = 14 \times 14$	8.22	11.44	15.54	19.90	20.30	24.07	25.08
	Layerwise Theory [52]	8.22	11.43	15.56	20.19	20.35	24.60	26.27
	Ritz Method - FSDT [53]	8.46	11.80	16.17	20.94	21.51	25.65	26.84
	Ritz Method - CPT [54]	8.46	11.80	16.18	21.09	21.56	25.98	27.48

Table 4.6: Frequencies for different FE meshes for the [0°/90°] laminate with $\alpha = 45°$

Element	Mesh	ω_1	Rel. diff. %	ω_3	Rel. diff %	ω_6	Rel. diff %
C3D20	$40 \times 40 \times 2$	42.038	−−	73.169	−−	95.472	−−
	$40 \times 40 \times 4$	41.297	1.79	72.139	1.43	94.274	1.27
	$40 \times 40 \times 8$	41.153	0.35	71.872	0.37	93.932	0.36
	$60 \times 60 \times 8$	41.150	0.01	71.867	0.01	93.925	0.01
C3D20R	$40 \times 40 \times 8$	41.126	−−	71.811	−−	93.844	−−
	$60 \times 60 \times 8$	41.122	0.01	71.805	0.01	93.837	0.01
S4	40×40	37.22	−−	64.397	−−	84.120	−−
	60×60	37.198	0.05	64.273	0.19	83.924	0.23
	100×100	37.188	0.03	64.209	0.1	83.823	0.12
S4R	40×40	37.209	−−	64.367	−−	84.092	−−
	60×60	37.194	0.04	64.259	0.17	83.911	0.22
	100×100	37.187	0.02	64.204	0.09	83.818	0.11

Table 4.7: For different orders of Jacobi polynomials, frequencies from the TSNDT solution for the $[\mathbf{0°/90°}]$ laminate with $\boldsymbol{\alpha = 45°}$

Polynomial Order	Mode 1	Rel. Diff %	Mode 3	Rel. Diff %	Mode 6	Rel. Diff %
5x5	42.041	-	73.269	-	96.690	-
6x6	42.040	0.00	73.110	0.22	95.771	0.96
7x7	42.040	0.00	73.094	0.02	95.563	0.22
8x8	42.039	0.00	73.091	0.00	95.528	0.04
9x9	42.039	0.00	73.092	0.00	95.523	0.00
10x10	42.039	0.00	73.092	0.00	95.522	0.00
11x11	42.039	0.00	73.092	0.00	95.522	0.00

Table 4.8: For three skew angles, first six natural frequencies of clamped skew $[\mathbf{0°/90°}]$ laminates (a/h=1, h/a=0.2) computed with the present method and by using C3D20, C3D20R, S4 and S4R elements in ABAQUS. (The maximum percentage error in the results obtained using C3D20R, S4, S4R, and present method are 0.08, 10.76, 12.07, and, 3.01, respectively)

Skew Angle	Method	ω_1 [Hz]	ω_2 [Hz]	ω_3 [Hz]	ω_4 [Hz]	ω_5 [Hz]	ω_6 [Hz]
0°	C3D20	28.738	46.743	46.743	60.300	69.483	69.748
	C3D20R	28.725	46.713	46.713	60.260	69.428	69.691
	Present	29.604	47.803	47.803	61.488	70.877	71.079
	S4	26.793	42.718	42.718	54.575	63.145	63.221
	S4R	26.793	42.717	42.717	54.574	63.144	63.220
30°	C3D20	33.323	49.266	58.117	63.804	78.6131	79.096
	C3D20R	33.305	49.233	58.075	63.757	78.548	79.031
	Present	34.217	50.333	59.232	65.016	80.060	80.455
	S4	30.678	44.792	52.475	57.594	70.857	70.997
	S4R	30.678	44.791	52.474	57.591	70.855	70.992
45°	C3D20	41.150	57.180	71.872	73.433	86.671	93.932
	C3D20R	41.122	57.132	71.805	73.362	86.583	93.837
	Present	42.039	58.254	73.092	74.630	88.010	95.522
	S4	37.188	51.340	64.209	65.547	77.102	83.823
	S4R	37.187	51.338	64.204	65.546	77.093	83.818

Table 4.9: For three skew angles, first six natural frequencies of clamped skew [0°/90°/0°/90°] laminates (a/h=1, h/a=0.2) computed with the present method and by using C3D20, C3D20R, S4 and S4R elements in ABAQUS (The maximum percentage error in the results obtained using C3D20R, S4, S4R, and present method are 0.02, 8.57, 8.57, and, 1.74, respectively)

Skew Angle	Method	ω_1 [Hz]	ω_2 [Hz]	ω_3 [Hz]	ω_4 [Hz]	ω_5 [Hz]	ω_6 [Hz]
0°	C3D20	31.384	50.074	50.074	63.888	73.195	73.275
	C3D20R	31.381	50.068	50.068	63.880	73.184	73.265
	Present	31.930	50.809	50.809	64.756	74.273	74.340
	S4	29.689	46.815	46.815	59.316	68.005	68.029
	S4R	29.689	46.814	46.814	59.315	68.005	68.029
30°	C3D20	35.803	52.372	61.512	67.069	82.354	82.409
	C3D20R	35.800	52.366	61.504	67.061	82.342	82.397
	Present	36.370	53.121	62.348	67.984	83.526	83.538
	S4	33.613	48.785	57.016	62.116	75.974	76.029
	S4R	33.613	48.785	57.015	62.115	75.972	76.028
45°	C3D20	43.307	59.989	74.751	76.916	89.561	97.825
	C3D20R	43.302	59.980	74.740	76.903	89.545	97.807
	Present	43.902	60.796	75.748	77.954	90.775	99.246
	S4	40.153	55.353	68.659	70.535	81.965	89.442
	S4R	40.153	55.352	68.658	70.535	81.963	89.440

Table 4.10: For three skew angles, first six natural frequencies of clamped skew $[0°/90°]_4$ laminates (a/h=1, h/a=0.2) computed with the present method and by using C3D20, C3D20R, S4 and S4R elements in ABAQUS

Skew Angle	Method	ω_1 [Hz]	ω_2 [Hz]	ω_3 [Hz]	ω_4 [Hz]	ω_5 [Hz]	ω_6 [Hz]
	C3D20	33.217	52.642	52.642	66.840	76.701	76.740
	C3D20R	33.216	52.641	52.641	66.838	76.698	76.737
0°	Present	33.747	53.663	53.663	68.171	78.564	78.610
	S4	32.468	51.210	51.210	64.858	74.448	74.475
	S4R	32.468	51.210	51.210	64.857	74.448	74.475
	C3D20	37.723	54.935	64.345	70.102	85.903	85.955
	C3D20R	37.722	54.934	64.344	70.100	85.900	85.953
30°	Present	38.360	56.024	65.710	71.637	88.004	88.101
	S4	36.770	53.375	62.388	67.965	83.158	83.234
	S4R	36.769	53.375	62.387	67.964	83.156	83.233
	C3D20	45.310	62.594	77.787	79.999	92.998	101.55
	C3D20R	45.308	62.593	77.785	79.996	92.995	101.55
45°	Present	46.187	63.956	79.660	81.971	95.464	104.33
	S4	43.942	60.581	75.156	77.209	89.749	97.931
	S4R	43.941	60.580	75.155	77.208	89.746	97.929

Table 4.11: the present method and by using C3D20 and S4 elements in ABAQUS

Skew angle	Method	ω_1	ω_2	ω_3	ω_4	ω_5	ω_6
0 deg	C3D20	21.288	37.128	37.128	48.649	57.905	58.121
	TSNDT	21.864	38.278	38.278	50.079	59.729	59.942
	S4	20.764	35.683	35.683	46.371	55.061	55.231
30 deg	C3D20	25.361	39.443	47.578	52.338	66.278	66.341
	TSNDT	26.075	40.630	49.013	53.911	68.221	68.270
	S4	24.550	37.721	45.205	49.724	62.510	62.570
45 deg	C3D20	32.629	46.911	60.199	62.285	73.893	81.135
	TSNDT	33.598	48.278	61.943	64.022	75.982	83.246
	S4	31.213	44.396	56.678	58.306	69.230	75.455

Table 4.12: For three skew angles, first six natural frequencies in Hertz of cantilever skew $[0/90 \text{ deg }]_4$ laminates $(a/h = 1, h/a = 0.1)$ computed wit the present method and by using C3D20, C3D20R, S4, and S4R elements in ABAQUS[a]

Skew angle	Method	ω_1	ω_2	ω_3	ω_4	ω_5	ω_6
0 deg	C3D20	2.9765	4.4609	13.384	15.611	17.529	18.617
	TSNDT	2.9925	4.4820	13.389	15.966	17.842	18.844
	S4	2.9714	4.4047	13.374	15.424	17.183	18.533
30 deg	C3D20	2.6385	6.1067	13.844	14.490	18.134	23.705
	TSNDT	2.6663	6.2663	13.922	14.743	18.474	24.181
	S4	2.6613	6.1058	13.842	14.443	18.047	23.462
45 deg	C3D20	2.7076	8.1107	13.817	14.906	19.854	25.288
	TSNDT	2.7442	8.2120	13.995	15.122	20.210	25.470
	S4	2.7406	8.1263	13.880	14.837	19.750	25.585

Table 4.13: For three skew angles, first six natural frequencies in Hertz of clamped skew [0/90 deg] laminates $(a/h = 1, h/a = 0.01)$ computed with the present method and by using C3D20, C3D20R, S4, and S4R elements in ABAQUS maximum error in the results obtained using S4 and present method are 0.07 and 0.29, respectively

Skew angle	Method	ω_1	ω_2	ω_3	ω_4	ω_5	ω_6
0 deg	C3D20	2.8513	5.8648	5.8648	7.9951	10.806	10.827
	TSNDT	2.8527	5.8725	5.8725	8.0060	10.829	10.850
	S4	2.8510	5.8658	5.8658	7.9943	10.814	10.835
30 deg	C3D20	3.5921	6.3824	8.1552	9.1940	12.618	12.654
	TSNDT	3.5950	6.3916	8.1686	9.2100	12.644	12.683
	S4	3.5915	6.3833	8.1551	9.1967	12.621	12.662
45 deg	C3D20	5.1110	8.1538	11.419	12.139	15.135	16.863
	TSNDT	5.1176	8.1680	11.444	12.169	15.179	16.906
	S4	5.1102	8.1550	11.425	12.139	15.150	16.869

Table 4.14: For three skew angles, first six natural frequencies in Hertz of cantilever skew [0/90 deg] laminates ($a/h = 1, h/a = 0.01$) computed the present method and by using C3D20, C3D20R, S4, and S4R elements in ABAQUS[a]

Skew angle	Method	ω_1	ω_2	ω_3	ω_4	ω_5	ω_6
0 deg	C3D20	0.30915	0.48433	1.9325	2.1106	2.1793	3.4213
	TSNDT	0.30918	0.48471	1.9335	2.1113	2.1809	3.4243
	S4	0.30912	0.48402	1.9327	2.1105	2.1787	3.4189
30 deg	C3D20	0.28482	0.68367	1.8210	2.2405	3.0866	3.5768
	TSNDT	0.28532	0.68451	1.8251	2.2441	3.0905	3.5835
	S4	0.28525	0.68400	1.8244	2.2429	3.0880	3.5816
45 deg	C3D20	0.29888	0.92176	1.8969	2.5758	3.8243	4.3467
	TSNDT	0.29954	0.92277	1.9015	2.5819	3.8318	4.3541
	S4	0.29959	0.92242	1.9017	2.5802	3.8335	4.3511

Table 4.15: For a of the a cantilever laminate with $\alpha = 45^\circ$ and $h/b = 0.2$, comparison of the number of DOFs and the run times for the present method and the FEM using C3D20 elements in ABAQUS

Method	Seeding (x, y, z)	No. of DOFs	CPU time, s	No. of layers
C3D20	$60 \times 60 \times 8$	387,411	639	2
C3D20	$60 \times 60 \times 16$	741,699	2,403	4
C3D20	$60 \times 60 \times 32$	1,450,275	10,262	8
Present	$--$	1,728	13	$--$

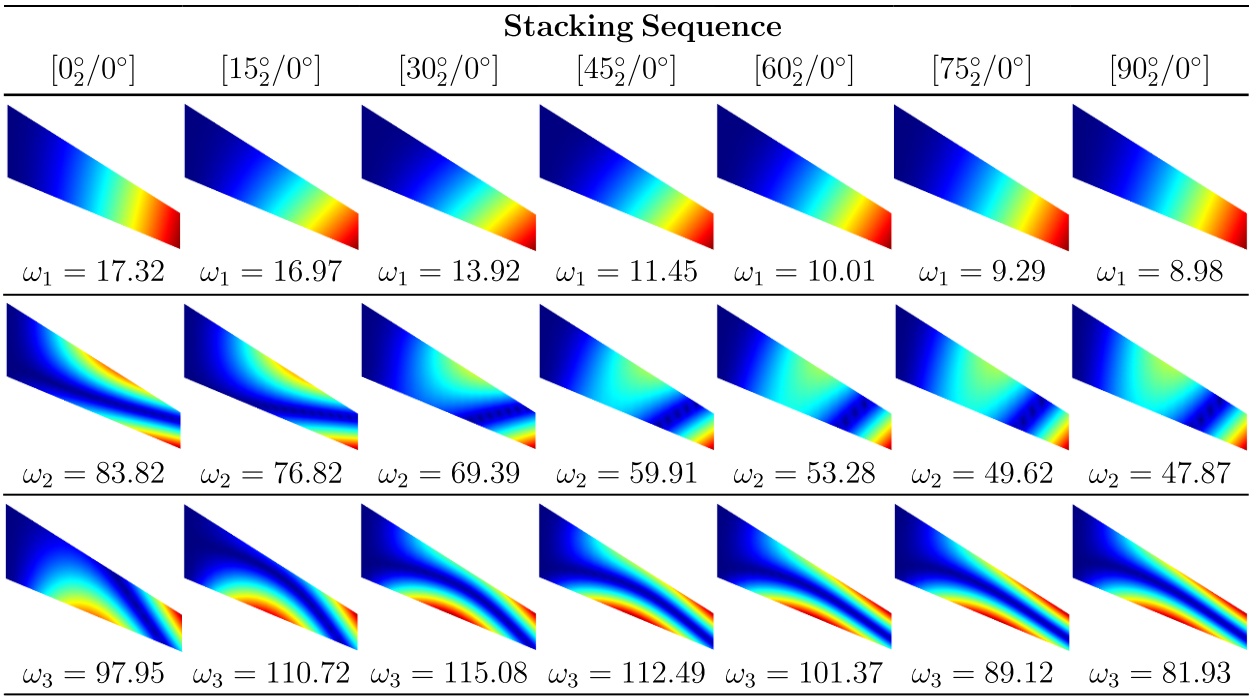

Figure 4.7: Mode shapes corresponding to the first three frequencies of the cantilever swept wing for different stacking sequences

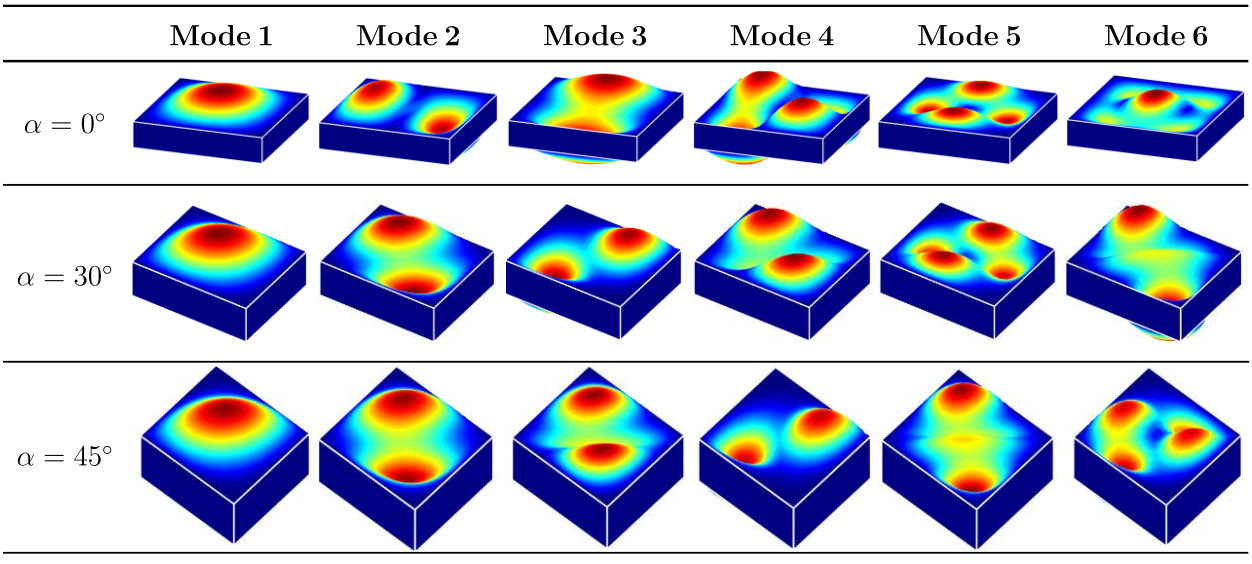

Figure 4.8: Mode shapes corresponding to the lowest six frequencies for the clamped skew [0/90 deg] laminates with $(h/a) = 0.2$ and $(a/b) = 1$

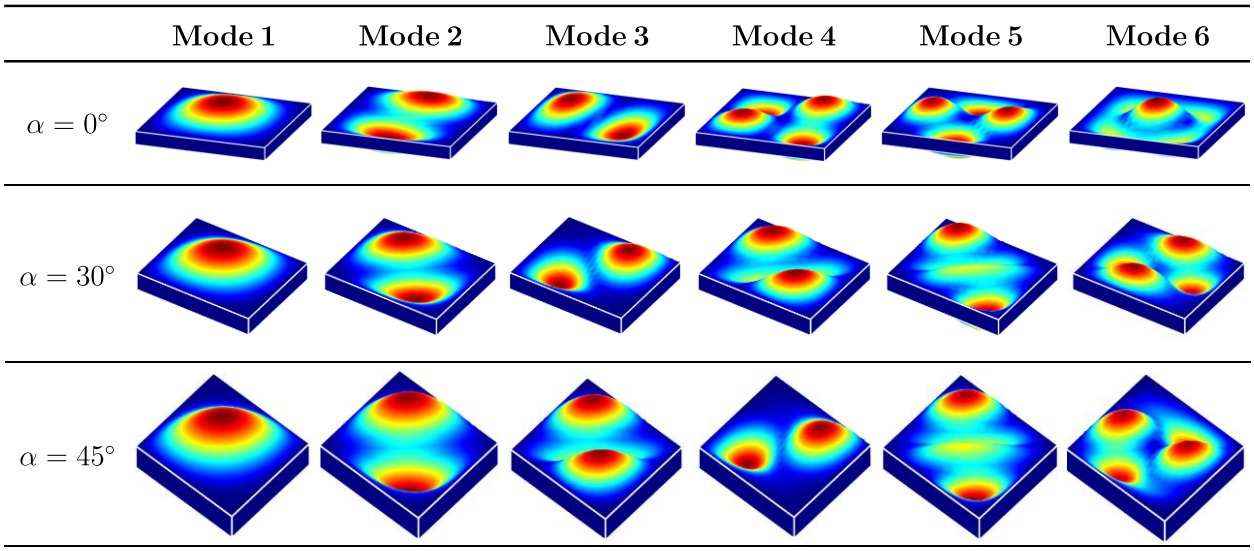

Figure 4.9: Mode shapes corresponding to the lowest six frequencies for the clamped skew [0/90 deg] laminates with $h/a = 0.1$ and $a/b = 1$

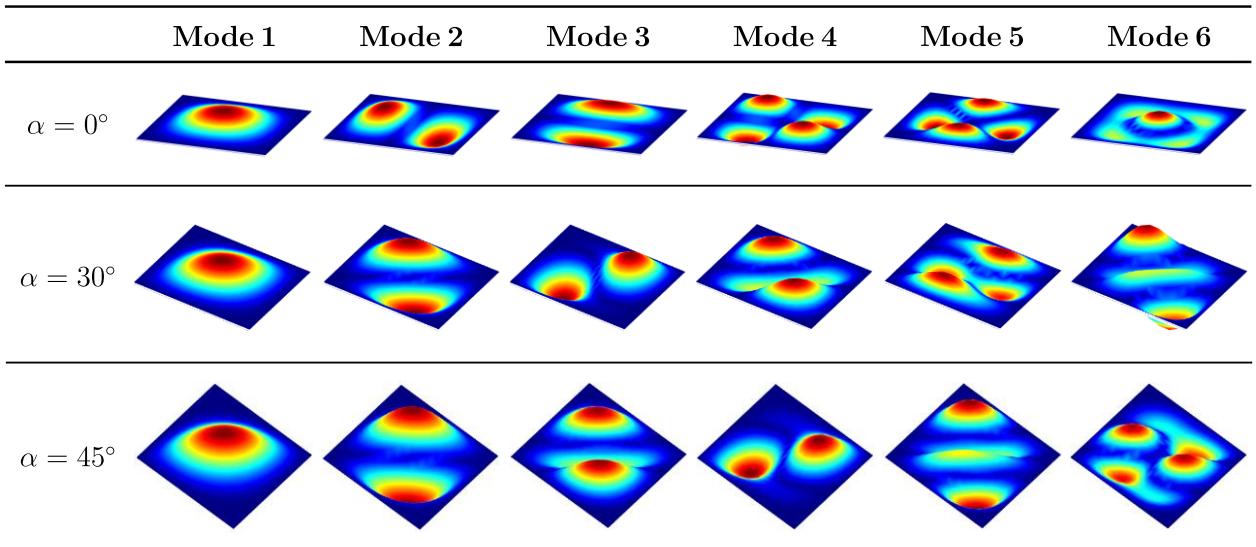

Figure 4.10: Mode shapes corresponding to the lowest six frequencies for the clamped skew [0/90 deg] laminates with $h/a = 0.01$ and $a/b = 1$

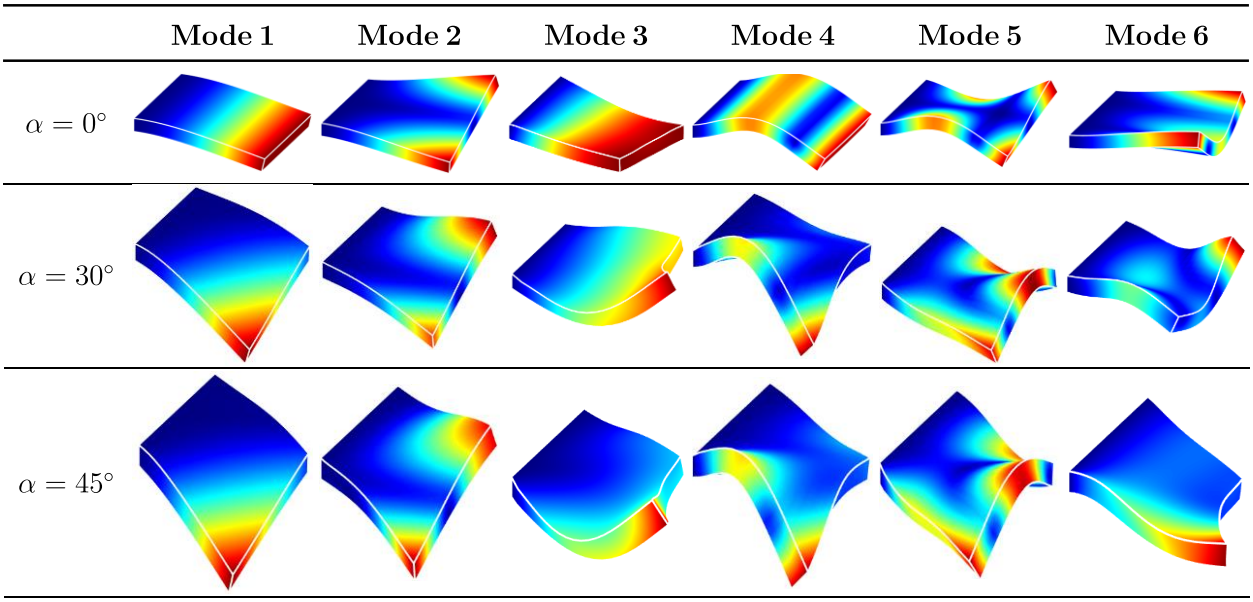

Figure 4.11: Mode shapes corresponding to the lowest six frequencies for the cantilever skew $h/a = 0.1$ and $a/b = 1$

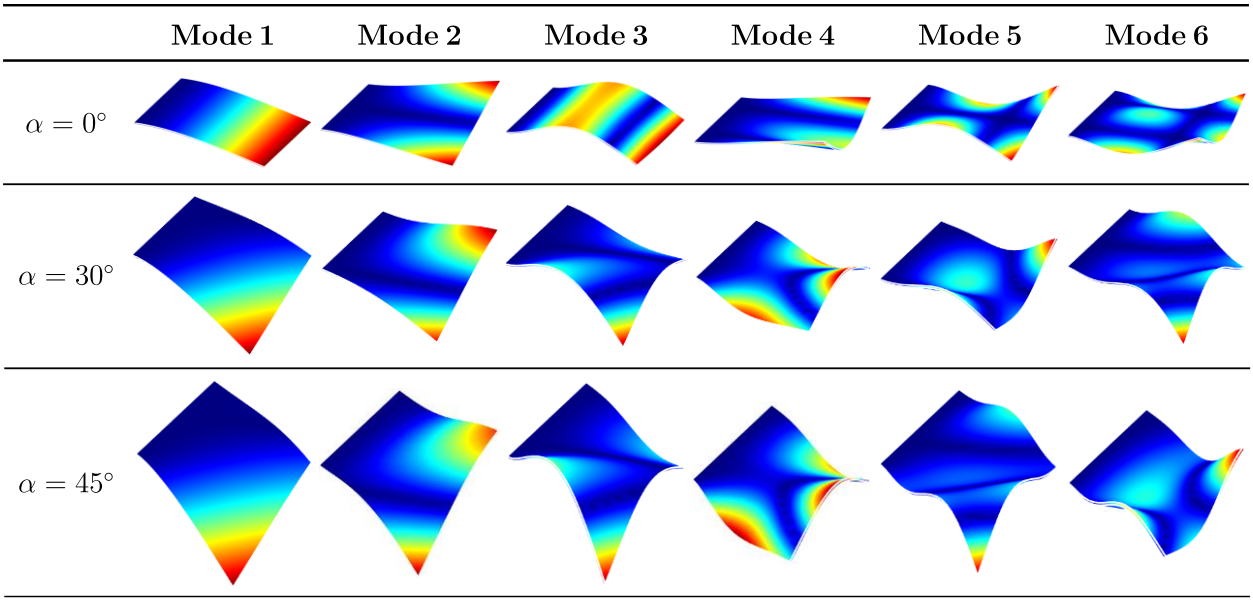

Figure 4.12: Mode shapes corresponding to the lowest six frequencies for the cantilever skew [0/90 deg] laminates with $h/a = 0.01$ and $a/b = 1$

Bibliography

[1] Love, A. E. H., 1888, "The Small Free Vibrations and Deformation of a Thin Elastic Shell," Philosophical Transactions of the Royal Society of London (A), **179**, pp. 491–546.

[2] Mindlin, R. D., 1951, "Influence of Rotatory Inertia and Shear on Flexural Motions of Isotropic, Elastic Plates," Journal of Applied Mechanics, **18**(1), pp. 31–38.

[3] Reissner, E., 1975, "On Transverse Bending of Plates, Including the Effect of Transverse Shear Deformation," International Journal of Solids and Structures, **11**(5), pp. 569–573.

[4] Kapania, R. K. and Raciti, S., 1989, "Recent Advances in Analysis of Laminated Beams and Plates, Part I: Shear Effects and Buckling," AIAA Journal, **27**(7), pp. 923–935.

[5] Batra, R. C., Vidoli, S., and Vestroni, F., 2002, "Plane Wave Solutions and Modal Analysis in Higher Order Shear and Normal Deformable Plate Theories," Journal of Sound and Vibration, **257**(1), pp. 63–88.

[6] Carrera, E. and Brischetto, S., 2009, "A Survey with Numerical Assessment of Classical and Refined Theories for the Analysis of Sandwich Plates," Applied Mechanics Reviews, **62**, p. 1.

[7] Noor, A. K., Burton, W. S., and Bert, C. W., 1996, "Computational Models for Sandwich Panels and Shells," Applied Mechanics Reviews, **49**(3), pp. 155–199.

BIBLIOGRAPHY

[8] Soedel, W., 2004, *Vibrations of Shells and Plates, 3rd ed.*, CRC Press, Boca Raton, FL.

[9] Mindlin, R. D., 2006, *An Introduction to the Mathematical Theory of Vibrations of Elastic Plates*, World Scientific, Singapore.

[10] Leissa, A. W. and Qatu, M. S., 2011, *Vibrations of Continuous Systems*, McGraw–Hill, New York.

[11] Elishakoff, I., 2019, *Handbook on Timoshenko-Ehrenfest beam and Uflyand-Mindlin Plate Theories*, World Scientific, Singapore.

[12] Liew, K. M. and Wang, C. M., 1993, "Vibration Studies on Skew Plates: Treatment of Internal Line Supports," Computers and Structures, **49**(6), p. 941–951.

[13] McGee, O. G. I., 2015, "Flexural Vibrations of Clamped-Free Rhombic Plates with Corner Stress Singularities Part I: Review of Research," Journal of Vibration and Control, **21**(13), p. 2583–2603.

[14] McGee, O. G. and Leissa, A. W., 1991, "Three-Dimensional Free Vibrations of Thick Skewed Cantilevered Plates," Journal of Sound and Vibration, **144**(2), pp. 305–322.

[15] Zhou, D., Liu, W., and Yang, Q., 2008, "Three-Dimensional Vibration Analysis of Cantilevered Skew Plates," Journal of Sound and Vibration, **313**(1), pp. 134–148.

[16] Lakshminarayana, H. V., Rajagopal, P. R., and Joshi, A., 1985, "Vibration Characteristics of a Swept Composite Wing Panel: Finite Element Analysis and Experimental Verification," Journal of the Aeronautical Society of India, **37**, pp. 289–295.

[17] Lee, I. and Lee, J. J., 1990, "Vibration Analysis of Composite Plate Wing," Computers and Structures, **37**(6), pp. 1077–1085.

[18] Kapania, R. K. and Singhvi, S., 1992, "Free Vibration Analyses of Generally Laminated Tapered Skew Plates," Composite Engineering, **2**(3), pp. 197–212.

[19] Kapania, R. K. and Lovejoy, A. E., 1996, "Free Vibration of Thick Generally Laminated Cantilever Quadrilateral Plates," AIAA Journal, **34**(7), pp. 1474–1486.

[20] Gurses, M., Civalek, O., Korkmaz, A. K., and Ersoy, H., 2009, "Free Vibration Analysis of Symmetric Laminated Skew Plates by Discrete Singular Convolution Technique Based on First-Order Shear Deformation Theory," International Journal for Numerical Methods in Engineering, **79**(3), pp. 290–313.

[21] Carrera, E., 2003, "Theories and Finite Elements for Multilayered Plates and Shells: A Unified Compact Formulation with Numerical Assessment and Benchmarking," Archives of Computational Methods in Engineering, **10**(3), pp. 215–296.

[22] Batra, R. C. and Vidoli, S., 2002, "Higher-Order Piezoelectric Plate Theory Derived from a Three-Dimensional Variational Principle," AIAA Journal, **40**(1), pp. 91–104.

[23] Demasi, L., 2008, "∞3 Hierarchy Plate Theories for Thick and Thin Composite Plates: The Generalized Unified Formulation," Composite Structures, **84**(3), pp. 256–270.

[24] Demasi, L., 2009, "∞6 Mixed Plate Theories Based on the Generalized Unified Formulation. Part IV: Zig-Zag Theories," Composite Structures, **87**(3), pp. 195–205.

[25] Demasi, L., 2009, "∞6 Mixed Plate Theories Based on the Generalized Unified Formulation. Part II: Layerwise Theories," Composite Structures, **87**(1), pp. 12–22.

[26] Demasi, L., 2009, "∞6 Mixed Plate Theories Based on the Generalized Unified Formulation. Part I: Governing Equations," Composite Structures, **87**(1), pp. 1–11.

[27] Demasi, L., 2009, "∞6 Mixed Plate Theories Based on the Generalized Unified Formulation. Part III: Advanced Mixed High Order Shear Deformation Theories," Composite Structures, **87**(3), pp. 183–194.

[28] Demasi, L., 2009, "∞6 Mixed Plate Theories Based on the Generalized Unified Formulation. Part V: Results," Composite Structures, **88**(1), pp. 1–16.

[29] Boscolo, M., 2013, "Analytical Solution for Free Vibration Analysis of Composite Plates with Layer-Wise Displacement Assumptions," Composite Structures, **100**(1), pp. 493–510.

[30] Boscolo, M. and Banerjee, J. R., 2014, "Layer-Wise Dynamic Stiffness Solution for Free Vibration Analysis of Laminated Composite Plates," Journal of Sound and Vibration, **333**(1), pp. 200–227.

[31] Dozio, L., 2014, "Exact Vibration Solutions for Cross-Ply Laminated Plates with Two Opposite Edges Simply Supported Using Refined Theories of Variable Order," Journal of Sound and Vibration, **333**(8), pp. 2347–2359.

[32] Fazzolari, F. A. and Carrera, E., 2011, "Advanced Variable Kinematics Ritz and Galerkin Formulations for Accurate Buckling and Vibration Analysis of Anisotropic Laminated Composite Plates," Composite Structures, **94**(1), pp. 50–67.

[33] Fazzolari, F. A., 2016, "Quasi-3D Beam Models for the Computation of Eigenfrequencies of Functionally Graded Beams with Arbitrary Boundary Conditions," Composite Structures, **154**(1), pp. 239–255.

[34] Marco, P. and Carrera, E., 2020, "Methods and Guidelines for the Choice of Shell Theories," Acta Mechanica, **231**(2), pp. 1–40.

BIBLIOGRAPHY

[35] Batra, R. C. and Aimmanee, S., 2005, "Vibrations of Thick Isotropic Plates with Higher Order Shear and Normal Deformable Plate Theories," Computers and Structures, **83**(12-13), pp. 934–955.

[36] Batra, R. C. and Aimmanee, S., 2007, "Vibration of an Incompressible Isotropic Linear Elastic Rectangular Plate with a Higher-Order Shear and Normal Deformable Theory," Journal of Sound and Vibration, **307**(3-5), pp. 961–971.

[37] Qian, L. F. and Batra, R. C., 2005, "Design of Bidirectional Functionally Graded Plate for Optimal Natural Frequencies," Journal of Sound and Vibration, **280**(1-2), pp. 415–424.

[38] Chattopadhyay, A. P. and Batra, R. C., 2019, "Free and Forced Vibrations of Monolithic and Composite Rectangular Plates with Interior Constrained Points," Journal of Vibration and Acoustics, **141**(1), p. 011018.

[39] Yuan, L. S. and Batra, R. C., 2019, "Vibrations of an Incompressible Linearly Elastic Plate Using Discontinuous Finite Element Basis Functions for Pressure," Journal of Vibration and Acoustics, **141**(5), p. 051016.

[40] Qian, L. F., Batra, R. C., and Chen, L. M., 2003, "Free and Forced Vibrations of Thick Rectangular Plates Using Higher-Order Shear and Normal Deformable Plate Theory and Meshless Petrov-Galerkin (MLPG) Method," Computer Modeling in Engineering and Sciences, **4**(5), pp. 519–534.

[41] Meirovitch, L. and Kwak, M. K., 1990, "Convergence of the Classical Rayleigh-Ritz Method and the Finite Element Method," AIAA Journal, **28**(8), pp. 1509–1516.

[42] Alanbay, B. and Kapania, R. K., 2018, ""On the Use of Classical Jacobi Orthogonal

Polynomials in the Ritz Method," 2018," AIAA/ASCE/AHS/ ASC Structures, Structural Dynamics, and Materials Conference, pp. 2018–1225.

[43] Alanbay, B., Singh, K., and Kapania, R. K., 2020, "Vibration of Curvilinearly Stiffened Plates Using Ritz Method with Orthogonal Jacobi Polynomials," Journal of Vibration and Acoustics, **142**(1), p. 011009.

[44] Alanbay, B., Batra, R. C., and Kapania, R. K., 2020, ""Lowest Twelve Frequencies of Sandwich Plates Using Third-Order Shear-Normal Deformation Theory,"," AIAA Journal, **58**(4), p. 1821–1835.

[45] Alanbay, B., Kapania, R. K., and Batra, R. C., 2020, "Up to Lowest 100 Frequencies of Rectangular Plates Using Jacobi Polynomials and TSNDT," Journal of Sound and Vibration, **480**(1), p. 115352.

[46] Datta, N. and Verma, Y., 2017, "Accurate Eigenvector-Based Generation and Computational Insights of Mindlin's Plate Modeshapes for Twin Frequencies," International Journal of Mechanical Sciences, **123**(1), p. 64–73.

[47] Qin, Z. and Batra, R. C., 2009, "Local Slamming Impact of Sandwich Composite Hulls," International Journal of Solids and Structures, **46**(10), p. 2011–2035.

[48] Hale, N. and Townsend, A., 2013, "Fast and Accurate Computation of Gauss-Legendre and Gauss-Jacobi Quadrature Nodes and Weights," SIAM Journal on Scientific Computing, **35**(2), p. A652–A674.

[49] Szegö, G., , and and, 1939, *Orthogonal Polynomials*, American Mathematical Society, Providence, Rhode Island.

[50] Fletcher, C. A. J., Methods, C. G., and , B., 1984, *Computational Galerkin Methods*, Springer-Verla.

BIBLIOGRAPHY

[51] Reddy, J. N., 2004, *Mechanics of Laminated Composite Plates and Shells: Theory and Analysis*, CRC Press, Boca Raton, FL.

[52] Malekzadeh, P., Maharloei, H. M., and Vosoughi, A. R., 2014, "A Three Dimensional Layerwise-Differential Quadrature Free Vibration of Thick Skew Laminated Composite Plates," Mechanics of Advanced Materials and Structures, **21**(10), p. 792–801.

[53] Wang, S., 1997, "Free Vibration Analysis of Skew Fibre-Reinforced Composite Laminates Based on First-Order Shear Deformation Plate Theory," Computers and Structures, **63**(3), p. 525–538.

[54] Anlas, G. and Goker, G., 2001, "Vibration Analysis of Skew FibreReinforced," Journal of Sound and Vibration, **242**(2), p. 265–276.

Chapter 5

Lowest Twelve Frequencies of Sandwich Plates Using TSNDT

The contents of this chapter have appeared in AIAA Journal. [1]

[1] **Alanbay, B.**, Batra, R. C., and Kapania, R. K., 2020, "Lowest Twelve Frequencies of Sandwich Plates Using Third-Order Shear-Normal Deformation Theory," AIAA Journal,58(4), p. 1821–1835.

5.1 Abstract

We delineate effects of 1) face-to-core stiffness ratio (FCSR) and mass density ratio (FCDR) in square laminates and sandwich plates and 2) the fiber and transverse direction elastic modulus ratio E_1/E_2 in cross-ply laminates on the first 12 distinct frequencies found by analytically solving the three-dimensional linear elasticity theory equations and using an equivalent single-layer third-order shear and normal deformation plate theory (TSNDT). Whereas the elasticity equations for simply supported plates are solved by using Srivinas and Rao's approach, the TSNDT equations are numerically solved by using weighted Jacobi polynomials and the Ritz method. We note that previous studies have generally compared only the fundamental frequency. For [0°/90°/0°/90°/0°] square laminates with a side-length/plate-thickness ratio of 100 (10), the maximum error in the TSNDT predicted first 12 frequencies is less than 0.4% (7%). For a FCSR less than 20 , the maximum difference in predictions from the two approaches for the first six distinct frequencies is 5.4%. However, the FCDR has little effect on the difference between frequencies from the two methods. The frequencies and mode shapes presented herein should help us better understand the dynamic behavior of laminated and sandwich plates and provide benchmark results for others to assess their theories.

5.2 Introduction

Because of superior properties, such as high specific strength and stiffness, composite structures have applications in many engineering fields, including automotive, aerospace, defense, and civilian infrastructure. However, due to differences in elastic moduli and possibly mass densities of individual layers as well as the existence of interfaces between adjoining layers, multilayered composite structures may exhibit complex dynamic behavior. Many equivalent

single-layer (ESL) plate theories generally do not represent aspects of transient deformations well since they usually fail to satisfy the continuity of surface tractions at the interfaces [1, 2]. In general, one cannot analytically solve the three-dimensional (3D) linear elasticity theory (LET) equations for transient deformations of composite structures. However, we can get some insights by studying their free vibrations found by analytically solving the 3 D LET equations. A typical sandwich structure consists of stiff outer face sheets (e.g., glass/carbon fiber-reinforced epoxy composite) and a soft core (e.g., aluminum, honeycomb, foam, and balsa wood) embedded between them [3]. Thus, it has a very high face-to-core stiffness ratio (FCSR). Several investigators have shown that an ESL plate theory in which the same displacement field is assumed through the plate thickness does not always satisfy the continuity of surface tractions across interfaces between adjoining layers, and thus may not predict accurate results. Reddy [4], Kant and Manjunatha [5], Pandya and Kant [6], Kant and Swaminathan [7], and Sayyad and Ghugal [8] have used different ESL plate theories to study free vibrations of the same sandwich plate with FCSR $= 19,000$ and reported significantly different frequencies. Carrera and Brischetto [9] compared accuracies of different plate theories for static and vibration analyses of sandwich plates, including ESL and layerwise plate theories. They concluded that using higher-order ESL plate theories provides improved predictions of their static and dynamic behaviors. However, the accuracy of their predictions worsens with an increase in the FCSR. Analytical solutions of the 3D-LET equations provide benchmark solutions for validating plate theories and their numerical solutions. Vlasov [10] seems to be the first one to have analytically solved plane strain deformations of a simply supported beam. A similar approach has been independently adopted by Srinivas and Rao [11], Srinivas et al. [12], and Pagano [13] to analyze free vibrations of simply supported thick laminated orthotropic plates. Following essentially the same technique, Fan and Ye [14] used a state-space method, in which the number of unknowns is independent of the number of layers, to analyze deformations of a laminate. Rao et al. [15]] employed

the propagator matrix technique to investigate free vibrations of a laminated plate. Messina [16] examined free vibrations of cross-ply laminated rectangular plates using two-dimensional displacementbased models and 3D-LET equations. Brischetto [17, 18] extended Messina's work to study 3D free vibrations of single-layer cy lindrical, spherical, and flat panels as well as multilayered cross-ply and sandwich plates/shells. Vel and Batra [19] have provided analytical frequencies of rectangular plates with through-the-thickness continuously varying (functionally graded) material properties. Batra et al. [20] have analytically solved fifth-order plate theory equations for symmetric and asymmetric bending modes of vibration and compared frequencies as well as through-the-thickness variations of stresses with those from Srivinas and Rao's approach and the Mindlin and the Kirchhoff plate theories. We note that most investigators have not provided stress distributions for different vibration modes.

The mentioned solutions of 3D-LET equations are obtained by expanding the three displacement components in terms of a double Fourier series in the plane of the plate with the coefficient of each term being a function of the thickness coordinate only. These expansions identically satisfy boundary conditions at simply supported edges, and the number of vibration waves in the x_1 and the x_2 directions (in-plane Cartesian coondinates) is defined by integers m and n appearing in the double Fourier series. The analysis procedure requires the solution of a resulting transcendental equation. For each (m, n), the transcendental equation yields an infinite number of frequencies, each corresponding to a different mode shape. For instance, when m and n both equal 1, the first root of the transcendental equation could correspond to the lowest vibration mode, while the second root could correspond to the 50 th mode. Furthermore, when either m or n equals zero, then only one in-plane displacement component is nonzero, there is no plate bending, and the solution of the transcendental equation gives frequencies of in-plane modes of vibration. Thus, obtaining natural frequencies and corresponding mode shapes in ascending order requires examination of the full spectrum of

values of (m, n). The sorted natural frequencies are needed since the dynamic characteristics of a structure are usually dominated by the lowest several modes. Furthermore, users of deterministic methods, such as the finite element method (FEM), can verify and ascertain the limits of their predictions by comparing them with the analytical results presented herein. We recall that obtaining higher vibration modes by using deterministic methods is computationally expensive and sometimes impossible due to the onset of numerical instabilities [21].

Most investigators, except possibly for Batra and Aimmanee [22] have reported frequencies for a few combinations of nonzero values of (m, n). Here, we present the lowest 12 distinct analytical frequencies and the corresponding mode shapes of simply supported crossply laminates and sandwich plates by using the state-space approach to solve 3D-LET equations and examine the full spectrum of modes to delineate the lowest 12. We find limits of applicability and the error in frequencies computed using an ESL third-order shear and normal deformable plate theory (TSNDT) that has been proven to be effective in analyzing free vibrations of monolithic, laminated, and sandwich plates [23, 24, 25, 26, 27, 28]. By varying the FCSR, the face sheet to the core mass density ratio (FCDR), and the elastic moduli of adjacent layers in a laminate, we examine how the relative errors between the TSNDT and 3D analytical solutions change. Novelties of the work include 1) quantifying the error in the first 12 distinct frequencies computed by the TSNDT relative to their analytical values (whereas most previous studies have compared only the first frequency), 2) demonstrating that using weighted Jacobi polynomials as basis functions in the Ritz method provides accurate values of the first 12 frequencies using the TSNDT. 3) considering in the third order plate theory transverse normal strains that have been assumed to be zero in most previous studies, and 4) ascertaining the critical FCSR and FCDR values beyond which frequencies from the TSNDT have unacceptable errors. It seems to us that the effect of the FCDR on

frequencies has not been addressed before.

5.3 Formulation of the Problem

Figure 5.1 shows a schematic sketch of a p -layer laminated rectangular plate of length a, width b, total thickness h, and the global and local rectangular Cartesian coordinate axes employed to describe the plate's infinitesimal deformations from the stress-free initial configuration. Each lamina is assumed to be made of a homogeneous material.

Equations, in the absence of the body forces, governing transient deformations of the k th lamina, are

$$\sigma_{ij,j}^{(k)} = \rho \ddot{u}_i^{(k)}, \qquad i,j = 1,2,3 \tag{5.1}$$

where $\sigma_{ij}^{(k)}$ are components of the Cauchy stress tensor, ρ is the mass density, and u_i is a displacement component. A repeated index, unless otherwise stated, implies summation over the range of the index; a comma followed by index j indicates partial differentiation with respect to the current position x_j of the particle; a superimposed dot represents partial derivative with respect to time t; and the superscript (k) implies quantities for the k^{th} layer.

With respect to the material principal axes, the constitutive relation for the k th lamina is

$$\begin{Bmatrix} \sigma_{11} \\ \sigma_{22} \\ \sigma_{33} \\ \sigma_{23} \\ \sigma_{13} \\ \sigma_{12} \end{Bmatrix}^{(k)} = \begin{bmatrix} C_{11} & C_{12} & C_{13} & 0 & 0 & 0 \\ C_{12} & C_{22} & C_{23} & 0 & 0 & 0 \\ C_{13} & C_{23} & C_{33} & 0 & 0 & 0 \\ 0 & 0 & 0 & C_{44} & 0 & 0 \\ 0 & 0 & 0 & 0 & C_{55} & 0 \\ 0 & 0 & 0 & 0 & 0 & C_{66} \end{bmatrix}^{(k)} \begin{Bmatrix} \varepsilon_{11} \\ \varepsilon_{22} \\ \varepsilon_{33} \\ 2\varepsilon_{23} \\ 2\varepsilon_{13} \\ 2\varepsilon_{12} \end{Bmatrix}^{(k)} \tag{5.2}$$

Here, $\varepsilon_{ij}^{(k)}$ is a component of the infinitesimal strain tensor, and $C_{ij}^{(k)}$ is an elastic constant

[29]. For infinitesimal deformations, the strain displacement relations are

$$\varepsilon_{ij}^{(k)} = \frac{1}{2}\left(u_{i,j}^{(k)} + u_{j,i}^{(k)}\right) \tag{5.3}$$

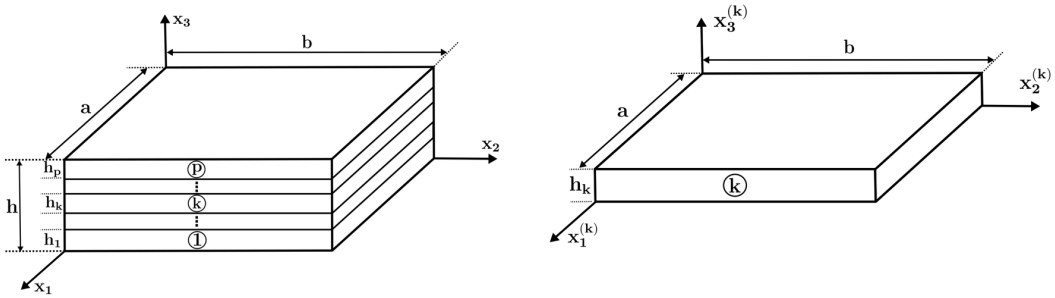

Figure 5.1: Nomenclature for a) p -layer laminated plate, and b) k^{th} lamina

5.3.1 Analytical solution for simply supported plate

Lamina

The state-space method [14] for finding analytical frequencies of simply supported cross-ply laminates is briefly described. We use the local coordinate system, $x_1^{(k)}, x_2^{(k)}, x_3^{(k)}$, defined in Figure 5.1b, and drop the superscript (k).

We rewrite Eqs. 5.1- 5.3 as the following first-order differential equations for the displace-

ments, u_1, u_2, u_3, and the transverse stresses, $\sigma_{33}, \sigma_{13}, \sigma_{23}$:

$$\begin{aligned}
u_{1,3} &= \frac{1}{C_{55}}\sigma_{13} - u_{3,1} \\
u_{2,3} &= \frac{1}{C_{44}}\sigma_{23} - u_{3,2} \\
u_{3,3} &= \frac{1}{C_{33}}\sigma_{33} - \frac{\bar{C}_{13}}{C_{33}}u_{1,1} - \frac{C_{23}}{C_{33}}u_{2,2} \\
\sigma_{13,3} &= \rho\ddot{u}_1 - \left(C_{11} - \frac{C_{13}^2}{C_{33}}\right)u_{1,11} - C_{66}u_{1,22} - \left(C_{12} - \frac{C_{13}C_{23}}{C_{33}}\right)u_{2,12} - \frac{C_{13}}{C_{33}}\sigma_{33,1} \\
\sigma_{23,3} &= -\left(C_{12} - \frac{C_{13}C_{23}}{C_{33}} + C_{66}\right)u_{1,12} + \rho\ddot{u}_2 - C_{66}u_{2,11} - \left(C_{22} - \frac{C_{23}^2}{C_{33}}\right)u_{2,22} - \frac{C_{23}}{C_{33}}\sigma_{33,2} \\
\sigma_{33,3} &= \rho\ddot{u}_3 - \sigma_{13,1} - \sigma_{23,2}
\end{aligned} \tag{5.4}$$

Following Srinivas and Rao [11] we use the following boundary conditions at edges of a simply supported plate:

$$\begin{aligned}
&\sigma_{11} = 0, \quad u_2 = u_3 = 0 \quad on \quad x_1 = 0,\ a \\
&\sigma_{22} = 0, \quad u_1 = u_3 = 0 \quad on \quad x_2 = 0,\ b
\end{aligned} \tag{5.5}$$

The following expressions for displacements identically satisfy boundary conditions [5]:

$$\left\{\begin{array}{c} u_1 \\ u_2 \\ u_3 \end{array}\right\} = \sum_{m=0}^{\infty}\sum_{n=0}^{\infty} \left\{\begin{array}{c} \bar{u}_1(x_3)\, cos\,(m\pi x_1/a)\, sin\,(n\pi x_2/b) \\ \bar{u}_2(x_3)\, sin\,(m\pi x_1/a)\, cos\,(n\pi x_2/b) \\ \bar{u}_3(x_3)\, sin\,(m\pi x_1/a)\, sin\,(n\pi x_2/b) \end{array}\right\} e^{i\omega t} \tag{5.6}$$

For the transverse stresses, we assume

$$\begin{Bmatrix} \sigma_{13} \\ \sigma_{23} \\ \sigma_{33} \end{Bmatrix} = \sum_{m=0}^{\infty}\sum_{n=0}^{\infty} \begin{Bmatrix} \bar{\sigma}_{13}\left(x_3\right) cos\left(m\pi x_1/a\right) sin\left(n\pi x_2/b\right) \\ \bar{\sigma}_{23}\left(x_3\right) sin\left(m\pi x_1/a\right) cos\left(n\pi x_2/b\right) \\ \bar{\sigma}_{33}\left(x_3\right) sin\left(m\pi x_1/a\right) sin\left(n\pi x_2/b\right) \end{Bmatrix} e^{i\omega t} \tag{5.7}$$

Here, ω is a natural frequency of the lamina. Substituting Eqs. 5.6 and 5.7 into Eq. 5.4 yields

$$\frac{\partial \mathbf{S}\left(x_3\right)}{\partial x_3} = \mathbf{A}\,\mathbf{S}\left(x_3\right) \tag{5.8}$$

where

$$\mathbf{S} = \left[\bar{u}_1 \;\; \bar{u}_2 \;\; \bar{\sigma}_{33} \;\; \bar{\sigma}_{13} \;\; \bar{\sigma}_{23} \;\; \bar{u}_3\right]^T, \qquad \mathbf{A} = \begin{bmatrix} \mathbf{0} & \mathbf{P} \\ \mathbf{Q} & \mathbf{0} \end{bmatrix} \tag{5.9}$$

$$\mathbf{P} = \begin{bmatrix} \frac{1}{C_{55}} & 0 & -M \\ 0 & \frac{1}{C_{44}} & -N \\ M & N & -\rho\omega^2 \end{bmatrix} \tag{5.10}$$

$$\mathbf{Q} = \begin{bmatrix} -\rho\omega^2 + \left(C_{11} - \frac{C_{13}^2}{C_{33}}\right)M^2 + C_{66}N^2 & \left(C_{12} + C_{66} - \frac{C_{13}C_{23}}{C_{33}}\right)MN & -\frac{C_{13}}{C_{33}}M \\ \left(C_{12} + C_{66} - \frac{C_{13}C_{23}}{C_{33}}\right)MN & -\rho\omega^2 + C_{66}M^2 + \left(C_{22} - \frac{C_{23}^2}{C_{33}}\right)N^2 & -\frac{C_{23}}{C_{33}}N \\ \frac{C_{13}}{C_{33}}M & \frac{C_{23}}{C_{33}}N & \frac{1}{C_{33}} \end{bmatrix}$$

$$M = m\pi/a, \quad N = n\pi/b \tag{5.11}$$

The solution of Eq. 5.8 for each M and N is

$$\mathbf{S}\left(x_3\right) = e^{\mathbf{A}x_3}\mathbf{S}\left(0\right) \tag{5.12}$$

We calculate the exponential matrix e^{Ax_3} by using the series expansion

$$\mathbf{D}\left(x_3\right) = e^{\mathbf{A}x_3} = \sum_{i=0}^{R} \frac{\mathbf{A}^i\, x_3^i}{i!} \tag{5.13}$$

Alternatively, e^{Ax_3} can be evaluated by using the Jordan decomposition of matrix A and the Cayley-Hamilton theorem [14, 30]

Laminate

Thus, for each lamina, we have

$$\mathbf{S}^{(k)}\left(x_3\right) = \mathbf{D}^{(k)}\left(x_3\right)\mathbf{S}^{(k)}\left(0\right), \qquad 0 \leq x_3^{(k)} \leq h_k \tag{5.14}$$

In a p -layered laminate, the interface continuity conditions to be satisfied are

$$\mathbf{S}^{(k+1)}\left(0\right) = \mathbf{S}^{(k)}\left(h_k\right) \tag{5.15}$$

Using Eqs. 5.14 and 5.15, the $\mathbf{S}$ matrix for the first lamina is related to that for the last lamina as follows by using the recursive formula:

$$\begin{aligned}
\mathbf{S}^{(p)}(h_p) =& \mathbf{D}^{(p)}(h_p)\mathbf{S}^{(p)}(0) = \mathbf{D}^{(p)}(h_p)\mathbf{S}^{(p-1)}(h_{p-1}) = \mathbf{D}^{(p)}(h_p)\mathbf{D}^{(p-1)}(h_{p-1})\mathbf{S}^{(p-1)}(0) \\
=& \mathbf{D}^{(p)}(h_p)\mathbf{D}^{(p-1)}(h_{p-1})\ldots\mathbf{D}^{(1)}(h_1)\mathbf{S}^{(1)}(0) \\
=& \bar{\mathbf{D}}\,\mathbf{S}^{(1)}(0)
\end{aligned} \tag{5.16}$$

Traction-free conditions at the top and the bottom surfaces of the p -layer laminate require that

$$\begin{aligned} \sigma_{33}^{(p)}(h_p) = \sigma_{13}^{(p)}(h_p) = \sigma_{23}^{(p)}(h_p) = 0 \\ \sigma_{33}^{(1)}(0) = \sigma_{13}^{(1)}(0) = \sigma_{23}^{(1)}(0) = 0 \end{aligned} \tag{5.17}$$

Substitution from Eq. 5.17 into Eq. 5.16 yields

$$\underbrace{\begin{bmatrix} \bar{D}_{31} & \bar{D}_{32} & \bar{D}_{36} \\ \bar{D}_{41} & \bar{D}_{42} & \bar{D}_{46} \\ \bar{D}_{51} & \bar{D}_{52} & \bar{D}_{56} \end{bmatrix}}_{\hat{\mathbf{D}}} \begin{Bmatrix} \bar{u}_1^{(1)}(0) \\ \bar{u}_2^{(1)}(0) \\ \bar{u}_3^{(1)}(0) \end{Bmatrix} = \{\mathbf{0}\} \tag{5.18}$$

where $\bar{D}_{ij}$ are components of the 6×6 matrix $\bar{\mathbf{D}}$ defined in Eq. 5.16. For Eq. 5.18 to have a nontrivial solution,

$$det\left(\hat{\mathbf{D}}\right) = 0 \tag{5.19}$$

For each combination of integer values of m and n, solutions of the characteristic Eq. 5.19 correspond to the plate vibration modes.

5.3.2 Brief Review of TSNDT

For the ESL formulation, we assume that the plane $x_3 = 0$ coincides with the plate midsurface, and the origin of the coordinate axes is at the plate geometric center. In the TSNDT [20], each component of the displacement vector, $\mathbf{u} = [u_1 \ u_2 \ u_3]^T$ is expressed as a complete polynomial of degree 3 in the thickness (the x_3) coordinate. That is,

$$u_i(x_1, x_2, x_3) = (x_3)^j u_{ij}(x_1, x_2), \qquad i = 1, 2, 3 \ and \ j = 0, 1, 2, 3 \tag{5.20}$$

Substitution for displacements from Eq. 5.20 into Eq. 5.3 yields

$$\boldsymbol{\epsilon} = \boldsymbol{Z}_i\left(x_3\right)\ \boldsymbol{L}\,\boldsymbol{d}_i\left(x_1, x_2\right), \qquad i = 0, 1, 2, 3 \tag{5.21}$$

Here,

$$\mathbf{d}_i = \left[u_{1i}\ \ u_{2i}\ \ u_{3i}\right]^T \tag{5.22}$$

$$\mathbf{L} = \begin{bmatrix} \dfrac{\partial}{\partial x_1} & 0 & 0 & 0 & 0 & \dfrac{\partial}{\partial x_2} & 1 & 0 \\ 0 & \dfrac{\partial}{\partial x_2} & 0 & 0 & 0 & \dfrac{\partial}{\partial x_1} & 0 & 1 \\ 0 & 0 & 1 & \dfrac{\partial}{\partial x_2} & \dfrac{\partial}{\partial x_1} & 0 & 0 & 0 \end{bmatrix}^T,$$

$$\mathbf{Z}_i = \begin{bmatrix} (x_3)^i & 0 & 0 & 0 & 0 & 0 & 0 & 0 \\ 0 & (x_3)^i & 0 & 0 & 0 & 0 & 0 & 0 \\ 0 & 0 & i\,(x_3)^{i-1} & 0 & 0 & 0 & 0 & 0 \\ 0 & 0 & 0 & (x_3)^i & 0 & 0 & 0 & i\,(x_3)^{i-1} \\ 0 & 0 & 0 & 0 & (x_3)^i & 0 & i\,(x_3)^{i-1} & 0 \\ 0 & 0 & 0 & 0 & 0 & (x_3)^i & 0 & 0 \end{bmatrix} \tag{5.23}$$

Recalling that the work done by external forces is zero, the Lagrangian of the plate at any time is given by

$$\Pi = U - T = \sum_{k=1}^{p} \frac{1}{2} \int_{\Omega^k} \left(\boldsymbol{\varepsilon}^T \boldsymbol{\sigma}^k - \rho^k\, \dot{\boldsymbol{u}}^T \dot{\boldsymbol{u}}\right) d\Omega^k \tag{5.24}$$

where

$$\dot{\boldsymbol{u}} = \begin{Bmatrix} u_{1,t} \\ u_{2,t} \\ u_{3,t} \end{Bmatrix} = \begin{bmatrix} x_3^i & 0 & 0 \\ 0 & x_3^i & 0 \\ 0 & 0 & x_3^i \end{bmatrix} \begin{Bmatrix} u_{1i,t} \\ u_{2i,t} \\ u_{3i,t} \end{Bmatrix} = \mathbf{Z}_\mathbf{i}^\mathbf{m} \dot{\mathbf{d}}_\mathbf{i}, \qquad i = 0, 1, 2, 3 \tag{5.25}$$

We approximate displacements in the plane of the plate by using the weighted Jacobian polynomials as basis functions. That is,

$$\mathbf{d}_i = \begin{Bmatrix} u_{1i} \\ u_{2i} \\ u_{3i} \end{Bmatrix} = \sum_{j=0}^{m_1} \sum_{k=0}^{m_1} \begin{Bmatrix} N_{1i}^{jk}(\xi,\eta)\ q_{1i}^{jk} \\ N_{2i}^{jk}(\xi,\eta)\ q_{2i}^{jk} \\ N_{3i}^{jk}(\xi,\eta)\ q_{3i}^{jk} \end{Bmatrix} = \mathbf{\Phi_i}\,\mathbf{q_i}, \qquad i = 0,1,2,3 \tag{5.26}$$

where the index i is not summed, $\mathbf{q}_i = [q_{1i}\ \ q_{2i}\ \ q_{3i}]^T$ is the vector of the generalized degrees of freedom (DOF), and $\mathbf{\Phi}_i = \text{diag}\,[\mathbf{N_{1i}},\ \mathbf{N_{2i}},\ \mathbf{N_{3i}}]$ is a matrix of basis functions that are chosen as the product of the Jacobi polynomials and a weight function. The details of constructing these basis functions and enforcing boundary conditions through the weight functions are given in [31, 32]. Substituting Eqs. 5.2 and 5.21 into Eq. 5.24 and taking the variation with respect to the unknown generalized DOF leads to the following eigenvalue problem:

$$\left[\mathbf{K} - \omega^2\,\mathbf{M}\right]\{\mathbf{q}\} = \{\mathbf{0}\} \tag{5.27}$$

In Eq. 5.27, $\mathbf{K}$ is the global stiffness matrix, $\mathbf{M}$ is the global mass matrix, ω is the natural frequency, and $\{\mathbf{q}\}$ is the eigenvector. The global stiffness and mass matrices, $\mathbf{K}$ and $\mathbf{M}$, have the expressions

$$\mathbf{K} = \begin{bmatrix} \mathbf{K_{00}} & \frac{1}{2}\left(\mathbf{K_{01}} + \mathbf{K_{10}}^T\right) & \frac{1}{2}\left(\mathbf{K_{02}} + \mathbf{K_{20}}^T\right) & \frac{1}{2}\left(\mathbf{K_{03}} + \mathbf{K_{30}}^T\right) \\ \frac{1}{2}\left(\mathbf{K_{10}} + \mathbf{K_{01}}^T\right) & \mathbf{K_{11}} & \frac{1}{2}\left(\mathbf{K_{12}} + \mathbf{K_{21}}^T\right) & \frac{1}{2}\left(\mathbf{K_{13}} + \mathbf{K_{31}}^T\right) \\ \frac{1}{2}\left(\mathbf{K_{20}} + \mathbf{K_{02}}^T\right) & \frac{1}{2}\left(\mathbf{K_{21}} + \mathbf{K_{12}}^T\right) & \mathbf{K_{22}} & \frac{1}{2}\left(\mathbf{K_{23}} + \mathbf{K_{32}}^T\right) \\ \frac{1}{2}\left(\mathbf{K_{30}} + \mathbf{K_{03}}^T\right) & \frac{1}{2}\left(\mathbf{K_{31}} + \mathbf{K_{13}}^T\right) & \frac{1}{2}\left(\mathbf{K_{32}} + \mathbf{K_{23}}^T\right) & \mathbf{K_{33}} \end{bmatrix} \tag{5.28}$$

$$\mathbf{M} = \begin{bmatrix} \mathbf{M_{00}} & \frac{1}{2}\left(\mathbf{M_{01}} + \mathbf{M_{10}}^T\right) & \frac{1}{2}\left(\mathbf{M_{02}} + \mathbf{M_{20}}^T\right) & \frac{1}{2}\left(\mathbf{M_{03}} + \mathbf{M_{30}}^T\right) \\ \frac{1}{2}\left(\mathbf{M_{10}} + \mathbf{M_{01}}^T\right) & \mathbf{M_{11}} & \frac{1}{2}\left(\mathbf{M_{12}} + \mathbf{M_{21}}^T\right) & \frac{1}{2}\left(\mathbf{M_{13}} + \mathbf{M_{31}}^T\right) \\ \frac{1}{2}\left(\mathbf{M_{20}} + \mathbf{M_{02}}^T\right) & \frac{1}{2}\left(\mathbf{M_{21}} + \mathbf{M_{12}}^T\right) & \mathbf{M_{22}} & \frac{1}{2}\left(\mathbf{M_{23}} + \mathbf{M_{32}}^T\right) \\ \frac{1}{2}\left(\mathbf{M_{30}} + \mathbf{M_{03}}^T\right) & \frac{1}{2}\left(\mathbf{M_{31}} + \mathbf{M_{13}}^T\right) & \frac{1}{2}\left(\mathbf{M_{32}} + \mathbf{M_{23}}^T\right) & \mathbf{M_{33}} \end{bmatrix} \tag{5.29}$$

where

$$\boldsymbol{K_{ij}} = \int_{-b/2}^{b/2}\int_{-a/2}^{a/2} \boldsymbol{B_i}^T \boldsymbol{R_{ij}} \boldsymbol{B_j} dx_1 dx_2, \quad \boldsymbol{B_i} = \boldsymbol{L}\boldsymbol{\Phi_i}, \qquad i,j = 0,1,2,3 \tag{5.30}$$

$$\boldsymbol{M_{ij}} = \int_{-b/2}^{b/2}\int_{-a/2}^{a/2} \boldsymbol{\Phi_i}^T \boldsymbol{m_{ij}} \boldsymbol{\Phi_j} dx_1 dx_2, \qquad i,j = 0,1,2,3 \tag{5.31}$$

$$\boldsymbol{R_{ij}} = \sum_{k=1}^{p} \int_{x_3^{(k)}}^{x_3^{(k+1)}} \boldsymbol{Z_i}^T \boldsymbol{C}^k \boldsymbol{Z_j} dx_3, \quad \boldsymbol{m_{ij}} = \sum_{k=1}^{p} \int_{x_3^{(k)}}^{x_3^{(k+1)}} \rho^k \left(\boldsymbol{Z_i^m}\right)^T \boldsymbol{Z_j^m} dx_3 \tag{5.32}$$

and repeated indices are not summed.

5.4 Numerical Examples

In this section, we present and discuss the lowest 12 distinct frequencies for numerous example problems. In tables and figures, repeated frequencies are signified by superscript $*$. We begin with studying vibrations of an orthotropic and homogeneous rectangular plate to verify our software and analysis technique by comparing the presently computed frequencies with those of Srinivas and Rao [11]. Subsequently, vibrations of a three-layered sandwich plate are analyzed, and the relative error between the analytical and the TSNDT results for different values of the FCSR and the FCDR are quantified. Next, the first 12 free vibration modes of a cross-ply laminated plate are found with different stacking sequences and two thickness-to-side length ratios for delineating the accuracy of the TSNDT frequencies. Also, the influence

Table 5.1: Material properties of aragonite crystals [11]

Elasticity ratio	Value	Elasticity ratio	Value
C_{22}/C_{11}	0.543103	C_{33}/C_{11}	0.530172
C_{12}/C_{11}	0.233190	C_{13}/C_{11}	0.010776
C_{23}/C_{11}	0.098276	C_{44}/C_{11}	0.266810
C_{55}/C_{11}	0.159914	C_{66}/C_{11}	0.262931

of the longitudinal (along the fiber) and the transverse (normal to the fiber) direction elastic moduli ratio E_1/E_2 on the relative error in the TSNDT predictions is examined. Finally, free vibrations of a five-layered sandwich plate are investigated by using the analytical approach, the TSNDT, and the 3D FEM.

5.4.1 Orthotropic Square Plate Studied by Srinivas and Rao [11]

For a first example, we consider the simply supported orthotropic plate analyzed by Srinivas and Rao[11] in order to establish the accuracy of the present analytical solution. The values of material elastic constants are listed in Table 5.1. The frequency parameters, $\lambda = \omega\sqrt{\rho h/C_{11}}$, for symmetric S, and antisymeric A, modes about the midplane are obtained for different sets of (m, n) values and are found to agree well with those of Srinivas and Rao; e.g., see Table 5.2 in which the maximum error of 0.06% is listed for $m = n = 5$.

The first 12 frequency parameters and the corresponding mode shapes of the orthotropic plate are presented in Figure 5.2. The red color represents the absolute maximum value of a displacement component (either deflection or an in-plane displacement), and the blue color represents the undeformed state. The fringe plots are for magnitudes of the most dominant deflection component; the scale for fringes is not included for brevity. Whereas Srinivas and Rao [11] considered frequencies for $m \geq 1$ and $n \geq 1$, we also include cases corresponding to in-plane pure distorional modes for which either m or n equals zero and there is no plate bending. The m and n values are listed as subscripts on the frequency parameter $\lambda_{m,n}$.

It is observed that the in-plane modes of vibration occur for low values of $\lambda_{m,n}$ and may play an important role in the dynamic behavior of a structure. As mentioned in [26], the occurrence of in-plane modes depends upon the plate aspect ratio. Strain energies associated with different modes of vibration are reported in [27] .

Table 5.2: Frequency parameters $\lambda = \omega\sqrt{\rho h/C_{11}}$ of a simply supported orthotropic square plate ($h/a = 0.1$)

		I-A (First antisymmetric mode)			I-S (First symmetric mode)			II-S (Second symmetric mode)		
Mode (m,n)		Srinivas and			Srinivas and			Srinivas and		
m	n	Rao [11]	Present	Diff %	Rao [11]	Present	Diff %	Rao [11]	Present	Diff %
1	1	0.04742	0.04742	0.00	0.21697	0.216953	-0.01	0.39405	0.394034	0.00
1	2	0.10329	0.10329	0.00	0.34501	0.344996	0.00	0.56242	0.562411	0.00
1	3	0.18881	0.18881	0.00	0.4953	0.495283	0.00	0.76004	0.760039	0.00
1	4	0.29690	0.29690	0.00	0.6519	0.651889	0.00	0.96901	0.969004	0.00
1	5	0.42124	0.42124	0.00	0.81071	0.810695	0.00	1.1825	1.18255	0.00
2	1	0.11880	0.11880	0.00	0.3515	0.35149	0.00	0.67278	0.672723	-0.01
2	2	0.16942	0.16941	0.00	0.43382	0.43379	-0.01	0.78796	0.787916	-0.01
2	3	0.24753	0.24754	0.00	0.55201	0.551971	-0.01	0.94433	0.944301	0.00
2	4	0.34755	0.34759	0.01	0.68957	0.689531	-0.01	1.1231	1.12312	0.00
2	5	0.46428	0.46428	0.00	0.83699	0.83696	0.00	1.3142	1.31415	0.00
3	1	0.21804	0.21803	-0.01	0.50291	0.5029	0.00	0.97278	0.972687	-0.01
3	2	0.26244	0.26243	0.00	0.56047	0.560444	0.00	1.0573	1.05717	-0.01
3	3	0.33200	0.33200	0.00	0.65043	0.650389	-0.01	1.1814	1.18137	0.00
3	4	0.42242	0.42241	0.00	0.76415	0.764096	-0.01	1.3321	1.33202	-0.01
3	5	0.52956	0.52956	0.00	0.8936	0.893549	-0.01	1.4994	1.49937	0.00
4	1	0.33189	0.33187	-0.01	0.65908	0.659073	0.00	1.2795	1.27933	-0.01
4	2	0.37066	0.37065	0.00	0.70277	0.702744	0.00	1.3453	1.34519	-0.01
4	3	0.43225	0.43224	0.00	0.77334	0.773295	-0.01	1.4463	1.4462	-0.01
4	4	0.51342	0.51341	0.00	0.86667	0.866611	-0.01	1.5736	1.57355	0.00
4	5	0.61092	0.61092	0.00	0.97769	0.977624	-0.01	1.7191	1.719	-0.01
5	1	0.45265	0.45263	-0.01	0.8172	0.817193	0.00	1.589	1.58878	-0.01
5	2	0.48680	0.48678	0.00	0.85223	0.852209	0.00	1.6425	1.64239	-0.01
5	3	0.54160	0.54159	0.00	0.90962	0.909579	0.00	1.7266	1.72651	-0.01
5	4	0.61465	0.61464	0.00	0.98732	0.987263	-0.01	1.8187	1.81865	0.00
5	5	0.70338	0.70338	0.00	1.0824	1.08228	-0.01	1.8559	1.85478	-0.06

5.4.2 Three-Ply Sandwich Plate Studied by Srinivas and Rao

Figure 5.3 shows a schematic sketch of the three-ply simply supported laminate with identical top and bottom face sheets studied in [11] having $a = b$, $h_1/h = 0.1$, $h_2/h = 0.8$, $a/h = 10$, and material properties provided in [11]. The FCSR and the FCDR, respectively, are defined as $\beta = C_{11}^{\text{face}}/C_{11}^{\text{core}}$ and $\gamma = \rho^{\text{face}}/\rho^{\text{core}}$ Srinivas and Rao [11] and Fan and Ye [14] considered

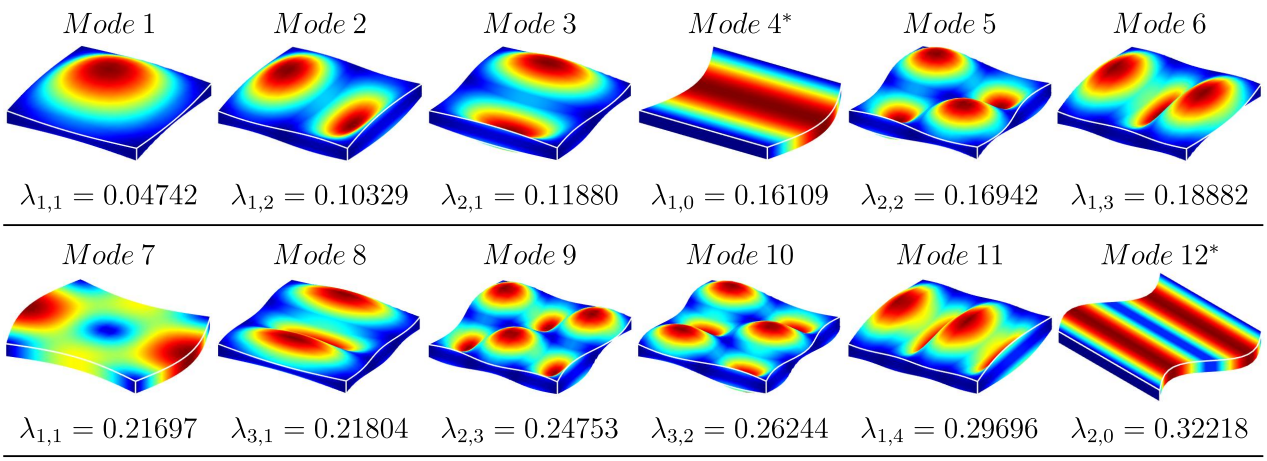

Figure 5.2: First 12 analytical frequencies and the corresponding mode shapes of the orthotropic plate. (Note that modes 1 and 7 are the first antisymmetric and the first symmetric modes for $m = n = 1$.

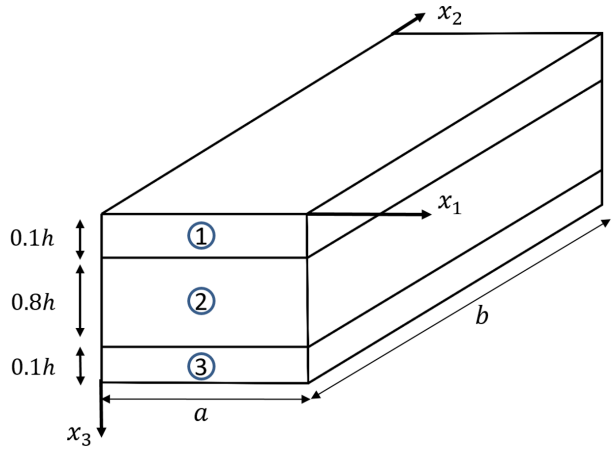

Figure 5.3: Schematic sketch of a three-ply laminate with identical top and bottom face sheets

β up to 15 . Depending on the application, a wide range of values of β and γ occurs in practical applications. It is known that for $\beta \gg 1$, the ESL plate theories give erroneous predictions [9]. However, it is not clear up to what values of β and γ the ESL plate theory yields acceptable results. Here, we try to address this question. The influence of β and γ on the relative error in the TSNDT predicted fundamental frequency (first six frequencies) is reported in Table 5.3 (Table 5.4) and Table 5.5 (Table 5.6), respectively. In Table 5.3, we have

also included fundamental frequencies computed by Srinivas and Rao and Fan and Ye. It is clear that the error between the TSNDT and the analytical results enormously increases with increasing β. For $\beta < 20$, the maximum difference in the TSNDT predictions and analytical values of the first six frequencies is 5.4% and can be accepted for many applications. The percent difference between the TSNDT and the analytical results with β values between 1 and 100 are plotted for the out-of-plane bending modes in Figure 5.4. It can be seen that the trend is monotonic and the percent difference increases with an increase in the mode number and the β value and exceeds 20 % for $\beta = 100$, suggesting that one should not use an ESL for plates with $\beta \geq 100$. In Figure 5.4, symbols denote computed values, and solid curves denote least-squares fit to the data for each in visualization. Equations of the curves with $x = \beta$ for β until 100 are

$$\begin{aligned} \lambda_{1,1}(x) &= -0.9205 + 0.2154x \\ \lambda_{1,2}(x) &= -0.4566 + 0.2446x \\ \lambda_{2,1}(x) &= -0.0832 + 0.2715x \\ \lambda_{2,2}(x) &= 0.1490 + 0.2690x \end{aligned} \tag{5.33}$$

Results included in Table 5.6 show that values of γ have very little effect on the first six frequencies. It is not clear why the error in the fifth frequency in Table 5.6 is less than that in the other frequencies. Note that the large error is due to our taking $\beta = 1000$. The critical value of the FCSR for which the lowest 12 frequencies from the TSNDT differed by less than 5% of their respective analytical values strongly depends upon values of m and n in Eq. 5.6. For the FCSR between 1 and 14 (1 and 22), the maximum error in the TSNDT frequencies was less than 5% (10%). For $(m, n) = (1, 1),\ (1, 2),\ (2, 1),\ (2, 2),\ (1, 3),\ (3, 1),\ (2, 3),\ (3, 2)$, the critical values of the FCSR respectively, were found to be 29, 19, 18, 20, 19, 14, 16and14.

Table 5.3: Influence of the FCSR on the fundamental frequency parameter, $\lambda_{1,1} = \omega h\sqrt{\rho_2/C_{11}^{\text{core}}}, \gamma = 1$

$\beta=\frac{C_{11}^{face}}{C_{11}^{core}}$	Present analytical	Srinivas and Rao analytical [11]	Fan and Ye analytical [14]	TSNDT	Difference %
1	0.047419	0.047419	0.047511	0.047419	0.00
2	0.057038	0.057041	0.057052	0.057062	0.04
5	0.077148	0.077148	0.077144	0.077456	0.40
10	0.098104	0.098104	0.098104	0.099315	1.23
15	0.112034	0.112034	0.112032	0.114495	2.20
20	0.122265	-	-	0.12621	3.23
50	0.153597	-	-	0.168708	9.84
100	0.173157	-	-	0.208935	20.66
500	0.20292	-	-	0.375258	84.93
1000	0.213214	-	-	0.507333	137.95
1500	0.220438	-	-	0.611127	177.23
2000	0.226723	-	-	0.6996	208.57
5000	0.258481	-	-	1.088426	321.09
10^4	0.302584	-	-	1.53071	405.88
10^5	0.718870	-	-	4.81590	569.9
10^6	1.611290	-	-	15.2214	844.7
10^7	1.612180	-	-	48.1318	2885

5.4.3 Cross-Ply Laminated Plates

For cross-ply laminates, we study the following two problems.

Effect of Different Stacking Sequence on Frequencies and Corresponding Mode Shapes

The first 12 frequencies of two-, three-, four-, and five-layer cross-ply square laminated plates for thickness ratios a/h of 10 and 100 obtained by the analytical solution and the TSNDT are listed in Tables 5.7– 5.10.The corresponding mode shapes are given in Figures 5.5– 5.12. Each layer has the same thickness, and the stacking sequences were constructed by starting with the fiber angle of 0 deg with respect to the x_1 axis and then alternating between 90

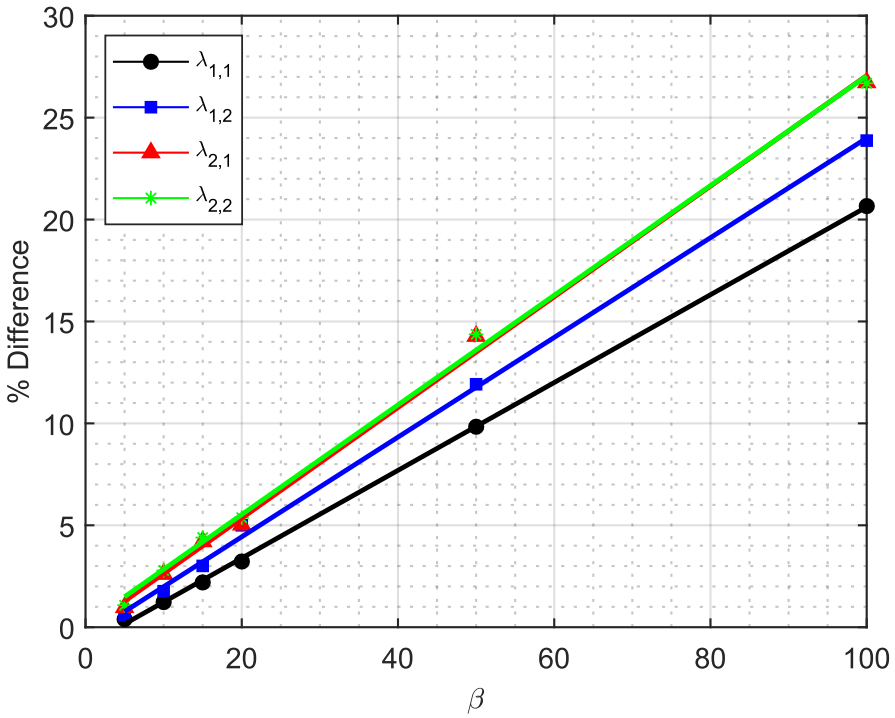

Figure 5.4: Percent difference between the TSNDT and the analytical results vs β (FCSR) values for the out-of-plane bending modes

and 0 deg. The material properties of the 0 deg layer, taken from [33], are listed below.

$$\begin{aligned} E_1 &= 25.1 \times 10^6\ psi \quad E_2 = 4.8 \times 10^6\ psi \quad E_3 = 0.75 \times 10^6\ psi \\ G_{12} &= 1.36 \times 10^6\ psi \quad G_{13} = 1.2 \times 10^6\ psi \quad G_{23} = 0.47 \times 10^6\ psi \\ \nu_{12} &= 0.036 \qquad \nu_{13} = 0.25 \qquad \nu_{23} = 0.171 \end{aligned} \tag{5.34}$$

For $a/h = 10$, natural frequencies for $(m, n) = (1, 1)$, $(1, 2)$, $(2, 1)$, and $(2, 2)$ have been reported by Nosier et al. [33] and Messina [16]. The present results for these four values of (m, n) match well with those included in [31, 32] and are not given here. For $a/h = 100$, the maximum difference in the presently computed analytical and the TSNDT values of the first 12 frequencies for the cross-ply laminates studied is 0.42%. However, the maximum difference increases to 7.2% for $a/h = 10$. We note that the in-plane frequencies are found to be the

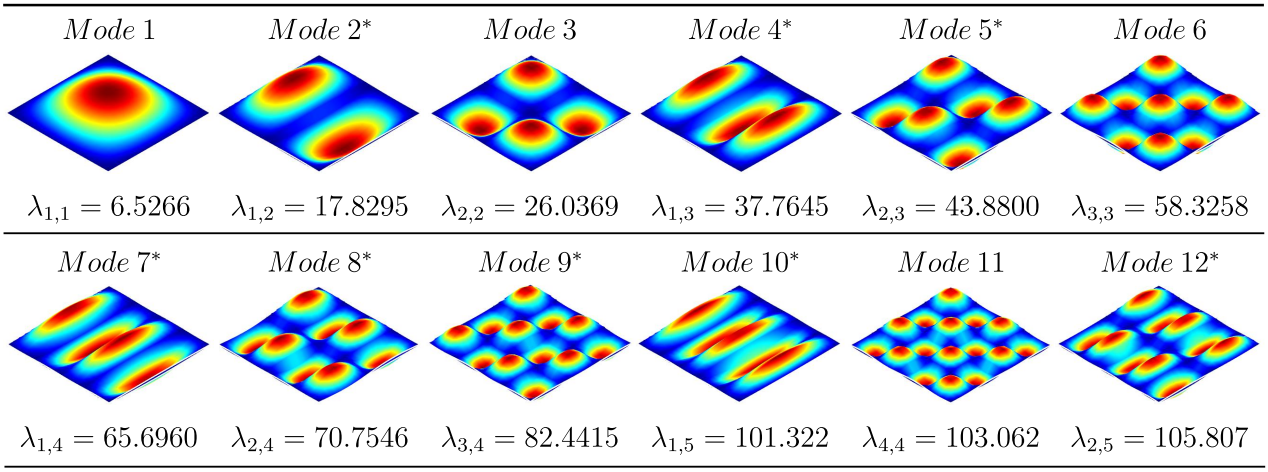

Figure 5.5: First 12 mode shapes of a square laminated plate; $[0°/90°], a/h = 100$. An $*$ indicates that the frequency is repeated with values of m and n interchanged

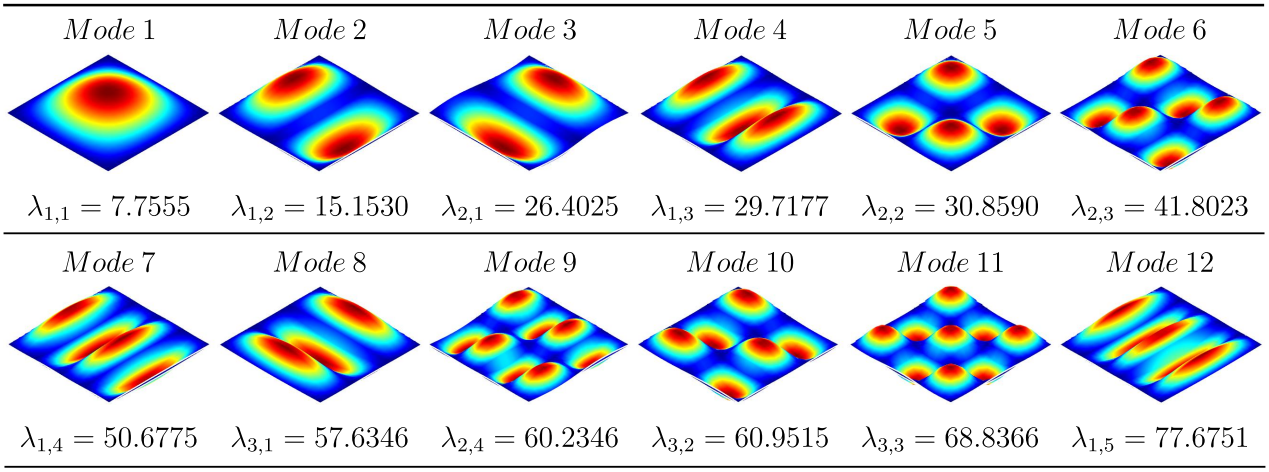

Figure 5.6: First 12 mode shapes of a square laminated plate; $[0°/90°/0°], a/h = 100$

same for the five stacking sequences and two thickness ratios considered here. For plates with $a/h = 100$, the first 12 vibration modes correspond to out-of-plane bending deformations. However, for $a/h = 10$, four in-plane modes are observed in the first 12 modes. Depending on the stacking sequence, the order of the lowest modes changes.

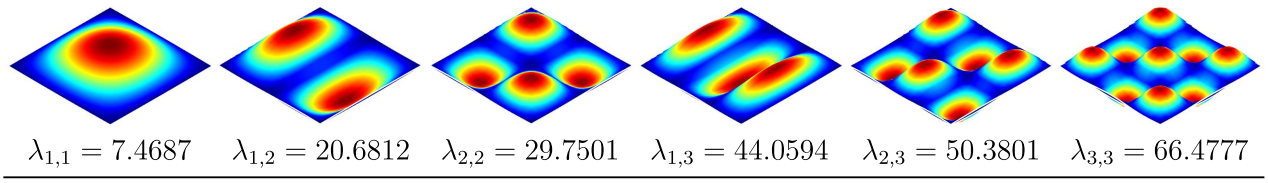

Figure 5.7: First 12 mode shapes of a square laminated plate; $[0°/90°/0°/90°]$, $a/h = 100$. An $*$ indicates that the frequency is repeated with values of m and n interchanged

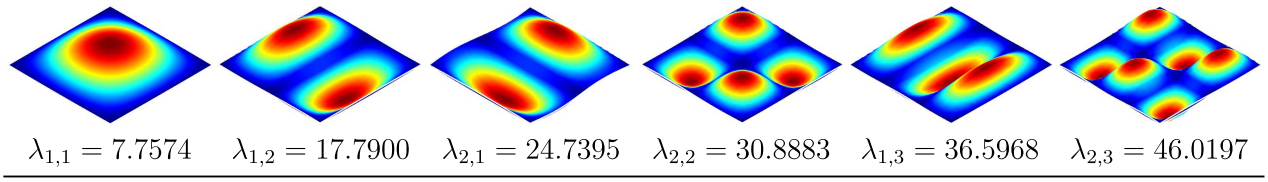

Figure 5.8: First 12 mode shapes of a square laminated plate; $[0°/90°/0°/90°/0°]$, $a/h = 100$

Influence of E_1/E_2, on Fundamental Frequency of Square Laminates Studied by Noor and Rao et al.

In Sec. III.B, we focused on changes in frequencies caused by the ratio of the elastic moduli of the face sheet and the core (FCSR) of a sandwich plate. However, distinct material properties of adjoining layers occur in laminated plates. For example, with one layer reinforced with carbon nanotubes and the other with carbon fibers, we may have $E_1/E_2 \geq 60$[34]. Here, we

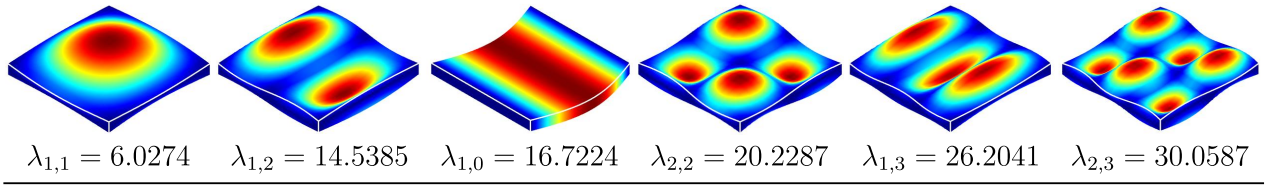

Figure 5.9: First 12 mode shapes of a square laminated plate; $[0°/90°]\,, a/h = 10$. An $*$ indicates that the frequency is repeated with values of m and n interchanged.

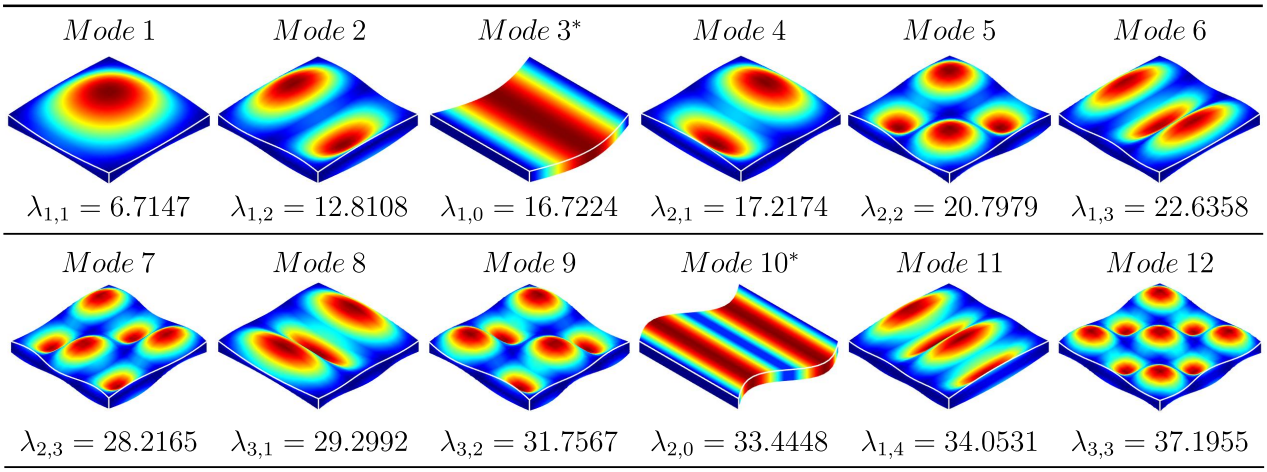

Figure 5.10: First 12 mode shapes of a square laminated plate; $[0°/90°/0°]\,, a/h = 10$. An $*$ indicates that the frequency is repeated with values of m and n interchanged.

investigate the influence of E_1/E_2, on the fundamental frequency of the square plate having $a/h = 5$, the same thickness of each layer, and the material properties listed in the following [35]:

$$\begin{gathered} E_1/E_2 = \text{ constant }, \quad E_3 = E_2, \quad G_{12} = G_{13} = 0.6E_2 \\ G_{23} = 0.5E_2, \quad v_{12} = v_{13} = v_{23} = 0.25 \end{gathered} \tag{5.35}$$

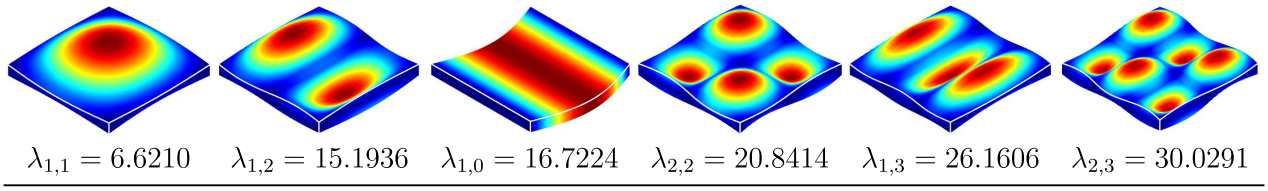

Figure 5.11: 11 First 12 mode shapes of a square laminated plate; $[0°/90°/0°/90°]$, $a/h = 10$. An * indicates that the frequency is repeated with values of m and n interchanged.

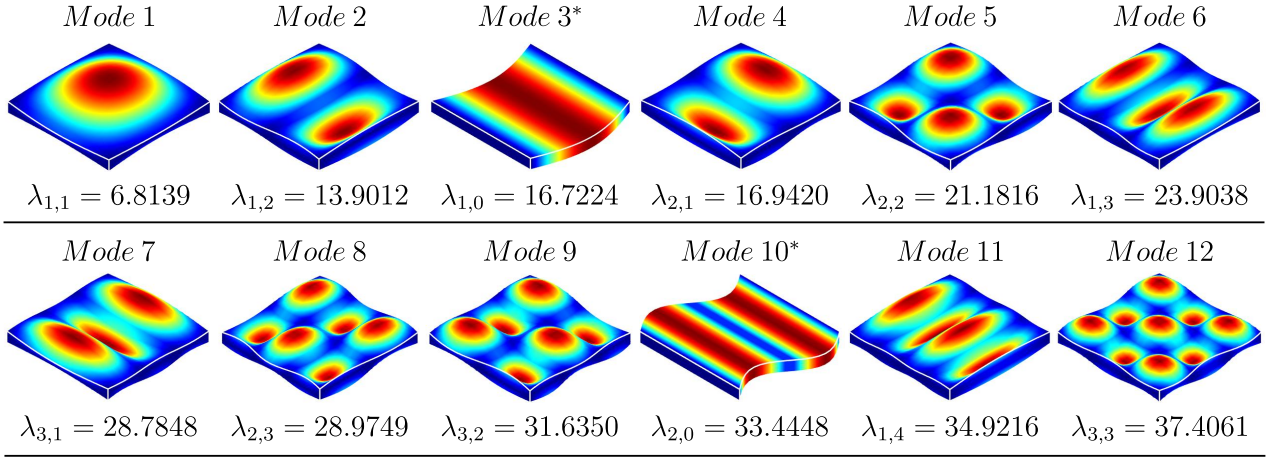

Figure 5.12: First 12 mode shapes of a square laminated plate; $[0°/90°/0°/90°/0°]$, $a/h = 10$. An $*$ indicates that the frequency is repeated with values of m and n interchanged.

We have listed in Table 5.11 for $80 \geq E_1/E_2 \geq 3$, frequencies obtained analytically, computed using the TSNDT; those found by Noor [35], who numerically solved the 3D LET equations by the finite difference method; and those found by Rao et al. [15], who used a different method to analyze the 3D LET equations. The percent difference between the present analytical solution and the results of other researchers is also reported in the table. The maximum percent differences between the present analytical results and those from the

TSNDT, Rao et al. [15], and Noor [35]are 4.5, 0.0, and 5.1, respectively. For $E_1/E_2 = 50$, the difference between the present analytical and the TSNDT results equals 9.1%, and that for the sandwich plate (cf. Table 5.3) is 9.8%.

5.4.4 $[0°/90°/$ core $/90°/0°]$ Sandwich Square Plate

We now analyze free vibrations of a five-layered sandwich plate having the core to face sheet thickness ratio $(t_c/t_f) = 10$, the side length to thickness ratio $(a/h) = 10$, and the following material properties [7]:

$$\begin{aligned}
&\text{Facesheets:}\\
&E_1 = 19 \times 10^6\, psi,\ \ E_2 = 1.5 \times 10^6,\ \ E_2 = E_3,\\
&G_{12} = G_{23} = 1 \times 10^6\, psi,\ \ G_{13} = 0.90 \times 10^6\, psi\\
&\nu_{12} = \nu_{13} = 0.22,\ \ \nu_{23} = 0.49,\ \ \rho = 0.057\, lb/inch^3\\
&\text{Core:}\\
&E_1 = E_2 = E_3 = 1000\, psi,\ \ G_{12} = G_{13} = G_{23} = 500\, psi\\
&\nu_{12} = \nu_{13} = \nu_{23} = 0,\ \ \rho = 0.003403\, lb/inch^3
\end{aligned} \tag{5.36}$$

In Table 5.12, we have compared the first 12 frequency parameters of the five-layered $[0°/90°/\text{core}/90°/0°]$ sandwich plate by using the present analytical method, the 3D FEM, and the TSNDT. The 3D FEM analysis is performed with the commercial finite element software, Abaqus, and employing mesh seeding of $70 \times 70 \times 33$ and $120 \times 120 \times 33$ [4(17) through the thickness in each face (core) layer] using eight-node brick elements (C3D8 in Abaqus terminology). The error in the TSNDT frequency is more than 100% for all modes and is attributed to $E_1/E_2 = 19,000$. On the other hand, the maximum difference of 6.1% is seen in the 3D FEM frequency for mode 10. The 3D mode shapes obtained using the

analytical solution and the FEM, presented in Figure 5.13, show excellent agreement with each other.

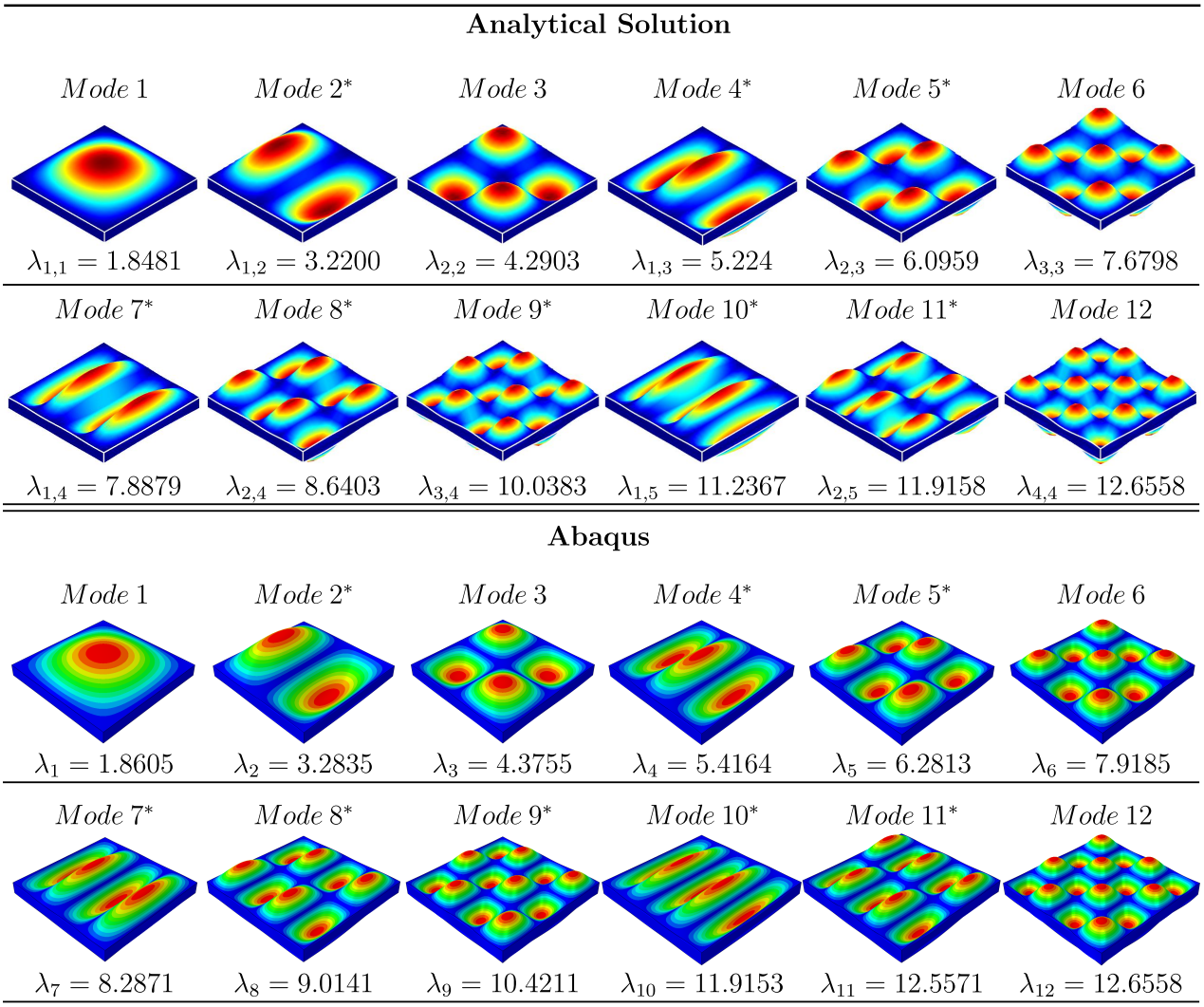

Figure 5.13: Frequency parameters and corresponding mode shapes of $[0°/90°/$ core $/90°/0°]$ sandwich plate, $a/b = 1$, $b/h = 10$, $t_c/t_f = 10$ $E_1^{\text{core}}/E_1^{\text{face}} = 1/19000$. An $*$ indicates that the frequency is repeated with values of m and n interchanged.

We remark that for a simply supported square homogeneous and isotropic plate with $h/a = 0.2$, Qian et al. [36] found that the second, the third, and the fourth order shear and normal deformable plate theory, respectively, give very good values of the first, the second and the fourth frequency. Furthermore, a 5th order shear and normal deformable plate theory gives

very good values of frequencies even for $h/a = 0.5$

Batra and Vidoli [37] deduced both compatible and mixed higherorder plate theories from a three dimensional theory. In the former stresses are deduced from the plate theory displacements and Hooke's law but in the latter they are found as a part of the solution of the problem. Groh and Weaver [38] have mentioned that the major advantage of the mixed theory is that it enforces stresses to satisfy the natural boundary conditions at the top and bottom surfaces, and by deriving transverse stresses from the plate equations directly, the stress fields are closer to 3D elasticity solutions than those derived from a compatible plate theory. Thus, boundary layers near clamped and free edges, and asymmetric stress profiles due to surface tractions on one surface only, can be captured more accurately in the mixed plate theory.

5.5 Conclusions

For a simply supported square orthotropic plate, a cross-ply laminate, and a sandwich plate, we have presented the first 12 natural frequencies and mode shapes found from the analytical solution of the 3 D linear elasticity theory equations (including in-plane modes), a third-order shear and normal deformable plate theory using weighted Jacobi polynomials as basis functions, and the 3 D finite element method using the commercial software Abaqus. The analytical results serve as benchmarks for assessing the accuracy of various plate theories.

It is found that for an equivalent single-layer TSNDT, the first six frequencies have a maximum error of 5% for the ratio of the maximum face sheet modulus to that of the orthotropic core (FCSR) of a sandwich plate less than 20. This percent error increases, respectively, to 16, 93, and 280 for FCSR = 50, 500, and 5000, making the use of the ESL unacceptable. The ratio of the mass densities of the face sheet and the core have a negligible effect on the first

six frequencies. For the [0°/90°/core/90°/0°] sandwich plate, the fundamental frequency predicted with the ESL TSNDT has an error of 168%, but that with the finite element method using the 3D LET equations has an error of only 0.7%.

For moderately thick cross-ply laminates with side length to plate thickness ratio, $a/h = 10$, the maximum difference between the analytical first 12 and the TSNDT frequencies is about 7.2%. However, this difference reduces to 0.42% for $a/h = 100$. Whereas the first 12 modes correspond to bending deformations for $a/h = 100$, those for $a/h = 10$ include four in-plane modes of vibrations for which the plate deflections vanish. The TSNDT, like the analytical solution, successfully predicts in-plane modes of vibration usually studied separately by many investigators.

This paper also presents the first 12 3D mode shapes for an improved understanding of the dynamic characteristics of the composite structures.

Table 5.4: Influence of the FCSR (β) on the first six frequencies, $\lambda_{m,n} = \omega h\sqrt{\rho_2/C_{11}^{\text{core}}}, \gamma = 1$

$\beta = \frac{C_{11}^{\text{face}}}{C_{11}^{\text{core}}}$	Method	Mode 1	Mode 2	Mode 3	Mode 4	Mode 5	Mode 6
1	$(m,n) \rightarrow$	(1, 1)	(1, 2)	(2, 1)	(0, 1)	(1, 0)	(2, 2)
	Analytical	0.047418	0.103289	0.118795	0.161090	0.161090	0.169420
	TSNDT	0.047419	0.103292	0.118804	0.161091	0.161091	0.169424
	Difference, %	0.00	0.00	0.01	0.00	0.00	0.00
2	$(m,n) \rightarrow$	(1, 1)	(1, 2)	(2, 1)	(0, 1)	(1, 0)	(2, 2)
	Analytical	0.057038	0.123267	0.139678	0.176443	0.176452	0.198247
	TSNDT	0.057062	0.123355	0.139849	0.176452	0.176458	0.198534
	Difference, %	0.04	0.07	0.12	0.01	0.00	0.14
5	$(m,n) \rightarrow$	(1, 1)	(1, 2)	(2, 1)	(0, 1)	(1, 0)	(2, 2)
	Analytical	0.077148	0.163324	0.178270	0.215847	0.215959	0.250467
	TSNDT	0.077456	0.164316	0.179999	0.216035	0.216071	0.253173
	Difference, %	0.40	0.61	0.97	0.09	0.05	1.08
10	$(m,n) \rightarrow$	(1, 1)	(1, 2)	(2, 1)	(1, 0)	(0, 1)	(2, 2)
	Analytical	0.098104	0.202289	0.211383	0.268455	0.268895	0.294361
	TSNDT	0.099315	0.205861	0.216884	0.269354	0.269435	0.302557
	Difference, %	1.23	1.77	2.60	0.33	0.20	2.78
15	$(m,n) \rightarrow$	(1, 1)	(1, 2)	(2, 1)	(0, 1)	(1, 0)	(2, 2)
	Analytical	0.112034	0.226547	0.229842	0.311758	0.312662	0.318692
	TSNDT	0.114495	0.233361	0.239499	0.313734	0.31385	0.332708
	Difference, %	2.20	3.01	4.20	0.63	0.38	4.40
20	$(m,n) \rightarrow$	(1, 1)	(1, 2)	(2, 1)	(2, 2)	(0, 1)	(1, 0)
	Analytical	0.122265	0.241862	0.243532	0.334595	0.349242	0.350713
	TSNDT	0.126210	0.253952	0.255765	0.352570	0.352715	0.354461
	Difference, %	3.23	5.00	5.02	5.37	0.99	1.07
50	$(m,n) \rightarrow$	(1, 1)	(2, 1)	(1, 2)	(2, 2)	(3, 1)	(1, 3)
	Analytical	0.153597	0.272589	0.291350	0.375954	0.401634	0.456818
	TSNDT	0.168708	0.311512	0.326075	0.429975	0.465686	0.520578
	Difference, %	9.84	14.28	11.92	14.37	15.95	13.96
100	$(m,n) \rightarrow$	(1, 1)	(2, 1)	(1, 2)	(2, 2)	(3, 1)	(1, 3)
	Analytical	0.173157	0.289244	0.318169	0.399045	0.420498	0.485742
	TSNDT	0.208935	0.366540	0.394128	0.505544	0.538346	0.614844
	Difference, %	20.66	26.72	23.87	26.69	28.03	26.58
500	$(m,n) \rightarrow$	(1, 1)	(2, 1)	(1, 2)	(2, 2)	(3, 1)	(1, 3)
	Analytical	0.202920	0.326177	0.359545	0.453320	0.495198	0.543794
	TSNDT	0.375258	0.622937	0.687318	0.859305	0.903670	1.046472
	Difference, %	84.93	90.98	91.16	89.56	82.49	92.44
1000	$(m,n) \rightarrow$	(1, 1)	(2, 1)	(1, 2)	(2, 2)	(3, 1)	(1, 3)
	Analytical	0.213214	0.354746	0.380330	0.496767	0.567247	0.587315
	TSNDT	0.507333	0.835463	0.924805	1.152644	1.211164	1.403375
	Difference, %	137.95	135.51	143.16	132.03	113.52	138.95
1500	$(m,n) \rightarrow$	(1, 1)	(2, 1)	(1, 2)	(2, 2)	(3, 1)	(1, 3)
	Analytical	0.220438	0.380052	0.397668	0.535137	0.625862	0.629861
	TSNDT	0.611127	1.003660	1.112159	1.384785	1.454840	1.685817
	Difference, %	177.23	164.08	179.67	158.77	132.45	167.65
2000	$(m,n) \rightarrow$	(1, 1)	(2, 1)	(1, 2)	(2, 2)	(1, 3)	(3, 1)
	Analytical	0.226723	0.403451	0.413661	0.570393	0.661501	0.685993
	TSNDT	0.699600	1.147393	1.272090	1.583155	1.663140	1.927181
	Difference, %	208.57	184.39	207.52	177.56	151.42	180.93
5000	$(m,n) \rightarrow$	(1, 1)	(1, 2)	(2, 1)	(2, 2)	(1, 3)	(3, 1)
	Analytical	0.258481	0.496326	0.520338	0.743298	0.838722	0.945565
	TSNDT	1.088426	1.780703	1.976045	2.457157	2.581120	2.990704
	Difference, %	321.09	258.78	279.76	230.57	207.74	216.29
10^4	$(m,n) \rightarrow$	(1, 1)	(1, 2)	(2, 1)	(2, 2)	(1, 3)	(3, 1)
	Analytical	0.302584	0.607034	0.667825	0.954554	1.057867	1.237555
	TSNDT	1.530710	2.502233	2.777564	3.452869	3.627030	4.202417
	Difference, %	405.88	312.21	315.91	261.73	242.86	239.57
10^5	$(m,n) \rightarrow$	(1, 1)	(1, 2)	(1, 3)	(2, 1)	(2, 2)	(1, 4)
	Analytical	0.71887	1.476399	1.672185	1.684856	1.715298	1.723897
	TSNDT	4.8159	7.866658	8.734611	10.85558	11.4031	13.21148
	Difference, %	569.93	432.83	422.35	544.30	564.79	666.37
10^6	$(m,n) \rightarrow$	(1, 1)	(1, 2)	(1, 3)	(2, 1)	(2, 2)	(1, 4)
	Analytical	1.607812	1.631458	1.669181	1.695309	1.71348	1.720772
	TSNDT	15.22138	24.86191	27.60575	34.30822	36.03863	41.75369
	Difference, %	846.71	1423.91	1553.85	1923.71	2003.24	2326.45
10^7	$(m,n) \rightarrow$	(1, 1)	(1, 2)	(1, 3)	(2, 1)	(2, 2)	(1, 4)
	Analytical	1.608683	1.631626	1.669218	1.695842	1.71365	1.720785
	TSNDT	48.13175	78.61565	87.29213	108.4858	113.9575	132.0289
	Difference, %	2892.00	4718.24	5129.52	6297.16	6549.99	7572.60

Table 5.5: Influence of the FCDR on the fundamental frequency parameter, $\lambda_{1,1} = \omega h\sqrt{\rho_2/C_{11}^{\text{core}}}$

$\beta=\frac{C_{11}^{face}}{C_{11}^{core}}$	$\gamma=\frac{\rho_1}{\rho_2}$	Present analytical	Srinivas and Rao analytical [11]	TSNDT	Difference %
1	1	0.047419	0.047419	0.047419	0.00
1	3	0.039970	-	0.039971	0.00
1	10	0.028170	-	0.028170	0.00
1	20	0.021485	-	0.021486	0.00
1	100	0.010306	-	0.010306	0.00
15	1	0.112034	0.112034	0.114495	2.20
15	3	0.094547	0.094548	0.096615	2.19
15	10	0.066724	-	0.068183	2.19
15	20	0.050918	-	0.052033	2.19
15	100	0.024437	-	0.024974	2.19
100	1	0.173157	-	0.208935	20.66
100	3	0.146281	-	0.176490	20.65
100	10	0.103352	-	0.124714	20.67
100	20	0.078903	-	0.095225	20.69
100	100	0.037884	-	0.045731	20.71
1000	1	0.213214	-	0.507333	137.95
1000	3	0.180168	-	0.428691	137.94
1000	10	0.127318	-	0.303055	138.03
1000	20	0.097202	-	0.231437	138.10
1000	100	0.046670	-	0.111166	138.20

Table 5.6: Influence of the FCDR (γ) on the first six frequencies, $\lambda_{m,n} = \omega h\sqrt{\rho_2/C_{11}^2}$, $\beta = 1000$

$\gamma = \frac{\rho_1}{\rho_2}$	Method	Mode 1 (1, 1)	Mode 2 (2, 1)	Mode 3 (1, 2)	Mode 4 (2, 2)	Mode 5 (3, 1)	Mode 6 (1, 3)
	Exact	0.213214	0.354746	0.380330	0.496767	0.567247	0.587315
1	TSNDT	0.507333	0.835463	0.924805	1.152644	1.211164	1.403375
	Diff %	137.95	135.51	143.16	132.03	113.52	138.95
	Exact	0.180168	0.299863	0.321336	0.420035	0.480368	0.496419
3	TSNDT	0.428691	0.706108	0.781542	0.974275	1.023857	1.186266
	Diff %	137.94	135.48	143.22	131.95	113.14	138.96
	Exact	0.127318	0.211831	0.226826	0.296499	0.339504	0.349941
10	TSNDT	0.303055	0.499297	0.552569	0.688998	0.724164	0.838958
	Diff %	138.03	135.71	143.61	132.38	113.30	139.74
	Exact	0.097202	0.161663	0.173042	0.226126	0.258996	0.266658
20	TSNDT	0.231437	0.381344	0.422009	0.526252	0.553144	0.640802
	Diff %	138.10	135.89	143.88	132.72	113.57	140.31
	Exact	0.046670	0.077576	0.083001	0.108407	0.124183	0.127701
100	TSNDT	0.111166	0.183191	0.202714	0.252813	0.265749	0.307848
	Diff %	138.20	136.14	144.23	133.21	114.00	141.07
	Exact	0.015018	0.024959	0.026701	0.034869	0.039943	0.041061
1000	TSNDT	0.035777	0.058959	0.065242	0.081368	0.085533	0.099081
	Diff %	138.23	136.22	144.34	133.36	114.13	141.30

Table 5.7: Frequencies, $\lambda = \omega b^2/h\sqrt{\rho/E_2}$, of simply supported [0°/90°] and [0°/90°/0°/90°] square laminates with $a/h = 100$ (* indicates the frequency is repeated with values of m and n interchanged)

			[0°/90°]						[0°/90°/0°/90°]		
Mode	m	n	Exact	TSNDT	Diff. %	Mode	m	n	Exact	TSNDT	Diff. %
1	1	1	6.5266	6.526989	0.01	1	1	1	7.4687	7.4710	0.03
2*	1	2	17.8295	17.83232	0.02	2*	1	2	20.6812	20.7022	0.10
3	2	2	26.0369	26.04277	0.02	3	2	2	29.7501	29.7851	0.12
4*	1	3	37.7645	37.77691	0.03	4*	1	3	44.0594	44.1604	0.23
5*	2	3	43.8800	43.89658	0.04	5*	2	3	50.3801	50.4916	0.22
6	3	3	58.3258	58.35467	0.05	6	3	3	66.4777	66.6508	0.26
7*	1	4	65.6960	65.81626	0.18	7*	1	4	76.6390	76.9477	0.40
8*	2	4	70.7546	70.87631	0.17	8*	2	4	81.6102	81.9296	0.39
9*	3	4	82.4415	82.56842	0.15	9*	3	4	94.0820	94.4490	0.39
10*	1	5	101.322	101.847	0.52	10	4	4	117.069	117.600	0.45
11	4	4	103.062	103.266	0.20	11*	1	5	117.876	118.616	0.63
12*	2	5	105.807	106.329	0.49	12*	2	5	122.132	122.885	0.62

Table 5.8: Frequencies, $\lambda = \omega b^2/h\sqrt{\rho/E_2}$, of simply supported [0°/90°/0°] and [0°/90°/0°/90°/0°] square laminates with $a/h = 100$ (* indicates the frequency is repeated with values of m and n interchanged)

			[0°/90°/0°]						[0°/90°/0°/90°/0°]		
Mode	m	n	Exact	TSNDT	Diff. %	Mode	m	n	Exact	TSNDT	Diff. %
1	1	1	7.7555	7.7574	0.02	1	1	1	7.7574	7.7597	0.03
2	1	2	15.1530	15.1562	0.02	2	1	2	17.7900	17.8033	0.07
3	2	1	26.4025	26.4301	0.10	3	2	1	24.7395	24.7687	0.12
4	1	3	29.7177	29.7268	0.03	4	2	2	30.8883	30.9249	0.12
5	2	2	30.8590	30.8885	0.10	5	1	3	36.5968	36.6663	0.19
6	2	3	41.8023	41.8366	0.08	6	2	3	46.0197	46.1051	0.19
7	1	4	50.6775	50.7017	0.05	7	3	1	53.7134	53.8676	0.29
8	3	1	57.6346	57.7678	0.23	8	3	2	58.0184	58.1792	0.28
9	2	4	60.2346	60.2834	0.08	9	1	4	63.1788	63.4453	0.42
10	3	2	60.9515	61.0894	0.23	10	3	3	68.9796	69.1751	0.28
11	3	3	68.8366	68.9810	0.21	11	2	4	70.4498	70.7243	0.39
12	1	5	77.6751	77.7375	0.08	12	3	4	88.9750	89.3287	0.40

Table 5.9: Frequencies, $\lambda = \omega b^2/h\sqrt{\rho/E_2}$, of simply supported [0°/90°] and [0°/90°/0°/90°] square laminates with $a/h = 10$ (* indicates the frequency is repeated with values of m and n interchanged)

			[0°/90°]						[0°/90°/0°/90°]		
Mode	m	n	Exact	TSNDT	Diff. %	Mode	m	n	Exact	TSNDT	Diff. %
1	1	1	6.0274	6.0541	0.44	1	1	1	6.6210	6.7735	2.30
2*	1	2	14.5385	14.6687	0.90	2*	1	2	15.1936	15.9472	4.96
3*	1	0	16.7224	16.7224	0.00	3*	1	0	16.7224	16.7224	0.00
4	2	2	20.2287	20.4553	1.12	4	2	2	20.8414	21.9733	5.43
5*	1	3	26.2041	26.5437	1.30	5*	1	3	26.1606	27.8803	6.57
6*	2	3	30.0587	30.4824	1.41	6*	2	3	30.0291	31.9836	6.51
7*	2	0	33.4448	33.4448	0.00	7*	2	0	33.4448	33.4448	0.00
8	3	3	37.5966	38.1865	1.57	8	3	3	37.1424	39.7102	6.91
9*	1	4	38.8548	39.4735	1.59	9*	1	4	37.8753	40.4885	6.90
10*	2	4	41.7328	42.4259	1.66	10*	2	4	40.7900	43.5856	6.85
11*	3	4	47.5893	48.4188	1.74	11*	3	4	46.3674	49.6511	7.08
12*	3	0	50.1672	50.1672	0.00	12*	1	5	49.9690	53.2643	6.59

Table 5.10: Frequencies, $\lambda = \omega b^2/h\sqrt{\rho/E_2}$, of simply supported [0°/90°/0°] and [0°/90°/0°/90°/0°] square laminates with $a/h = 10$ (* indicates the frequency is repeated with values of m and n interchanged)

			[0°/90°/0°]						[0°/90°/0°/90°/0°]		
Mode	m	n	Exact	TSNDT	Diff. %	Mode	m	n	Exact	TSNDT	Diff. %
1	1	1	6.71469	6.824989	1.64	1	1	1	6.8139	6.9708	2.30
2	1	2	12.8108	12.98228	1.34	2	1	2	13.9012	14.4825	4.18
3*	1	0	16.7224	16.7224	0.00	3*	1	0	16.7224	16.7224	0.00
4	2	1	17.2174	17.84931	3.67	4	2	1	16.9420	17.8773	5.52
5	2	2	20.7979	21.44634	3.12	5	2	2	21.1816	22.3407	5.47
6	1	3	22.6358	23.01292	1.67	6	1	3	23.9038	25.3302	5.97
7	2	3	28.2165	28.97916	2.70	7	3	1	28.7848	30.7815	6.94
8	3	1	29.2992	30.49465	4.08	8	2	3	28.9749	30.9457	6.80
9	3	2	31.7567	32.96373	3.80	9	3	2	31.6350	33.9120	7.20
10*	2	0	33.4448	33.44481	0.00	10*	2	0	33.4448	33.4448	0.00
11	1	4	34.0531	34.7744	2.12	11	1	4	34.9216	37.2516	6.67
12	3	3	37.1955	38.47417	3.44	12	3	3	37.4061	40.1074	7.22

Table 5.11: Influence of E_1/E_2 of the individual layers on the fundamental frequency, $\lambda = \omega b^2/h\sqrt{\rho/E_2}$, of simply supported cross-ply laminated composite plates

No. of Layers	E_1/E_2	3	10	20	30	40	50	60	70	80
2	Present analytical	6.2317	6.9555	7.6427	8.1423	8.5269	8.8338	9.0852	9.2953	9.4740
	TSNDT	6.2336	6.9741	7.7140	8.2775	8.7272	9.0962	9.4054	9.6687	9.8959
	Difference %	0.03	0.27	0.93	1.66	2.35	2.97	3.52	4.02	4.45
	Rao et al. [15]	6.2317	6.9555	7.6427	8.1423	8.5269	-	-	-	-
	Difference %	0.00	0.00	0.00	0.00	0.00	-	-	-	-
	Noor [35]	6.25775	6.9845	7.6745	8.17625	8.5625	-	-	-	-
	Difference %	0.42	0.42	0.42	0.42	0.42	-	-	-	-
3	Present analytical	6.5681	8.1636	9.2378	9.8354	10.2318	10.5217	10.7472	10.9302	11.0831
	TSNDT	6.5712	8.1697	9.2513	9.8595	10.2687	10.5732	10.8143	11.0137	11.1834
	Difference %	0.05	0.07	0.15	0.24	0.36	0.49	0.62	0.76	0.90
	Noor [35]	6.6185	8.2103	9.5603	10.2723	10.7515	-	-	-	-
	Difference %	0.77	0.57	3.49	4.44	5.08	-	-	-	-
4	Present analytical	6.5043	8.0927	9.3453	10.0997	10.6111	10.9839	11.2695	11.4965	11.6822
	TSNDT	6.5146	8.1482	9.4675	10.2733	10.8221	11.2218	11.5269	11.7681	11.9639
	Difference %	0.16	0.69	1.31	1.72	1.99	2.17	2.28	2.36	2.41
	Rao et al. [15]	6.5044	8.0928	9.3453	10.0998	10.6111	-	-	-	-
	Difference %	0.00	0.00	0.00	0.00	0.00	-	-	-	-
	Noor [35]	6.5455	8.1445	9.4055	10.1650	10.6798	-	-	-	-
	Difference %	0.63	0.64	0.64	0.65	0.65	-	-	-	-
5	Present analytical	6.59	8.40	9.75	10.53	11.06	11.44	11.72	11.95	12.14
	TSNDT	6.60	8.44	9.82	10.64	11.20	11.60	11.90	12.15	12.17
	Difference %	0.13	0.42	0.78	1.05	1.25	1.41	1.54	1.64	0.23
	Noor [35]	6.65	8.52	9.95	10.79	11.34	-	-	-	-
	Difference %	0.79	1.42	2.05	2.39	2.59	-	-	-	-

Table 5.12: Comparison of first 12 frequencies of [0°/90°/core/90°/0°] sandwich plate (numbers in parentheses equal percent deviation of the frequency from the analytical one, $*$ indicates the frequency is repeated with values of m and n interchanged)

Mode	m	n	Analytical	3D FEM($70 \times 70 \times 33$)	3D FEM($120 \times 120 \times 33$)	TSNDT
1	1	1	1.8481	1.8887 (2.20)	1.8605 (0.67)	4.9603 (168)
2*	1	2	3.2200	3.4180 (6.15)	3.2835 (1.97)	8.1904 (154)
3	2	2	4.2903	4.5643 (6.39)	4.3755 (1.98)	10.5154 (145)
4*	1	3	5.2244	5.8049 (11.1)	5.4164 (3.67)	11.9821 (129)
5*	2	3	6.0959	6.6766 (9.53)	6.2813 (3.04)	13.7479 (126)
6	3	3	5.2244	8.4380 (9.87)	7.9185 (3.11)	16.1927 (111)
7*	1	4	7.6798	9.0727 (15.0)	8.2871 (5.06)	16.4550 (109)
8*	2	4	7.8879	9.7775 (13.2)	9.0141 (4.33)	17.6198 (104)
9*	3	4	10.0383	11.2332 (11.9)	10.4211 (3.81)	19.9228 (109)
10*	1	5	11.2367	13.2027 (17.5)	11.9153 (6.04)	20.8422 (99)
11*	2	5	11.9158	13.2245 (11.0)	12.5571 (5.38)	22.0522 (86)
12	4	4	12.1878	13.3374 (9.43)	12.6558 (3.84)	22.5368 (85)

Bibliography

[1] Liew, K. M., Pan, Z. Z., and Zhang, L. W., 2019, "An Overview of Layerwise Theories for Composite Laminates and Structures: Development, Numerical Implementation and Application," Composite Structures, **216**, pp. 240–259.

[2] Carrera, E., 1997, "CZ Requirements-Models for the Two-Dimensional Analysis of Multilayered Structures," Composite Structures, **37**(3-4), pp. 373–383.

[3] Birman, V. and Kardomateas, G. A., 2018, "Review of Current Trends in Research and Applications of Sandwich Structures," Composites Part B: Engineering, **142**, pp. 221–240.

[4] Reddy, J. N., 1984, "A Simple Higher-Order Theory for Laminated Composite Plates," Journal of Applied Mechanics, **51**(4), pp. 745–752.

[5] Kant, T. and Manjunatha, B. S., 1988, "An Unsymmetric FRC Laminate C° Finite Element Model with 12 Degrees of Freedom Per Node," Engineering Computations, **5**(4), pp. 300–308.

[6] Pandya, B. N. and Kant, T., 1988, "Finite Element Analysis of Laminated Composite Plates Using a Higher-Order Displacement Model," Composites Science and Technology, **32**(2), pp. 137–155.

BIBLIOGRAPHY

[7] Kant, T. and Swaminathan, K., 2002, "Analytical Solutions for the Static Analysis of Laminated Composite and Sandwich Plates Based on a Higher Order Refined Theory," Composite Structures, **56**(4), pp. 329–344.

[8] Sayyad, A. S. and Ghugal, Y. M., 2015, "On the Free Vibration Analysis of Laminated Composite and Sandwich Plates: A Review of Recent Literature with Some Numerical Results," Composite Structures, **129**, pp. 177–201.

[9] Carrera, E. and Brischetto, S., 2009, "A Survey with Numerical Assessment of Classical and Refined Theories for the Analysis of Sandwich Plates," Applied Mechanics Reviews, **62**(1), p. 010803.

[10] Vlasov, V. Z., 1957, "The Method of Initial Functions in Problems of the Theory of Thick Plates and Shells," *Proceedings of 9th Congress for Applied Mechanics*, Univ. of Brussels, Brussels, Belgium.

[11] Srinivas, S. and Rao, A. K., 1970, "Bending, Vibration and Buckling of Simply Supported Thick Orthotropic Rectangular Plates and Laminates," International Journal of Solids and Structures, **6**(11), pp. 1463–1481.

[12] Srinivas, S., Rao, C. J., and Rao, A. K., 1970, "An Exact Analysis for Vibration of Simply-Supported Homogeneous and Laminated Thick Rectangular Plates," Journal of Sound and Vibration, **12**(2), pp. 187–199.

[13] Pagano, N. J., 1970, "Exact Solutions for Rectangular Bidirectional Composites and Sandwich Plates," Journal of Composite Materials, **4**(1), pp. 20–34.

[14] Fan, J. and Ye, J., 1990, "An Exact Solution for the Statics and Dynamics of Laminated Thick Plates with Orthotropic Layers," International Journal of Solids and Structures, **26**(5-6), pp. 655–662.

[15] Rao, M. K., Scherbatiuk, K., Desai, Y. M., and Shah, A. H., 2004, "Natural Vibrations of Laminated and Sandwich Plates," Journal of Engineering Mechanics, **130**(11), pp. 1268–1278.

[16] Messina, A., 2012, "Three-Dimensional Free Vibration Analysis of Cross-Ply Laminated Rectangular Plates Through 2D and Exact Models," Mechanics of Advanced Materials and Structures, **19**(4), pp. 250–264.

[17] Brischetto, S., 2014, "An Exact 3D Solution for Free Vibrations of Multilayered Cross-Ply Composite and Sandwich Plates and Shells," International Journal of Applied Mechanics, **6**(6), p. 479738.

[18] Brischetto, S., 2014, "Three-Dimensional Exact Free Vibration Analysis of Spherical, Cylindrical, and Flat One-Layered Panels," Shock and Vibration, **2014**(1), p. 479738.

[19] Vel, S. S. and Batra, R. C., 2004, "Three-Dimensional Exact Solution for the Vibration of Functionally Graded Rectangular Plates," Journal of Sound and Vibration, **272**(3-5), pp. 703–730.

[20] Batra, R. C., Vidoli, S., and Vestroni, F., 2002, "Plane Wave Solutions and Modal Analysis in Higher Order Shear and Normal Deformable Plate Theories," Journal of Sound and Vibration, **257**(1), pp. 63–88.

[21] Desmet, W., 2002, "Mid-Frequency Vibro-Acoustic Modelling: Challenges and Potential Solutions," *Proceedings of ISMA*, B. Leuven, ed.

[22] Batra, R. C. and Aimmanee, S., 2003, "Missing Frequencies in Previous Exact Solutions of Free Vibrations of Simply Supported Rectangular Plates," Journal of Sound and Vibration, **265**(4), pp. 887–896.

BIBLIOGRAPHY

[23] Batra, R. C. and Aimmanee, S., 2007, "Vibration of an Incompressible Isotropic Linear Elastic Rectangular Plate with a Higher-Order Shear and Normal Deformable Theory," Journal of Sound and Vibration, **307**(3-5), pp. 961–971.

[24] Batra, R. C. and Aimmanee, S., 2005, "Vibrations of Thick Isotropic Plates with Higher Order Shear and Normal Deformable Plate Theories," Computers & Structures, **83**(12-13), pp. 934–955.

[25] Batra, R. C., Qian, L. F., and Chen, L. M., 2004, "Natural Frequencies of Thick Square Plates Made of Orthotropic, Trigonal, Monoclinic, Hexagonal and Triclinic Materials," Journal of Sound and Vibration, **270**(4), pp. 1074–1086.

[26] Qian, L. F., Batra, R. C., and Chen, L. M., 2003, "Free and Forced Vibrations of Thick Rectangular Plates Using Higher-Order Shear and Normal Deformable Plate Theory and Meshless Petrov–Galerkin (MLPG) Method," Computer Modeling in Engineering and Sciences, **4**(5), pp. 519–534.

[27] Chattopadhyay, A. P. and Batra, R. C., 2019, "Free and Forced Vibrations of Monolithic and Composite Rectangular Plates with Interior Constrained Points," Journal of Vibration and Acoustics, **141**(1), p. 011018.

[28] Yuan, L. S. and Batra, R. C., 2019, "Vibrations of an Incompressible Linearly Elastic Plate Using Discontinuous Finite Element Basis Functions for Pressure," Journal of Vibration and Acoustics, **141**(5), p. 051016.

[29] Reddy, J. N., 2004, *Mechanics of Laminated Composite Plates and Shells: Theory and Analysis*, CRC Press, Boca Raton, FL.

[30] Vel, S. S. and Batra, R. C., 2001, "Exact Solution for Rectangular Sandwich Plates with Embedded Piezoelectric Shear Actuators," AIAA Journal, **39**(7), pp. 1363–1373.

BIBLIOGRAPHY

[31] Alanbay, B. and Kapania, R. K., 2018, "On the Use of Classical Jacobi Orthogonal Polynomials in the Ritz Method," AIAA/ASCE/AHS/ ASC Structures, Structural Dynamics, and Materials Conference, pp. 2018–1225.

[32] Alanbay, B., Singh, K., and Kapania, R. K., 2020, "Vibration of Curvilinearly Stiffened Plates Using Ritz Method with Orthogonal Jacobi Polynomials," Journal of Vibration and Acoustics, **142**(1), p. 011009.

[33] Nosier, A., Kapania, R. K., and Reddy, J. N., 1993, "Free Vibration Analysis of Laminated Plates Using a Layerwise Theory," AIAA Journal, **31**(12), p. 2335–2346.

[34] Shi, Z., Yao, X., Pang, F., and Wang, Q., 2017, "An Exact Solution for the Free-Vibration Analysis of Functionally Graded Carbon-Nanotube Reinforced Composite Beams with Arbitrary Boundary Conditions," Scientific Reports, **7**(1), pp. 1–18.

[35] Noor, A. K., 1973, "Free Vibrations of Multilayered Composite Plates," AIAA Journal, **11**(7), p. 1038–1039.

[36] Qian, L. F., Batra, R. C., and Chen, L. M., 2003, "Free and Forced Vibrations of Thick Rectangular Plates by Using Higher-Order Shear and Normal Deformable Plate Theory and Meshless Petrov-Galerkin (MLPG)Method," Computer Modeling in Engineering and Sciences, **4**, p. 519–534.

[37] Batra, R. C. and Vidoli, S., 2002, "Higher-Order Piezoelectric Plate Theory Derived from a Three-Dimensional Variational Principle," AIAA Journal, **40**(1), p. 91–104.

[38] Groh, R. M. J. and Weaver, P. M., 2016, "Computationally Efficient 2D Model for Inherently Equilibrated 3D Stress Predictions in Heterogeneous Laminated Plates Part I: Model Formulation," Composite Structures, **156**, p. 171–185.

Chapter 6

Free vibration and static deformations of sandwich plates using N^{th} order equivalent-single-layer and layer-wise theories

6.1 Abstract

We analyzed the free vibrations and static deformations of laminated and sandwich plates using an equivalent single layer (ESL), and a layerwise (LW) Nth order shear and normal deformation theory. For both the theories, the numerical solution is obtained using the Ritz method with weighted Jacobi polynomials in the in-plane directions and hierarchic Legendre polynomials in the thickness direction as basis functions. Transverse stresses are calculated using a stress recovery scheme (SRS). Moreover, the deformations of sandwich structures are solved analytically using the three-dimensional, linear, small deformation theory of elasticity (3D-LET) by following Srivinas and Rao's approach. By comparing the natural frequencies and stress values obtained from various order ESL and LW theories with those of analytical solutions, we investigate the influence of face-to-core stiffness ratio (FCSR) on the accuracy of these plate theories. We tried to find whether or not ESL and LW theories give accurate natural frequencies and stress values while increasing the FCSR for different thickness ratios,and if so, which minimum order of plate theory is required to reduce the difference with analytical results under 5%. Furthermore, we have used the realistic material properties to see what are the values of the typical elastic modulus ratio in the thickness direction, $E_{33}^{face}/E_{33}^{core}$, and that of in the fiber direction $E_{11}^{face}/E_{11}^{core}$ and it is found that, $E_{33}^{face}/E_{33}^{core}$, has a higher influence than $E_{11}^{face}/E_{11}^{core}$ on the accuracy of the results obtained using ESL theories.

6.2 Introduction

The high strength and stiffness ratios of laminated and sandwich plates have resulted in their growing applications across various engineering fields over the last few decades. However, due to the distinct material properties of individual layers, their static and dynamic behaviors

are more complicated than that of the monolithic structures. Hence, developing efficient and accurate mathematical models for capturing these behaviors has been of considerable interest and concern for many researchers.

Linear elasticity theories in analyzing composite laminated plates can be categorized depending on dimensionality variables; 3D – 2D, variable description; Equivalent Single Layer (ESL) or Layerwise (LW), formulation type; displacement-based formulation or mixed formulation [1, 2, 3, 4]. Additionally, Carrera [5] reiterated the importance of C_z^0 requirements, namely C^0 continuity of displacements (zig-zag, ZZ) and transverse stresses (interlaminar equilibrium, IC) at interfaces between adjoining layers, on the accuracy and effectiveness of the used theory. Each theory that lies under these categories has its own merits and demerits, and some may satisfy the C_z^0 requirements as a priori, other may need additional treatment.

Among them, 3D analytical solutions for laminated plates that assume both the displacements and stresses as unknowns at each layer and satisfy the C_z^0 requirements as a priori are considered as benchmark solutions and used to assess the validity of approximate methods and plate theories. Some of these solutions are contributed to the literature by Srinivas and Rao [6], Srinivas et al. [7], Pagano [8], Ye and Soldatos [9], Fan and Ye [10], and Vel and Batra [11, 12, 13]. However, these 3D analytical solutions are limited to simple geometries and boundary conditions; furthermore, they are computationally more expensive as compared to 2D theories.

Computational expenses of 3D analysis led researchers to refine 2D theories. In ESL theories the variables are the same in the whole plate; hence the number of variables is independent of the number of layers. The ESL theories include classical laminate plate theory [14], first-order shear deformation theory [15], high-order shear deformable theories [16], and high-order shear and normal deformable theories [17]. A detailed examination and review of 2D−ESL

theories can be found in Kapania and Raciti [18, 19], Leissa [20], and Noor et al. [21]. Since most of the ESL theories are displacement-based and do not take account of C_z^0 requirements, transverse stresses obtained from constitutive law may not be accurate. These drawbacks of the ESL theories lead to the development of zig-zag theories (see Carrera [22], Lekhnitskii [23], Ren [24], Gherlone [25]) and eventually layerwise theories for multilayered plates and shells. Layerwise theories that use mixed formulations (i.e., Reissner's mixed variational theorem [26, 27, 28]) satisfies the C_z^0 retirements as a priori, however, they introduce considerably more unknowns into the problem, hence the computational cost is high. For more details and examination of layerwise theories reader should consult reviews by Liew et al. [3], Reddy [29], Carrera and Brischetto [30], and Khandan et al. [31].

The drawback of displacement based ESL and LW theories for the calculation of transverse stresses can be significantly improved by the use of stress recovery scheme (SRS) in which 3D equilibrium equations are integrated along the thickness direction to compute the transverse stresses from the in-plane stresses [32]. The SRS procedure requires the first and second derivatives of strains for computation of transverse shear (σ_{13}, σ_{23}) and normal (σ_{23}) stresses, respectively. Pagano [33] obtained (σ_{13}, σ_{23}) CLPT based analytical closed-form solutions of transverse stresses using the derivatives of in-plane stresses for simply supported laminated plate. Ahmadi [34] investigated the transverse stress of sandwich plates with various boundary conditions using a displacement-based 3D-LET and an SRS scheme. He reported that the computed stresses agreed well with those of analytical 3D-LET solutions of Batra and Vel [12] and Pagano [8]. Kapoor et al. [35], Duffor et al. [36], and Patton et al. [37] incorporated SRS with FSDT based isogeometric analysis to compute the transverse stresses of simply supported laminates. They directly use the high-order derivatives of NURBS basis in the SRS. Reddy and Barbero [38] calculated the transverse shear stresses of laminated plates using the first derivatives of finite element shape functions. However,

obtaining higher-order derivatives directly from finite element shape functions is not always possible [39, 40]. To overcome this problem, many researchers used interpolation techniques with finite element solutions to calculate various high-order derivatives. Byun and Kapania [41] developed a post processor for displacement-based finite element solutions based on CLPT and FSDT to compute the transverse stresses. They used a weighted least-squares method with Chebyshev and other orthogonal polynomials to obtain global interpolations of finite element nodal displacement solutions and calculate the higher-order derivatives of in-plane strain. Shah and Batra used the third-order shear and normal deformable theory (TSNDT) in conjunction with SRS to compute the transverse stresses of laminated plates [42] and doubly-curved shells [43, 44, 45] under static loads. They calculated the required stress gradients by the least-square fitting of a complete quadratic polynomial to computed in-plane stresses at 3x3 Gauss quadrature points in each finite element. Later, Yuan and Batra [46] used TSNDT with SRS to find the optimum first failure load design of sandwich plates under blast loads. Shah and Batra [42] found that while TSNDT coupled with SRS could accurately predict the transverse stresses away from the edge (a distance greater than 10% edge-length), in the vicinity of the edge, the stresses could differ up to 40% from those of 3D-LET for some cases of thick laminates (span/thickness = 5).

The most popular common practice for solving initial boundary value problems is the finite element method (FEM). Compared to the FEM, the Ritz method uses global shape functions, which satisfy the essential boundary conditions as a priori over the entire domain. Ritz method could provide superior results with lesser degrees of freedoms (DoFs) than FEM [47, 48]. Many researchers (i.e., see Leissa and Zhang [49], Liew and Yang [50], Zhou et al. [51]) investigated the three-dimensional free vibrations of monolithic plates using the Ritz method based on 3D-LET. There are also several applications of the three-dimensional Ritz method to multilayered structures. Fazzolari and Carrera [52] investigated the free vibrations and

buckling of simply supported multilayered shells using the hierarchical Ritz method. They used the method of the principle of virtual displacements to derive the governing equations and evaluated their theory under the equivalent single-layer plate category according to Carrera's unified formulation.

Here we present a method for static and free vibration analysis of laminated and sandwich plates using ESL and LW N^{th}-order shear and normal deformation theories with Ritz method for arbitrary boundary conditions. The analysis uses displacement-based formulations and the displacement field is approximated by weighted Jacobi polynomials [53, 54, 55, 56] in the in-plane directions and hierarchic Legendre polynomials in the thickness direction. The essential boundary conditions are exactly satisfied using the weight of the Jacobi polynomials. For the computation of transverse stresses, the present approach is coupled with a stress recovery scheme (SRS).In addition to plate theory solutions, we found the deformations of sandwich structures by solving the 3D-LET equations analytically using Srinivas and Rao's approach.

It is well-known that the structural analysis of sandwich structures with a soft core is a challenging problem for most of the existing plate theories due to their high face-to-core stiffness ratio (FCSR). However, it is not clear the critical values of FCSR that cause the solutions of various high-order ESL plate theories to diverge from those of 3D-LET solution. In our previous work [57], we seek an answer to whether ESL third-order shear and normal deformation theory (TSNDT) provides accurate natural frequencies of sandwich structures for different face-to-core-stiffness ratios. We found that for an ESL- TSNDT, the first six frequencies have a maximum error of 5% for FCSR less than 20. This percent error increases, respectively, to 16, 93, and 280 for FCSR= 50, 500, and 5000; making the use of the ESL-TSNDT unacceptable. Here, we want to see if we can reduce these errors to acceptable limits by using higher order ESL and LW plate theories. By varying the face-to-core stiffness

ratios of sandwich plates, we aim to find the plate order N that reduces the error between the ESL predictions and analytical solutions for natural frequencies, static deformations and stress values to less than 5%. Furthermore, when the face sheets or core are made of orthotropic materials, it would results in different face-to-core stiffness ratios in fiber and thickness directions. Whether the FCSR in fiber or thickness direction is more influential on the accuracy of the various plate theories are also not investigated in our knowledge. To address this issue, we have considered case studies which use typical face sheet and core materials and results in different face-to-core modulus ratios in thickness $\left(E_{33}^{\text{face}}/E_{33}^{\text{core}}\right)$ and fiber directions ($E_{11}^{\text{face}}/E_{11}^{\text{cor}}$). It is found that $E_{33}^{\text{face}}/E_{33}^{\text{core}}$ has a higher influence than $E_{11}^{\text{face}}/E_{11}^{\text{core}}$ on the accuracy of the natural frequency and stress results obtained from various plate theories, such that one needs to use higher-order ESL plate theories in the case of high $E_{33}^{\text{face}}/E_{33}^{\text{core}}$ than those of high $E_{11}^{\text{face}}/E_{11}^{\text{core}}$ ratio to obtain the same accuracy. On the other hand, LW theories provided very close results compared to analytical results in almost all the cases and were not affected much by the change of FCSR.

Novelties of the work include: (i) demonstrating the use of weighted Jacobi polynomials and hierarchic Legendre shape functions as basis functions to solve ESL and LWN^{th} -order shear and normal deformation theory for the natural frequencies and static deformations of multilayered plates is computationally very efficient, (ii) Ascertaining the critical ESL and LW plate theory orders for predicting the natural frequency and stress results within 5% of their analytical values for various FCSR ratios (iii) providing 3D analytical solutions for static deformations of sandwich plates which could be used as benchmark solutions for validating plate theories and their numerical solution. (iv) showing that face-to-core modulus ratio in thickness direction $E_{33}^{\text{face}}/E_{33}^{\text{core}}$ is more influential on the accuracy of ESL theories in predicting the natural frequencies and the stresses of sandwich plates than those of in fiber direction $E_{11}^{\text{face}}/E_{11}^{\text{core}}$. In addition to that the limiting $E_{33}^{\text{face}}/E_{33}^{\text{core}}$ values beyond which

frequencies/stress variables from the ESL theories have unacceptable errors are identified.

6.3 Formulation of the Problem

Figure 6.1 depicts a schematic sketch of a p-layered laminated plate of length a, width b, and thickness h. We use rectangular Cartesian coordinate axes to describe the plate's infinitesimal deformations from the stress-free undeformed and configuration. We assume that each ply material is homogeneous, orthotropic and linearly elastic, and plane $x_3 = 0$ coincides with the plate mid-surface. The x_3 coordinates of the bottom and the top surfaces of the k^{th} ply are denoted by $x_3^{(k)}$ and $x_3^{(k+1)}$, respectively. Components of the displacements

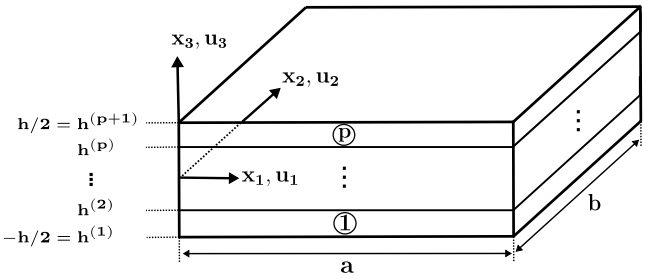

Figure 6.1: Schematic sketch of a laminated plate, and of rectangular Cartesian coordinate axes

field of the plate undergoing harmonic oscillations can be expressed as

$$u_j\left(x_1, x_2, x_3, t\right) = U_j\left(x_1, x_2, x_3\right)\ sin\left(\omega t\right), \qquad j = 1, 2, 3 \tag{6.1}$$

Components of the infinitesimal strain tensor, $\boldsymbol{\varepsilon}$, are defined as

$$\epsilon_{ij} = \frac{1}{2}\left(u_{i,j} + u_{j,i}\right) \tag{6.2}$$

Alternatively,

$$\boldsymbol{\epsilon} = \begin{bmatrix} \frac{\partial}{\partial x_1} & 0 & 0 & 0 & \frac{\partial}{\partial x_3} & \frac{\partial}{\partial x_2} \\ 0 & \frac{\partial}{\partial x_2} & 0 & \frac{\partial}{\partial x_3} & 0 & \frac{\partial}{\partial x_1} \\ 0 & 0 & \frac{\partial}{\partial x_3} & \frac{\partial}{\partial x_2} & \frac{\partial}{\partial x_1} & 0 \end{bmatrix}^T \begin{Bmatrix} u_1 \\ u_2 \\ u_3 \end{Bmatrix} = \mathbf{L}\,\boldsymbol{u} \tag{6.3}$$

For a linearly elastic orthotropic material, stress-strain relations for the k^{th} lamina with respect to the material principal axes are [2]

$$\begin{Bmatrix} \sigma_{11} \\ \sigma_{22} \\ \sigma_{33} \\ \sigma_{23} \\ \sigma_{13} \\ \sigma_{12} \end{Bmatrix}^{(k)} = \begin{bmatrix} C_{11} & C_{12} & C_{13} & 0 & 0 & 0 \\ C_{12} & C_{22} & C_{23} & 0 & 0 & 0 \\ C_{13} & C_{23} & C_{33} & 0 & 0 & 0 \\ 0 & 0 & 0 & C_{44} & 0 & 0 \\ 0 & 0 & 0 & 0 & C_{55} & 0 \\ 0 & 0 & 0 & 0 & 0 & C_{66} \end{bmatrix}^{(k)} \begin{Bmatrix} \varepsilon_{11} \\ \varepsilon_{22} \\ \varepsilon_{33} \\ 2\varepsilon_{23} \\ 2\varepsilon_{13} \\ 2\varepsilon_{12} \end{Bmatrix} \tag{6.4}$$

Here $\sigma_{ij}^{(k)}$ is a component of Cauchy stress tensor, and $C_{ij}^{(k)}$ is an elastic constant with respect to the material principal axes. These are transformed by using the tensor transformation rules to the global rectangular Cartesian coordinate axes when the material principle and the global axes do not coincide with each other.

6.3.1 Variational formulation

Letting $\delta\boldsymbol{u}$ be an admissible virtual displacement field that satisfies

$$\begin{gathered} \delta\boldsymbol{u} = \mathbf{0} \text{ on } \Gamma_u \text{ for all } t \\ \delta\boldsymbol{u}\left(\boldsymbol{x}, t_1\right) = \delta\boldsymbol{u}\left(\boldsymbol{x}, t_2\right) = \mathbf{0} \text{ for all } \boldsymbol{x} \end{gathered} \tag{6.5}$$

where Γ_u, t_1, and t_2 identify the part of the plate boundary where the displacement vector $\boldsymbol{u}$ is specified, initial time, and final time, respectively. That is, in considering variations in $\boldsymbol{u}$ the states at $t = t_1,\ t_2$ are kept fixed. Equations governing plate's deformations can be derived by using the following Hamilton's principle [58]

$$\int_{t_1}^{t_2} \delta L \, dt = \int_{t_1}^{t_2} (\delta T - \delta U + \delta W) \, dt = 0 \tag{6.6}$$

where L denotes the Lagrangian function, T the kinetic energy, U the strain energy, and W the work done by applied forces. The expressions for δT, δU, and δW are

$$\delta T = \sum_{k=1}^{p} \int_{\Omega^k} \rho^k \dot{\boldsymbol{u}} \, \delta \dot{\boldsymbol{u}}^T \, d\Omega^k, \quad \delta U = \sum_{k=1}^{p} \int_{\Omega^k} \delta(\boldsymbol{\epsilon}^k)^T \boldsymbol{\sigma}^k d\Omega^k, \quad \delta W = \int_{\bar{A}} \delta \boldsymbol{u}^T \bar{\boldsymbol{f}} \, d\bar{A} \tag{6.7}$$

where Ω^k is the region occupied by the k^{th} layer, ρ^k the mass density, $\bar{f}$ the surface traction specified on the plate surface $\bar{A}$, and a superimposed dot represents differentiation with respect to time. Substituting expressions from Eq. 6.7 into Eq. 6.6, using integration by parts, and requiring that Eq. 6.6 holds for arbitrary values of t_1 and t_2, we get

$$\sum_{k=1}^{p} \int_{\Omega^k} \left[\delta(\boldsymbol{\epsilon}^k)^T \boldsymbol{\sigma}^k + \rho^k \delta \boldsymbol{u}^T \ddot{\boldsymbol{u}} \right] d\Omega^k - \int_{\bar{A}} \delta \boldsymbol{u}^T \bar{\boldsymbol{f}} \, d\bar{A} = 0 \tag{6.8}$$

6.3.2 Approximating Displacement Field in the Ritz Method

We defined non-dimensionalized coordinates global coordinates as follows.

For the ESL theory:

$$x_1 = \frac{(\xi_1 + 1)\, a}{2}, \quad x_2 = \frac{(\xi_2 + 1)\, b}{2}, \quad x_3 = \frac{\xi_3 h}{2} \tag{6.9}$$

For the LW theory:

$$x_1^k = \frac{\left(\xi_1^k + 1\right) a}{2}, \quad x_2^k = \frac{\left(\xi_2^k + 1\right) b}{2}, \quad x_3^k = \left(\frac{h^{k+1} - h^k}{2}\right) \xi_3^k + \left(\frac{h^{k+1} + h^k}{2}\right) \tag{6.10}$$

The ESL Theory

Each displacement component (U_1, U_2, U_3) at a point is approximated as

$$U_i(\xi_1, \xi_2, \xi_3) = \sum_{k=0}^{n_1} \sum_{l=0}^{n_2} \sum_{m=0}^{n_3} d_{iklm} T_k(\xi_1) T_l(\xi_2) T_m(\xi_3) = \boldsymbol{N_i}\, \boldsymbol{d_i}, \qquad i = 1, 2, 3 \tag{6.11}$$

In Eq. 6.11, repeated indices do not imply summation. $\boldsymbol{N_i}$ contains Ritz shape functions, and $\boldsymbol{d_i}$ is the unknown generalized DoFs vector.They are given as,

$$\begin{aligned} N_i &= \{T_0(\xi_1)\, T_0(\xi_2)\, T_0(\xi_3), \cdots, T_{n_1}(\xi_1)\, T_{n_2}(\xi_2)\, T_{n_3}(\xi_3)\} \\ d_i &= \{d_{000}, \cdots, d_{n_1 n_2 n_3}\}^T \end{aligned} \tag{6.12}$$

where

$$T_i(\xi_j) = (1 - \xi_j)^\alpha (1 + \xi_j)^\beta P_i^{(2\alpha, 2\beta)}(\xi_j) \tag{6.13}$$

where $P_n^{(\alpha,\beta)}(\xi)$ is the n^{th} order Jacobi polynomial with shape parameters α and β. These polynomials are orthogonal with respect to the weight $(1-\xi)^\alpha(1+\xi)^\beta$ on the interval $[-1, 1]$, i.e.,

$$\int_{-1}^{1} (1 - \xi)^\alpha (1 + \xi)^\beta P_i^{(\alpha,\beta)}(\xi) P_j^{(\alpha,\beta)}(\xi)\, d\xi = f(\alpha, \beta, n)\, \delta_{ij}, \quad \alpha, \beta > -1 \tag{6.14}$$

Exponents α and β in Eq. 6.13 are assigned values to enforce essential boundary conditions at the plate edges. We set

$$\alpha = \begin{cases} 1, & \text{if } U_i \text{ is fixed at face } \xi_i = 1 \\ 0, & \text{if } U_i \text{ is free at face } \xi_i = 1 \end{cases}, \qquad \beta = \begin{cases} 1, & \text{if } U_i \text{ is fixed at face } \xi_i = -1 \\ 0, & \text{if } U_i \text{ is free at face } \xi_i = -1 \end{cases} \tag{6.15}$$

The three-term recursive formula for Jacobi polynomials is given by

$$\begin{aligned} 2n\, c_n\, c_{2n-2}\, P_n^{(\alpha,\beta)}(\xi) = c_{2n-1}\, (c_{2n-2}\, c_{2n}\, \xi + \alpha^2 - \beta^2)\, P_{n-1}^{(\alpha,\beta)}(\xi) \\ -2(n-1+\alpha)(n-1+\beta)\, c_{2n}\, P_{n-2}^{(\alpha,\beta)}(\xi) \end{aligned} \tag{6.16}$$

where

$$c_n = n + \alpha + \beta \tag{6.17}$$

$$P_0^{(\alpha,\beta)}(\xi) = 1; \qquad P_1^{(\alpha,\beta)}(\xi) = \frac{\alpha - \beta}{2} + \left(1 + \frac{\alpha + \beta}{2}\right) \xi \tag{6.18}$$

The m^{th} derivative of the nth order Jacobi polynomial is given by [59],

$$\frac{\mathrm{d}^m}{\mathrm{d}\xi^m} \left[P_n^{(\alpha,\beta)}(\xi)\right] = \frac{\Gamma\left(\alpha + \beta + n + m\right)}{2^m\, \Gamma\left(\alpha + \beta + n + 1\right)}\, P_{n-m}^{(\alpha+m,\beta+m)}(\xi) \tag{6.19}$$

where $\Gamma\left(n\right) = (n-1)!$ is the gamma function and n a positive integer.

We note that because of the displacement field Eq. 6.11, we may say that we are using a shear and normal deformable plate theory of order n_3 with DoFs $= 3 \times (n_1+1) \times (n_2+1) \times (n_3+1)$.

The LW Theory

In the LW theory, the displacements of a point in the k^{th} layer are expressed as

$$U_i^k(\xi_1, \xi_2, \xi_3) = \sum_{j=0}^{n_1} \sum_{l=0}^{n_2} \sum_{m=1}^{n_3+1} d_{iklm} T_j(\xi_1^k) T_l(\xi_2^k) V_m(\xi_3^k) = \boldsymbol{N_i^k}\, \boldsymbol{d_i^k}, \qquad i = 1, 2, 3 \tag{6.20}$$

In the ξ_1 and ξ_2 directions, Jacobi polynomials are used and the essential boundary conditions are satisfied as for the ESL. In the thickness direction, the following hierarchic shape functions based on Legendre polynomials are used [60] . For polynomial order $n_p = 1$,

$$V_1 = \frac{1-\xi_3}{2}, \quad V_2 = \frac{1+\xi_3}{2} \tag{6.21}$$

For polynomial order $n_p > 1$,

$$V_i = \frac{1}{\sqrt{2\,(2i-3)}} \left(L_{i-1}\left(\xi\right) - L_{i-3}\left(\xi\right)\right), \quad i = 3, 4, ... \tag{6.22}$$

Here L_i represents the i^{th} order Legendre polynomial and can be obtained from Jacobi polynomials' three-term recursive formula (Eq. 6.16) by setting α and β equal to zero. The hierarchic shape functions V1 through V6 are shown in Figure 6.2.

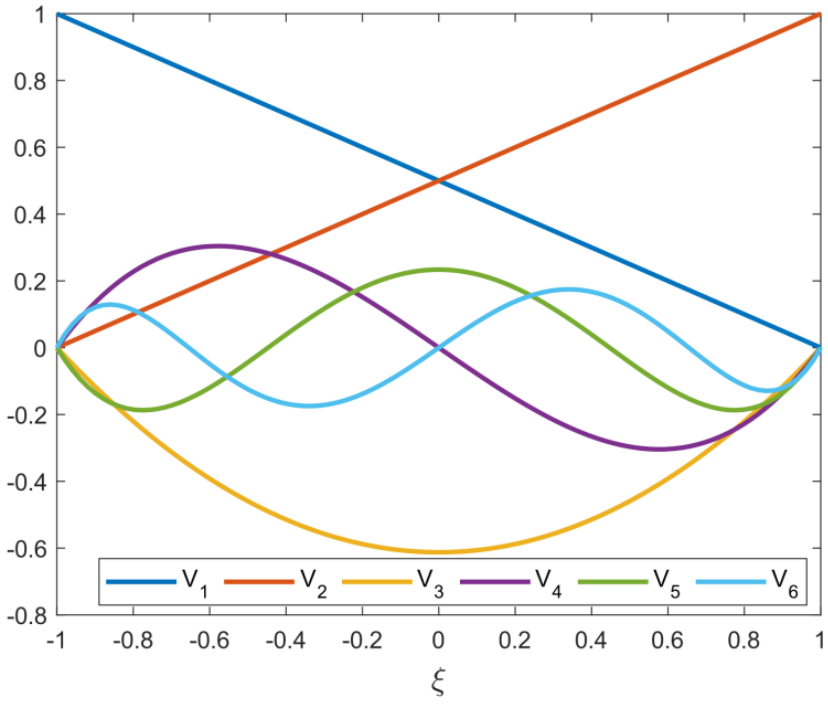

Figure 6.2: Hierarchic shape functions V_1 through V_6

In the FE terminology, one can think of each layer as a 1D FE in the thickness direction having 2 physical nodes – one at the top and the other at the bottom surface of the layer, and $n_p - 1$ fictitious interior nodes. These nodes and the local coordinates for the 1st layer of a 4-layered laminate are shown in Figure 6.3.

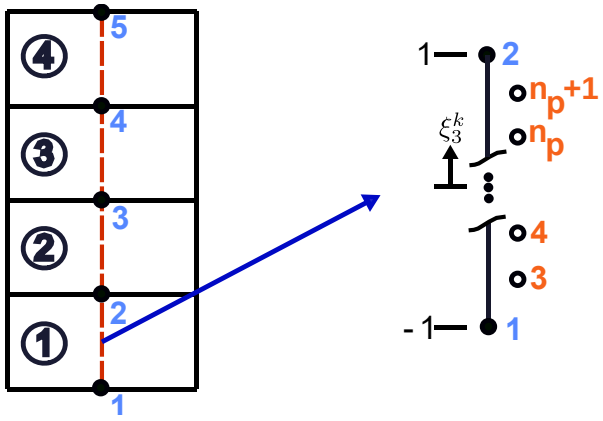

Figure 6.3: Four-layered laminate and representation of 1D-finite element in local coordinates (physical nodes: blue color; interior nodes: orange color)

In Figure 6.4, a two-layer laminate with each layer having 4 nodes and an illustration of assembling layer stiffness matrices into the global stiffness matrix is shown for the LW theory. The layer-1 and layer- 2 share node 4 and $\boldsymbol{K_1}$ and $\boldsymbol{K_2}$ correspond to the stiffness matrices of layer -1 and layer- 2 , respectively. The assemblage procedure given in Figure 6.4 ensures the continuity of the displacements at the interfaces. It should be noted that, since the present LW theory formulations are displacement based, the continuity of transverse stresses are not guaranteed during the solution. However, they are satisfied through a stress recovery scheme. The total DoFs for LW theory is equal to $3 \times (n_1 + 1) \times (n_2 + 1) \times (p \times (n_3 + 1) - (p - 1))$ where p is the total number of layer, $(n_3 + 1)$ corresponds to the number of nodes in thickness direction per layer, and $(p - 1)$ is the number of shared nodes at the interfaces.

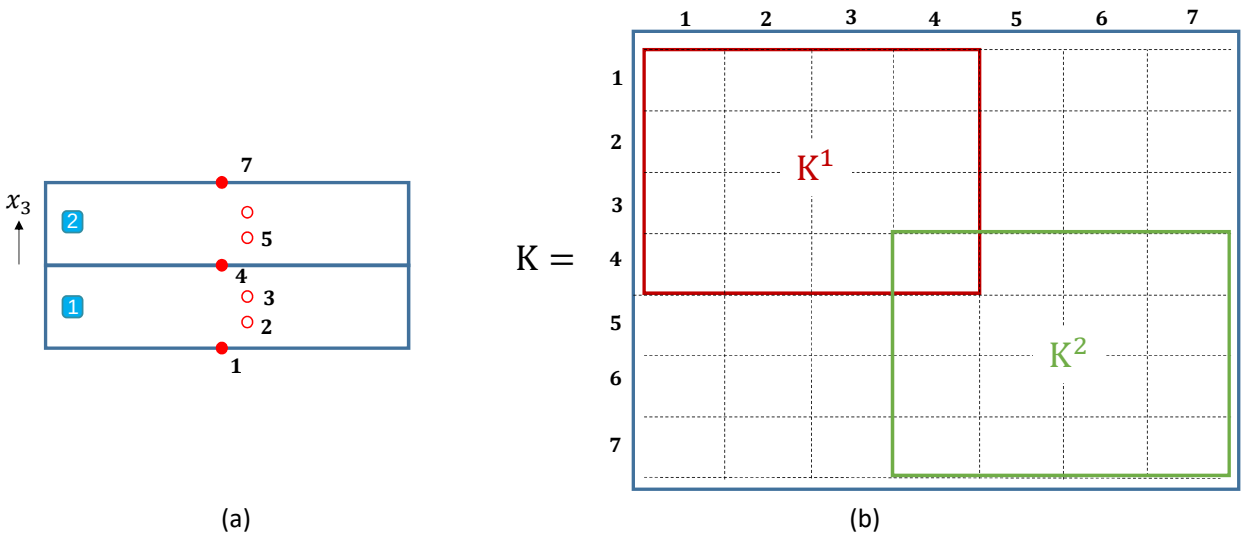

Figure 6.4: An example showing a) through-the-thickness nodes for the 3^{rd} order LW theory for a 2-layered laminate, b) assembly of layer stiffness matrices into the global stiffness matrix

Boundary Conditions

Boundary conditions at a simply supported (S), a clamped (C), and a free (F) edge are specified as follows.

$$\begin{aligned}
S: &\quad U_2 = U_3 = 0,\ \ \sigma_{11} = 0 \quad \text{on } \xi_1 = -1,\ 1 \\
&\quad U_1 = U_3 = 0,\ \ \sigma_{22} = 0 \quad \text{on } \xi_2 = -1,\ 1 \\
C: &\quad U_1 = U_2 = U_3 = 0 \quad \text{on } \xi_1 = -1,\ 1;\ \xi_2 = -1,\ 1 \\
F: &\quad \sigma_{11} = \sigma_{12} = \sigma_{13} = 0 \quad \text{on } \xi_1 = -1,\ 1 \\
&\quad \sigma_{12} = \sigma_{22} = \sigma_{23} = 0 \quad \text{on } \xi_2 = -1,\ 1
\end{aligned} \tag{6.23}$$

Note that in Eq. 6.23, the layer number k is dropped from superscripts of displacement and stress components, for LW theory these conditions should be satisfied for each layer.

6.3.3 Free Vibration Analysis

For free vibration analysis, we set the force $\bar{\boldsymbol{f}}$ equal to zero in Eq. 6.8, and substitute the displacement from Eq. 6.11 into Eq. 6.1 and the result into Eq. 6.8 and the following eigenvalue problem for the frequency ω :

$$\left[\mathbf{K} - \omega^2 \, \mathbf{M}\right] \{\mathbf{d}\} = \{\mathbf{0}\} \tag{6.24}$$

where $\mathbf{K}$ and $\mathbf{M}$ are the global stiffness and the mass matrices, respectively. They have the following expressions. For the LW theory:

$$\boldsymbol{K}^k = \int_{-1}^{1}\int_{-1}^{1}\int_{-1}^{1} \boldsymbol{B}^{kT}\boldsymbol{C}^k \, \boldsymbol{B}^k \, \frac{abh_k}{8} \, d\xi_1^k d\xi_2^k d\xi_3^k \tag{6.25}$$

$$\boldsymbol{M}^k = \int_{-1}^{1}\int_{-1}^{1}\int_{-1}^{1} \rho^k \boldsymbol{H}^{kT}\boldsymbol{H}^k \, \frac{abh}{8} \, d\xi_1^k d\xi_2^k d\xi_3^k \tag{6.26}$$

For the ESL theory:

$$\boldsymbol{K} = \int_{-1}^{1}\int_{-1}^{1}\sum_{k=1}^{p}\int_{\xi_3^{(k)}}^{\xi_3^{(k+1)}} \boldsymbol{B}^{T}\boldsymbol{C}^k \, \boldsymbol{B} \, \frac{abh}{8} \, d\xi_1 d\xi_2 d\xi_3 \tag{6.27}$$

$$\boldsymbol{M} = \int_{-1}^{1}\int_{-1}^{1}\sum_{k=1}^{p}\int_{\xi_3^{(k)}}^{\xi_3^{(k+1)}} \rho^k \boldsymbol{H}^{T}\boldsymbol{H} \, \frac{abh}{8} \, d\xi_1 d\xi_2 d\xi_3 \tag{6.28}$$

in which

$$\boldsymbol{B} = \begin{bmatrix} \frac{2}{a}\frac{\partial \boldsymbol{N_1}}{\partial \xi_1} & 0 & 0 & 0 & \frac{2}{h}\frac{\partial \boldsymbol{N_1}}{\partial \xi_3} & \frac{2}{b}\frac{\partial \boldsymbol{N_1}}{\partial \xi_2} \\ 0 & \frac{2}{b}\frac{\partial \boldsymbol{N_2}}{\partial \xi_2} & 0 & \frac{2}{h}\frac{\partial \boldsymbol{N_2}}{\partial \xi_3} & 0 & \frac{2}{a}\frac{\partial \boldsymbol{N_2}}{\partial \xi_1} \\ 0 & 0 & \frac{2}{h}\frac{\partial \boldsymbol{N_3}}{\partial \xi_3} & \frac{2}{b}\frac{\partial \boldsymbol{N_3}}{\partial \xi_2} & \frac{2}{a}\frac{\partial \boldsymbol{N_3}}{\partial \xi_1} & 0 \end{bmatrix}^T, \quad \mathbf{H} = \begin{bmatrix} \mathbf{N_1} & 0 & 0 \\ 0 & \mathbf{N_2} & 0 \\ 0 & 0 & \mathbf{N_3} \end{bmatrix} \tag{6.29}$$

6.3.4 Static deformations

Setting the time derivatives terms to zero and proceeding as above for the vibration problem, we get

$$\boldsymbol{K}\boldsymbol{d} = \boldsymbol{F} \tag{6.30}$$

where $\boldsymbol{F}$ is the global load vector with

$$\boldsymbol{F} = \boldsymbol{Q_1^+} + \boldsymbol{Q_1^-} + \boldsymbol{Q_2^+} + \boldsymbol{Q_2^-} + \boldsymbol{Q_3^+} + \boldsymbol{Q_3^-} \tag{6.31}$$

and

$$\boldsymbol{Q_1^\pm} = \int_{-1}^{1}\int_{-1}^{1} \boldsymbol{N}\, \boldsymbol{q_1^\pm}\, \frac{bh}{4}\, d\xi_2 d\xi_3 \tag{6.32}$$

$$\boldsymbol{Q_2^\pm} = \int_{-1}^{1}\int_{-1}^{1} \boldsymbol{N}\, \boldsymbol{q_2^\pm}\, \frac{ah}{4}\, d\xi_1 d\xi_3 \tag{6.33}$$

$$\boldsymbol{Q_3^\pm} = \int_{-1}^{1}\int_{-1}^{1} \boldsymbol{N}\, \boldsymbol{q_3^\pm}\, \frac{ab}{4}\, d\xi_1 d\xi_2 \tag{6.34}$$

where q_1^+, q_1^-, q_2^+, q_2^-, q_3^+ and q_3^- are surface tractions prescribed on the edge surfaces $x_1 = a$, $x_1 = 0$, $x_2 = b$, $x_2 = 0$ $x_3 = h/2$, and $x_3 = -h/2$, respectively.

6.3.5 Calculation of Transverse Stresses

For the displacement-based ESL, the transverse stresses computed from the plate theory displacements generally are inaccurate. This shortcoming is remedied by using a one-step stress recovery scheme (SRS) in which the in-plane stresses are first computed from the displacement field and the constitutive relation, and the transverse stresses are then calculated by integrating the equilibrium equations in the thickness direction. Equilibrium equations in the absence of body forces for the k^{th} lamina are

$$\sigma^k_{i1,1} + \sigma^k_{i2,2} + \sigma^k_{i3,3} = 0, \qquad i = 1, 2, 3 \tag{6.35}$$

Integrating Eq. 6.35 along the thickness yields

$$\sigma^k_{i3}\left(x_3\right) = -\int_{\bar{h}^k}^{x_3} \left(\sigma^k_{i1,1} + \sigma^k_{i2,2}\right) dx_3 + \sigma^k_{i3}(\bar{h}^k), \qquad i = 1, 2, 3 \tag{6.36}$$

where $\bar{h}^k$ denotes the x_3-coordinate of the bottom surface of the k^{th} layer. The values of $\sigma^k_{i3}\left(x_3\right)$ equal prescribed surface tractions at the bottom surface of the first layer. For the remaining layers, they are found from Eq. 6.36 with $x_3 = h^{k+1}$. Ideally, transverse stresses on the top-most surface of the laminate derived from this procedure should equal the tractions prescribed on that surface. Substitution for displacement field from Eq. 6.11 into the strain-displacement relation (Eq. 6.2), for strains into Hooke's law (Eq. 6.4) and the result into the right-hand side of Eq. 6.36, we see that the integrand involves second-order derivatives of displacements. Since the assumed displacement is a polynomial of degree greater than 2 in x_1 and x_2, the right-hand sides of Eq. 6.36 are well defined. Furthermore, the powers of x_3 in these integrands determine the through-the-thickness variation of the transverse stresses.

6.4 Numerical Examples for Free Vibrations

In our previous work [57], we have presented the first 12 natural frequencies of three-layered sandwich plates having various face-to-core stiffness ratios (FCSR) from the analytical solution of 3D linear elasticity theory equations and a third-order shear and normal deformable theory (TSNDT) using Jacobi polynomials as basis functions. When FCSR =1, the material properties of the face sheets and core becomes identical, i.e., a homogeneous plate. However, with increasing FCSR, the core becomes softer compared to face sheets. We found that the error of the TSNDT in estimating natural frequencies for FCSR of a sandwich plate greater than 20 is unacceptable. Here, it is aimed to see whether these limitations of TSNDT could be eliminated by using higher order either ESL or LW theories. By comparing the natural frequencies obtained from various order ESL, LW plate theories, and the 3D FEM using ABAQUS with those found by analytically solving the 3D-LET equations, we investigate the influence of FCSR on the accuracy of these methods in predicting the lowest six natural frequencies of the sandwich plates. Next, we analyzed the free vibrations of sandwich structures with typical face sheet and core materials to study the influence of face-to-core elastic modulus ratio in the thickness direction ($E_{33}^{face}/E_{33}^{core}$) and in the fiber direction ($E_{11}^{face}/E_{11}^{core}$) on the accuracy of ESL and LW plate theories.

Before presenting numerical results, we note that integrands for the stiffness matrix and the mass matrix involve polynomials of degree much higher than those encountered in the FEM. These integrands are numerically evaluated by using an appropriate Gauss quadrature rule with the number of integration points in each direction depending upon the degree of the polynomial.

6.4.1 Influence of face sheet to core stiffness ratio on the convergence of frequencies

Figure 6.5 shows a cross-section of the simply supported square sandwich plate having h/a =0.1 with identical top and bottom face sheets and a core in between along with material properties of Aragonite crystals [6]. Note that elasticity constants of Aragonite crystals are expressed in terms of C_{11} and these material properties are assigned to both face sheets and the core. By keeping C_{11}^{core} fixed and changing C_{11}^{face}, the different face-to-core-stiffness ratios (FCSR = $C_{11}^{face}/C_{11}^{core}$) are obtained.

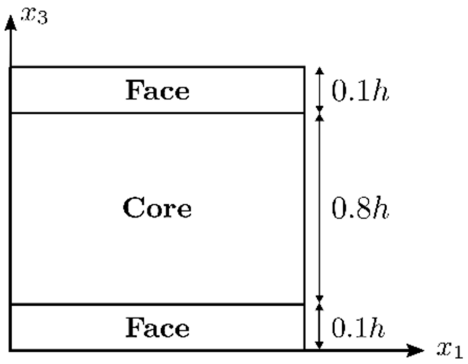

Material properties of Aragonite crystals	
$C_{22}/C_{11} = 0.543103$	$C_{33}/C_{11} = 0.530172$
$C_{12}/C_{11} = 0.233190$	$C_{13}/C_{11} = 0.010776$
$C_{23}/C_{11} = 0.098276$	$C_{44}/C_{11} = 0.266810$
$C_{55}/C_{11} = 0.159914$	$C_{66}/C_{11} = 0.262931$

Figure 6.5: Cross-section of the sandwich plate and orthotropic properties assumed in face sheets and the core [6]

In Figure 6.6, we have presented the convergence (up to the fourth significant digit) of the 1^{st} and 6^{th} frequency parameters ($\lambda = \omega\sqrt{\rho h/C_{11}^{\text{core}}}$) obtained from ESL-5 theory with an increase in the degree of Jacobi polynomials n_1 and n_2 in the x_1 and the x_2, respectively, for sandwich plate having FCSR = 10. As a result of the convergence study, the degree of polynomials, n_1 and n_2, is set to 6 for ESL-N theories.By varying the FSCR, we have listed ESL- N^{th}-order shear and normal deformable theory predictions and analytical values of the lowest six frequency parameters of the sandwich plate in Table 6.1. We aim to find the plate order N that reduces the error between the ESL predictions and analytical solutions to less

than 5%. It is clear that for FCSR = 1, i.e., a homogeneous plate, ESL-1 suffices. However, for FSCR = $10^2, 10^5$, one needs, respectively, ESL-15, ESL-31 to get results within the 5% error limit. For 10^7, ESL-45 was able to reduce the error to under 7%. Note that even for ESL-45, the model has only 6762 degrees of freedom (DoFs) that is negligible as compared to those in the FEM. In Figure 6.7, the percentage error, $\left(100 \times \left|\lambda_{\text{analytical}} - \lambda_{\text{present}}\right| / \lambda_{\text{analytical}}\right)$, in the fundamental frequency parameter λ_1 versus plate order n_3 is presented. Except for FCSR = 10^6 and 10^7, ESL-17 (-45) reduces the error to less than 5% (2%) for the fundamental frequency. For FCSR = 10^6 and 10^7, the error in λ_1 is reduced to less than 9% with ESL $-$ 45. Insights for the slower convergence of the error for FCSR = 10^6 and 10^7 can be gained by looking at the plot of the analytical values of λ_1 versus FCSR exhibited in Figure 6.8. It is clearly seen that with increasing FCSR, λ_1 converges to $\sim$ 1.608 for FCSR = 10^6 and remains unchanged when FCSR is increased to 10^7.

For the sandwich plate studied above, the results of the LW theory are presented in Table 6.2. The number of polynomials in the x_1- and the x_2- directions are set equal to 12 as a result of the convergence study. Except for FCSR = 10^5, the frequency parameters obtained from LW-3 and LW-5 match exactly with the analytical results. For FCSR = 10^5, LW-3 with 5070 DoFs gives the maximum error of 5.8 % for the lowest six frequency parameters.

We now find the number of DoFs needed in the FEM to accurately (within 5% of its analytical value) compute λ_1 through λ_6 for different values of FCSR. For this purpose, we use the commercial FE software, ABAQUS with 8-node brick elements (C3D8) and four elements in each face sheet and the core. We compare results computed with different FE meshes with their analytical values in Table 6.3. For FCSR greater than 10^2, the $120 \times 120 \times 18$ (790614 DoFs) FE mesh result in a maximum error of 8% for the lowest six frequency parameters. Due to the computational cost, we did not further refine the FE mesh to reduce the error to 5%. The percentage error in λ_1 versus the number of elements plotted in Figure 6.9 reveals

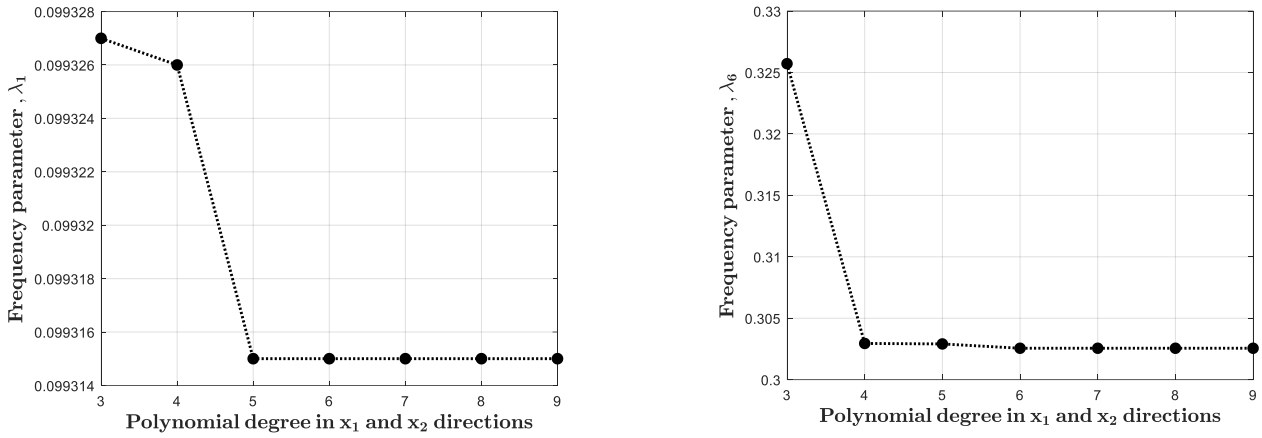

Figure 6.6: Convergence of the 1st and the 6th frequencies with the increase in the degree of Jacobi polynomials in the x_1- and the x_2- directions ($n_3 = 5, FCSR = 10$)

that for FCSR up to 1000, the $40 \times 40 \times 14$ (75645 DoFs) and $120 \times 120 \times 18$ (790614 DoFs) FE meshes result in errors of less than 5% and 1% in λ_1, respectively. However, for FCSR $= 10^4$ and 10^5, the $120 \times 120 \times 18$ (790614 DoFs) FE mesh is needed to compute λ_1 within 5% of its analytical value. Furthermore, the influence of different FE meshes on the $\sim 3\%$ error in λ_1 for FCSR $= 10^6$ and 10^7 is rather minuscule.

6.4.2 Sandwich plates with typical face sheet and core materials

Recall that different values of the FCSR used in section 6.4.1 are obtained by modifying the elastic constant C_{11}. Since the remaining elastic constants are expressed in terms of C_{11}, the same value of the FCSR applies to all elastic parameters. However, that is not the case for practical problems. To remedy the situation, we now study free vibrations of a [0°/90°/ core /90°/0°] square sandwich plate with the face sheet and the core material parameters listed in Tables 6.4 and 6.5, respectively. The schematic of the plate cross-section is shown in Figure 6.10. We begin by studying the effects of different boundary conditions and thickness-to-side ratios of a [0°/90°/core/90°/0°] square sandwich plate with graphite/epoxy face sheets and balsa S45 core $\left(E_{11}^{face}/E_{11}^{\text{core}} = 2454, E_{33}^{face}/E_{33}^{core} = 8\right)$. The

Table 6.1: SSSS Square 3-ply sandwich plate: convergence of frequency parameters, λ, in ESL Ritz method

FCSR	Solution	DoF	λ_1	λ_2	λ_3	λ_4	λ_5	λ_6
1	ESL-1	294	0.04787	0.1052	0.1209	0.1611	0.1611	0.1731
	ESL-3	588	0.04742	0.1033	0.1188	0.1611	0.1611	0.1694
	ESL-5	882	0.04742	0.1033	0.1188	0.1611	0.1611	0.1694
	Analytical [57]		0.04742	0.1033	0.1188	0.1611	0.1611	0.1694
10^2	ESL-3	588	0.2089	0.3665	0.39413	0.5056	0.5401	0.6177
	ESL-9	1470	0.1814	0.3064	0.33528	0.4227	0.4486	0.5163
	ESL-15	2352	0.1776	0.2983	0.32726	0.4115	0.4359	0.5028
	ESL-25	3822	0.1759	0.2949	0.32382	0.4068	0.4306	0.4970
	ESL-31	4704	0.1754	0.2939	0.32287	0.4055	0.4291	0.4954
	Analytical [57]		0.1732	0.2892	0.318169	0.3990	0.4205	0.4857
10^5	ESL-3	588	4.816	7.867	8.735	10.86	11.45	13.26
	ESL-7	1176	0.7522	1.646	1.947	2.746	2.845	3.140
	ESL-15	2352	0.7322	1.553	1.801	1.974	1.991	1.996
	ESL-25	3822	0.7270	1.524	1.757	1.794	1.817	1.818
	ESL-31	4704	0.7252	1.515	1.744	1.746	1.770	1.770
	Analytical [57]		0.7189	1.476	1.672	1.685	1.715	1.724
10^7	ESL-3	588	48.13	78.62	87.29	108.5	114.4	132.5
	ESL-9	1470	6.995	8.820	15.52	18.56	18.81	22.44
	ESL-15	2352	2.431	2.45	2.450	2.466	2.473	2.492
	ESL-25	3822	1.894	1.914	1.919	1.939	1.948	1.971
	ESL-35	5292	1.797	1.818	1.823	1.844	1.854	1.878
	ESL-45	6762	1.740	1.763	1.768	1.789	1.799	1.824
	Analytical [57]		1.612	1.633	1.669	1.696	1.714	1.722

first six computed frequencies using the ESL Ritz method and the ABAQUS for SSSS, CCCC and CFFF plates and thickness-to-side ratios $= 0.01, 0.1$, and 0.2 are listed in Tables 6.6 - 6.8. The seeding of the FE mesh is determined as $120 \times 120 \times 30$ from a convergence study in which the seeding is systematically increased from coarse to fine mesh until the results are within 1% of their values. For the ESL Ritz method, 12^{th} -degree polynomials are used in both x_1 and x_2 directions. For $h/a = 0.01$, the maximum discrepancy between frequencies calculated by ESL- 3 and ABAQUS is 0.9%. For thicker plates ($h/a = 0.1, 0.2$), the ESL-9 (17) is needed to reduce the maximum discrepancy to less than 5%(1.92%). It should be

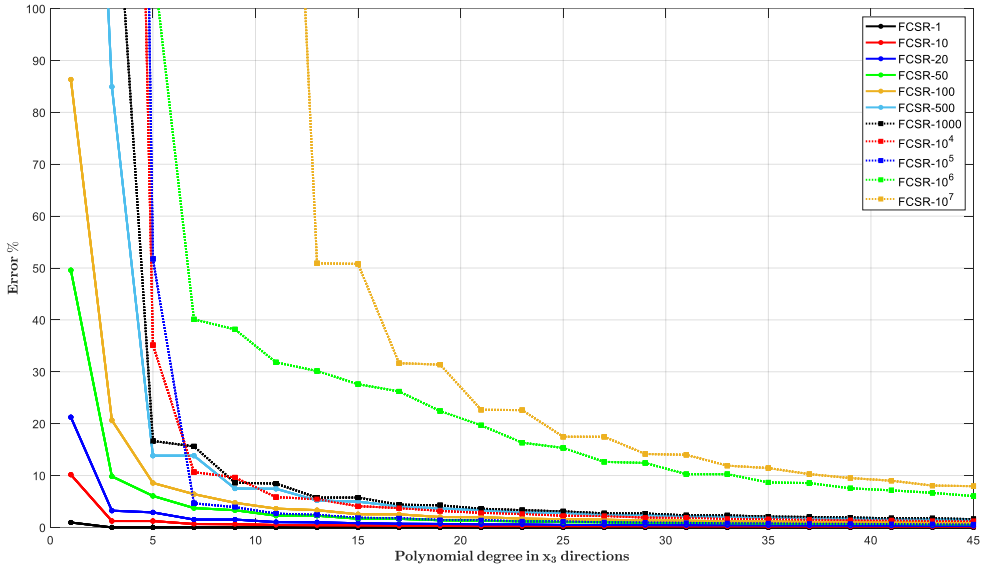

Figure 6.7: Percentage error in the fundamental frequency versus the polynomial degree in the x_3- direction for different FCSR values

noted that the Ritz method with the ESL-17 (7290 DoFs) requires only 0.54% of the number of DoFs need for ABAQUS (1, 361, 613 DoFs).

As the last set of example problems and to explore the effect of different $E_{11}^{\text{face}}/E_{11}^{\text{core}}$ and $E_{33}^{\text{face}}/E_{33}^{\text{core}}$ ratios, we analyze free vibration of sandwich plates with boron/epoxy face sheets and the core made of either aluminum Honeycomb, or foam H45, or Balsa S45. For the Foam H45 and the Balsa S45 cores, $E_{11}^{\text{face}}/E_{11}^{\text{core}} =\sim 3800$, however, $E_{33}^{\text{face}}/E_{33}^{\text{core}} = 376$ and 15, respectively. Here, we aimed see how the convergence behavior and the accuracy of the ESL and LW-Ritz estimations of natural frequencies are changing with different core materials resulting in different $E_{11}^{\text{face}}/E_{11}^{\text{core}}$ and $E_{33}^{\text{face}}/E_{33}^{\text{core}}$ ratios. In Table 6.8 we compare the ESL and LW results with those of ABAQUS (120x120x30 FE mesh and 1,361,613 DoFs). For Balsa 45 and Honeycomb cases, the results from the ESL-9 (with 7290 DoF) and ABAQUS have a relative difference of less than 5%. However, to reduce the relative error under 5% for Foam 45 case, ESL-17 is required. Even the ESL-3 solutions are enough to achieve $\sim 10\%$ relative difference for Balsa S45 $\left(E_{33}^{\text{face}} = 15\right)$ and Honeycomb $\left(E_{33}^{\text{face}} = 11\right)$ cases, as

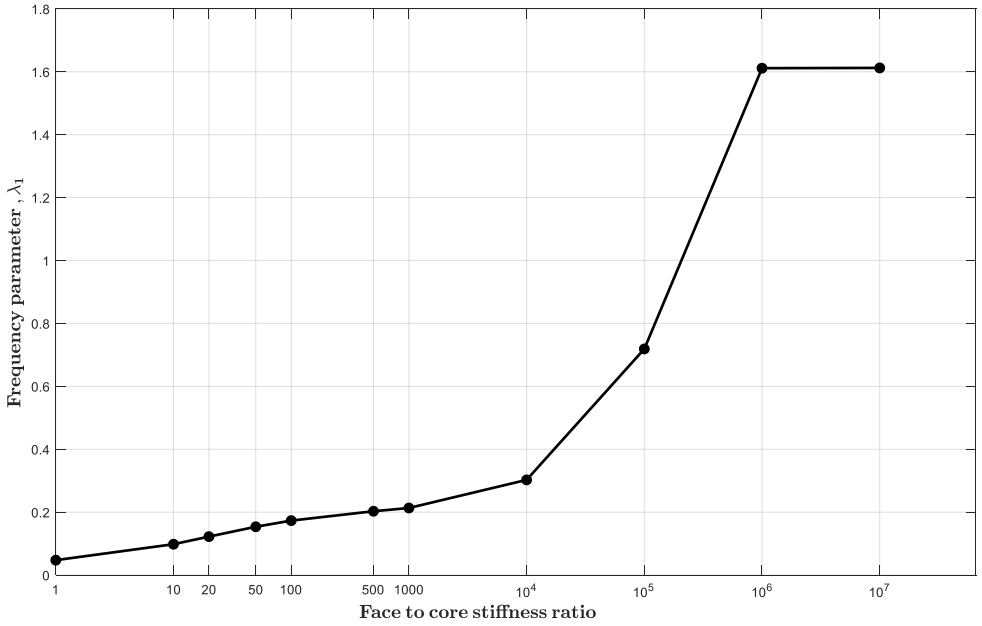

Figure 6.8: SSSS Square sandwich plate: convergence of frequency parameters, λ, in the LW Ritz method

compared to the difference of 78% for Foam H45. In fact, the observed error trend with respect to increasing plater order for different FCSR ratios in Figure 6.7 seems to agree with the current observation in terms of $E_{33}^{\text{face}}/E_{33}^{\text{core}}$ ratio. Thus, it can be concluded that $E_{33}^{\text{face}}/E_{33}^{\text{core}}$ has a higher influence than $E_{11}^{\text{face}}/E_{11}^{\text{core}}$ on the convergence of results. $\text{LW}-3$ and $\text{LW}-5$ results matched very closely with ABAQUS results.

Table 6.2: SSSS Square sandwich plate: convergence of frequency parameters, λ, in the LW Ritz method

FCSR	Solution	DoF	λ_1	λ_2	λ_3	λ_4	λ_5	λ_6
1	LW-1	2028	0.04760	0.1040	0.1195	0.1611	0.1611	0.1707
	LW-3	5070	0.04742	0.1033	0.1188	0.1611	0.1611	0.1694
	LW-5	8112	0.04742	0.1033	0.1188	0.1611	0.1611	0.1694
	Analytical [57]		0.04742	0.1033	0.1188	0.1611	0.1611	0.1694
10^2	LW-1	2028	0.1732	0.2893	0.3182	0.3992	0.4206	0.4861
	LW-3	5070	0.1732	0.2892	0.3182	0.3990	0.4205	0.4857
	LW-5	8112	0.1732	0.2892	0.3182	0.3990	0.4205	0.4857
	Analytical [57]		0.1732	0.2892	0.3182	0.3990	0.4205	0.4857
10^3	LW-1	2028	0.2133	0.3549	0.3810	0.4977	0.5688	0.5896
	LW-3	5070	0.2132	0.3548	0.3803	0.4968	0.5673	0.5873
	LW-5	8112	0.2132	0.3548	0.3803	0.4968	0.5673	0.5873
	Analytical [57]		0.2132	0.3548	0.3803	0.4968	0.5673	0.5873
10^4	LW-1	2028	0.3034	0.6147	0.6758	0.9813	1.098	1.307
	LW-3	5070	0.3026	0.6070	0.6678	0.9546	1.058	1.238
	LW-5	8112	0.3026	0.6070	0.6678	0.9546	1.058	1.238
	Analytical [57]		0.3026	0.6070	0.6678	0.9546	1.058	1.238
10^5	LW-1	2028	0.7344	1.636	1.937	2.600	2.845	3.123
	LW-3	5070	0.7189	1.477	1.586	1.613	1.615	1.640
	LW-5	8112	0.7189	1.476	1.576	1.603	1.605	1.630
	Analytical [57]		0.7189	1.476	1.672	1.685	1.715	1.724

Table 6.3: SSSS Square sandwich plate: convergence of frequency parameter, λ, using ABAQUS

FCSR	Solution	DoF	λ_1	λ_2	λ_3	λ_4	λ_5	λ_6
10^2	$40 \times 40 \times 14$	75645	0.1742	0.2934	0.3245	0.4061	0.4342	0.5063
	$60 \times 60 \times 14$	167445	0.1736	0.2910	0.3210	0.4020	0.42632	0.4948
	$80 \times \times 80 \times 14$	295245	0.1734	0.2902	0.3197	0.4006	0.4235	0.4908
	$100 \times 100 \times 15$	489648	0.1733	0.2898	0.3191	0.3999	0.4222	0.4889
	$120 \times 120 \times 18$	790614	0.1732	0.2895	0.3188	0.3996	0.4215	0.4878
	Analytical [57]		0.1732	0.2892	0.3182	0.3990	0.4205	0.4857
10^4	$40 \times 40 \times 14$	75645	0.3642	0.8356	0.8816	1.209	1.538	1.558
	$60 \times 60 \times 14$	167445	0.3301	0.7415	0.7440	1.074	1.371	1.392
	$80 \times 80 \times 14$	295245	0.3173	0.6841	0.7085	1.020	1.246	1.323
	$100 \times 100 \times 15$	489648	0.3112	0.6555	0.6913	0.9929	1.180	1.288
	$120 \times 120 \times 18$	790614	0.3078	0.6393	0.6817	0.9779	1.141	1.268
	Analytical [57]		0.3026	0.6070	0.6678	0.9546	1.058	1.238
10^5	$40 \times 40 \times 14$	75645	0.9429	1.557	1.580	1.585	1.607	1.615
	$60 \times 60 \times 14$	167445	0.8233	1.558	1.582	1.585	1.609	1.619
	$80 \times 80 \times 14$	295245	0.7757	1.558	1.583	1.585	1.609	1.621
	$100 \times 100 \times 15$	489648	0.7524	1.563	1.588	1.591	1.608	1.615
	$120 \times 120 \times 18$	790614	0.7393	1.565	1.568	1.594	1.596	1.621
	Analytical [57]		0.7189	1.476	1.672	1.685	1.715	1.724
10^7	$40 \times 40 \times 14$	75645	1.560	1.581	1.588	1.607	1.616	1.640
	$60 \times 60 \times 14$	167445	1.560	1.583	1.589	1.610	1.620	1.644
	$80 \times 80 \times 14$	295245	1.560	1.583	1.589	1.610	1.621	1.646
	$100 \times 100 \times 15$	489648	1.565	1.589	1.594	1.616	1.627	1.652
	$120 \times 120 \times 18$	790614	1.570	1.594	1.600	1.622	1.633	1.659
	Analytical [57]		1.609	1.632	1.670	1.696	1.714	1.721

Table 6.4: Values of the engineering constants for typical face sheet materials

	E_{11}	E_{22}	E_{33}	G_{12}	G_{13}	G_{23}	v_{12}	v_{13}	v_{23}	ρ
Units	(GPa)	(GPa)	(GPa)	(GPa)	(GPa)	(GPa)				kg/m^3
Graphite/Epoxy	132.5	10.8	10.8	5.7	5.7	3.4	0.24	0.24	0.49	1540
Boron/Epoxy [2]	206.84	20.68	20.68	6.89	4.14	6.89	0.3	0.25	0.25	2000

Table 6.5: Values of the engineering constants for typical core materials

	E_{11}	E_{22}	E_{33}	G_{12}	G_{13}	G_{23}	v_{12}	v_{13}	v_{23}	ρ
Units	(MPa)	(MPa)	(MPa)	(MPa)	(MPa)	(MPa)				kg/m^3
Balsa S45 [61]	54	54	1355	59	201	201	0.36	0.014	0.014	600
Foam H45 [62]	55	55	55	15	15	15	0.4	0.4	0.4	48
Honeycomb [63]	0.884	0.918	1812.3	0.64	262.981	390.83 3	0.98	1.61E− 04	1.67E -04	69.9

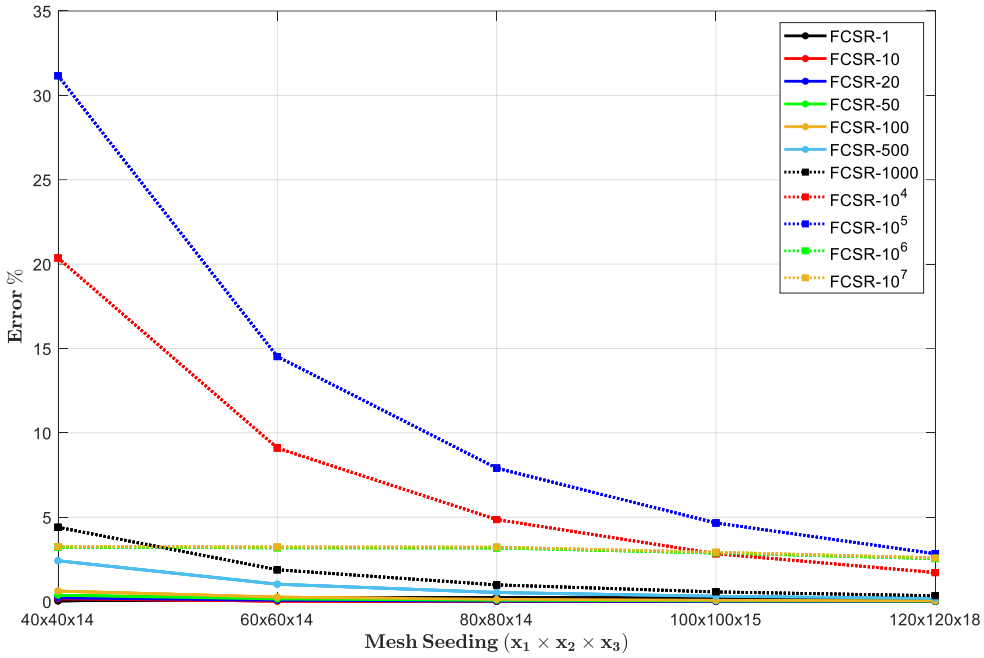

Figure 6.9: The percentage error in the fundamental frequency versus the FE mesh for different FCSR values

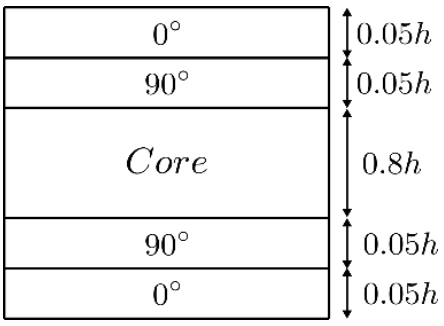

Figure 6.10: Cross-section of the [0°/90°/core/90°/0°] square sandwich plate (a = b = 10m)

Table 6.6: Frequencies (Hz) of SSSS square [0°/90°/core/90°/0°] sandwich plate from the ESL-Ritz method and ABAQUS (Face sheets: Graphite/Epoxy, Core: Balsa S45)

h/a	Modes	ESL-1	ESL-3	ESL-7	ESL-9	ESL-13	ESL-17	ABAQUS
	1	4.82	4.66	4.65	4.65	4.65	4.65	4.70
	2	12.82	12.30	12.25	12.24	12.23	12.23	12.40
0.01	3	13.76	13.25	13.21	13.20	13.19	13.18	13.34
	4	19.17	18.27	18.19	18.19	18.17	18.16	18.36
	5	27.09	25.54	25.34	25.34	25.29	25.27	25.63
	6	29.37	27.79	27.65	27.64	27.59	27.57	27.90
	1	41.38	30.22	29.30	29.30	29.03	28.89	28.53
	2	61.37	54.66	52.18	52.17	51.51	51.16	50.28
0.1	3	61.37	57.21	55.18	55.17	54.54	54.21	53.36
	4	90.23	61.34	61.09	61.06	61.03	61.02	60.98
	5	92.89	61.34	61.11	61.08	61.05	61.03	60.98
	6	122.74	73.17	70.06	70.06	69.17	68.70	67.51
	1	61.37	36.59	35.03	35.03	34.59	34.35	33.75
	2	61.37	60.21	57.15	57.14	56.35	55.93	54.84
0.2	3	62.14	61.23	60.03	60.02	59.24	58.84	57.79
	4	114.84	61.24	60.23	60.12	60.01	59.96	59.79
	5	115.81	62.58	60.30	60.19	60.05	59.99	59.80
	6	122.74	78.94	75.26	75.25	74.23	73.71	72.32

Table 6.7: Frequencies (Hz) of CCCC square [0°/90°/core/90°/0°] sandwich plate from the ESL-Ritz method and ABAQUS (Face sheets: Graphite/Epoxy, Core: Balsa S45)

h/a	Modes	ESL-1	ESL-3	ESL-7	ESL-9	ESL-13	ESL-17	ABAQUS
	1	10.14	9.71	9.67	9.67	9.66	9.65	9.78
	2	20.12	18.87	18.72	18.71	18.68	18.66	18.93
0.01	3	21.41	20.12	20.00	19.99	19.95	19.93	20.19
	4	28.39	26.41	26.20	26.19	26.14	26.10	26.44
	5	36.61	33.45	33.05	33.04	32.94	32.89	33.33
	6	39.51	36.21	35.90	35.89	35.79	35.73	36.11
	1	63.97	37.68	36.05	36.04	35.59	35.35	34.80
	2	105.50	58.84	56.12	56.10	55.37	54.98	54.04
0.1	3	106.88	61.20	58.88	58.86	58.13	57.76	56.85
	4	137.05	76.64	73.43	73.40	72.45	71.97	70.76
	5	159.36	85.78	81.26	81.24	80.14	79.56	78.26
	6	161.70	90.19	86.63	86.61	85.50	84.95	83.70
	1	76.34	40.99	39.06	39.05	38.52	38.26	37.86
	2	120.40	64.29	61.15	61.11	60.32	59.91	59.28
0.2	3	121.15	66.62	63.93	63.89	63.05	62.66	62.03
	4	153.84	83.50	79.81	79.76	78.72	78.22	77.31
	5	175.93	92.89	88.13	88.09	87.04	86.49	86.05
	6	176.90	96.97	93.25	93.19	91.96	91.42	91.00

Table 6.8: Frequencies (Hz) of CFFF square [0°/90°/core/90°/0°] sandwich plate from the ESL-Ritz method and ABAQUS (Face sheets: Graphite/Epoxy, Core: Balsa S45)

h/a	Modes	ESL-1	ESL-3	ESL-7	ESL-9	ESL-13	ESL-17	ABAQUS
0.01	1	1.15	1.13	1.13	1.13	1.13	1.13	1.14
	2	1.68	1.66	1.66	1.66	1.66	1.66	1.66
	3	7.03	6.91	6.89	6.89	6.89	6.88	6.97
	4	7.26	7.03	7.01	7.01	7.01	7.00	7.09
	5	7.88	7.67	7.65	7.65	7.64	7.64	7.70
	6	11.91	11.53	11.49	11.49	11.48	11.47	11.56
0.1	1	10.69	9.01	8.87	8.86	8.81	8.79	8.72
	2	14.70	11.75	11.52	11.52	11.45	11.41	11.30
	3	26.82	26.80	26.77	26.77	26.77	26.76	26.75
	4	50.34	33.16	32.20	32.19	31.88	31.71	31.25
	5	55.20	37.28	36.24	36.24	35.90	35.73	35.23
	6	60.21	43.61	42.04	42.04	41.62	41.40	40.82
0.2	1	18.10	12.46	12.10	12.10	11.98	11.91	11.77
	2	23.18	15.90	15.48	15.48	15.34	15.27	15.11
	3	26.83	26.78	26.69	26.68	26.67	26.66	26.64
	4	65.05	39.46	38.18	38.17	37.74	37.52	37.08
	5	72.81	45.47	43.94	43.93	43.43	43.18	42.63
	6	78.90	52.51	49.92	49.92	49.25	48.91	48.07

Table 6.9: Frequencies (Hz) of SSSS square [0°/90°/ core /90°/0°] sandwich plates (Face sheets: Boron/Epoxy,$a/h = 0.1$)

Core		ESL					LW		ABAQUS
Material	$n_3 \rightarrow$	3	9	17	25	35	3	5	
Honeycomb	ω_1	49.40	48.09	47.46	47.30	47.20	46.94	46.94	46.94
	ω_2	86.94	86.08	84.29	83.84	83.57	82.89	82.89	82.90
$E_{11}^{face}/E_{11}^{core} = 233981$	ω_3	86.94	86.93	86.92	86.92	86.92	86.92	86.92	86.92
	ω_4	89.83	86.93	86.93	86.93	86.93	86.93	86.93	86.92
$E_{33}^{face}/E_{3}^{core} = 11$	ω_5	93.28	90.39	89.15	88.84	88.61	88.07	88.07	88.08
	ω_6	119.8	115.1	113.1	112.6	112.2	111.4	111.4	111.4
Foam H45	ω_1	24.05	14.52	14.05	13.88	13.76	13.50	13.50	13.51
	ω_2	38.18	24.01	23.33	23.07	22.90	22.52	22.52	22.61
$E_{11}^{face}/E_{11}^{core} = 3761$	ω_3	41.78	25.15	24.39	24.11	23.92	23.50	23.50	23.58
	ω_4	51.50	32.02	31.11	30.77	30.54	30.05	30.05	30.15
$E_{33}^{face}/E_{33}^{core} = 376$	ω_5	55.64	37.36	36.47	36.13	36.16	35.43	35.43	35.72
	ω_6	62.90	39.31	38.26	37.90	37.89	37.07	37.07	37.35
Balsa S45	ω_1	31.42	30.08	29.53	29.37	29.28	29.06	29.06	29.06
	ω_2	53.96	51.33	50.29	49.98	49.80	49.38	49.38	49.39
$E_{11}^{face}/E_{11}^{core} = 3830$	ω_3	57.82	54.61	53.29	52.92	52.73	52.21	52.21	52.22
	ω_4	63.60	63.33	63.28	63.27	63.26	63.23	63.23	63.23
$E_{33}^{face}/E_{33}^{core} = 15$	ω_5	63.60	63.35	63.29	63.27	63.26	63.24	63.24	63.24
	ω_6	72.58	68.63	67.05	66.60	66.35	65.73	65.73	65.73

6.5 Numerical Examples for Static Deformations

In this section, by using ESL and LW plate theories, we analyze the static deformations of monolithic beams, laminates, and sandwich plates with tractions applied on the top and/or the bottom surfaces. The in-plane stresses $(\sigma_{11}, \sigma_{22}, \sigma_{12})$ and transverse stresses $(\sigma_{13}, \sigma_{23}, \sigma_{33})$ are obtained from the constitutive relations and by using a stress recovery scheme (SRS), respectively. First, we have studied static deformations of monolithic beams without using SRS to see which order ESL theory is required for accurately calculating through-the-thickness stress variations in the cantilevered monolithic beams at the vicinity of free and clamped edges. Next, we have compared the displacement and stress values obtained from ESL theories with those of 3D analytical solutions from the literature for different boundary conditions. Finally, we consider the sandwich plates that we analyzed in the free vibrations section to investigate the effects of FCSR and face to core modulus ratios on the accuracy of ESL and LW plate theories. First, we have solved the 3D -LET equations analytically by following Srinivas and Rao's approach, then these analytical solutions are used as a reference to calculate relative errors of ESL and LW plate theories.

For monolithic beams and each layer of laminated plates, the below material properties are used.

$$E_1 = 25 \times 10^6 \text{psi}, \quad E_2 = E_3 = 10^6 \text{psi}, \quad G_{23} = 0.2 \times 10^6 \text{psi}$$

$$G_{12} = G_{13} = 0.5 \times 10^6 \text{psi}, \quad v_{12} = v_{13} = v_{23} = 0.25$$

Thus each layer is comprised of a transversely isotropic material with the axis of transverse isotropy along the x_1 -axis.

6.5.1 Cantilever beam with uniform pressure on the top surface

We investigate static deformations of a monolithic thick cantilever beam having length/thickness $(a/h) = 2$ and width/thickness $(b/h) = 0.001$ clamped at the edge $x_1 = 0$, traction free at $x_1 = a$, and subjected to uniformly distributed normal tractions on its top and bottom surfaces given by $q_3^+ = [0, 0, -q_0/2]^T, q_3^- = [0, 0, q_0/2]^T$. Because of the very small width of the beam and no tractions on the front and the back faces, the beam undergoes plane stress deformations. The degrees of polynomials in the displacement approximations for x_1 and x_2 directions are determined as 16 and 1 through a convergence study, and for x_3 direction the polynomial degree is varied. Here, we test the efficiency of the ESL Ritz method without using the SRS for calculating transverse stresses. Vel and Batra [61] analytically solved this problem by using the Eshelby-Stroh formalism and assuming generalized plane strain deformations that are valid for a beam with $b >> a$. Batra and Vidoli [62] analyzed deformations for this problem with their Kth-order mixed plate theory. In Figure 6.11, we compare presently computed through-the-thickness distributions of σ_{11} on sections $x_1/a = 0.4$ and 0.6 with those reported in [61]. It is clear that when $n_3 = 3$, which corresponds to the third-order polynomial expansion in the thickness direction, the present results deviate from the analytical solutions. However, for $n_3 = 5$ and 7 the two sets of results, respectively, show good and excellent agreements with each other. The through-the-thickness distributions of the transverse stresses on the sections $x_1/a = 0.02$, 0.1, 0.3, and 0.85 are exhibited in Figure 12 along with predictions from the 7^{th} -order mixed plate theory [65]. Note that the section $x_1/a = 0.02$ is close to the clamped edge. In Figure 6.12-a, σ_{33} on $x_1/a = 0.02$ by the current theory with $n_3 = 7$ and with the 7^{th} -order mixed plate theory [62] has oscillatory behavior with similar amplitudes not present in the analytical solutions. However, σ_{33} found using $n_3 = 15$ agrees very well with that from the analytical solution. Also, it is seen that $n_3 = 7$ is not sufficient to satisfy the natural boundary conditions at the top and bottom surfaces

near the clamped edge. On the other hand, in the interior sections ($x_1/a = 0.1$, 0.3 and $0.85, n_3 = 7$ provides a solution that not only agrees well with the analytical solution but also satisfies the natural boundary conditions on the top and the bottom surfaces. However, for the transverse stress σ_{13} to vanish everywhere on the top and the bottom surfaces, one needs $n_3 = 15$. As pointed out above, the total number of DoFs for $n_3 = 15$ is quite small.

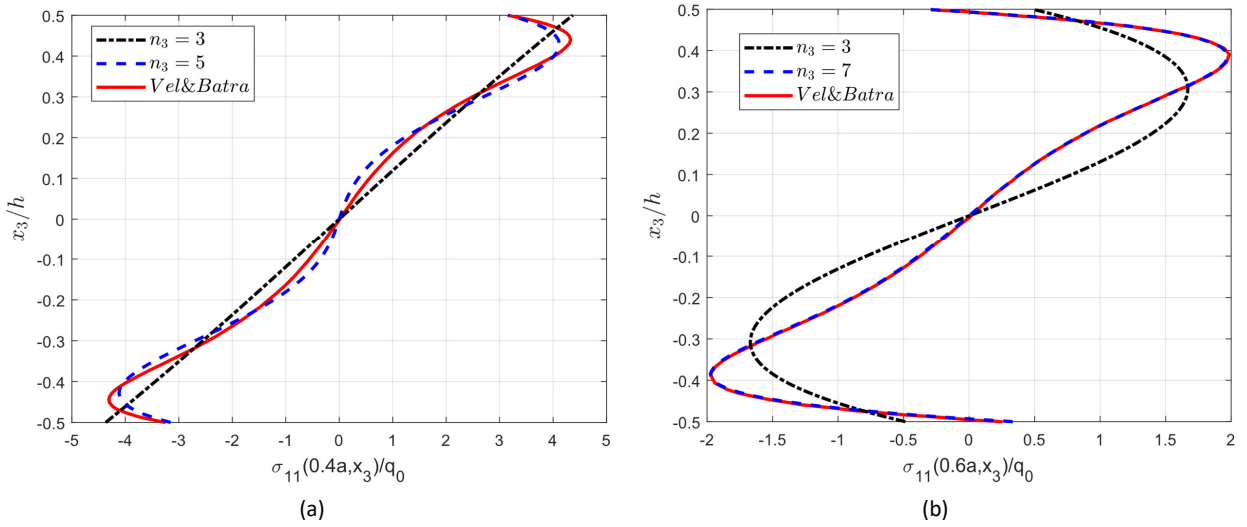

Figure 6.11: Through-the-thickness distribution of the axial stress σ_{11} on a) $x_1 = 0.4a$, and b) $x_1 = 0.6a$

6.5.2 Cantilever beam with uniformly distributed tangential tractions on the top and the bottom surfaces

We now study deformations of the cantilever beam of subsection 6.5.1 but loaded with tangential tractions, $q_3^+ = [q_0/2, 0, 0]^T, q_3^- = [-q_0/2, 0, 0]^T$, on top and bottom surfaces. Computed transverse shear and normal stress distributions on several sections by the present theory and the 7^{th} -order mixed plate theory [62] are presented in Figures 6.14 and 6.15 respectively. It is observed that $n_3 = 7$ is unable to satisfy natural boundary conditions near the edge sections, but $n_3 = 15$ is. However, except for the boundary layers near the top and

bottom surfaces of the beam, results obtained with $n_3 = 7$ have good agreement with those of Batra and Vidoli [62].

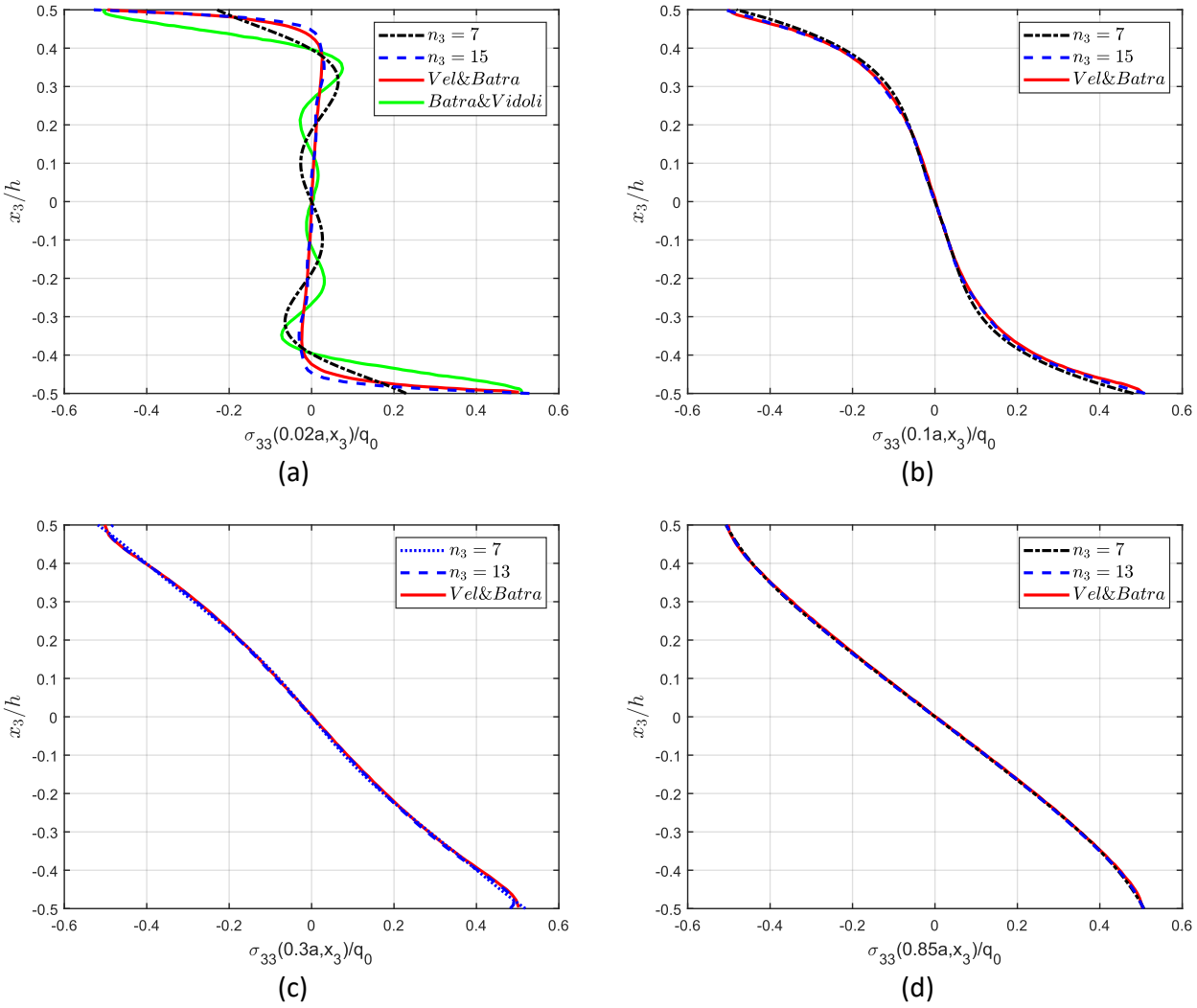

Figure 6.12: Through-the-thickness distribution of the transverse normal stress, σ_{33}, on a) $x_1 = 0.02a$, b)$x_1 = 0.1a$, c) $x_1 = 0.3a$, and d) $x_1 = 0.85a$

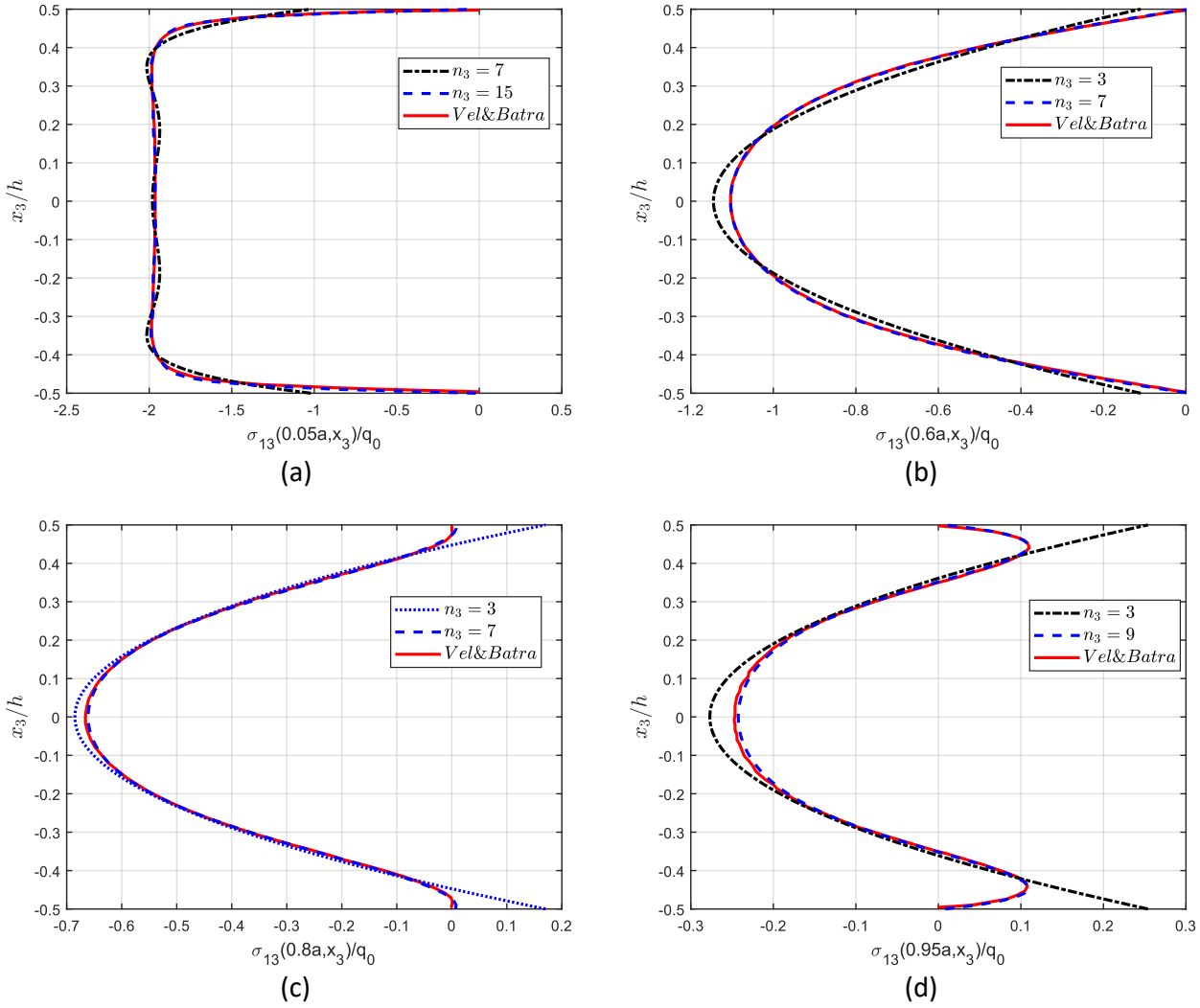

Figure 6.13: Through-the-thickness distribution of the transverse shear stress, σ_{13} on a) $x_1 = 0.05a$, b)$x_1 = 0.6a$, c) $x_1 = 0.8a$, and d) $x_1 = 0.95a$

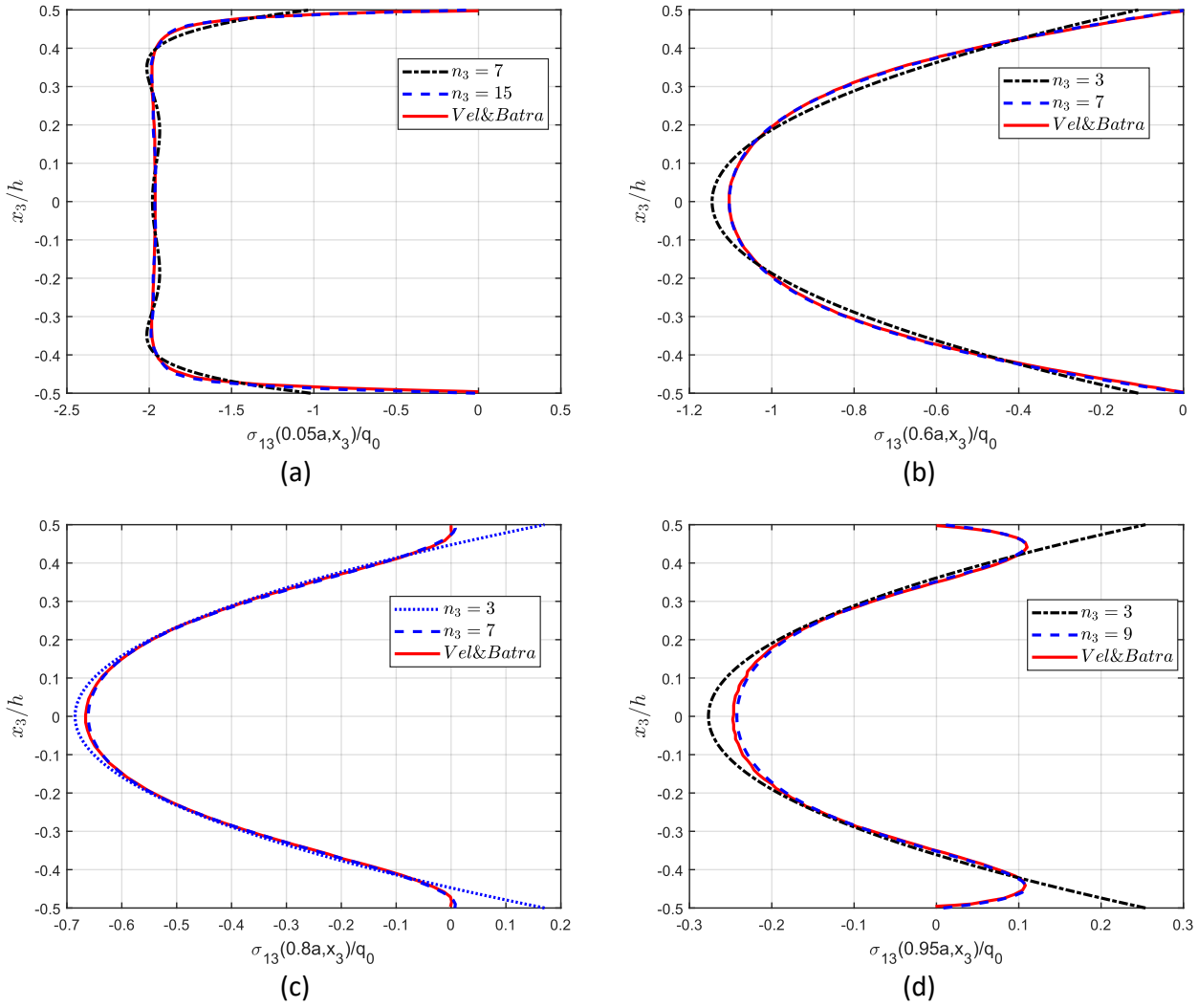

Figure 6.14: Through-the-thickness distribution of the transverse shear stress σ_{13} on sections a) $x_1 = 0.05a$, b) $x_1 = 0.6a$, c) $x_1 = 0.8a$, and $x_1 = 0.95a$

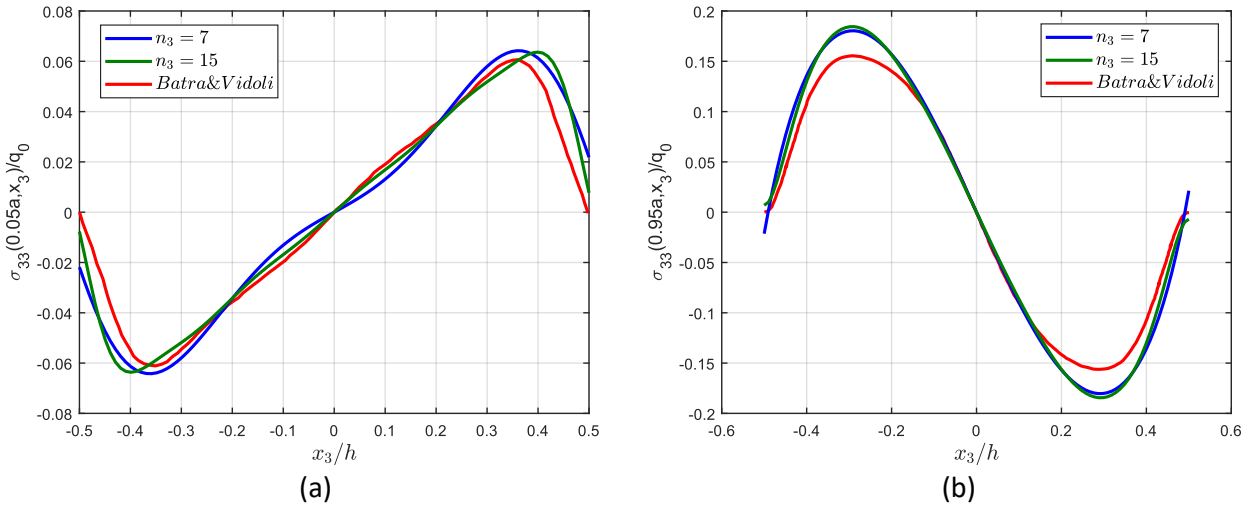

Figure 6.15: Through-the-thickness distribution of the transverse normal stress, σ_{33} on sections a) $x_1 = 0.05a$ and b) $x_1 = 0.95a$

6.5.3 Simply Supported [0°/90°/0°] Laminated Plate with Various Thicknesses: Reference Solution of Pagano [8]

To verify the accuracy of the present ESL coupled with the SRS for finding transverse stresses in laminated plates, we now study deformations of an SSSS square [0°/90°/0°] plate subjected to the sinusoidal normal traction $q(x_1, x_2) = q_0 \sin(\pi x_1/a) \sin(\pi x_2/a)$ on the top surface, and compare our results with the analytical solution of Pagano [8] by using his following non-dimensionalization for stresses.

$$(\bar{\sigma}_{11}, \bar{\sigma}_{22}, \bar{\sigma}_{12}) = \frac{h^2}{a^2 q_0}(\sigma_{11}, \sigma_{22}, \sigma_{12}), \quad (\bar{\sigma}_{13}, \bar{\sigma}_{23}) = \frac{h}{a q_0}(\sigma_{13}, \sigma_{23}), \quad \overline{u}_3 = \frac{100 E_2 h^3 u_3}{a^4 q_0}$$

For $n_1 = n_2 = 8$, Figure 6.16 shows the influence of n_3 on the percentage error ($100\times \mid \sigma_{\text{analytical}} - \sigma_{\text{Abaqus}} \mid /\sigma_{\text{analytical}}$) in $\sigma_{11}, \sigma_{22}, \sigma_{13}$, and σ_{23} for side-to-thickness ratios, $a/h = 2, 4, 10, 20, 50, 100$. The presently computed with $n_3 = 45$ are compared with those from the exact solution using Pagano's method in Table 6.10. It is evident that when $a/h = 50$ and 100, $n_3 = 3$ provides

a minuscule percentage error. However, with a decrease in a/h higher polynomial order n_3 needed for small % error increases. For example, to reduce the error to under 1% in σ_{13} the required n_3 values for $a/h = 2,\ 4,\ 10,\ 20$ are 3, 7, 15, and 25, respectively. For ESL-45 the error is less than 0.5% for all stress components except for σ_{22} for which the error is reduced to 3.4%. It should be pointed out that since the transverse shear stresses are calculated from the in-plane stresses in the SRS, their values depend upon how accurately the in-plane stresses are calculated. It provides a means of assessing the accuracy of plate theories and the associated SRS. For example, a fifth-order shear and normal deformable plate theory may give σ_{22} with more than 14% error for $a/h = 2$ according to Figure 6.16-b.

Table 6.10: Comparison of present results for stresses with those of Pagano for square SSSS $[0°/90°/0°]$ plate

a/h	Solution	$\bar{\sigma}_{11}$ $(a/2, b/2, \pm h/2)$		$\bar{\sigma}_{22}$ $(a/2, b/2, \pm h/6)$		$\bar{\sigma}_{13}$ $(0, b/2, 0)$	$\bar{\sigma}_{23}$ $(a/2, 0, 0)$	$\bar{\sigma}_{12}$ $(0, 0, \pm h/2)$	
2	Pagano	1.436	-0.938	0.669	-0.742	0.164	0.2591	-0.0859	0.0702
	Present	1.4321	-0.9337	0.6460	-0.7273	0.1647	0.2585	-0.0858	0.0700
4	Pagano	0.801	-0.755	0.534	-0.556	0.256	0.2172	-0.0511	0.0505
	Present	0.7988	-0.7528	0.5293	-0.5519	0.2568	0.2165	-0.0509	0.0504
10	Pagano	0.59	-0.59	0.285	0.288	0.357	0.1228	-0.0289	0.0289
	Present	0.59	-0.5893	0.2835	-0.2872	0.3578	0.1225	-0.0288	0.0289
20	Pagano	0.552	-0.552	0.21	-0.21	0.385	0.0938	-0.0234	0.0234
	Present	0.5522	-0.5523	0.2089	-0.2098	0.3848	0.0937	-0.0233	0.0234
50	Pagano	0.541	-0.541	0.185	-0.185	0.393	0.0842	-0.0216	0.0216
	Present	0.5409	-0.5409	0.1844	-0.1846	0.3935	0.0842	-0.0216	0.0216
100	Pagano	0.539	-0.539	0.181	-0.181	0.395	0.0828	-0.0213	0.0213
	Present	0.5392	-0.5393	0.1808	-0.1808	0.3948	0.0828	-0.0214	0.0214

6.5.4 Through-the-thickness Stress Distributions Near Edges of Laminated Plates: Reference Solution of Vel and Batra [12]

We now study the deformations of a thick, $a/h = 5, [0°/90°]$ and $[0°/90°/0°]$ laminated square plates subjected to the sinusoidal normal traction $q(x_1, x_2) = q_0 \sin(\pi x_1/a)(\pi x_2/b)$ on the top surface. The displacements and stresses at specific locations on the $x_1 - x_2$ plane

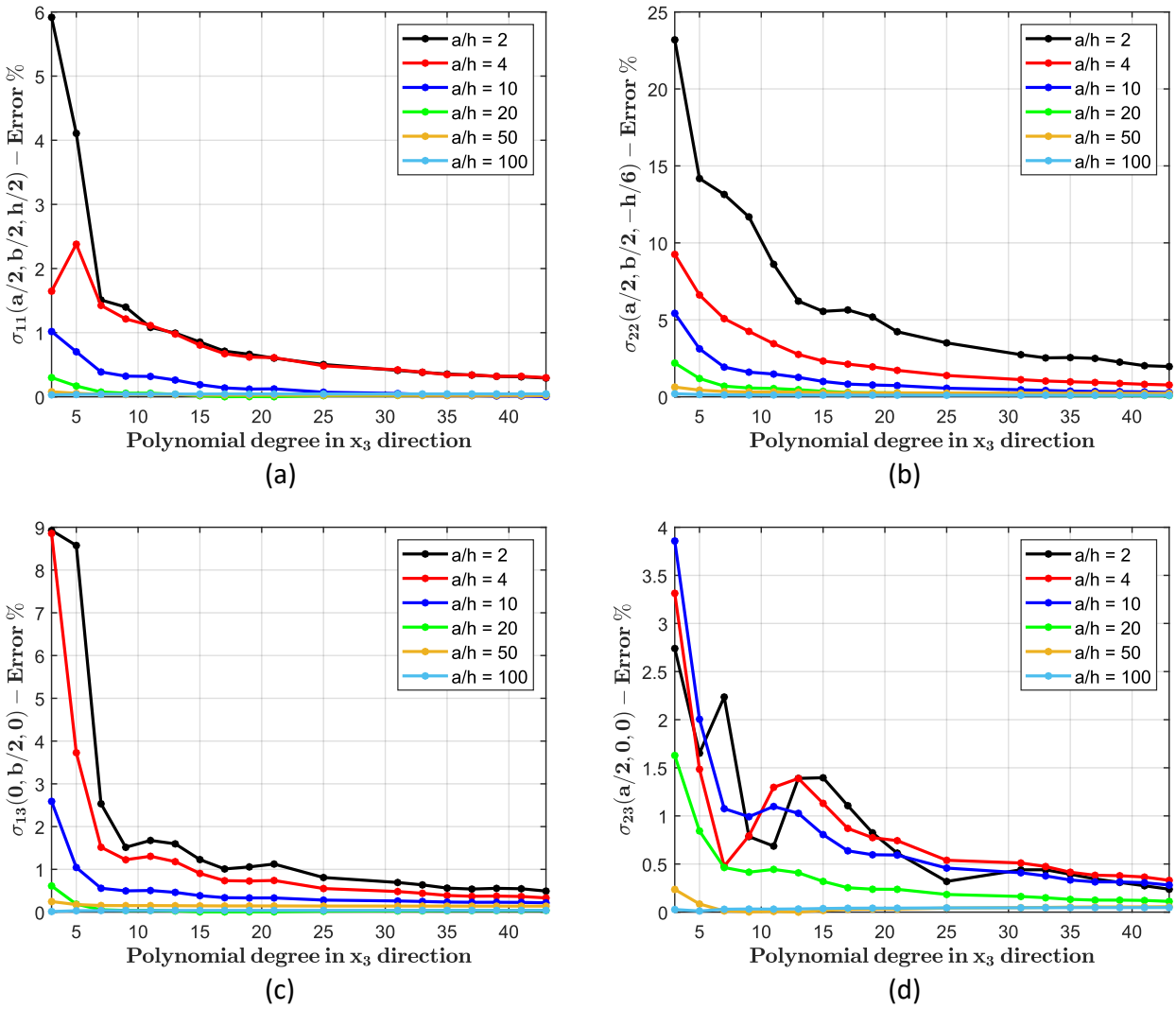

Figure 6.16: For various thickness ratios (a/h), dependence of the percentage error in (a) σ_{11}, (b) σ_{22}, (c) σ_{13}, (d) σ_{23} upon the polynomial degree in x_3 -direction for a square SSSS $[0°/90°/0°]$ plate

are normalized as in [12]:

$$[\bar{u}_1(x_3), \bar{u}_2(x_3)] = \frac{100E_2h^2}{q_0a^3}\left[u_1\left(\frac{a}{4}, \frac{b}{2}, x_3\right), u_2\left(\frac{a}{2}, \frac{b}{4}, x_3\right)\right], \quad \bar{u}_3 = \frac{100E_2h^3}{q_0a^4}u_3\left(\frac{a}{2}, \frac{b}{2}, x_3\right)$$

$$[\bar{\sigma}_{11}(x_3), \bar{\sigma}_{22}(x_3), \bar{\sigma}_{12}(x_3)] = \frac{10h^2}{q_0a^2}\left[\sigma_{11}\left(\frac{a}{2}, \frac{b}{2}, x_3\right), \sigma_{22}\left(\frac{a}{2}, \frac{b}{2}, x_3\right), \sigma_{12}\left(\frac{a}{8}, 0, x_3\right)\right]$$

$$[\bar{\sigma}_{13}(x_3), \bar{\sigma}_{23}(x_3)] = \frac{10h}{q_0a}\left[\sigma_{13}\left(\frac{a}{8}, \frac{b}{2}, x_3\right), \sigma_{23}\left(\frac{a}{2}, 0, x_3\right)\right], \quad \bar{\sigma}_{33}(x_3) = \frac{1}{q_0}\sigma_{33}\left(\frac{a}{2}, \frac{b}{2}, x_3\right)$$

In Table 6.11, we listed the normalized stresses and displacements of [0°/90°] laminated plate obtained from the ESL theory together with those computed analytically by Vel and Batra [12] for SSSS and CSCS boundary conditions. The maximum discrepancy between the results of the two methods is 0.5%. Through-the-thickness distributions of σ_{13} and σ_{23} obtained from ESL Ritz method using SRS and that reported by Vel and Batra [12] are plotted at the near edge sections in Figure 6.17. Excellent agreement between the present and analytical results is observed.

For [0°/90°/0°] laminated plate, the normalized stresses and displacements computed using the current method and those of analytical solutions of Vel and Batra are presented in Table 12. The maximum discrepancy between the results of the two methods is 1.2%. In Figures 6.18 and 6.19 the present results for through-the-thickness distributions of transverse shear and normal stresses in the vicinity of the edges are plotted together with those of Vel and Batra. Excellent agreements between the two methods are observed for all the plots. The polynomial degrees used in the ESL theory for SSSS and CSCS plates are $n_1 \times n_2 \times n_3 = 8 \times 8 \times 43$ and $n_1 \times n_2 \times n_3 = 12 \times 12 \times 25$, respectively.

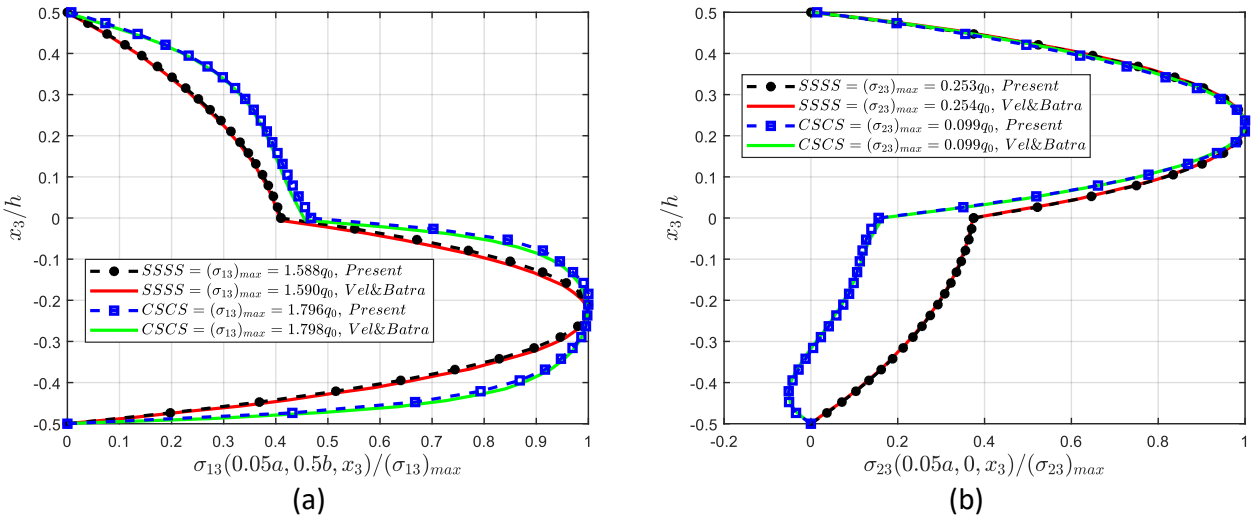

Figure 6.17: For a [0°/90°] laminate subjected to sinusoidal load on top surface, through-the-thickness distribution of a) σ_{13}, b) σ_{23} for SSSS and CSCS boundary conditions

Table 6.11: Displacements and stresses for a square [0°/90°] laminate subjected to sinusoidal normal traction on the top surface

	$\bar{u}_1(h/2)$	$\bar{u}_2(-h/2)$	$\bar{u}_3(0)$	$\bar{\sigma}_{11}(-h/2)$	$\bar{\sigma}_{22}(h/2)$	$\bar{\sigma}_{33}(0)$	$\bar{\sigma}_{12}(-h/2)$	$\bar{\sigma}_{13}(0)$	$\bar{\sigma}_{23}(0)$
				SSSS					
Vel & Batra [12]	-1.867	1.899	1.712	-7.671	7.894	0.495	0.527	1.216	1.211
Present	-1.871	1.899	1.711	-7.666	7.889	0.495	0.527	1.218	1.213
				CSCS					
Vel & Batra [12]	-1.047	1.341	1.217	-4.630	5.723	0.579	0.313	1.550	0.875
Present	-1.047	1.341	1.215	-4.609	5.749	0.574	0.313	1.558	0.876

Table 6.12: Displacements and stresses for a square [0°/90°/0°] laminate subjected to sinusoidal normal traction on the top surface

	$\bar{u}_1(h/2)$	$\bar{u}_2(-h/2)$	$\bar{u}_3(0)$	$\bar{\sigma}_{11}(-h/2)$	$\bar{\sigma}_{22}(h/6)$	$\bar{\sigma}_{33}(h/6)$	$\bar{\sigma}_{12}(-h/2)$	$\bar{\sigma}_{13}(0)$	$\bar{\sigma}_{23}(0)$
				SSSS					
Vel & Batra [12]	-0.620	1.353	1.525	-6.987	4.639	0.726	0.404	2.653	1.911
Present	-0.619	1.349	1.519	-6.969	4.605	0.727	0.403	2.660	1.905
				CSCS					
Vel & Batra [12]	-0.331	1.053	1.180	-4.235	3.573	0.701	0.256	2.093	1.470
Present	-0.329	1.048	1.172	-4.280	3.530	0.702	0.255	2.110	1.462

6.5.5 Sandwich Plate with Various Face to Core Stiffness Ratios

Here, we studied the deformations of simply supported three layered sandwich plate subjected to the sinusoidal normal traction $q(x_1, x_2) = q_0 \sin(\pi x_1/a)(\pi x_2/b)$ on the top surface. The material properties and the plate geometry and material are the same as in Srinivasa and Rao [6] and shown in Figure 6.5. First, we have solved the 3D -LET equations analytically, and with using ESL, LW Ritz methods. For the analytical solution, we followed Srivinas and Rao's approach. The face-to-core stiffness ratio is again defined as, $FCSR = C_{11}^{\text{face}}/C_{11}^{\text{core}}$. In Tables 6.13 - 6.14 results from ESL-Ritz method, LW-Ritz method, and the analytical solutions are compared for $FCSR = 1, 10^2, 10^3, 10^4, 10^5$ and $h/a = 0.1$, and 0.25. For ESL-Ritz and LW-Ritz method solution, $n_1 = n_2 = 12$ is used, the value of n_3 is written next to corresponding theory notation, i.e. ESL-3 means $n_3 = 3$ or third-order shear and normal deformable plate theory. $LW-3$ results are matching well with analytical results for all FCSR values and both aspect ratios. ESL theories are able to provide results with less than

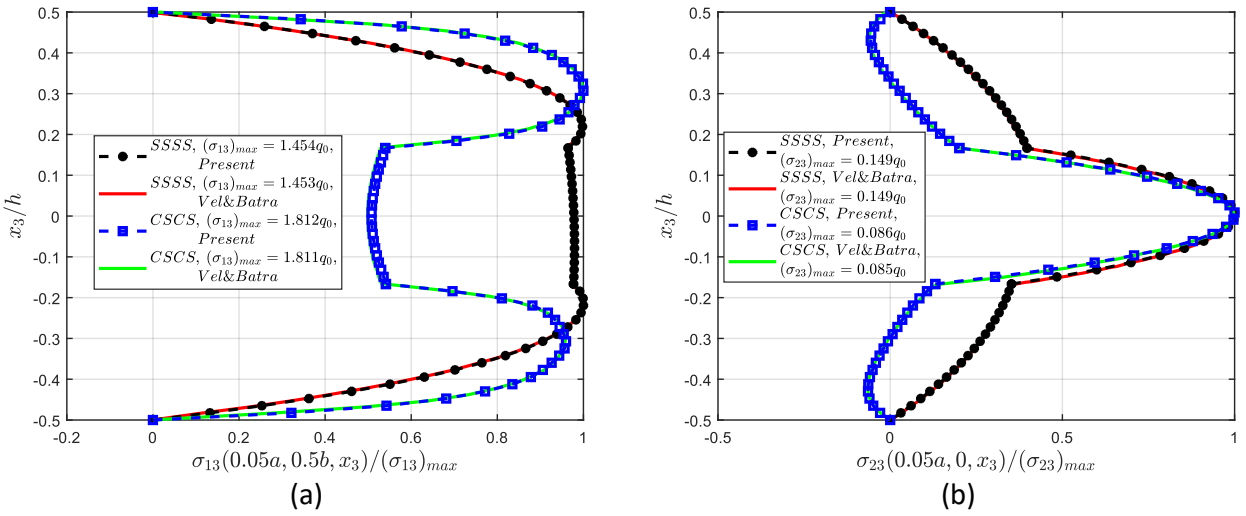

Figure 6.18: For a $[0°/90°/0°]$ laminate subjected to sinusoidal load on top surface, through-the thickness distribution of a) σ_{13}, b) σ_{23} for SSSS and CSCS boundary conditions

5% error up to FCSR = 10^2 for both aspect ratios. However, for FCSR = 10^2 and above, the ESL predictions have unacceptably high errors. We have depicted in Figure 6.20, the change in the error with respect to increase in the plate theory for $\sigma_{11}, \sigma_{22}, \sigma_{13}$, and σ_{33} at selected locations. In Figures, if the evaluation point is located at the interface, we have used superscript + and − for showing that the point is located to the top and bottom layer, respectively. Even with very high order ESL- 25 theory, the maximum error in estimating σ_{22} for FCSR = 10^3 is above 20%. It can be said that for FCSR values higher than 10^2 one should not be using ESL theories for estimating stresses in sandwich plates.

In Figures 6.21 - 6.25, we have displayed the effect of FCSR on through-the-thickness variation of $U_3, \sigma_{11}, \sigma_{22}, \sigma_{32}$, and σ_{13}. The results from LW Ritz method match very well with the analytical solution for all the variables. With increasing FCSR; 1) U_3 profile at the faces starts becoming a vertical line and after that curvature of U_3 profile for the core section starts decreasing until it became a straight line, 2) The faces starts carrying normal stresses σ_{11} and σ_{22} completely after FCSR of 10, 3) The transverse normal stress, σ_{33}, , the transition from the face to sheet the core becomes sharper and the bottom face starts carrying more

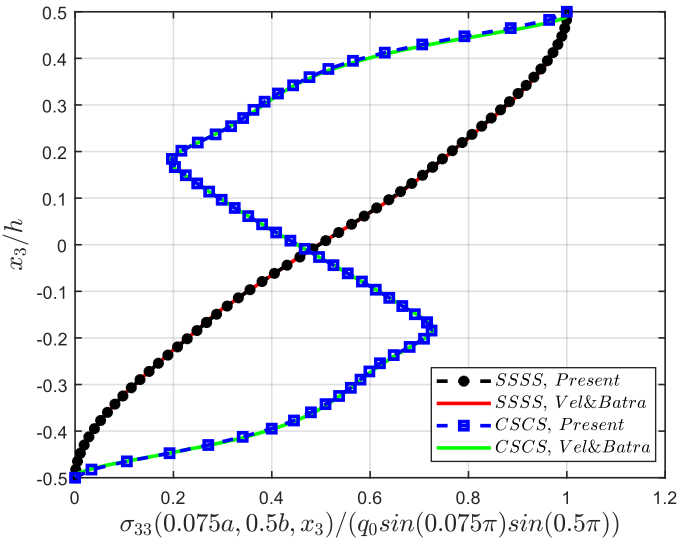

Figure 6.19: For a [0°/90°/0°] laminate subjected to sinusoidal load on top surface, through-the thickness distribution of σ_{33} for SSSS and CSCS boundary conditions

stress, 4) Although, the transverse shear stress, σ_{13}, is mainly carried by the core up to FCSR of 10^2, just like I-beam, after FCSR of 10^2, σ_{13} in the core approaches zero with increasing FSCR.

6.5.6 Sandwich plates with typical face sheet and core materials

We next analyzed the deformations of the [0°/90°/core/90°/0°] square sandwich plates with typical industrial face and core materials. The geometry of the sandwich plate is shown in Figure 6.10 and the material properties for face sheets and the core are given in Tables 6.4 and 6.5. The problem is solved analytically, and by using ESL, LW-Ritz methods for three different core materials, namely Honeycomb, Foam H45, Balsa S45, and three aspect ratios, $h/a = 0.01$, 0.1, and 0.2. For all the cases, the face material of Boron/Epoxy is used. Here, we aim to see the effect of different aspect ratios, $E_{11}^{\text{face}}/E_{11}^{\text{core}}$ and $E_{33}^{\text{face}}/E_{33}^{\text{core}}$ ratios on the accuracy of LW and ESL N$^{\text{th}}$ -order shear and normal deformable theories on estimating displacement and stress variables. In Tables 6.15 - 6.17, we have compared

selected displacement and stress variables obtained from ESL and LW-Ritz method with different plate order with those of analytical solution. The variables listed in Tables 6.15 - 6.17, are non-dimensionalized as below:

$$\hat{\sigma}_{33} = \frac{1}{q_0}\sigma_{33}\left(0.5a, 0.5b, 0.45h^{+}\right)$$

$$[\hat{\sigma}_{11},\ \hat{\sigma}_{22}] = \frac{h^2}{q_0 a^2}\left[\sigma_{11}\left(0.5a, 0.5b, 0.5h\right),\ \sigma_{22}\left(0.5a, 0.5b, -0.5h\right)\right]$$

$$[\hat{\sigma}_{13},\ \hat{\sigma}_{23}] = \frac{h}{q_0 a}\left[\sigma_{13}\left(0.05a, 0.5b, 0.4h^{+}\right),\ \sigma_{23}\left(0.5a, 0.05b, -0.4h^{-}\right)\right]$$

As can be seen from Table 6.15 for $h/a = 0.01$, LW-3 and LW-5 results are exactly matching with analytical results. ESL-3 and ESL-25 predictions for σ_{22} have maximum 2.84% and 0.61% error, respectively.

As can be seen from Table 15, for h/a $= 0.01$, LW-3 and LW-5 results are exactly matching with analytical results and ESL-3 results have a maximum 2.84% error for all cases.

For h/a $= 0.1$, again LW-3 and LW-5 results are exactly matching with analytical results. Now, we are able to see the effect of $E_{33}^{\text{face}}/E_{33}^{\text{core}}$ ratio on the accuracy of ESL theories. ESL-3 is able to provide results with maximum error of 3% for Balsa S45 and Honeycomb cases. Note that both Balsa S45 and Honeycomb have $E_{33}^{\text{face}}/E_{33}^{\text{core}}$ ratios less than 20 while having $E_{11}^{\text{face}}/E_{11}^{\text{core}}$ ratios of 3800 and 234,000, respectively. However, When we look into the Foam H45 case, the maximum error increases to 49.18%. ESL-25 reduces the maximum error to 4.3% for Foam H45. It should be noted that for Foam H45 and Balsa S45 cases, $E_{11}^{\text{face}}/E_{11}^{\text{core}}$ ratios are similar and equal to approximately 3800, however, their $E_{33}^{\text{face}}/E_{33}^{\text{core}}$ ratios are 376 and 15, respectively. Although Balsa S45 has a high $E_{11}^{\text{face}}/E_{11}^{\text{core}}$ ratio, ESL-3 is able to provide results within 1.5% error, the reason would be the effect of $E_{33}^{\text{face}}/E_{33}^{\text{core}}$ more dominant than those of $E_{11}^{\text{face}}/E_{11}^{\text{core}}$ on the accuracy of ESL plate theories.

For h/a $= 0.2$, LW-3 results are exactly matching with analytical results for all the cases.

ESL-Ritz method accuracy getting degraded for all the cases when the h/a increased to 0.2. Still, ESL-3 is able the predict the results within 5% of their analytical values for Balsa S45 and Honeycomb. However, ESL-25 is needed to reduce the error under 5% for Foam H45 case. It should be pointed out that even though we are using SRS for calculating transverse stresses, the accuracy of SRS solutions depends on how accurately the in-plane stresses are calculated from plate theories. Thus one should be careful about using low order plate theories especially if the $E_{33}^{\text{face}}/E_{33}^{\text{core}}$ and aspect ratios are high.

Table 6.13: Comparison of normalized displacements and stresses SSSS sandwich plate subjected to sinusoidal normal traction on the top surface, $h/a = 0.1$

		$\bar{\sigma}_{11}$		$\bar{\sigma}_{22}$		$\bar{\sigma}_{13}$	$\bar{\sigma}_{23}$	$\bar{\sigma}_{12}$	
FCSR	Solution	$(a/2, b/2, \pm h/2)$		$(a/2, b/2, \pm h/4)$		$(0, b/2, 0)$	$(a/2, 0, 0)$	$(0, 0, \pm h/2)$	
	Analytical	0.2467	-0.2460	0.1240	-0.1234	0.2723	0.2036	-0.1066	0.1070
	LW-3	0.2467	-0.2460	0.1240	-0.1234	0.2723	0.2036	-0.1066	0.1070
1	ESL-3	0.2467	-0.2460	0.1240	-0.1235	0.2723	0.2036	-0.1066	0.1070
	ESL-9	0.2467	-0.2460	0.1240	-0.1234	0.2723	0.2037	-0.1066	0.1070
	ESL-25	0.2467	-0.2460	0.1240	-0.1234	0.2723	0.2037	-0.1066	0.1070
	Analytical	0.4511	-0.4488	0.2314	-0.2343	0.2081	0.1659	-0.2050	0.2064
	LW-3	0.4511	-0.4488	0.2314	-0.2343	0.2081	0.1659	-0.2050	0.2064
10	ESL-3	0.4532	-0.4513	0.2355	-0.2336	0.2081	0.1647	-0.2046	0.2061
	ESL-9	0.4525	-0.4499	0.2363	-0.2344	0.2083	0.1655	-0.2048	0.2063
	ESL-25	0.4514	-0.4491	0.2354	-0.2343	0.2082	0.1657	-0.2049	0.2064
	Analytical	0.5220	-0.5150	0.2386	-0.2455	0.1664	0.1832	-0.2946	0.2948
	LW-3	0.5220	-0.5150	0.2386	-0.2455	0.1664	0.1832	-0.2946	0.2948
10^2	ESL-3	0.5003	-0.4985	0.2771	-0.2515	0.1768	0.1740	-0.2654	0.2666
	ESL-9	0.5152	-0.5087	0.2609	-0.2521	0.1686	0.1808	-0.2865	0.2870
	ESL-25	0.5200	-0.5123	0.2578	-0.2461	0.1671	0.1824	-0.2918	0.2921
	Analytical	1.556	-1.507	-0.4348	0.4024	0.1237	0.1911	-0.7853	0.7679
	LW-3	1.556	-1.507	-0.4349	0.4024	0.1237	0.1911	-0.7853	0.7679
10^3	ESL-3	0.5550	-0.5539	0.2759	-0.2156	0.1619	0.1852	-0.3171	0.3172
	ESL-9	1.354	-1.318	-0.2482	0.2916	0.1267	0.1930	-0.6994	0.6856
	ESL-25	1.480	-1.434	-0.3319	0.3564	0.1248	0.1919	-0.7521	0.7362
	Analytical	6.947	-6.494	-3.998	3.717	0.0613	0.1016	-3.036	2.845
	LW-3	6.947	-6.494	-3.998	3.717	0.0613	0.1016	-3.036	2.845
10^4	ESL-3	0.5714	-0.5705	0.2727	-0.2037	0.1595	0.1870	-0.3287	0.3285
	ESL-9	5.771	-5.473	-3.051	3.114	0.0730	0.1207	-2.552	2.419
	ESL-25	6.639	-6.236	-3.659	3.609	0.0643	0.1066	-2.910	2.736
	Analytical	13.29	-9.416	-8.119	5.737	0.0105	0.0175	-5.688	4.036
	LW-3	13.29	-9.416	-8.119	5.737	0.0105	0.0175	-5.688	4.036
10^5	ESL-3	0.5733	-0.5724	0.2722	-0.2023	0.1593	0.1872	-0.3300	0.3298
	ESL-9	12.11	-9.552	-7.121	5.982	0.0160	0.0267	-5.196	4.098
	ESL-25	12.95	-9.506	-7.616	6.025	0.0118	0.0197	-5.551	4.071

Table 6.14: Comparison of normalized displacements and stresses SSSS sandwich plate subjected to sinusoidal normal traction on the top surface, $h/a = 0.25$

FCSR	Solution	$\bar{\sigma}_{11}$ $(a/2, b/2, \pm h/2)$		$\bar{\sigma}_{22}$ $(a/2, b/2, \pm h/4)$		$\bar{\sigma}_{13}$ $(0, b/2, 0)$	$\bar{\sigma}_{23}$ $(a/2, 0, 0)$	$\bar{\sigma}_{12}$ $(0, 0, \pm h/2)$	
	Analytical	0.2498	-0.2448	-13.08	-0.1297	0.2619	0.2095	-0.1110	0.1118
	LW-3	0.2498	-0.2448	-13.08	-0.1297	0.2618	0.2095	-0.1110	0.1118
1	ESL-3	0.2499	-0.2448	0.083	-0.1298	0.2618	0.2094	-0.1110	0.1118
	ESL-9	0.2498	-0.2448	-11.85	-0.1297	0.2619	0.2096	-0.1110	0.1118
	ESL-25	0.2498	-0.2448	0.1326	-0.1297	0.2619	0.2096	-0.1110	0.1118
	Analytical	0.4608	-0.4410	0.2369	-0.2483	0.1890	0.1808	-0.2328	0.2338
	LW-3	0.4608	-0.4410	0.2369	-0.2483	0.1890	0.1808	-0.2328	0.2338
10	ESL-3	0.4644	-0.4472	0.2557	-0.2482	0.1880	0.1771	-0.2312	0.2328
	ESL-9	0.4643	-0.4437	0.2574	-0.2499	0.1890	0.1796	-0.2322	0.2334
	ESL-25	0.4613	-0.4417	0.2530	-0.2486	0.1890	0.1804	-0.2326	0.2337
	Analytical	0.8951	-0.8055	0.0043	-0.0611	0.1386	0.1971	-0.4880	0.4622
	LW-3	0.8951	-0.8055	0.0042	-0.0611	0.1386	0.1971	-0.4880	0.4622
10^2	ESL-3	0.6911	-0.6478	0.2374	-0.1515	0.1476	0.1923	-0.3888	0.3782
	ESL-9	0.8377	-0.7568	0.1131	-0.1029	0.1396	0.1954	-0.4591	0.4374
	ESL-25	0.8773	-0.7873	0.0868	-0.0679	0.1388	0.1965	-0.4781	0.4537
	Analytical	4.4688	-3.7374	-2.3458	1.8940	0.0899	0.1483	-2.0021	1.7020
	LW-3	4.4688	-3.7374	-2.3459	1.8942	0.0899	0.1483	-2.0021	1.7020
10^3	ESL-3	1.0390	-0.9643	0.1178	0.0834	0.1358	0.1967	-0.5579	0.5282
	ESL-9	3.8867	-3.2964	-1.7701	1.6701	0.0944	0.1556	-1.7618	1.5142
	ESL-25	4.2583	-3.5717	-2.0220	1.8140	0.0915	0.1510	-1.9119	1.6323
	Analytical	13.03	-7.3448	-7.9070	4.4110	0.0230	0.0387	-5.5890	3.1702
	LW-3	13.03	-7.3448	-7.9075	4.4113	0.0230	0.0387	-5.5890	3.1702
10^4	ESL-3	1.126	-1.0433	0.0864	0.1432	0.1342	0.1969	-0.5974	0.5629
	ESL-9	11.52	-7.3211	-6.451	4.6962	0.0303	0.0512	-4.9718	3.1565
	ESL-25	12.63	-7.3803	-7.280	4.6889	0.0247	0.0417	-5.4312	3.1804
	Analytical	21.29	-2.8304	-13.08	1.7278	0.0027	0.0046	-9.1012	1.2144
	LW-3	21.29	-2.8305	-13.08	1.7279	0.0027	0.0046	-9.1012	1.2145
10^5	ESL-3	1.136	-1.0523	0.0828	0.1501	0.1340	0.1969	-0.6019	0.5669
	ESL-9	19.92	-3.8750	-11.85	2.6663	0.0043	0.0073	-8.5214	1.6594
	ESL-25	20.93	-3.1159	-12.49	2.2133	0.0031	0.0052	-8.9549	1.3305

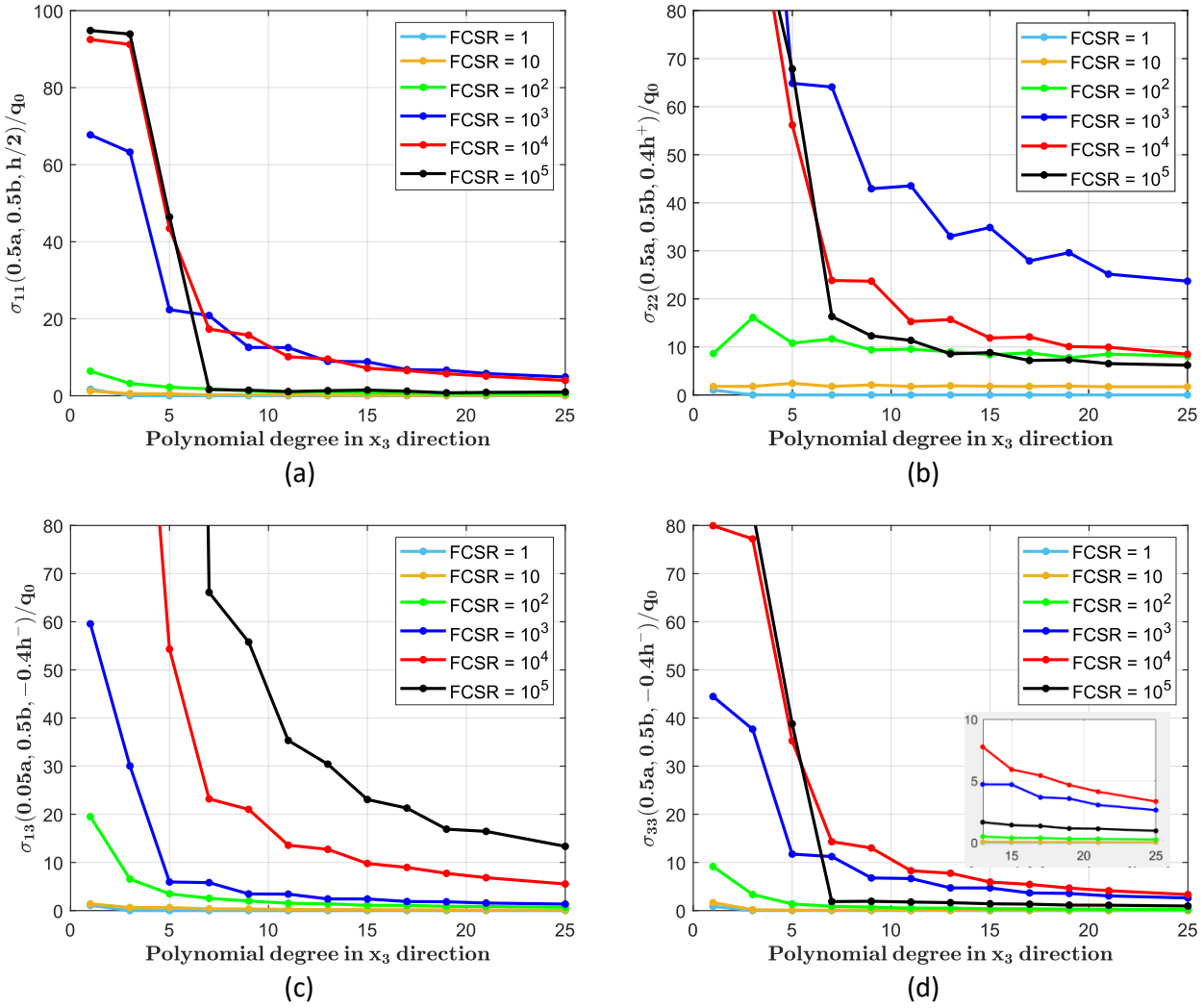

Figure 6.20: For various FCSR values, dependence of the percentage error in (a) σ_{11}, (b) σ_{22}, (c) σ_{13}, (d) σ_{33} upon the polynomial degree in x_3 -direction (order of ESL theory) for a sandwich plate

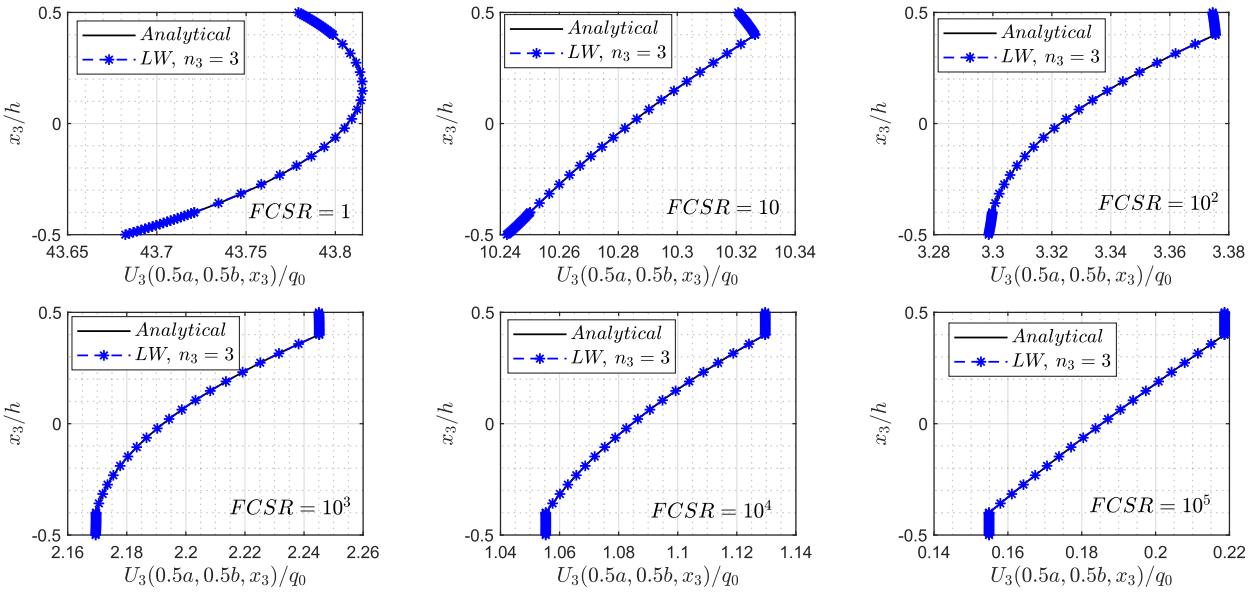

Figure 6.21: Influence of the FCSR on the through-thickness distribution of the displacement U_3 for a square SSSS sandwich plate: $h/a = 1/10$

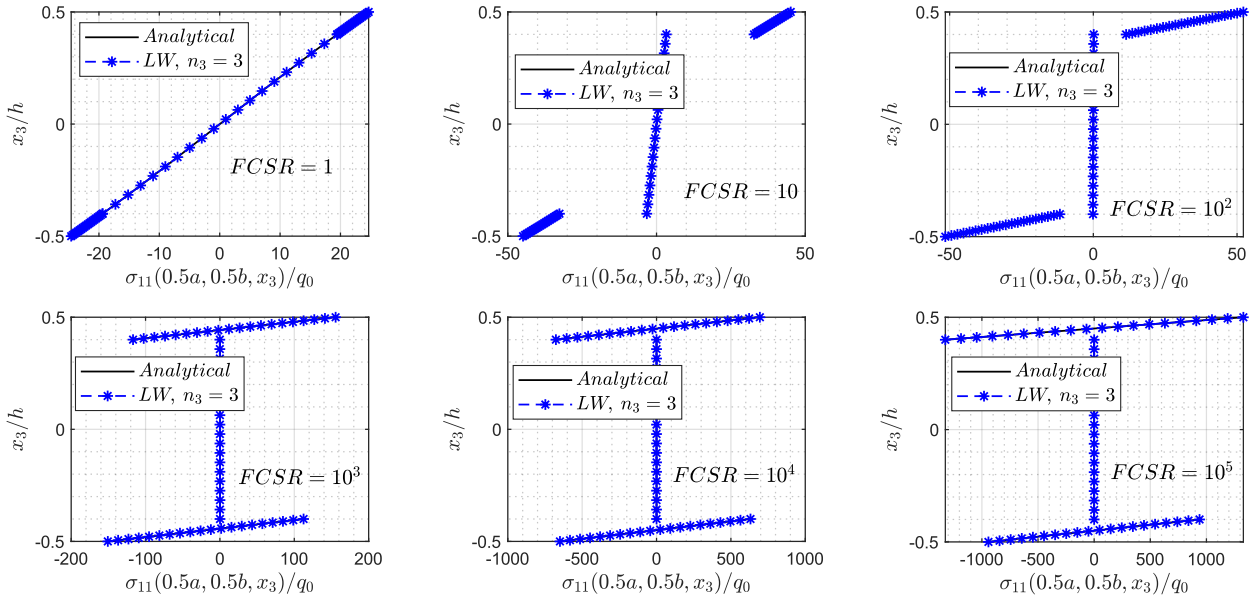

Figure 6.22: Influence of the FCSR on the through-thickness distribution of the displacement σ_{11} for a square SSSS sandwich plate: $h/a = 1/10$

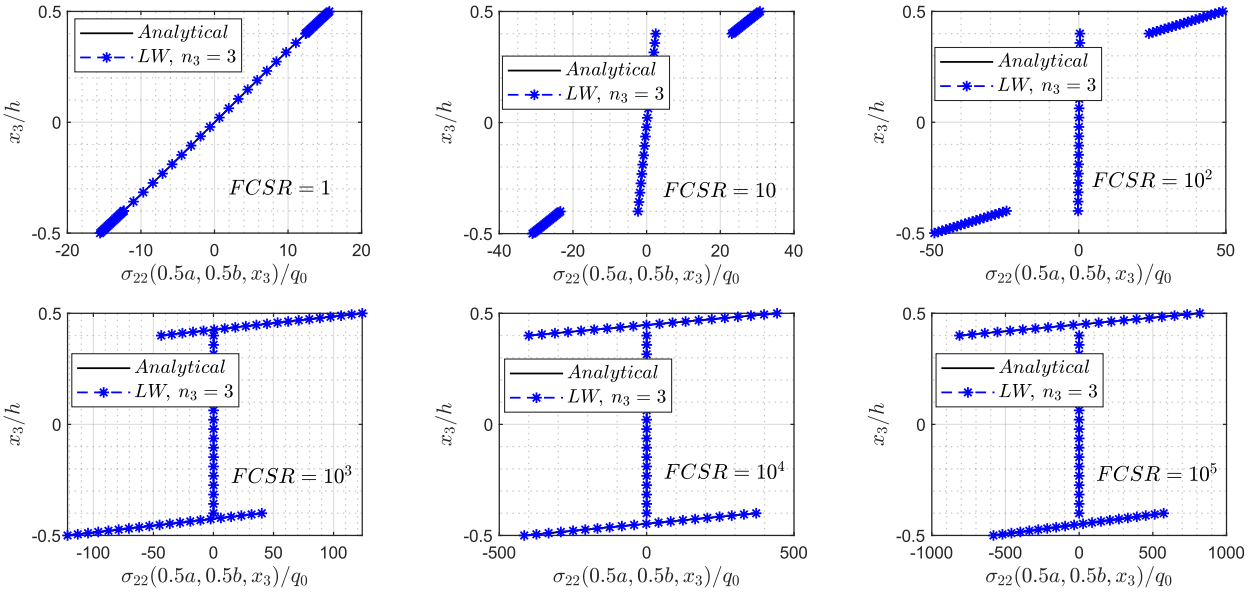

Figure 6.23: Influence of the FCSR on the through-thickness distribution of the displacement σ_{22} for a square SSSS sandwich plate: $h/a = 1/10$

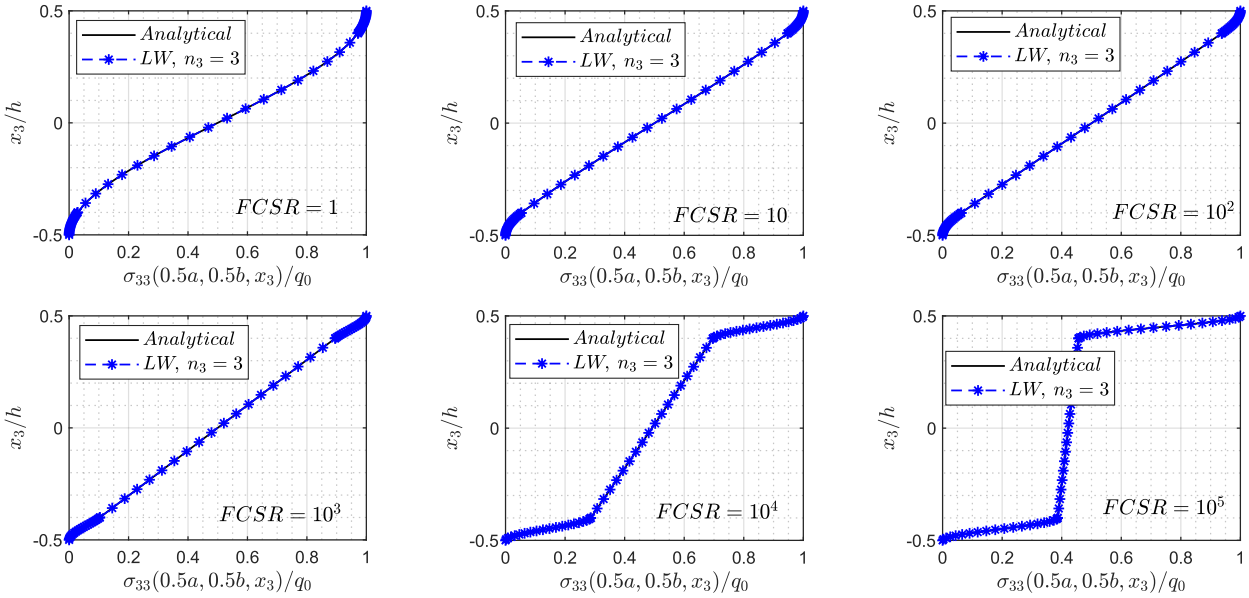

Figure 6.24: Influence of the FCSR on the through-thickness distribution of the displacement σ_{33} for a square SSSS sandwich plate: $h/a = 1/10$

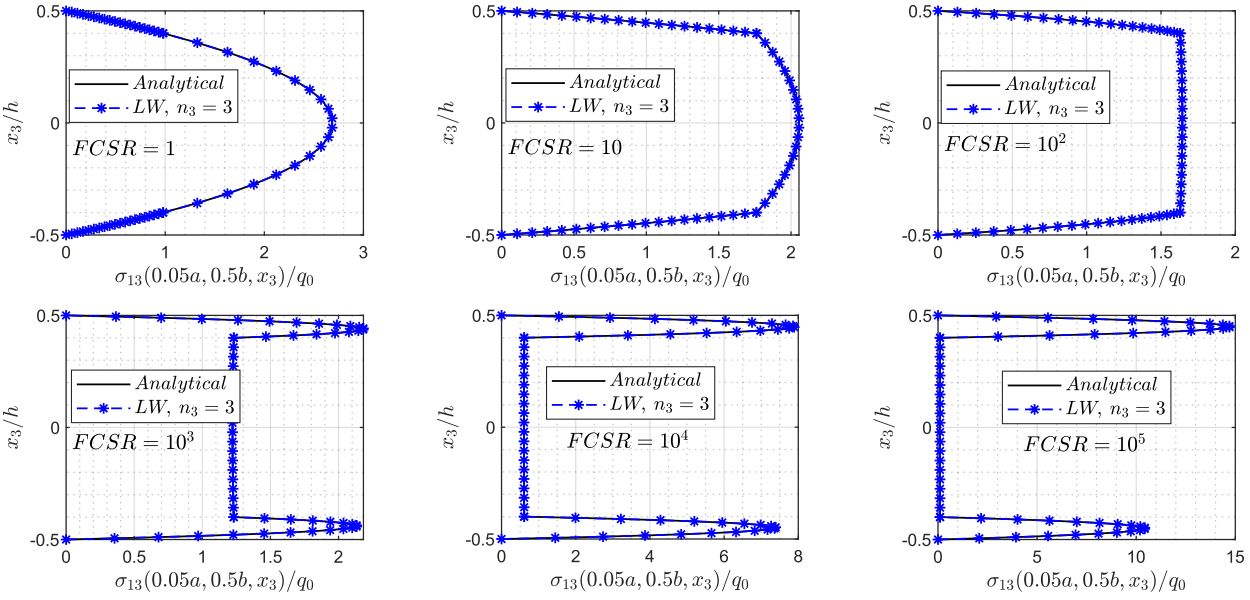

Figure 6.25: Influence of the FCSR on the through-thickness distribution of the displacement σ_{13} for a square SSSS sandwich plate: $h/a = 1/10$

Table 6.15: Through the thickness stress distributions for a square [0°/90°/ core /90°/0°] sandwich plate with different core materials (Face sheets: Boron/Epoxy, $h/a = 0.01$)

Core Material	$n_3 \rightarrow$	ESL 3	ESL 9	ESL 17	ESL 25	LW 3	LW 5	Analytical
	$\hat{\sigma}_{11}$	0.9872	0.9879	0.9867	0.9857	0.9863	0.9863	0.9863
Honeycomb	$\hat{\sigma}_{22}$	-0.1258	-0.1262	-0.1253	-0.1247	-0.1251	-0.1251	-0.1251
$E_{11}^{face}/E_{11}^{core} = 233981$	$\hat{\sigma}_{13}$	0.1795	0.1794	0.1793	0.1793	0.1793	0.1793	0.1793
$E_{33}^{face}/E_{3}^{core} = 11$	$\hat{\sigma}_{23}$	0.1668	0.1668	0.1668	0.1668	0.1668	0.1668	0.1668
	$\hat{\sigma}_{33}$	0.9852	0.9852	0.9852	0.9852	0.9852	0.9852	0.9852
	$\hat{\sigma}_{11}$	1.003	1.011	1.012	1.013	1.014	1.014	1.014
Foam H45	$\hat{\sigma}_{22}$	-0.1267	-0.1293	-0.1295	-0.1296	-0.1304	-0.1304	-0.1304
$E_{11}^{face}/E_{11}^{core} = 3761$	$\hat{\sigma}_{13}$	0.1811	0.1808	0.1807	0.1807	0.1807	0.1807	0.1807
$E_{33}^{face}/E_{33}^{core} = 376$	$\hat{\sigma}_{23}$	0.1661	0.1665	0.1665	0.1665	0.1666	0.1666	0.1666
	$\hat{\sigma}_{33}$	0.9851	0.9850	0.9850	0.9850	0.9850	0.9850	0.9850
	$\hat{\sigma}_{11}$	0.9930	0.9950	0.9938	0.9926	0.9932	0.9932	0.9932
Balsa S45	$\hat{\sigma}_{22}$	-0.1262	-0.1271	-0.1261	-0.1251	-0.1255	-0.1255	-0.1255
$E_{11}^{face}/E_{11}^{core} = 3830$	$\hat{\sigma}_{13}$	0.1805	0.1804	0.1804	0.1804	0.1804	0.1804	0.1804
$E_{33}^{face}/E_{33}^{core} = 15$	$\hat{\sigma}_{23}$	0.1669	0.1669	0.1669	0.1669	0.1669	0.1669	0.1669
	$\hat{\sigma}_{33}$	0.9851	0.9852	0.9852	0.9852	0.9852	0.9852	0.9852

We have also depicted in Figures 6.26 - 6.29 comparison of though-the-thickness variations of $\sigma_{13}, \sigma_{23}, \sigma_{33}$ and σ_{13} from LW-Ritz method and analytical solutions. For all the cases, the LW theory results match pretty closely with those from the analytical solution. For $h/a = 0.01$, through the thickness variations of $\sigma_{13}, \sigma_{23}, \sigma_{33}$ and σ_{13} seem to be independent of the core materials and consequently also of $E_{11}^{\text{face}}/E_{11}^{\text{core}}$ and $E_{33}^{\text{face}}/E_{33}^{\text{core}}$ ratios. Increasing the aspect ratio h/a plays a similar role as in the FCSR investigation case performed in Section 6.5.5. For example, in the previous section we observed that when FCSR ratio is increased the faces carried the most of the stresses, and after some point even transverse shear stresses become zero. Here we are seeing the same effect in Foam H45 case when the aspect ratio is increased.

We also compared the ESL-Ritz method estimations with $n_3 = 3, 9$, and 25 for through-the-thickness variation of σ_{13} and σ_{11} in Figures 32 and 33. As expected the σ_{13} and σ_{11} profiles

Table 6.16: Through the thickness stress distributions for a square [0°/90°/ core /90°/0°] sandwich plate with different core materials (Face sheets: Boron/Epoxy, $h/a = 0.1$)

Core Material	$n_3 \rightarrow$	ESL 3	ESL 9	ESL 17	ESL 25	LW 3	LW 5	Analytical
	$\hat{\sigma}_{11}$	0.9928	0.9795	0.9719	0.9676	0.9676	0.9676	0.9676
Honeycomb	$\hat{\sigma}_{22}$	-0.1596	-0.1566	-0.1566	-0.1568	-0.1588	-0.1588	-0.1588
$E_{11}^{face}/E_{11}^{core} = 233981$	$\hat{\sigma}_{13}$	0.1653	0.1629	0.1615	0.1611	0.1604	0.1604	0.1604
$E_{33}^{face}/E_{3}^{core} = 11$	$\hat{\sigma}_{23}$	0.1819	0.1840	0.1853	0.1856	0.1862	0.1862	0.1862
	$\hat{\sigma}_{33}$	0.9854	0.9855	0.9856	0.9856	0.9856	0.9856	0.9856
	$\hat{\sigma}_{11}$	1.688	2.608	2.726	2.772	2.849	2.849	2.849
Foam H45	$\hat{\sigma}_{22}$	-0.3164	-0.5697	-0.5918	-0.5959	-0.6226	-0.6226	-0.6226
$E_{11}^{face}/E_{11}^{core} = 3761$	$\hat{\sigma}_{13}$	0.1847	0.1689	0.1669	0.1664	0.1644	0.1644	0.1644
$E_{33}^{face}/E_{33}^{core} = 376$	$\hat{\sigma}_{23}$	0.1557	0.1586	0.1578	0.1573	0.1567	0.1567	0.1567
	$\hat{\sigma}_{33}$	0.9794	0.9702	0.9693	0.9690	0.9680	0.9680	0.9680
	$\hat{\sigma}_{11}$	1.142	1.141	1.142	1.139	1.143	1.143	1.143
Balsa S45	$\hat{\sigma}_{22}$	-0.1649	-0.1610	-0.1615	-0.1615	-0.1642	-0.1642	-0.1642
$E_{11}^{face}/E_{11}^{core} = 3830$	$\hat{\sigma}_{13}$	0.1823	0.1813	0.1807	0.1805	0.1802	0.1802	0.1802
$E_{33}^{face}/E_{33}^{core} = 15$	$\hat{\sigma}_{23}$	0.1635	0.1644	0.1648	0.1649	0.1652	0.1652	0.1652
	$\hat{\sigma}_{33}$	0.9839	0.9838	0.9838	0.9838	0.9837	0.9837	0.9837

obtained from ESL- 3 matched well with those of analytical ones for aspect ratio of 0.01 for all core materials. For Balsa S45 and Honeycomb cases, ESL-3 is also able to predict stress values close to those of analytical ones for all aspect ratios. However, for aspect ratios of 0.1 and 0.2, ESL-3 leads to unacceptable results for Foam H45 case. Increasing the ESL theory order to 25 was able to reduce the maximum error to 5% for Foam H45 case.

6.6 Conclusions

Free vibration and static analysis of sandwich and laminated plates are performed using LW and ESL N$^{\text{th}}$ order shear and normal deformation theories. Furthermore, analytical solutions of 3D -LET equations for static deformations of sandwich structures having various FCSR are provided by following Srinivasa and Rao solution procedure. For ESL and *LW* theories, the numerical solution is obtained using Ritz method in which weighted Jacobi polynomials in the

Table 6.17: Through the thickness stress distributions for a square [0°/90°/ core /90°/0°] sandwich plate with different core materials (Face sheets: Boron/Epoxy, $h/a = 0.2$)

Core		ESL				LW		Analytical
Material	$n_3 \rightarrow$	3	9	17	25	3	5	
	$\hat{\sigma}_{11}$	1.213	1.194	1.188	1.179	1.187	1.187	1.187
Honeycomb	$\hat{\sigma}_{22}$	-0.2422	-0.2256	-0.2271	-0.2293	-0.2350	-0.2350	-0.2350
$E_{11}^{face}/E_{11}^{core} = 233981$	$\hat{\sigma}_{13}$	0.1558	0.1521	0.1500	0.1497	0.1485	0.1485	0.1485
$E_{33}^{face}/E_{3}^{core} = 11$	$\hat{\sigma}_{23}$	0.1909	0.1929	0.1943	0.1947	0.1952	0.1952	0.1952
	$\hat{\sigma}_{33}$	0.9837	0.9837	0.9837	0.9838	0.9837	0.9837	0.9837
	$\hat{\sigma}_{11}$	3.492	6.510	6.882	7.022	7.227	7.227	7.227
Foam H45	$\hat{\sigma}_{22}$	-0.8442	-1.589	-1.641	-1.644	-1.719	-1.719	-1.719
$E_{11}^{face}/E_{11}^{core} = 3761$	$\hat{\sigma}_{13}$	0.1724	0.1354	0.1304	0.1291	0.1237	0.1237	0.1237
$E_{33}^{face}/E_{33}^{core} = 376$	$\hat{\sigma}_{23}$	0.1513	0.1455	0.1418	0.1404	0.1377	0.1377	0.1377
	$\hat{\sigma}_{33}$	0.9650	0.9341	0.9315	0.9306	0.9274	0.9274	0.9274
	$\hat{\sigma}_{11}$	1.555	1.556	1.571	1.568	1.584	1.584	1.584
Balsa S45	$\hat{\sigma}_{22}$	-0.2805	-0.2613	-0.2653	-0.2684	-0.2772	-0.2772	-0.2772
$E_{11}^{face}/E_{11}^{core} = 3830$	$\hat{\sigma}_{13}$	0.1812	0.1793	0.1781	0.1779	0.1773	0.1773	0.1773
$E_{33}^{face}/E_{33}^{core} = 15$	$\hat{\sigma}_{23}$	0.1606	0.1617	0.1622	0.1623	0.1624	0.1624	0.1624
	$\hat{\sigma}_{33}$	0.9804	0.9799	0.9798	0.9798	0.9796	0.9796	0.9796

in-plane directions and hierarchic Legendre polynomials in the thickness direction are used as basis functions. Transverse stresses are calculated using a stress recovery scheme (SRS). ESL theories up to order 45 were employed without encountering any ill-conditioning. The presently computed results agree well with those from either analytical solutions or solutions of the corresponding 3 -dimensional linearly elastic problems obtained with the commercial FE software, ABAQUS.

The main conclusions of the paper can be listed as:

1. The free vibration analysis of simply supported square three-ply sandwich plate with $h/a = 0.1$ considered showed that for FSCR = 10^2 and 10^5, one needs, respectively, ESL-15 and ESL-31 to get the lowest six natural frequencies within 5% of their analytical values. For FSCR = 10^7, ESL-45 is able to get results with maximum 7% error. It would be impossible to use such high order theories with simple polynomials due

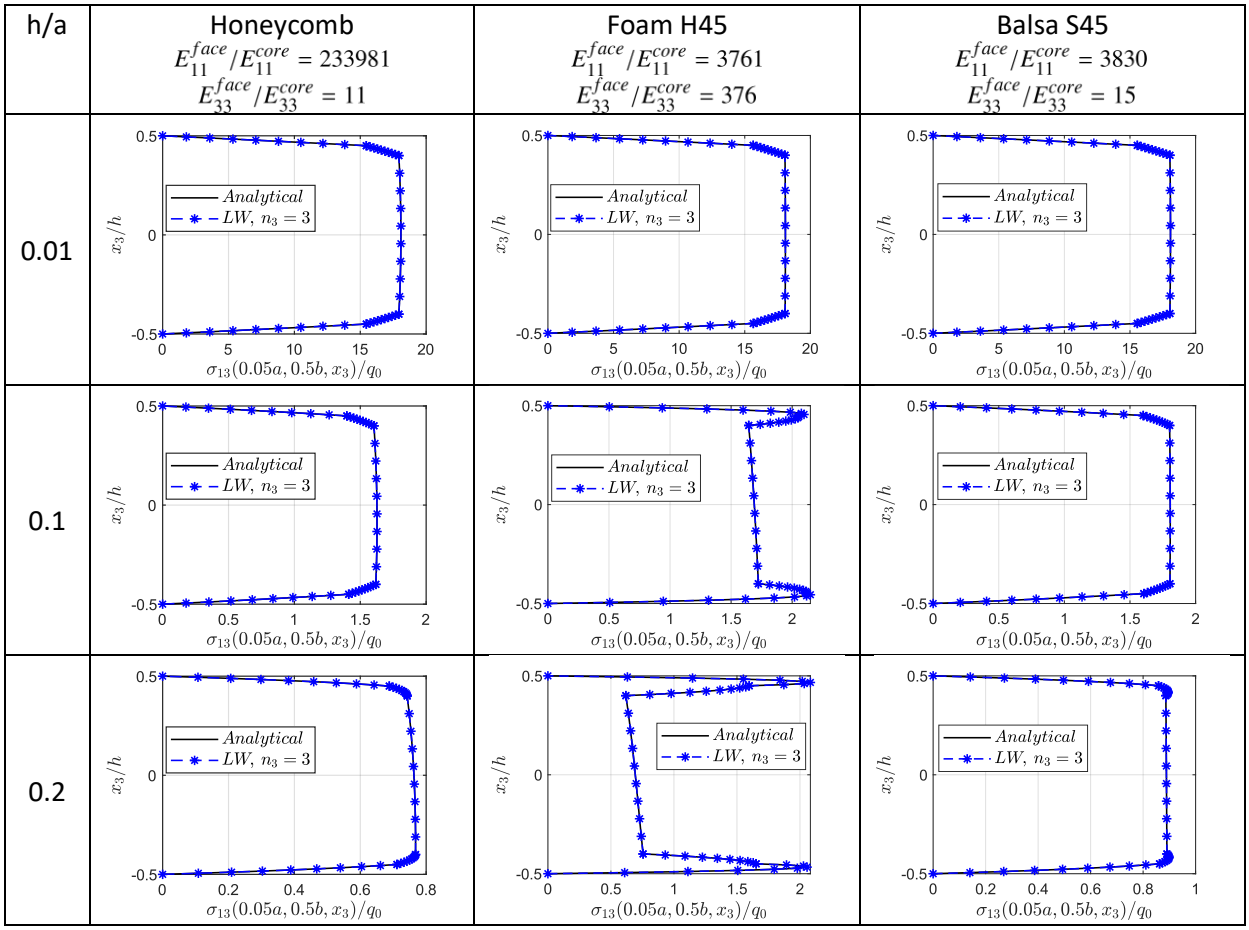

Figure 6.26: The through-thickness distribution of the transverse shear stress σ_{13} for a square [0°/90°/ core /90°/0°] sandwich plate (Face sheets: Boron/Epoxy)

to ill-conditioning. It is observed that results LW-3 is able match very closely with analytical results for all FCSR values up to 10^5. For an FCSR greater than 10^2, the $120 \times 120 \times 18$ (7906 14 DoFs) FE mesh provides results with the maximum error of 8% for the lowest six frequency parameters.

2. The current ESL Ritz method (even though it's higher-order) is able to produce accurate natural frequency results compared to FEM with considerably lesser DOFs.

3. It is observed that $E_{33}^{\text{face}}/E_{33}^{\text{core}}$ has a higher influence than $E_{11}^{\text{face}}/E_{11}^{\text{core}}$ on the accuracy of the natural frequency results and stress results. Also when the $E_{33}^{\text{face}}/E_{33}^{\text{core}}$ is less than

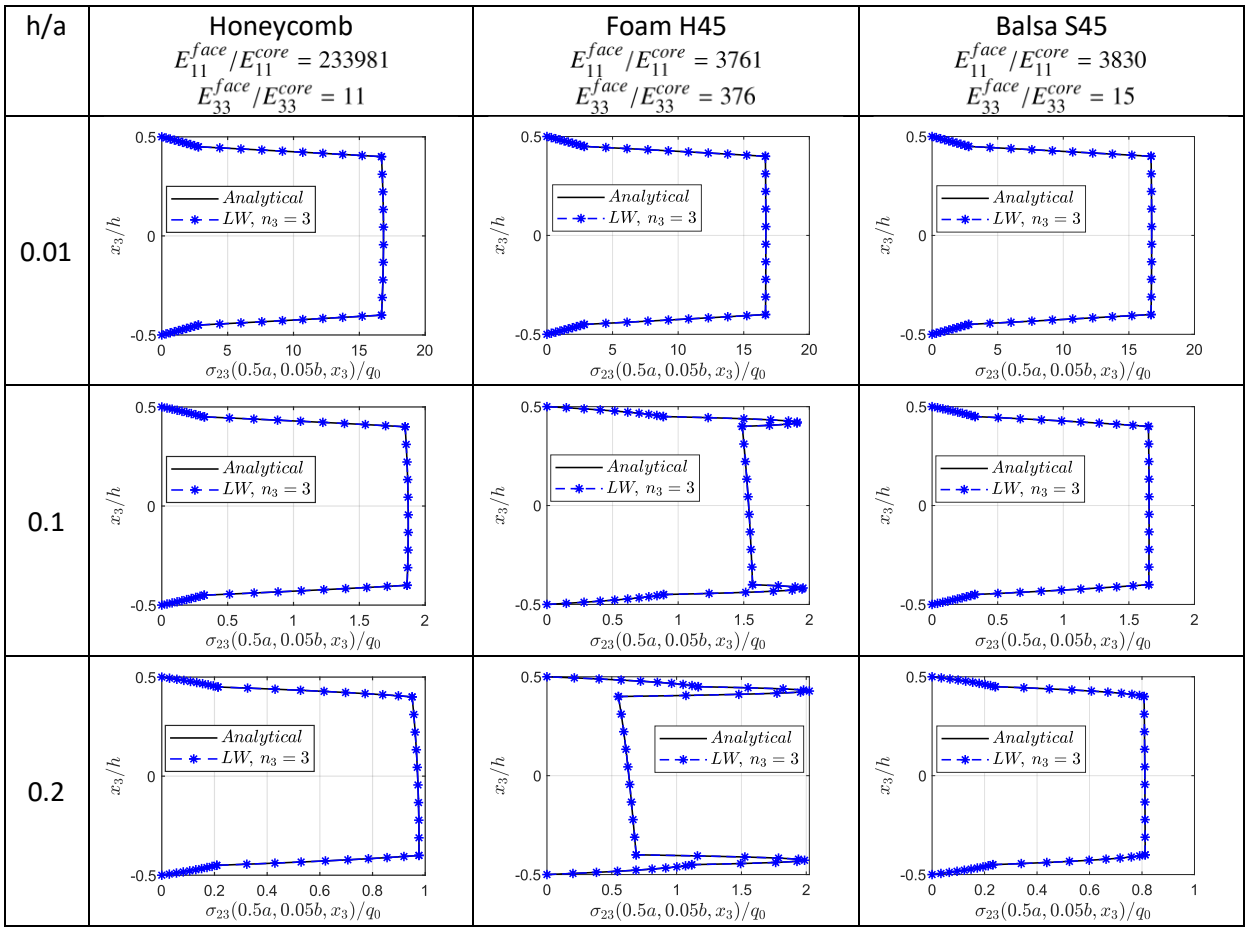

Figure 6.27: The through-thickness distribution of the transverse shear stress σ_{23} for a square [0°/90°/ core /90°/0°] sandwich plate (Face sheets: Boron/Epoxy)

20 (i.e., Graphite/Epoxy - Honeycomb, Graphite/Epoxy - Balsa S45, Boron/Epoxy - Honeycomb and Boron/Epoxy - Balsa S45 combinations) ESL-3 with SRS could provide stress values having a maximum error of 3% for simply supported sandwich plates for all considered aspect ratios of 0.01, 0.1, and 0.2.

4. In the analysis of static deformations of cantilevered orthotropic beams subjected to normal and tangential tractions on the top and bottom surfaces, the stresses are calculated directly using constitutive law without SRS. It is found that, $n_3 = 3$ is not able to satisfy natural boundary conditions, $n_3 = 7$ satisfies natural boundary conditions

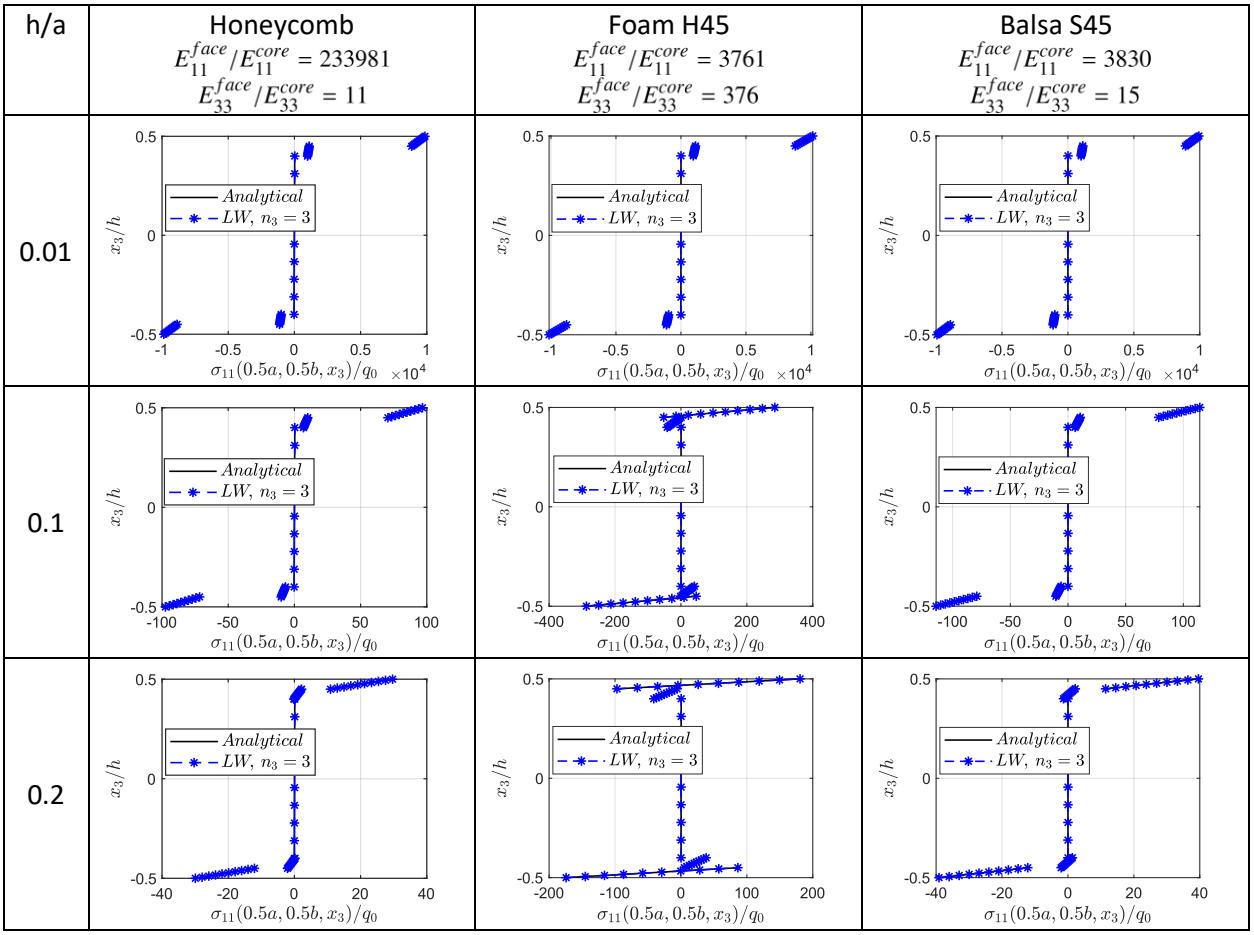

Figure 6.28: The through-thickness distribution of the transverse shear stress σ_{11} for a square [0°/90°/ core /90°/0°] sandwich plate (Face sheets: Boron/Epoxy)

and has a close agreement with analytical solution only at the interior sections, and $n_3 = 15$ captures well the boundary layer effects near the clamped and free edges.

5. Low order displacement-based ESL plate theories like CPT, FSDT, TSNDT, even with the use of SRS, may not be able to provide accurate stresses at the sections in the vicinity of the edges.

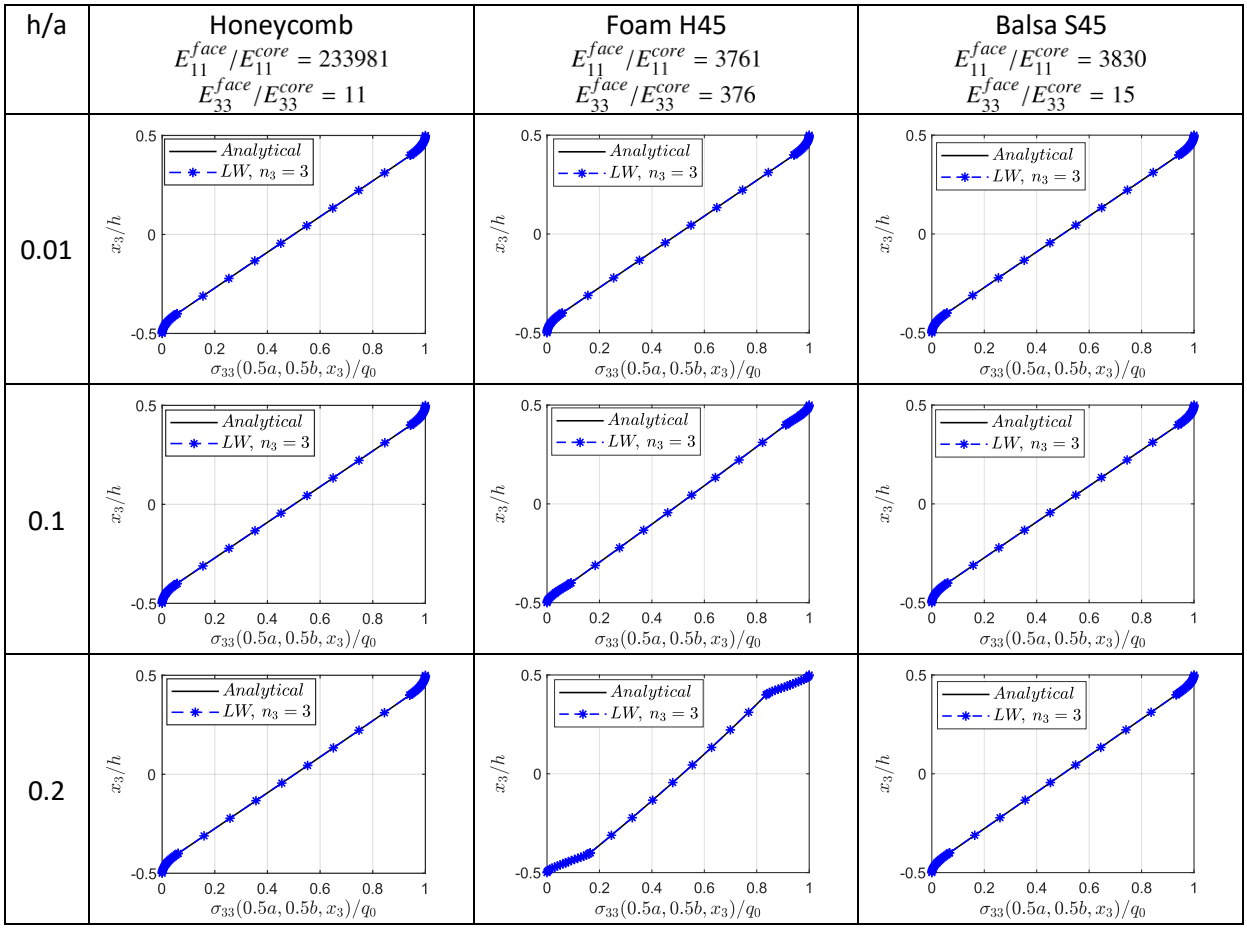

Figure 6.29: The through-thickness distribution of the transverse shear stress σ_{33} for a square [0°/90°/ core /90°/0°] sandwich plate (Face sheets: Boron/Epoxy)

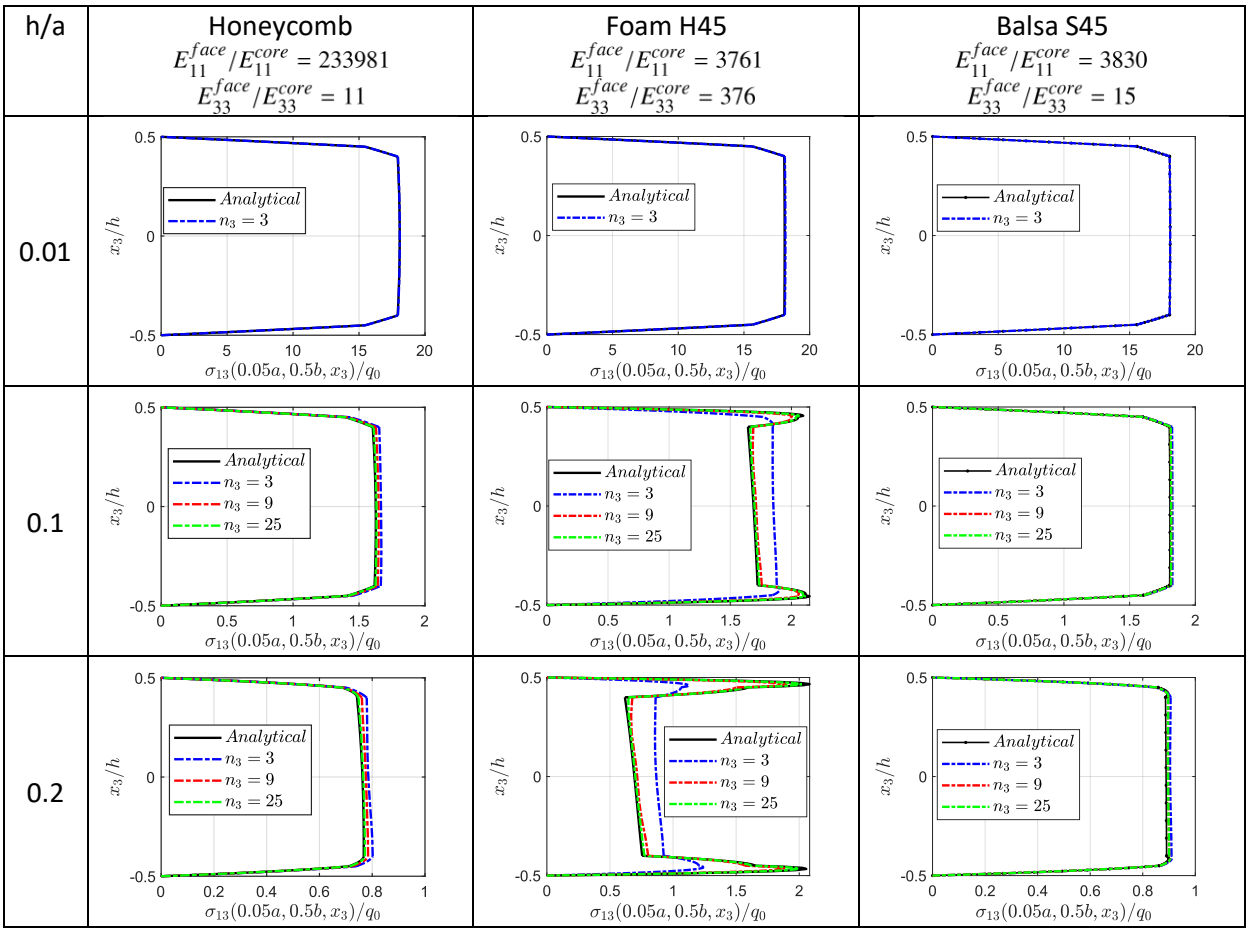

Figure 6.30: Comparison of n^{th} order ESL-Ritz estimates of through-thickness distribution of the transverse shear stress σ_{13} for a SSSS square [0°/90°/ core /90°/0°] sandwich plate (Face sheets: Boron/Epoxy)

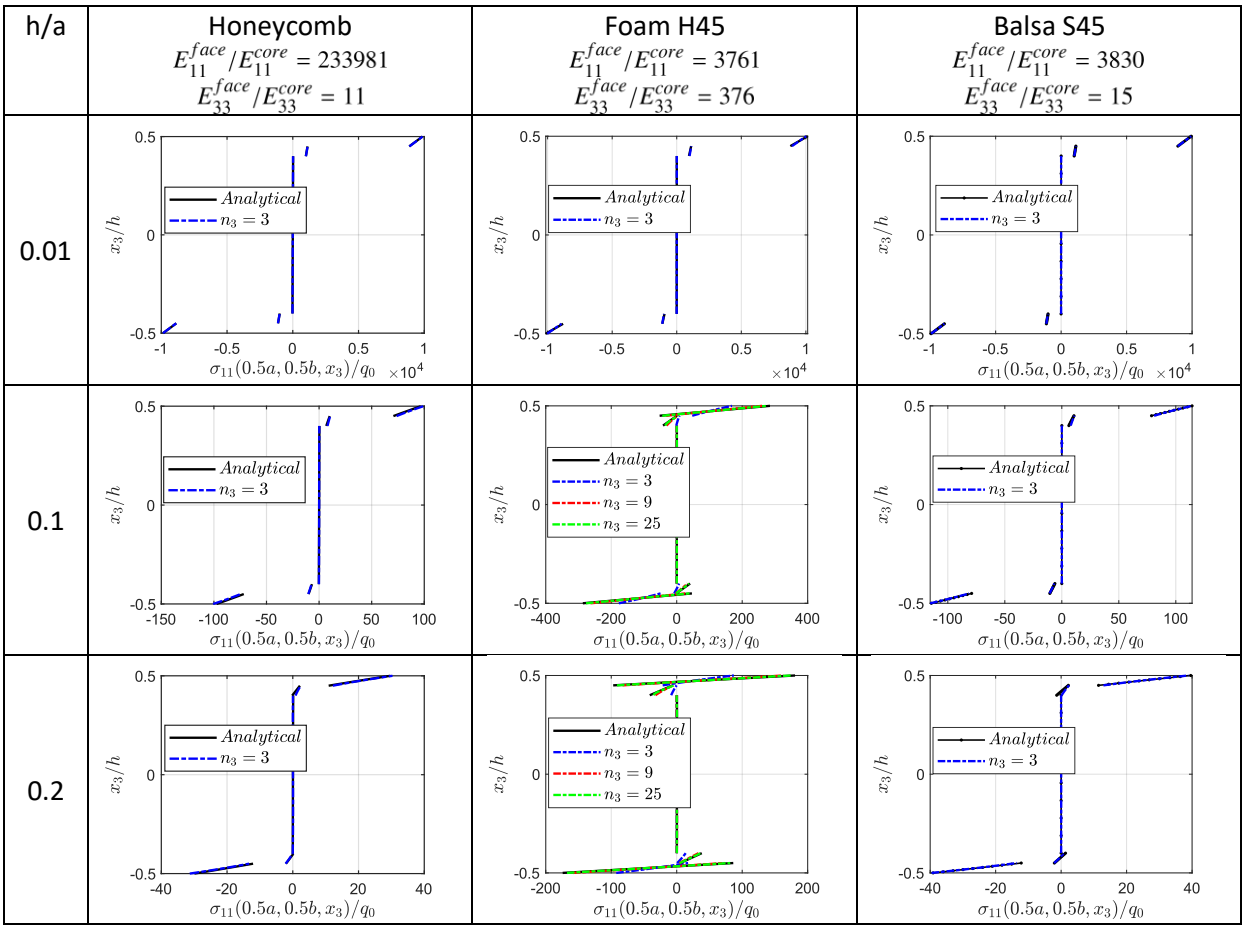

Figure 6.31: Comparison of n^{th} order ESL-Ritz estimates of through-thickness distribution of the transverse shear stress σ_{11} for a SSSS square [0°/90°/ core /90°/0°] sandwich plate (Face sheets: Boron/Epoxy)

Bibliography

[1] Carrera, E., 2003, "Theories and finite elements for multilayered plates and shells: a unified compact formulation with numerical assessment and benchmarking," Archives of Computational Methods in Engineering, **10**(3), pp. 215–296.

[2] Reddy, J. N., 2004, *Mechanics of laminated composite plates and shells: theory and analysis*, CRC Press.

[3] Liew, K. M., Pan, Z. Z., and Zhang, L. W., 2019, "An overview of layerwise theories for composite laminates and structures: Development, numerical implementation and application," Composite Structures, **216**, pp. 240–259.

[4] Kreja, I., 2011, "A literature review on computational models for laminated composite and sandwich panels," Open Engineering, **1**(1), pp. 59–80.

[5] Carrare, E., 1997, "CZ requirements—models for the two dimensional analysis of multilayered structures," Composite Structures, **37**(3-4), pp. 373–383.

[6] Srinivas, S. and Rao, A. K., 1970, "Bending, vibration and buckling of simply supported thick orthotropic rectangular plates and laminates," International Journal of Solids and Structures, **6**(11), pp. 1463–1481.

[7] Srinivas, S., Rao, C. J., and Rao, A. K., 1970, "An exact analysis for vibration of simply-

supported homogeneous and laminated thick rectangular plates," Journal of Sound and Vibration, **12**(2), pp. 187–199.

[8] Pagano, N. J., 1970, "Exact solutions for rectangular bidirectional composites and sandwich plates," Journal of Composite Materials, **4**(1), pp. 20–34.

[9] Ye, J. and Soldatos, K. P., 1994, "Three-dimensional vibration of laminated cylinders and cylindrical panels with symmetric or antisymmetric cross-ply lay-up," Composites Engineering, **4**(4), pp. 429–444.

[10] Fan, J. and Ye, J., 1990, "An exact solution for the statics and dynamics of laminated thick plates with orthotropic layers," International Journal of Solids and Structures, **26**(5-6), pp. 655–662.

[11] Vel, S. S. and Batra, R. C., 2001, "Exact solution for rectangular sandwich plates with embedded piezoelectric shear actuators," AIAA Journal, **39**(7), pp. 1363–1373.

[12] Vel, S. S. and Batra, R. C., 1999, "Analytical solution for rectangular thick laminated plates subjected to arbitrary boundary conditions," AIAA Journal, **37**(11), pp. 1464–1473.

[13] Vel, S. S. and Batra, R. C., 2000, "Three-dimensional analytical solution for hybrid multilayered piezoelectric plates," Journal of Applied Mechanics, **67**(3), pp. 558–567.

[14] Reissner, E. and Stavsky, Y., 1961, "Bending and stretching of certain types of heterogeneous aeolotropic elastic plates," Journal of Applied Mechanics, **28**(3), pp. 402–408.

[15] Mindlin, R. D., 1951, "Influence of rotatory inertia and shear on flexural motions of isotropic, elastic plates," Journal of Applied Mechanics, **18**, pp. 31–38.

[16] Reddy, J. N., 1984, "A simple higher-order theory for laminated composite plates," Journal of Applied Mechanics, **51**(4), pp. 745–752.

[17] Batra, R. C., Vidoli, S., and Vestroni, F., 2002, "Plane wave solutions and modal analysis in higher order shear and normal deformable plate theories," Journal of Sound and Vibration, **257**(1), pp. 63–88.

[18] Kapania, R. K. and Raciti, S., 1989, "Recent advances in analysis of laminated beams and plates. Part I-Shear effects and buckling," AIAA Journal, **27**(7), pp. 923–935.

[19] Kapania, R. K. and Raciti, S., 1989, "Recent advances in analysis of laminated beams and plates, part II: Vibrations and wave propagation," AIAA Journal, **27**(7), pp. 935–946.

[20] Leissa, A. W., 1987, "A review of laminated composite plate buckling," Applied Mechanics Reviews, **40**(5), pp. 575–591.

[21] Noor, A. K., Burton, W. S., and Bert, C. W., 1996, "Computational models for sandwich panels and shells," Applied Mechanics Reviews, **49**(3), pp. 155–199.

[22] Carrera, E., 2003, "Historical review of Zig-Zag theories for multilayered plates and shells," Applied Mechanics Reviews, **56**(3), pp. 287–308.

[23] Lekhnitskii, S. G., 1935, "Strength calculation of composite beams," Vestnik inzhen i tekhnikov, **9**, pp. 137–148.

[24] Ren, J. G., 1986, "Bending theory of laminated plate," Composites Science and Technology, **27**(3), pp. 225–248.

[25] Gherlone, M., 2013, "On the use of zigzag functions in equivalent single layer theories for laminated composite and sandwich beams: a comparative study and some observations on external weak layers," Journal of Applied Mechanics, **80**(6), p. 061004.

[26] Reissner, E., 1984, "On a certain mixed variational theorem and a proposed application," International Journal for Numerical Methods in Engineering, **20**(7), pp. 1366–1368.

[27] Reissner, E., 1986, "On a mixed variational theorem and on shear deformable plate theory," International Journal for Numerical Methods in Engineering, **23**(2), pp. 193–198.

[28] Carrera, E., 1999, "A Reissner's mixed variational theorem applied to vibration analysis of multilayered shell," Journal of Applied Mechanics, **66**(1), pp. 68–78.

[29] Reddy, J. N., 1993, "An evaluation of equivalent-single-layer and layerwise theories of composite laminates," Composite Structures, **25**(1-4), pp. 21–35.

[30] Carrera, E. and Brischetto, S., 2009, "A survey with numerical assessment of classical and refined theories for the analysis of sandwich plates," Applied Mechanics Reviews, **62**(1), p. 010803.

[31] Khandan, R., Noroozi, S., Sewell, P., and Vinney, J., 2012, "The development of laminated composite plate theories: a review," Journal of Materials Science, **47**(16), pp. 5901–10.

[32] Kant, T. and Swaminathan, K., 2000, "Estimation of transverse/interlaminar stresses in laminated composites–a selective review and survey of current developments," Composite Structures, **49**(1), pp. 65–75.

[33] Pagano, N. J., 1969, "Exact solutions for composite laminates in cylindrical bending," Journal of Composite Materials, **3**(3), pp. 398–411.

[34] Ahmadi, I., 2020, "Stress analysis in transverse loading of soft core sandwich plates with various boundary conditions," Journal of Sandwich Structures & Materials, **22**(8), pp. 2692–2734.

[35] Kapoor, H., Kapania, R. K., and Soni, S. R., 2013, "Interlaminar stress calculation in

composite and sandwich plates in NURBS Isogeometric finite element analysis," Composite Structures, **106**(1), pp. 537–548.

[36] Dufour, J. E., Antolin, P., Sangalli, G., Auricchio, F., and Reali, A., 2018, "A cost-effective isogeometric approach for composite plates based on a stress recovery procedure," Composites Part B: Engineering, **138**(1), pp. 12–18.

[37] Patton, A., Dufour, J. E., Antolin, P., and Reali, A., 2019, "Fast and accurate elastic analysis of laminated composite plates via isogeometric collocation and an equilibrium-based stress recovery approach," Composite Structures, **225**(1), p. 111026.

[38] Reddy, J. N. and Barbero, E. J., 1989, "A plate bending element based on a generalized laminate plate theory," International Journal for Numerical Methods in Engineering, **28**, pp. 2275–2292.

[39] Rolfes, R., Rohwer, K., and Ballerstaedt, M., 1998, "Efficient linear transverse normal stress analysis of layered composite plates," Computers and Structures, **68**(6), pp. 643–652.

[40] Rohwer, K., Friedrichs, S., and Wehmeyer, C., 2005, "Analyzing laminated structures from fibre-reinforced composite material – an assessment," Technische Mechanik, **25**(1), pp. 59–79.

[41] Byun, C. and Kapania, R. K., 1992, "Prediction of interlaminar stresses in laminated plates using global orthogonal interpolation polynomials," AIAA Journal, **30**(11), pp. 2740–2749.

[42] Shah, P. H. and Batra, R. C., 2015, "Through-the-thickness stress distributions near edges of composite laminates using stress recovery scheme and third order shear and normal deformable theory," Composite Structures, **131**, pp. 397–413.

[43] Shah, P. H. and Batra, R. C., 2018, "Stretching and bending deformations due to normal and shear tractions of doubly curved shells using third-order shear and normal deformable theory," Mechanics of Advanced Materials and Structures, **25**(15-16), pp. 1276–1296.

[44] Shah, P. H. and Batra, R. C., 2016, "Stress singularities and transverse stresses near edges of doubly curved laminated shells using TSNDT and stress recovery scheme," European Journal of Mechanics-A/Solids, **63**, pp. 68–83.

[45] Shah, P. H. and Batra, R. C., 2019, *Effect of Reissner's parameter on strain energies of spherical sandwich shells*, AIAA Journal.

[46] Yuan, L. and Batra, R. C., 2019, "Optimum first failure load design of one/two-core sandwich plates under blast loads, and their ultimate loads," Composite Structures, **224**, p. 111022.

[47] Meirovitch, L. and Kwak, M. K., 1990, "Convergence of the classical Rayleigh-Ritz method and the finite element method," AIAA Journal, **28**(8), pp. 1509–1516.

[48] Wang, C. M., Wang, Y. C., and Reddy, J. N., 2002, "Problems and remedy for the Ritz method in determiningstress resultants of corner supported rectangular plates," Computers and Structures, **80**, pp. 145–154.

[49] Leissa, A. W. and Zhang, Z. D., 1983, "On the three-dimensional vibrations of the cantilevered rectangular parallelepiped," Journal of the Acoustical Society of America, **73**, pp. 2013–2021.

[50] Liew, K. M. and Yang, B., 1999, "Three-dimensional elasticity solutions for free vibrations of circular plates: a polynomials-Ritz analysis," Computer Methods in Applied Mechanics and Engineering, **175**(1-2), pp. 189–201.

[51] Zhou, D., Cheung, Y. K., Au, F., and Lo, S. H., 2002, "Three-dimensional vibration analysis of thick rectangular plates using Chebyshev polynomial and Ritz method," International Journal of Solids and Structures, **39**(26), pp. 6339–6353.

[52] Fazzolari, F. A. and Carrera, E., 2014, "Refined hierarchical kinematics quasi-3D Ritz models for free vibration analysis of doubly curved FGM shells and sandwich shells with FGM core," Journal of Sound and Vibration, **333**(5), pp. 1485–1508.

[53] Alanbay, B. and Kapania, R. K., 2018, *On the use of classical Jacobi orthogonal polynomials in the Ritz method*, in 2018 AIAA/ASCE/AHS/ASC Structures, Structural Dynamics, and Materials Conference, Kissimmee, Florida.

[54] Alanbay, B., Singh, K., and Kapania, R. K., 2020, "Vibration of curvilinearly stiffened plates using Ritz method with orthogonal Jacobi polynomials," Journal of Vibration and Acoustics, **142**(1), p. 011009.

[55] Alanbay, B., Kapania, R. K., and Batra, R. C., 2020, "Up to lowest 100 frequencies of rectangular plates using Jacobi polynomials and TSNDT," Journal of Sound and Vibration, **480**(1), p. 115352.

[56] Alanbay, B., Kapania, R. K., and Batra, R. C., 2020, "Free Vibration of Thick Quadrilateral Laminates Using Third-Order Shear-Normal Deformation Theory," AIAA Journal, **58**(10), pp. 4580–4594.

[57] Alanbay, B., Batra, R. C., and Kapania, R. K., 2020, "Lowest Twelve Frequencies of Sandwich Plates Using Third-Order Shear-Normal Deformation Theory," AIAA Journal, **58**(4), pp. 1821–1835.

[58] Reddy, J. N., 2017, *Energy principles and variational methods in applied mechanics*, 3rd ed., John Wiley & Sons.

[59] Szegö, G., 1967, *Orthogonal polynomials*, American Mathematical Society, Providence, Rhode Island.

[60] Szabo, B. and Babuska, I., 2011, *Introduction to Finite Element Analysis: Formulation, Verification and Validation*, John Wiley & Sons, Ltd, West Sussex, United Kingdom.

[61] Vel, S. S. and Batra, R. C., 2000, "The generalized plane strain deformations of thick anisotropic composite laminated plates," International Journal of Solids and Structures, **37**(5), pp. 715–733.

[62] Batra, R. C. and Vidoli, S., 2002, "Higher-order piezoelectric plate theory derived from a three-dimensional variational principle," AIAA Journal, **40**(1), pp. 91–104.

Chapter 7

Conclusions and Future Work

7.1 Conclusions

In this study, the Ritz method and weighted Jacobi polynomials are used to analyze free vibrations and static deformations of rectangular composite laminates and sandwich structures under different boundary conditions. The details and the contributions of these studies are summarized below.

In Chapter 2, the free vibrations of quadrilateral plates with curvilinear stiffeners have been analyzed using a first order shear deformation theory (FSDT). The accuracy of the present work is established by comparing the present results with those available in the open literature or found by a detailed finite element model using commercial software MSC NASTRAN. Since the presented approach is not dependent upon the mesh, the changes in stiffeners' location does not require recalculation of the plate stiffness matrix.

In Chapter 3, a third-order shear and normal deformation theory (TSNDT) is used to find the lowest 100 natural frequencies of vibrations of thick isotropic plates under different boundary conditions. Obtaining higher-order vibrations modes, which are particularly important in vibroacoustic applications, requires use of higher order polynomials in the Ritz method. Unlike the polynomial-based trial functions, the weighted Jacobi polynomials do not show any ill-conditioning issues when higher order polynomials are used. The results obtained from the present method agree well with those found either analytically or numerically solving the 3D linear elasticity theory (3D-LET) equations with the commercial FE software, ABAQUS. It is shown that computational resources needed for the present approach are significantly less than those needed for the traditional FEM. For instance, the number of degree of freedoms (DoFs) and the CPU time for the present method to compute the lowest 100 frequencies were 1200 and 5s, respectively; for ABAQUS solution, the two numbers were 2×10^6 and 3h.

In Chapter 4, the TSNDT-based Ritz method formulations are extended to analyze thick quadrilateral laminates. We delineate effects of the skew angle, the number of layers, and thickness-to-side ratio on the frequencies computed with the present method, the FSDT-based shell elements (S4 and S4R), and with 20-node brick elements (C3D20) in ABAQUS. It is found that the computed first six natural frequencies of clamped skew laminates with thickness/side length of 0.2 differ at most by 3% from those found by numerically solving the 3-D linear elasticity theory equations using brick elements (C3D20) in ABAQUS. On the other hand, the FSDT-based shell elements provide frequencies that differ by 11% from those computed using either the 3-D FEM or the present TSNDT-based method. This finding suggests that one should be careful in using the shell elements based on the FSDT when analyzing skew plates for critical applications.

In Chapter 5, the lowest 12 distinct natural frequencies and the corresponding mode shapes of simply supported cross-ply laminates and sandwich plates are found from the analytical solution of the 3D-LET equations and the numerical solution of the TSNDT equations using the Ritz method. It was of interest to find out whether the TSNDT still provides accurate natural frequencies when highly flexible cores, i.e., sandwich plates with very large face-to-core stiffness ratio (FCSR), are used. It is found that for the TSNDT, the first six natural frequencies have a maximum error of 5% for a sandwich plate with and FCSR of less than 20. This percent error increases, respectively, to 16, 93, and 280 for sandwich panels of FCSR of 50, 500, and 5000, making the use of TSNDT unacceptable for sandwich panels with large values of FCSR.

In Chapter 6, free vibrations and static deformations of laminated and sandwich plates are analyzed using an equivalent single layer theory (ESL) and a layerwise (LW) theory of variable order accounting for both shear and normal deformations. A one-step stress

recovery scheme is utilized to calculate transverse stresses. In Chapter 5, we found that the error of the TSNDT in estimating natural frequencies for FCSR of a sandwich plate greater than 20 is unacceptable. Here, it is aimed to see whether these limitations could be eliminated by using higher order either ESL or LW theories. By comparing the natural frequencies and stress values obtained from various order ESL and LW theories with those of the analytical solution, we investigate the influence of FCSR on the accuracy of these plate theories. Furthermore, we have used the realistic material properties to see what are the typical values of the elastic modulus ratio in the thickness direction, $E_{33}^{face}/E_{33}^{core}$, and that of in the fiber direction $E_{11}^{face}/E_{11}^{core}$ and it is found that, $E_{33}^{face}/E_{33}^{core}$, has higher influence than $E_{11}^{face}/E_{11}^{core}$ on the accuracy of the results obtained using ESL theories.

7.2 Recommendations for Future Work

In this research, we have developed efficient methods based on the Ritz method using Jacobi polynomials as the trial functions. The possible future directions for this research can be listed as below:

1. The present code for curvilinearly stiffened plates could be extended to develop an equivalent plate model of built-up aircraft wings, which consist of curvilinear spars and ribs. Then the developed equivalent plate structural model can be integrated into the multidisciplinary design, analysis, and optimization (MDAO) framework developed at Virginia Tech for fast preliminary design and optimization of the internal structure of a wing.

2. The present Ritz codes based on ESL and LW plate theories could be extended to deal with different geometries (i.e., doubly curved shells), transient loads (i.e., blast and impact loads), and progressive damage analysis of fiber reinforced composite lam-

inates (including 3D fiber and matrix damage initiation/evaluation, and delamination between the adjacent layers). Due to the higher computational efficiencies of present methods compared to the FEM, these could be beneficial in optimization studies for finding the optimal geometry and materials to minimize weight (or maximize the energy absorption capabilities) of the laminated and sandwich structures.

3. The presented higher order plate theories could be integrated into commercial finite element code, ABAQUS, for modelling individual layers (or sub groups of laminates) as a single super element using user element subroutine (UEL) in ABAQUS. This could enable one to leverage the built-in capabilities of ABAQUS (i.e. cohesive zone model, solvers, visualization tools, post processing, and contact algorithms) while increasing the computational efficiency of the ABAQUS for dealing with multilayered structures. Furthermore, these super elements could be used together with ABAQUS standard/explicit elements.

Appendix A

Sample MATLAB Code

Appendix A. Sample MATLAB Code

Here, we have provided a MATLAB code for analyzing free vibrations of laminated plates using third order shear and normal deformable theory (TSNDT) and weighted Jacobi polynomials.

```
% Main File for TSNDT-Ritz method
% Formulation Reference: Alanbay, B., Kapania, R. K., and Batra, R. C.,
% 2020,  Free  Vibration of Thick Quadrilateral Laminates Using ...
    Third-Order
% Shear-Normal Deformation Theory,   AIAA Journal, 58(10), p. 4580-4594.

% Cross-ply laminate example in Alanbay, B., Batra, R. C., and
% Kapania, R. K., 2020,  Lowest  Twelve Frequencies of Sandwich Plates
% Using Third-Order Shear-Normal Deformation Theory,
% AIAA Journal,58(4), p. 1821  1835.
% Result comparison can be find in Table 10

clear all; clc; close all;

n =8; % degree of Jacobi Polynomials in x and y directions

% Plate geometry
tau=0.1; %thickness ratio t/b
b=10;
hp=tau*b; %thickness
h=hp;
aspectratio=1; %a/b
a=aspectratio*b;

% Coordinates of the corner points of the plate
xvec=[0, a, a, 0]; % (x1,x2,x3,x4)
yvec=[0, 0, b, b]; % (y1,y2,y3,y4)

% Essential boundary conditions (BC = [e1 e2 e3 e4])
% e1-e3 in x direction
% e2-e4 in y direction
bcType = 'SSSS'; % S = Simply Supported, F = Free, C= Clamped
[BC] = BoundaryCondition(bcType);
bc1 = BC(:,1); % for u1i at the edges
bc2 = BC(:,2); % for u2i at the edges
bc3 = BC(:,3); % for u3i at the edges

% Properties
nlayer=3; % Number of layers
Nosier_Mat; % To update material Properties go to Nosier_Mat.m
layer(1) = Material_1; % Assing material Properties
layer(1).Thickness = hp/nlayer; % Thickness of 1st layer
layer(1).Theta=0;  % Fiber angle
layer(2) = Material_1;
layer(2).Thickness = hp/nlayer;
```

```
layer(2).Theta=90;
layer(3) = Material_1;
layer(3).Thickness = hp/nlayer;
layer(3).Theta=0;

% Eq. 22
D = zeros(8,8,4,4);
for i =  0:1:3
    for j =  0:1:3
        D(:,:,i+1,j+1) = D_ij(i,j,layer);
    end
end
mp = CompositeMassProperty(layer); %Eq. 22
%% Calculate Integrals with Gauss Quadrature
%n-point Gauss quadrature integrates polynomials degree 2n-1 or less
%exactly
 Ng=ceil((2*(n+1)+1)/2); % ceil rounds up
[xgauss,wgauss] = legendre_gauss_quad(Ng); %Quadrature points and weights

% Preallocate  the matrices;
subksize = 3*(n+1)^2;
Nsize = (n+1)^2;
K = zeros(subksize,subksize,4,4); % 12 stiffness sub matrices
B = zeros(9,subksize,4); % strain-displacement relations
NJ = zeros(3,Nsize,3,4); % for shape function storage
MP = zeros(12*Nsize, 12*Nsize); % Global mass matrix
KP = zeros(12*Nsize, 12*Nsize); % Global stiffness matrix

% Stiffness and mass matrix calculation
for i=1:Ng
    eta=xgauss(i);
    for j=1:Ng
        ksi=xgauss(j);
        % Mapping (Eqs. 8-13)
        [JB,detJ] = invjacobian(xvec,yvec,ksi,eta);
        [T]=quad_transformation(JB);
        % Ritz basis functions (Eqs. 24-25)
        [N1i] = ritz_basis(bc1,n,ksi,eta); % for u1i
        [N2i] = ritz_basis(bc2,n,ksi,eta); % for u2i
        [N3i] = ritz_basis(bc3,n,ksi,eta); % for u3i
        NJ(:,:,1,1)=N1i;
        NJ(:,:,1,2)=N1i;
        NJ(:,:,1,3)=N1i;
        NJ(:,:,1,4)=N1i;
        NJ(:,:,2,1)=N2i;
        NJ(:,:,2,2)=N2i;
        NJ(:,:,2,3)=N2i;
        NJ(:,:,2,4)=N2i;
        NJ(:,:,3,1)=N3i;
        NJ(:,:,3,2)=N3i;
        NJ(:,:,3,3)=N3i;
```

```
96          NJ(:,:,3,4)=N3i;
97          % Strain fisplacement matrices (Eq. 21)
98          B(:,:,1) = BM(N1i,N2i,N3i,Nsize);
99          B(:,:,2) = BM(N1i,N2i,N3i,Nsize);
100         B(:,:,3) = BM(N1i,N2i,N3i,Nsize);
101         B(:,:,4) = BM(N1i,N2i,N3i,Nsize);
102         % Shape function matrix for mass matrix (Eq. 23)
103         [H] = mass_shape_f_matrix(NJ,Nsize);
104         for i1 = 1:4
105             for j1 = 1:4
106                 K(:,:,i1,j1)=K(:,:,i1,j1)+transpose(B(:,:,i1))*...
107                     transpose(T)*D(:,:,i1,j1)*T*B(:,:,i1)*...
108                     detJ*wgauss(j)*wgauss(i);
109             end
110         end
111         MP=MP+transpose(H)*mp*H*detJ*wgauss(j)*wgauss(i);
112     end
113 end
114
115 % Global stiffness matrix (Eq. 17)
116 KP(1:subksize, 1:subksize) = K(:,:,1,1);
117 KP(1:subksize, subksize+1:2*subksize) = K(:,:,1,2);
118 KP(1:subksize, 2*subksize+1:3*subksize) = K(:,:,1,3);
119 KP(1:subksize, 3*subksize+1:4*subksize) = K(:,:,1,4);
120 KP(subksize+1:2*subksize, 1:subksize) = K(:,:,2,1);
121 KP(subksize+1:2*subksize,  subksize+1:2*subksize) = K(:,:,2,2);
122 KP(subksize+1:2*subksize,  2*subksize+1:3*subksize) = K(:,:,2,3);
123 KP(subksize+1:2*subksize,  3*subksize+1:4*subksize) = K(:,:,2,4);
124 KP(2*subksize+1:3*subksize, 1:subksize ) = K(:,:,3,1);
125 KP(2*subksize+1:3*subksize, subksize+1:2*subksize) = K(:,:,3,2);
126 KP(2*subksize+1:3*subksize, 2*subksize+1:3*subksize) = K(:,:,3,3);
127 KP(2*subksize+1:3*subksize, 3*subksize+1:4*subksize) = K(:,:,3,4);
128 KP(3*subksize+1:4*subksize, 1:subksize) = K(:,:,4,1);
129 KP(3*subksize+1:4*subksize, subksize+1:2*subksize) = K(:,:,4,2);
130 KP(3*subksize+1:4*subksize, 2*subksize+1:3*subksize) = K(:,:,4,3);
131 KP(3*subksize+1:4*subksize, 3*subksize+1:4*subksize) = K(:,:,4,4);
132
133 % Solution
134  nmode=12; %Desired number of modes
135 [v1,d1]=eigs(KP,MP,nmode,'sm');
136 [eval,ix] = sort(diag(d1));
137 evec = v1(:,ix); % Re-order eigenvectors to match sorted eigenvalues
138 d2=double(eval); % Eigenvalues
139 omega=sqrt(d2);
140 freq_parameter= omega*b^2/hp*sqrt(layer(1).Density/layer(1).E2);
141 disp('Frequency parameters')
142 disp(freq_parameter(1:10,1))
143 % disp('freq Hz')
144 % freq_Hz=sqrt(d2)/(2*pi);
145 % disp(freq_Hz(1:10))
```

Subroutines

```
function [N] = ritz_basis(bc,n,x,y)
%
%  Generates Ritz basis functions for TSNDT
%
%  INPUT:
%  bc = According to bc at the edges arranges the Jacobi shape parameter
%  n  - number of Jacobi Polynomials terms
%  x    - coordinate input
%  y    - coordinate input
%
%  Output:
%  N(1,:) = basis function of x and y
%  N(2,:) = dN/dx
%  N(3,:) = dN/dy

% Set Jacobi polynomials to zero if uij at specific edge is constrained
    e1 = bc(1,1); e2 = bc(2,1); e3 = bc(3,1); e4 = bc(4,1);

% Weight of Jacobi polynomials
    WX = JacobiWeight(e1,e3,x);
    WY = JacobiWeight(e2,e4,y);

%  Derivatives of Jacobi weight functions
    WXD = JacobiWeightD(e1,e3,x);
    WYD = JacobiWeightD(e2,e4,y);

% Jacobi polynomials in x and y directions
    [Pout1, PX] = JacobiPol(n,2*e3,2*e1,x);
    [Pout2, PY] = JacobiPol(n,2*e4,2*e2,y);

% Derivatives of the Jacobi polynomials in x and u directions
    [Pout, PDX] = JacobiPolD(n,2*e3,2*e1,x);
    [Pout, PDY] = JacobiPolD(n,2*e4,2*e2,y);

% Preallocation
    phi = zeros(1,(n+1)^2); % basis function - N(1,:)
    phidx = zeros(1,(n+1)^2); % dNdx - N(2,:)
    phidy = zeros(1,(n+1)^2); % dNdy - N(3,:)

% Calculate product basis function
    for i = 1:(n+1)
        for j = 1:(n+1)
            % Locator index
            k = (i-1)*(n+1)+j; % index k=1,2,...,N

            % x direction
            % Derivative of 1D Jacobi polynomial
```

```
48              a1 = PDX(i)*WX+WXD*PX(i);
49              % Jacobi polynomial
50              a2 = PX(i)*WX;
51
52              % y direction
53              b1 = PY(j)*WY;
54              b2 = PDY(j)*WY+WYD*PY(j);
55
56              % Basis function and derivatives
57              phi(k) = a2*b1;
58              phidx(k) = a1*b1;
59              phidy(k) = a2*b2;
60          end
61      end
62      N(1,:) = phi;
63      N(2,:) = phidx;
64      N(3,:) = phidy;
65  end
```

```
function [Pout,P] = JacobiPol(n,a,b,x)
%
% This code generates Jacobi Polynomials
% Input:
% n = is degree of the polynomials
% a = alpha and b=beta (Jacobi Shape Parameters)
% x = coordinate
%
% Output:
% Pout = only includes term related tp nth degree
% P =  all terms up to nth degree
% P(1) is the zeroth order .. P(n+1) is the nth order
%
    P(1)=1; % 0th term
    P(2)=(a-b)/2+(1+(a+b)/2)*x; %1st Term
%
    if(n==0)Pout=P(1);end
    if(n==1)Pout=P(2);end
%
    if n≥2
        for i=3:n+1
            t=i-1;
            a1=(ci(2*t-1,a,b)*(ci(2*t-2,a,b)*ci(2*t,a,b)*x+a^2-b^2))/...
                (2*t*ci(t,a,b)*ci(2*t-2,a,b));
            b1=(2*(t-1+a)*(t-1+b)*ci(2*t,a,b))/(2*t*ci(t,a,b)*ci(2*t-2,a,b));
            P(i)=a1*P(i-1)-b1*P(i-2);
        end
    Pout=P(n+1);
    end
%
    function [Out]=ci(i,a,b)
        Out=i+a+b;
    end
end
```

```
function [Pout] = JacobiWeight(a,b,x)
% This function calculates the weight of Jacobi Polynomials
    Pout=(x+1)^a*(x-1)^b;
end
```

Appendix A. Sample MATLAB Code

```
function [Pout,PD] = JacobiPolD(n,a,b,x)
%
% This code generates 1st derivative of the Jacobi polynomials at given x
% P is the output of [P] = JacobiPol(n,a,b,x)
% Ref:"http://mathworld.wolfram.com/JacobiPolynomial.html"
% n is the max degree of polynomials
% a= alpha and b=beta
% Written by Berkan Alanbay 02-13-2018
% All rights are reserved
    PD(1)=0; % 0th term
    if(n==0) Pout=0;end% 0th term
    [Pout,Pv]=JacobiPol(n,a+1,b+1,x);
    if n≥1
        for i=2:n+1
           t=i-1;
           PD(i)=1/2*(t+a+b+1)*Pv(i-1);
        end
        Pout=PD(n+1);
    end
end
```

```
function [Pout] = JacobiWeightD(a,b,x)
%This function calculates 1st derivative of the Jacobi weight function
    Pout=a*(x-1)^b*(1+x)^(a-1)+b*(x-1)^(b-1)*(1+x)^a;
end
```

```
function [B] = BM(N1i,N2i,N3i,Nsize)

zm=zeros(1,Nsize);

B1=[N1i(2,:),zm,zm];
B2=[N1i(3,:),zm,zm];
B3=[zm,N2i(2,:),zm];
B4=[zm,N2i(3,:),zm];
B5=[zm,zm,N3i(2,:)];
B6=[zm,zm,N3i(3,:)];
B7=[N1i(1,:),zm,zm];
B8=[zm,N2i(1,:),zm];
B9=[zm,zm,N3i(1,:)];

B=[B1;B2;B3;B4;B5;B6;B7;B8;B9];

end
```

```
function [H] = mass_shape_f_matrix(NJ,Nsize)

H = zeros(12, 12*Nsize);
H(1, 1:Nsize) = NJ(1,:,1,1);
H(2, Nsize+1:2*Nsize) = NJ(1,:,2,1);
H(3, 2*Nsize+1:3*Nsize) = NJ(1,:,3,1);
H(4, 3*Nsize+1:4*Nsize) =  NJ(1,:,1,2);
H(5, 4*Nsize+1:5*Nsize) =  NJ(1,:,2,2);
H(6, 5*Nsize+1:6*Nsize) =  NJ(1,:,3,2);
H(7, 6*Nsize+1:7*Nsize) =  NJ(1,:,1,3);
H(8, 7*Nsize+1:8*Nsize) =  NJ(1,:,2,3);
H(9, 8*Nsize+1:9*Nsize) =  NJ(1,:,3,3);
H(10, 9*Nsize+1:10*Nsize) = NJ(1,:,1,4);
H(11, 10*Nsize+1:11*Nsize) =  NJ(1,:,2,4);
H(12, 11*Nsize+1:12*Nsize) =  NJ(1,:,3,4);

end
```

```
function [BC] = BoundaryCondition(type)

    switch type(1)
        case 'S'
            edge1 = [0,1,1];
        case 'C'
            edge1 = [1,1,1];
        case 'F'
            edge1 = [0,0,0];
    end

    switch type(2)
        case 'S'
            edge2 = [1,0,1];
        case 'C'
            edge2 = [1,1,1];
        case 'F'
            edge2 = [0,0,0];
    end

    switch type(3)
        case 'S'
            edge3 = [0,1,1];
        case 'C'
            edge3 = [1,1,1];
        case 'F'
            edge3 = [0,0,0];
    end

    switch type(4)
```

```
        case 'S'
            edge4 = [1,0,1];
        case 'C'
            edge4 = [1,1,1];
        case 'F'
            edge4 = [0,0,0];
    end

    BC=[edge1' edge2' edge3' edge4']';
end
```

```
% Material Properties
% Update below values for different material

Material_1 = LaminateData; %Assign class property
Material_1.Type = 'Lamina';

Material_1.E1 = 25.1e6; %Psi
Material_1.E2 = 4.8e6; %Psi
Material_1.E3 = 0.75e6; %Psi

Material_1.Nu12 = 0.036;
Material_1.Nu13 = 0.25;
Material_1.Nu23 = 0.171;

Material_1.G12 = 1.36e6; %Psi
Material_1.G13 = 1.2e6; %Psi
Material_1.G23 = 0.47e6; %Psi

Material_1.Density = 1800;

% The values are taken from Nosier, Asghar, Rakesh K. Kapania,
% and J. N. Reddy. "Free vibration analysis of laminated plates using
% a layerwise theory." AIAA journal 31.12 (1993): 2335-2346.
```

```
function [C] = lamina(Mat)

% This subroutine calculates the transformed elastic coefficients for a
% lamina

% The Components of the Elastic Compliance Matrix

S11=1/Mat.E1;
S22=1/Mat.E2;
S33=1/Mat.E3;
S12=-Mat.Nu12/Mat.E1;
S13=-Mat.Nu13/Mat.E1;
S23=-Mat.Nu23/Mat.E2;
```

```
S44=1/Mat.G23;
S55=1/Mat.G13;
S66=1/Mat.G12;

% The Components of the Stiffness Matrix

S=S11*S22*S33 - S11*S23*S23 - S22*S13*S13 - S33*S12*S12 + 2*S12*S23*S13;
C11=(S22*S33 - S23*S23)/S;
C22=(S33*S11 - S13*S13)/S;
C33=(S11*S22 - S12*S12)/S;
C12=(S13*S23 - S12*S33)/S;
C13=(S12*S23 - S13*S22)/S;
C23=(S12*S13 - S23*S11)/S;
C44=1/S44;
C55=1/S55;
C66=1/S66;

% Transformed elastic coefficients referred to the (x,y,z)
% JN Reddy Mechanics of Laminated Composite Plates and Shells p96

Theta = Mat.Theta;
C11b = C11*cosd(Theta)^4 + 2*(C12 + 2*C66)*cosd(Theta)^2*sind(Theta)^2 ...
    + ...
    C22*sind(Theta)^4;
C12b = C12*cosd(Theta)^4 + (C11 + C22 - ...
    4*C66)*cosd(Theta)^2*sind(Theta)^4 +...
    C12*sind(Theta)^4;
C13b = C13*cosd(Theta)^2 + C23*sind(Theta)^2;
C16b = (C11 - C12 - 2*C66)*cosd(Theta)^3*sind(Theta) + ...
    (2*C66 + C12 - C22)*cosd(Theta)*sind(Theta)^3;
C22b = C22*cosd(Theta)^4 + 2*(C12 + 2*C66)*cosd(Theta)^2*sind(Theta)^2+...
    C11*sind(Theta)^4;
C23b = C23*cosd(Theta)^2 + C13*sind(Theta)^2;
C26b = (C12 - C22 + 2*C66)*cosd(Theta)^3*sind(Theta) + ...
    (C11 - C12 -2*C66)*cosd(Theta)*sind(Theta)^3;
C33b = C33;
C36b = (C13 - C23)*cosd(Theta)*sind(Theta);
C44b = C44*cosd(Theta)^2 + C55*sind(Theta)^2;
C45b = (C55 - C44)*cosd(Theta)*sind(Theta);
C55b = C55*cosd(Theta)^2 + C44*sind(Theta)^2;
C66b = (C11 + C22 -2*C12 -2*C66)*cosd(Theta)^2*sind(Theta)^2 + ...
    C66*(cosd(Theta)^4 + sind(Theta)^4);

C = [ C11b, C12b, C13b, 0, 0, C16b;
      C12b, C22b, C23b, 0, 0, C26b;
      C13b, C23b, C33b, 0, 0, C36b;
      0, 0, 0, C44b, C45b, 0;
      0, 0, 0, C45b, C55b, 0;
      C16b, C26b, C36b, 0, 0, C66b];
end
```

Appendix A. Sample MATLAB Code

```
% Laminate class is defined with below properties
classdef LaminateData
   properties
      Material
      Type
      E1
      E2
      E3
      Nu12
      Nu13
      Nu23
      G12
      G13
      G23
      Alpha1
      Alpha2
      Alpha3
      Beta1
      Beta2
      Beta3
      Thickness
      Density
      Theta
   end
end
```

```
function mp = CompositeMassProperty(layer)
% Calculate mp matrix in TSNDT formulations
% Input:
%       layer is a class contains properties of each layer
% Output:
%       mp = sum_{k=1}^{N} int_{h_k}^{h_{k+1}} rho ZZ  dz
%%%%%%%%%%%%%%%%%%%%%%%%%%%%%%%%%%%%%%%%%%%%%%%%%%%%%%%%%%%%%%%%%%%%%%%%%%%%

% Number of layer in laminated composite
    nLayer = length(layer);

% Calculate total thickness
    h = sum([layer(1:nLayer).Thickness]);

% z cordinates of each laminate
    zc = zeros(nLayer+1,1);
    zc(1) = -h/2; % bottom of the plate

    for n=1:nLayer
        zc(n+1)=zc(n)+layer(n).Thickness;
    end

```

```
% Gauss quadtature data
    Ng = 4; % Number of Gauss Points
    [Qz, Wz] = legendre_gauss_quad (Ng); % Gauss Points and Weights

    mp = 0;
    for k=1:nLayer
        a = zc(k);
        b = zc(k+1);
        for m=1:Ng
            zeta = (b - a)/2*Qz(m) + (b + a)/2;
            mp = mp + (b - a)/2 *layer(k).Density * ZZ(zeta) * Wz(m);
        end
    end
end
```

```
function D = D_ij(i,j,layer)
% Calculate Dij matrix in TSNDT formulations
% Input:
%       layer is a class contains properties of each layer
% Output:
%       Dij = sum_{k=1}^{N} int_{h_k}^{h_{k+1}} Z_i^T C^k Zj dz
%%%%%%%%%%%%%%%%%%%%%%%%%%%%%%%%%%%%%%%%%%%%%%%%%%%%%%%%%%%%%%%%%%%%%%%%%%%%

% Number of layer in laminated composite
    nLayer = length(layer);

% Calculate total thickness
    h = sum([layer(1:nLayer).Thickness]);

% z cordinates of each laminate
    zc = zeros(nLayer+1,1);
    zc(1) = -h/2; % bottom of the plate

    for n=1:nLayer
        zc(n+1)=zc(n)+layer(n).Thickness;
    end

% Gauss quadtature data
    Ng = 4; % Number of Gauss Points
    [Qz, Wz] = legendre_gauss_quad (Ng); % Gauss Points and Weights

    D = 0;
    for k=1:nLayer
        a = zc(k);
        b = zc(k+1);
        C = lamina(layer(k));
        for m=1:Ng
            zeta = (b - a)/2*Qz(m) + (b + a)/2;
            D = D + (b - a)/2*transpose(Z1(i,zeta))*C*Z1(j,zeta)*Wz(m);
```

```
        end
    end
end
```

```
function [Z] = Z1(i,z)
    Z = [z^i, 0, 0, 0, 0, 0, 0, 0;...
        0, z^i, 0, 0 ,0, 0, 0, 0;...
        0, 0, i*z^(i-1), 0, 0, 0, 0, 0;...
        0, 0, 0, z^(i), 0, 0, 0, i*z^(i-1);...
        0, 0, 0, 0, z^(i), 0,i*z^(i-1), 0;...
        0, 0, 0, 0, 0, z^(i), 0, 0];
end
```

```
function [ZZ] = ZZ(z)

ZZ = [1, 0, 0, z, 0, 0, z^2, 0, 0, z^3, 0, 0;...
      0, 1, 0, 0, z, 0, 0, z^2, 0, 0, z^3, 0;...
      0, 0, 1, 0, 0, z, 0, 0, z^2, 0, 0, z^3;...
      z, 0, 0, z^2, 0, 0, z^3, 0, 0, z^4, 0, 0;...
      0, z, 0, 0, z^2, 0, 0, z^3, 0, 0, z^4, 0;...
      0, 0, z, 0, 0, z^2, 0, 0, z^3, 0, 0, z^4;...
      z^2, 0, 0, z^3, 0, 0, z^4, 0, 0, z^5, 0, 0;...
      0, z^2, 0, 0, z^3, 0, 0, z^4, 0, 0, z^5, 0;...
      0, 0, z^2, 0, 0, z^3, 0, 0, z^4, 0, 0, z^5;...
      z^3, 0, 0, z^4, 0, 0, z^5, 0, 0, z^6, 0, 0;...
      0, z^3, 0, 0, z^4, 0, 0, z^5, 0, 0, z^6, 0;...
      0, 0, z^3, 0, 0, z^4, 0, 0, z^5, 0, 0, z^6];
end
```

```
function [x,w] = legendre_gauss_quad (N)
% Nodes and weights for N-point Legendre Gaussian quadrature
    n = [0:N-2]; beta = (n+1)./sqrt((2*n+1).*(2*n+3));
    J = diag(beta,-1)+diag(beta,1); % Symmetric tridiagonal matrix
    [V,D] = eig(J); % Solve eigenvalue problem
    x = diag(D); [x,i] = sort(x); % Gauss quadrature nodes
    x = flipud(x); w = 2*V(1,i).^2; % Gauss quadrature weights
end
```

```
function [JB,detj]=invjacobian(x,y,ksi,eta)
%
%   Calculates inverse of Jacobian matrix, [J]^(-1)
%
%  format:
%
```

```
%  [jb11,jb12,jb21,jb22,detj]=Fun1(x,y,ksi,eta)
%
%  x    - vector of x coordinates
%  y    - vector of y coordinates
%  xi  - local coordinate 1
%  eta  - local coordinate 2
%
%  jb11 - output matrix term
%  jb12 - output matrix term
%  jb21 - output matrix term
%  jb22 - output matrix term
%  detj - determinant of [J]

      x1 = x(1); x2=x(2); x3=x(3); x4=x(4);
      y1 = y(1); y2=y(2); y3=y(3); y4=y(4);
      % Shape functions
      pxk = ((1+eta)*(x3-x4)+(1-eta)*(x2-x1))/4;
      pxe = ((1+ksi)*(x3-x2)+(1-ksi)*(x4-x1))/4;
      pyk = ((1+eta)*(y3-y4)+(1-eta)*(y2-y1))/4;
      pye = ((1+ksi)*(y3-y2)+(1-ksi)*(y4-y1))/4;
      % Determinant of the Jacobian matrix
      detj = pxk*pye-pxe*pyk;
      % Inverse of Jacobian matrix
      jb11 = pye/detj;
      jb12 = -pxe/detj;
      jb21 = -pyk/detj;
      jb22 = pxk/detj;
      JB = [jb11,jb12;jb21,jb22];
end
```

```
function [T]=quad_transformation(JB)

G11 = JB(1,1);
G12 = JB(2,1);
G21 = JB(1,2);
G22 = JB(2,2);

% Transformation matrix
T = [G11, G12, 0, 0, 0, 0, 0, 0, 0;...
    0, 0, G21, G22, 0, 0, 0, 0, 0;...
    0, 0, 0, 0, 0, 0, 0, 0, 1;...
    0, 0, 0, 0, G21, G22, 0, 0, 0;...
    0, 0, 0, 0, G11, G12, 0, 0, 0;...
    G21, G22, G11, G12, 0, 0, 0, 0, 0;...
    0, 0, 0, 0, 0, 0, 1, 0, 0;...
    0, 0, 0, 0, 0, 0, 0, 1, 0];

end
```